

# FUSION APPROACH ON LOW RESOLUTION SATELLITE IMAGES FOR LAND COVER APPLICATION

## A THESIS

*Submitted in partial fulfilment of the  
requirements for the award of the degree*

*of*

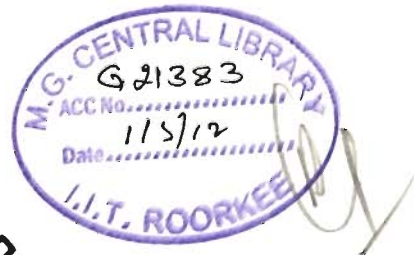
DOCTOR OF PHILOSOPHY

*in*

ELECTRONICS AND COMPUTER ENGINEERING

*by*

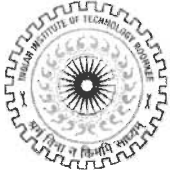
**HARISH KUMAR G R**



DEPARTMENT OF ELECTRONICS AND COMPUTER ENGINEERING  
INDIAN INSTITUTE OF TECHNOLOGY ROORKEE  
ROORKEE-247 667 (INDIA)

SEPTEMBER, 2010

**©INDIAN INSTITUTE OF TECHNOLOGY ROORKEE, ROORKEE, 2010  
ALL RIGHTS RESERVED**



# INDIAN INSTITUTE OF TECHNOLOGY ROORKEE ROORKEE

## CANDIDATE'S DECLARATION

I hereby certify that the work which is being presented in the thesis entitled **FUSION APPROACH ON LOW RESOLUTION SATELLITE IMAGES FOR LAND COVER APPLICATION** in partial fulfilment of the requirements for the award of the Degree of Doctor of Philosophy and submitted in the Department of Electronics and Computer Engineering of the Indian Institute of Technology Roorkee, Roorkee is an authentic record of my own work carried out during a period from July 2005 to September 2010 under the supervision of Dr. Dharmendra Singh, Associate Professor, Department of Electronics and Computer Engineering, Indian Institute of Technology Roorkee, Roorkee.

The matter presented in this thesis has not been submitted by me for the award of any other degree of this or any other Institute.



(**HARISH KUMAR G R**)

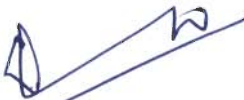
This is to certify that the above statement made by the candidate is correct to the best of my knowledge.



(**Dharmendra Singh**)  
Supervisor

Date: 20/09/2010

The Ph.D. Viva-Voce Examination of **Mr. Harish Kumar G R**, Research Scholar, has been held on ..... 11/3/2011 .....



Signature of Supervisor



Signature of External Examiner

# Abstract

Since the launch of Landsat-1, the first Earth resource satellite in 1972, satellite image processing has become an increasingly important tool for the inventory, monitoring, management of earth resources and many other applications (Draeger et al. 1997). The increasing availability of information products generated from satellite images has added greatly to our ability to understand the patterns and dynamics of the earth resource systems at all scales of inquiry (Lambin et al. 2001).

Satellite remote sensors can be divided into two major types of imaging systems: optical (optical and thermal) and radar imaging systems. Optical imaging systems operate in the visible and IR (Infra Red) regions of the spectrum. Their operational use is weather dependent, since clouds are not transparent at visible/IR wavelengths (0.4-14  $\mu\text{m}$ ). Some of the satellite images working on optical and thermal images can be listed as AVHRR (Advanced Very High Resolution Radiometer), MODIS (Moderate Resolution Imaging Spectroradiometer), Landsat (land Satellite), LISS (Linear Imaging Self Scanner), SPOT (Satellite Pour L'Observation de la Terra or earth observing satellites) and many others. On the other hand, radar imaging systems works in microwave region (1 GHz to 30 GHz), and are very much atmosphere and weather independent. ERS (European remote sensing satellite), JERS (Japanese earth remote sensing), ENVISAT (Environmental Satellite Advanced Synthetic Aperture Radar), RADARSAT (Radar Satellite), and PALSAR

(Phased Array L-band Synthetic Aperture Radar) are some of the radar satellite sensors available for various applications.

One of the important application of satellite image processing is the generation of landuse/ land-cover maps (Anderson et al. 1976) in comparison to more traditional mapping approaches such as terrestrial survey and basic aerial photo interpretation which is quite cumbersome. Land-use mapping/ classification using satellite imagery has the advantages of low cost, large area coverage, repetitively, and computitivity. Eventually maximum high resolution satellite images is expensive with some extent. Therefore, it is need of current research to explore some techniques by which utilization of freely available satellite image may be enhanced. The increasing availability of satellite imagery with significantly improved spectral and spatial resolution has offered greater potential for more detailed land cover classification. The availability of MODIS image with greatly improved spectral, spatial, geometric, and radiometric attributes provides significant new opportunities and challenges for remote sensing-based land cover classification (Friedl et al. 2002) as well as other applications. MODIS has several spectral bands with are useful for various application in one hand and in other hand its spatial resolution varies from 250 m to 1000 m. This spatial resolution is not so enough to get good classification accuracy on MODIS images. Therefore, there is a need to explore the possibility of the use of techniques like fusion that may be helpful to increase the utilization of MODIS image for land cover classification/ land use maps. Time series analysis is another important aspect by which changes may be identified in a particular class of the land cover.

Alparone et al. 2004 have demonstrated the benefit of combining optical and radar image for improved land cover mapping in several studies. With the availability of multifrequency and high-resolution space borne radar data, such as Advanced Land Observation Satellite (ALOS) Phase Array L-type Synthetic Aperture Radar (PALSAR), an increased interest in tools to exploit the full information content of both image types is arising.

Unsupervised clustering is a fundamental tool in image processing for geosciences and satellite imaging applications (Stuckens et al. 2000). A well review of clustering method is reported by Jain et al. in 1999. For example, unsupervised

clustering is often used to obtain vegetation maps of an area of interest. This approach is useful when reliable training image are either scarce or expensive, and when relatively little a priori information about the image is available. Unsupervised clustering methods play a significant role in the pursuit of unsupervised classification (Richards and Jia 1999). Eventually this unsupervised clustering can be used for hotspot and non-hotspot region classification.

Recent advances in satellite image processing have expanded opportunities to characterize the seasonal and inter-annual dynamics of natural and managed Land use/ land cover communities. The development of a regional-scale monitoring procedure is challenging because it requires remotely sensed image that have wide geographic coverage, high temporal resolution, adequate spatial resolution and minimal cost. The MODIS offers an opportunity for detailed, large-area Land use/ land cover characterization by providing global coverage of science quality image with high temporal resolution (1–2 days) and intermediate spatial resolution (Justice and Townshend 2002). The spatial, spectral, and temporal components of the MODIS may be appropriate for multitemporal harmonic analysis. Harmonic analysis is useful for analyzing seasonal and inter-annual variation in land surface condition (Wan et al. 2004). This type of analysis may develop the possibility to quantify and classify some fundamental characteristics, related to the phenology of vegetation, water and others.

The main aim of this thesis was to study and to maximize the utilization of low resolution freely available satellite image for various land cover classification. For this purpose, freely available MODIS image has been used and it is attempted to develop suitable algorithm for fusion technique for land cover classification and harmonic analysis.

This thesis is organized in seven chapters. The first chapter presents the introduction of the thesis which includes motivation, major research gaps, and details about the study area and satellite image used. Brief review of related work is presented in chapter II.

We have explored the fusion technique for enhancing the land cover classification of low resolution satellite image especially freely available satellite image like MODIS in the chapter III. One of the aim of this chapter is to analyze the

effect of classification accuracy on major type of land cover types like agriculture, water and urban bodies with fusion of ASTER image to MODIS image and enhance the classification accuracy of MODIS image at spatial level. For this purpose, we have considered to fuse, high resolution i.e., like 15m resolution ASTER image with moderate resolution i.e., like 250 m MODIS satellite data. MODIS band 1 and band 2 are used as a moderate resolution data, where as ASTER band 2 and band 3 are considered as high resolution data. Curvelet transformation has been applied for fusion of these two satellite images and Minimum Distance classification technique has been applied on the resultant fused image for classifying the fused image in major land cover classes (i.e., agriculture, urban and water). The fuzzy based fusion is also applied for fusion of these two satellite images. After the fusion by fuzzy based approach, the minimum distance classification technique is used to classify the resultant fused image in major land cover classes (i.e., agriculture, urban and water). It is quantitatively observed that the overall classification accuracy of MODIS image after fusion is enhanced at spatial level. The quality of fused image is assessed by quality indicators. Another important point which one should consider while doing the time-series analysis, where every MODIS image may require the same number of high resolution image for fusion in one hand and in another hand every time one has to carry out the complex computation of fusion. Generally high resolution image i.e., ASTER is not freely available. So, it is another point of research to develop such a methodology or coefficients by which use of high spatial resolution image(i.e., ASTER in our case) for fusion for time series analysis may be minimized. Therefore, in this chapter, we have attempted to explore to find the possible methodology to search some fusion coefficient by which ASTER image use may be minimized, while analyzing time series image for observing the land cover classification. For this purpose, firstly we have carried out fusion of MODIS (band 1 and band 2) image with ASTER (band 2 and band 3) image using curvelet transform and fuzzy based technique. After this, we have obtained a fusion coefficient that may be minimizing the use of ASTER image(i.e., every time of fusion of MODIS image with ASTER data, we may use this derived coefficient). Another advantage of this fusion coefficient is that every time we do not have to carry out curvelet transform on ASTER image by which it reduces the computation complexity up to a certain extent. We have obtained the fusion coefficient with three MODIS and one ASTER image of

month March 2001. The obtained coefficient is validated with the MODIS image of another year and gives the satisfactory result.

In the chapter IV, another important aspect of fusion of different sensors image like optical and radar images (where both can provide the complimentary information) is carried out and the quality of fused image is assessed by various assessment indicators. For this purpose an attempt has been made to fuse the PALSAR image with MODIS image using curvelet based fusion and quality assessment of fused image has been done. PALSAR image has a advantage of availability of image in four different channels. These four channels are HH (Transmitted horizontal polarization and received also in horizontal polarization), HV(Transmitted horizontal polarization and received vertical polarization), VH (Transmitted vertical polarization and received horizontal polarization) and VV (Transmitted vertical polarization and received vertical polarization)(www2 2009), which provides various landcover information. We have used the curvelet and fuzzy based technique for fusing the PALSAR (HH, HV and VV) image to MODIS (band 1 and 2) image in spatial resolution. Each band of PALSAR (i.e., HH, HV and VV) is individually fused with MODIS band 1 and Band 2 separately in one hand and in other hand fused image of MODIS band 1 and 2 is individually fused PALSAR (HH, HV and VV) bands separately. The quality of fused image is assessed by assessment indicator like Correlation, RMSE (root mean squared error), Relative Mean Difference, Relative Variation Difference, Deviation Index, PSNR (Peak signal-to-noise ratio) and Universal Image Quality Index. These indicators are applied to measure and compare the performance of the fused images. The results are quite encouraging and we get quite a good overall classification accuracy after fusion. Thereby in near future it may provide a better platform for the maximize the use of MODIS images.

Classification of various class is one aspect whereas focus for certain class is another aspect, therefore in this thesis, we have considered for both type of objective where in case 1, we have classified image into three major land cover classes (Agriculture, water and urban) and in second case we have attempted to focus the subsurface fire (i.e., hotspots) in the image and considered it as one class. We have considered Jharia, region of India as a test area for this purpose. In the chapter V, we



have explored the application of MODIS and LISS-III image for hotspot and non-hotspot regions. Although MODIS provides a special product MOD14A2 for fire product classification. But this special product is not only sufficient for hotspot and non-hotspot regions. Therefore objective of this chapter is to use various information of different corresponding bands to focus the hotspot in the images. For this purpose, in this chapter, an approach based on Binary Division Algorithm is used for hotspot and non-hotspot regions using band 1 and band 2 of MODIS and band 2 and band 3 of LISS - III for the Jharia (India) Region. Results are compared with the MOD14A2, the exclusive MODIS product for thermal anomalies and fire, and it is found that the proposed approach gives quite satisfactory results in comparison to MOD14A2 products.

It is important to analyze the changes in the classes from year to year therefore harmonic analyses is another aspect to see the respective changes in different classes, hence in the next chapter, i.e., chapter VI, we have tried to characterized the changes for agricultural and water land use/land cover in Western Uttar Pradesh and part of Uttarakhand of India from the year 2001 to 2008. In this perspective, we have considered the MODIS NDVI (Normalized difference vegetation index) and NDWI (Normalized difference water index) images for agricultural and water regions respectively. Harmonic analysis, also known as Fourier analysis, decomposes a time-dependent periodic phenomenon into a series of sinusoidal functions in which each defined by unique additive and amplitude values. In consequence, the additive image  $A_0$  and the amplitude images  $A_1$  were produced, respectively. With these images we have checked the changes in agricultural and water land use/land cover in the test area, in one hand we have analyzed the changes or variation in agriculture and water for the whole image, whereas in the other hand, we have analyzed the changes or variation in agriculture and water for the selected region of interest. Such type of study is very helpful in near future to optimize the use of MODIS image in one hand and in another hand to develop monitoring system by which changes during the particular month may be observed.

Finally in chapter VII, the contributions made in the thesis are summarized and scope of future work is outlined.

# Acknowledgements

*"If I have seen further than others, it is by standing upon the shoulders of giants"*

.....Isaac Newton

*"The mere formulation of a problem is far more often essential than its solution, which may be merely a matter of mathematical or experimental skill. To raise new questions, new possibilities, to regard old problems from a new angle requires creative imagination and marks real advances in science"*

*"One should never impose one's views on a problem; one should rather study it, and in time a solution will reveal itself"*

*'Problems cannot be solved at the same level of awareness that created them.'*

.....Albert Einstein

*"If you're not making mistakes, then you're not doing anything. I'm positive that a doer makes mistakes"*

.....John Wooden

*"Research is to see what everybody else has seen, and to think what nobody else has thought."*

..... Albert Szent-Gyorgyi

This doctoral work had been difficult to reach the final stage without the support of several people. It's tough to put words together to acknowledge the help I got from them.

I am deeply and humbly grateful to my guide Dharmendra Singh for helping to create the best possible academic environment I could have hoped for during my stay at IIT Roorkee. His scientific vision, enthusiasm and brilliance have been nothing short of a model for me. His invaluable discussions, suggestions, meticulous, guidance and selfless efforts despite his very busy schedule was always extended to me, whenever I needed. The research directions that we have explored together are in my own opinion very exciting; and for this I feel very obliged. "Teachers open the door, student has to enter themselves" the self-explanatory sentence, which has been scribed on the board in his room, explains the kindness of opening the door for the students. His motivation and energy has always been a driving force for successful completion of this thesis work. His enduring patience and supervision during the review of this thesis helped me to reframe it in the present form.

My sincere thanks to research committee members; Prof. R.P.Gupta, Prof. Manoj Mishra and SRC chairman Prof. R. C. Joshi for their critic views that have helped me in improving the quality of my research work. I am indebted to the Ministry of Human Resource Development (MHRD), Government of India for providing me financial support during my research work.

I am thankful to the Head of Department, Prof. S. N. Sinha for providing computing and other important facilities for my research work. He has been the Chairman, Department Research Committee during tenure of my research work. I am thankful for the support and encouragement extended to me with his valuable suggestions.

It is a pleasure to acknowledge the support extended by my friends, colleagues and many others who had been in my contact during my research; Rohit, Vijaya, Gunjan, Rishi, Triloki, Abhay Gayakwad, Dharmveer, Vivek for the congenial cheering work environment in the Remote Sensing Lab and rounds of discussions where many naive thoughts have generated. I wish to convey my appreciation to my colleagues and friends for their encouragement and timely support.

I avail this privilege to express the heartfelt thanks to my dear mother (Mrs. Nagarathnamma) and father (Mr. Rangaiyah), whose prayers and wishes adhere with me in every situation of my life and also for providing me the much needed motivation and moral support during these grueling years. I am blessed to have the affectionate and empathetic support from my brothers (Vijay Kumar , Raghunath), sister (Kokila) who have been the stirring source behind my work.

I want to express my sincere thanks to all those who directly or indirectly helped me at various stages of this work. Above all, I express my indebtedness to the "ALMIGHTY" for all his blessings and kindness. "Shanta Karam Bhujaga Shayanam, Padmanabham Suresham, Vishvadharam Gagana Sadrsham, Megha Varnam Shubhangam, Lakshmi Kantam Kamala Nayanam, Yogibhir Dhyana Gamyam, Vande Vishnum, Vande Madhusoodanam, Vande Madhavam, Bhava Bhaya Haram, Sarva Lokaiaka Natham". I thank him for blessing me with the people around me that helped me at various steps of my life. I also thank him for that inner strength which I always feel within me even in my most depressing moments.

Harish Kumar G R

# Table of Contents

<b>CANDIDATE’S DECLARATION</b>	i
<b>Abstract</b>	iii
<b>Acknowledgements</b>	ix
<b>Table of Contents</b>	xiii
<b>List of Figures</b>	xix
<b>List of Tables</b>	xxxi
<b>Acronyms</b>	xxxiii
<b>Chapter 1</b>	
<b>Introduction</b>	1
1.1. Motivation	8
1.2. Problem Statement	12
1.3. Study Area	12
1.3.1. Study area for fusion techniques	13

1.3.2. Study area for hotspot and non-hotspot classification	13
1.3.3. Study area for multitemporal harmonic analysis	13
1.4. Satellite Data	15
1.4.1. Satellite data used for land cover classification	15
1.4.1a. MODIS	16
1.4.1b. ASTER	18
1.4.1c. PALSAR	19
1.4.2. Satellite data for hotspot and non-hotspot region classification	20
1.4.3. Satellite data for multitemporal harmonic analysis	21
1.5. Framework of the Research	21
1.6. Organization of the Thesis	23
<b>Chapter 2</b>	
<b>Brief Literature survey</b>	<b>25</b>
2.1. Introduction	25
2.2. Fusion processing levels	26
2.3. Commonly Used Fusion Techniques	28
2.3.1. Intensity Hue Saturation (IHS)	28
2.3.2. Brovey Transform	29
2.3.3. Principal Component Analysis (PCA)	30
2.3.4. Wavelet based fusion technique	31
2.3.5. Fuzzy based fusion technique	32

2.4. Fusion of Optical Images	34
2.5. Fusion of Optical and Radar Images	35
2.6. Hotspot and non-Hotspot Classification	35
2.7. Multitemporal Harmonic Analysis of MODIS Indexes	38

### **Chapter 3**

#### **Analysis of Fusion of Optical (MODIS and ASTER) Images for Land Cover Classification** 43

3.1. Introduction	43
3.2. Data Used/ Study Area	49
3.3. Theoretical Basis	50
3.3.1. Curvelet transform based Fusion	50
3.3.1.1. ATrous wavelet transform	50
3.3.1.2. Ridgelet transform	51
3.3.1.3. Curvelet transform	52
3.3.2. Fuzzy based fusion	54
3.3.2.1 Fuzzy logic approach	54
3.3.3. Quality assessment indicators	59
3.3.4. Minimum distance classification techniques	63
3.4. Implementation and Results	64
3.4.1. Curvelet based fusion	64
3.4.2. Fuzzy based fusion	65
3.4.3. Fusion coefficients	69

3.4.3.1. Methodology for deriving the fusion coefficient	69
3.5. Analysis of Experimental Results	71
3.5.1. Classification Accuracy	71
3.5.1.1. Curvelet based fusion	79
3.5.1.2. Fuzzy based fusion	83
3.5.1.3. Fusion coefficients	91
3.5.2. Quality assessment	103
3.6. Conclusion	103
<b>Chapter 4</b>	
<b>Optical (MODIS) and Radar (PALSAR) Image Fusion for Land Cover Classification</b>	<b>105</b>
4.1. Introduction	106
4.2. Data Used/ Study Area	107
4.3. Theoretical Basis	107
4.3.1. Curvelet transform based fusion	107
4.3.2. Fuzzy based fusion	107
4.3.3. Quality assessment indicators	108
4.4. Implementation and Results:	108
4.4.1. Curvelet based fusion	108
4.4.2. Fuzzy based fusion	112
4.5. Analysis of Experimental Results	119
4.5.1. Curvelet based fusion	119



4.5.2. Fuzzy based fusion	120
4.6. Conclusion	153
<b>Chapter 5</b>	
<b>MODIS Image Application for Hotspot and non-Hotspot Region Classification</b>	<b>155</b>
5.1. Introduction	155
5.2. Data Used/Study Area	159
5.3. Theoretical Basis	163
5.3.1. Curvelet transform	164
5.3.2. Binary Division Algorithm	165
5.3.3. Normalized Difference Vegetation Index (NDVI)	170
5.4. Implementation and Results	170
5.5. Analysis of Experimental Results	173
5.6. Conclusion	182
<b>Chapter 6</b>	
<b>Multitemporal Harmonic Analysis of MODIS Indexes</b>	<b>183</b>
6.1. Introduction	183
6.2. Data Used/Study Area	184
6.2.1. Data used	185
6.3. Theoretical Basis	186
6.3.1. Normalized Difference Vegetation Index (NDVI)	186
6.3.2. Normalized Difference Water Index (NDWI)	187

6.3.3. Harmonic Analysis	187
6.4. Implementation of Proposed Approach	190
6.5. Experimental Results	191
6.6. Conclusion	201
<b>Chapter 7</b>	
<b>Conclusions and Future Scope</b>	<b>203</b>
7.1. Contributions of the Thesis	203
7.2. Future Scope	206
<b>Bibliography</b>	<b>209</b>
<b>Author's Publications</b>	<b>247</b>

# List of Figures

Fig. 1.1. Location of the study area (Roorkee region) for fusion techniques, in the Haridwar district, India.	14
Fig. 1.2. Location of the study area (Jharia region) for hotspot and non-hotspot regions classification, in the Dhanbad district, Jharkhand state, India.	14
Fig. 1.3. Location of the study area for multitemporal harmonic analysis is indicated by the box in the top of the map	15
Fig. 1.4. Framework of the proposed research work	22
Fig. 2.1. Processing levels of image fusion	27
Fig. 3.1. Curvelet transform flowgraph. The figure illustrates the decomposition of the original image into subbands followed by the spatial partitioning of each subband(i.e., each subband is decomposed into blocks). The ridgelet transform is then applied to each block	54
Fig. 3.2. Basic fuzzy inference system	58
Fig. 3.3. Flowchart for fusion of ASTER and MODIS images through curvelet based fusion	66
Fig. 3.4. Fuzzy interference system editor for the fusion of ASTER and MODIS image	67

Fig. 3.5. Membership fusion editor implying the Membership Fusion (MF) for the ASTER and MODIS image	67
Fig. 3.6. Rule editor for the fusion of ASTER and MODIS image	68
Fig. 3.7. Flowchart for the fusion of ASTER and MODIS image through fuzzy based fusion	68
Fig. 3.8. The flowchart implying the fusion of the MODIS image with the AST_avg	71
Fig. 3.9a. ASTER band 2 image of as1	72
Fig. 3.9b. ASTER band 3 image of as1	72
Fig. 3.10a. MODIS band 1 image of d2	73
Fig. 3.10b. MODIS band 2 image of d2	73
Fig. 3.11. Toposheet of the study area (Roorkee region) in the Haridwar district, India	74
Fig. 3.12a. Spectral response of ASTER Band 2 (as1) for different class	74
Fig. 3.12b. Spectral response of ASTER Band 3 (as1) for different class	75
Fig. 3.13a. Spectral response of MODIS Band 1 (d2) for different class	75
Fig. 3.13b. Spectral response of MODIS Band 2 (d2) for different class	76
Fig. 3.14a. Minimum distance classified image of ASTER band 2 image of as1	77
Fig. 3.14b. Minimum distance classified image of ASTER band 3 image of as1	77
Fig. 3.15a. Minimum distance classified image of MODIS band 1 image of d2	78
Fig. 3.15b. Minimum distance classified image of MODIS band 2 image of d2	78

of d2

Fig. 3.16a. Resultant curvelet based fused MOD12 image of d2	80
Fig. 3.16b. Minimum Distance classified of the resultant curvelet based fused MOD12 image of d2	80
Fig. 3.17a. Resultant curvelet based fused AST23 image of as1	81
Fig. 3.17b. Minimum distance classified of the resultant curvelet based fused AST23 image of as1	81
Fig. 3.18a. Interpolated resultant curvelet based fused MOD12 (1186*1186) image of d2	83
Fig. 3.18b. Resultant curvelet based fused AS_MO	84
Fig. 3.18c. Minimum distance classified of the resultant curvelet based fusion AS_MO	84
Fig. 3.19a. Resultant fuzzy based fused MOD12 image of d2	87
Fig. 3.19b. Minimum distance classified of the resultant fuzzy based fused MOD12 image of d2	87
Fig. 3.20a. Resultant fuzzy based fused AST23 image of as1	88
Fig. 3.20b. Minimum distance classified of the resultant fuzzy based fused AST23 image of as1	88
Fig. 3.21a. Interpolated resultant fuzzy based fused MOD12 (1186*1186) image of d2	89
Fig. 3.21b. Resultant fuzzy based fused AS_MO	89
Fig. 3.21c. Minimum distance classified of the resultant fuzzy based fused AS_MO	90
Fig. 3.22. Fuzzy vs curvelet	90

Fig. 3.23a. Resultant curvelet based fused MOD12 of image d1	92
Fig. 3.23b. Minimum distance classified of the resultant Curvelet based fused MOD12 of image d1	93
Fig. 3.24a. Resultant curvelet based fused AS_MO of image d1	93
Fig. 3.24b. Minimum distance classified of the resultant curvelet based fused AS_MO of image d1	94
Fig. 3.25. AST_avg (fusion coefficients)	94
Fig. 3.26a. AST_avg curvelet based fused with MOD12 of image d1 (i.e., AST_avg_d1)	97
Fig. 3.26b. Minimum distance classified AST_avg_d1	97
Fig. 3.27a. AST_avg curvelet based fused with MOD12 of image d2 (i.e., AST_avg_d2)	98
Fig. 3.27b. Minimum distance classified AST_avg_d2	98
Fig. 3.28a. . Resultant curvelet based MOD12 of image d3	99
Fig. 3.28b. Minimum distance classified MOD12 of image d3	99
Fig. 3.39a. AS_MO of image d3 (i.e., MOD12 of d3 is fused with AST23)	100
Fig. 3.29b. Minimum distance classified AS_MO of image d3	100
Fig. 3.30a. AST_avg curvelet based fused with MOD12 of image d3 (i.e., AST_avg_d3)	101
Fig. 3.30b. Minimum distance classified AST_avg_d3	101
Fig. 3.31. Graph implying the classification accuracy of fused MODIS image with ASTER image and MODIS image with AST_avg (fusion coefficients)	102

Fig. 4.1. Flowchart for the fusion of MODIS(Band 1) on PALSAR images	110
Fig. 4.2. Flowchart for the fusion of MODIS(Band 2) on PALSAR images	110
Fig. 4.3. Flowchart for the fusion of MODIS(Band 1 and Band 2) on PALSAR images	111
Fig. 4.4. Fuzzy Interference System Editor for the fusion of PALSAR and MODIS image	114
Fig. 4.5. Membership Fusion Editor implying the Membership Fusion (MF) for the PALSAR and MODIS image	114
Fig. 4.6. Rule editor for the fusion of PALSAR and MODIS image	115
Fig. 4.7. Flowchart for the fusion of MODIS (Band 1) on PALSAR images	115
Fig. 4.8. Flowchart for the fusion of MODIS (Band 2) on PALSAR images	116
Fig. 4.9. Flowchart for the fusion of MODIS (Band 1 and Band 2) on PALSAR images	116
Fig. 4.10a. PALSAR HH-Pol image	117
Fig. 4.10b. PALSAR HV-Pol image	117
Fig. 4.10c. PALSAR VV-Pol image	118
Fig. 4.11a. MODIS Band 1 image	118
Fig. 4.11b. MODIS Band 2 image	119
Fig. 4.12a. MO1_PA(HH), the resultant fused image of MODIS Band 1 and HH-Pol image fused by curvelet based fusion .	121
Fig. 4.12b. MO1_PA(HV), the resultant fused image of MODIS Band 1	121

and HV–Pol image fused by curvelet based fusion.

Fig. 4.12c. MO1\_PA(VV), the resultant fused image of MODIS Band 1 122  
and VV–Pol image fused by curvelet based fusion.

Fig. 4.13a. MO2\_PA(HH), the resultant fused image of MODIS Band 2 122  
and HH–Pol image fused by curvelet based fusion.

Fig. 4.13b. MO2\_PA(HV), the resultant fused image of MODIS Band 2 123  
and HV–Pol image fused by curvelet based fusion.

Fig. 4.13c. MO2\_PA(VV), the resultant fused image of MODIS Band 2 123  
and VV–Pol image fused by curvelet based fusion.

Fig. 4.14a. MOD12, the resultant fused image of MODIS band 1 and 124  
MODIS band 2 fused by curvelet based fusion.

Fig. 4.14b. MO\_PA(HH), the resultant fused image of MOD12 and HH– 124  
Pol image fused by curvelet based fusion.

Fig. 4.14c. MO\_PA(HV), the resultant fused image of MOD12 and HV– 125  
Pol image fused by curvelet based fusion.

Fig. 4.14d. MO\_PA(VV), the resultant fused image of MOD12 and VV– 125  
Pol image fused by curvelet based fusion.

Fig. 4.15a. MO1\_PA(HH), the resultant fused image of MODIS Band 1 126  
and HH–Pol image fused by fuzzy based fusion.

Fig. 4.15b. MO1\_PA(HV), the resultant fused image of MODIS Band 1 126  
and HV–Pol image fused by fuzzy based fusion.

Fig. 4.15c. MO1\_PA(VV), the resultant fused image of MODIS Band 1 127  
and VV–Pol image fused by fuzzy based fusion.

Fig. 4.16a. MO2\_PA(HH), the resultant fused image of MODIS Band 2 127  
and HH–Pol image fused by fuzzy based fusion.

Fig. 4.16b. MO2\_PA(HV), the resultant fused image of MODIS Band 2 128



and HV–Pol image fused by fuzzy based fusion.

Fig. 4.16c. MO2\_PA(VV), the resultant fused image of MODIS Band 2 128  
and VV–Pol image fused by fuzzy based fusion.

Fig. 4.17a. MOD12, the resultant fused image of MODIS band 1 and 129  
MODIS band 2 fused by fuzzy based fusion.

Fig. 4.17b. MO\_PA(HH), the resultant fused image of MOD12 and HH- 129  
Pol image fused by fuzzy based fusion.

Fig. 4.17c. MO\_PA(HV), the resultant fused image of MOD12 and HV- 130  
Pol image fused by fuzzy based fusion.

Fig. 4.17d. MO\_PA(VV), the resultant fused image of MOD12 and VV- 130  
Pol image fused by fuzzy based fusion.

Fig. 4.18a. Minimum distance classified PALSAR HH-Pol image. 133

Fig. 4.18b. Minimum distance classified PALSAR HV-Pol image. 133

Fig. 4.18c. Minimum distance classified PALSAR VV-Pol image. 134

Fig. 4.19a. Minimum distance classified MODIS band 1. 134

Fig. 4.19b. Minimum distance classified MODIS band 2. 135

Fig. 4.20a. Minimum distance classified of the curvelet based fused 137  
resultant MO1\_PA(HH).

Fig. 4.20b. Minimum distance classified of the curvelet based fused 137  
resultant MO1\_PA(HV).

Fig. 4.20c. Minimum distance classified of the curvelet based fused 138  
resultant MO1\_PA(VV).

Fig. 4.21a. Minimum distance classified of the curvelet based fused 138  
resultant MO2\_PA(HH).

Fig. 4.21b. Minimum distance classified of the curvelet based fused 139

resultant MO2\_PA(HV).

Fig. 4.21c. Minimum distance classified of the curvelet based fused 139  
resultant MO2\_PA(VV).

Fig. 4.22a. Minimum distance classified of the curvelet based fused 140  
resultant MOD12

Fig. 4.22b. Minimum distance classified of the curvelet based fused 140  
resultant MO\_PA(HH).

Fig. 4.22c. Minimum distance classified of the curvelet based fused 141  
resultant MO\_PA(HV).

Fig. 4.22d. Minimum distance classified of the curvelet based fused 141  
resultant MO\_PA(VV).

Fig. 4.23a. Minimum distance classified of the fuzzy based fused 145  
resultant MO1\_PA(HH).

Fig. 4.23b. Minimum distance classified of the fuzzy based fused 145  
resultant MO1\_PA(HV).

Fig. 4.23c. Minimum distance classified of the fuzzy based fused 146  
resultant MO1\_PA(VV).

Fig. 4.24a. Minimum distance classified of the fuzzy based fused 146  
resultant MO2\_PA(HH).

Fig. 4.24b. Minimum distance classified of the fuzzy based fused 147  
resultant MO2\_PA(HV).

Fig. 4.24c. Minimum distance classified of the fuzzy based fused 147  
resultant MO2\_PA(VV).

Fig. 4.25a. Minimum distance classified of the fuzzy based fused 148  
resultant MOD12

Fig. 4.25b. Minimum distance classified of the fuzzy based fused 148

resultant MO\_PA(HH).

Fig. 4.25c. Minimum distance classified of the fuzzy based fused 149  
resultant MO\_PA(HV).

Fig. 4.25d. Minimum distance classified of the fuzzy based fused 149  
resultant MO\_PA(VV).

Fig 5.1a. Spectral response of hotspot and non-hotspot regions in the 161  
MODIS band 1(d1).

Fig 5.1b. Spectral response of hotspot and non-hotspot regions in the 161  
MODIS band 2 (d1).

Fig 5.2a. Spectral response of hotspot and non-hotspot regions in the 162  
LISS band 2 (L1).

Fig 5.2b. Spectral response of hotspot and non-hotspot regions in the 162  
LISS band 3 (L1).

Fig. 5.3. Spectral response of hotspot and non-hotspot regions in the 163  
MODIS NDVI (d1)

Fig 5.4. Proposed Methodology 165

Fig. 5.5. BDA flowgraph. 167

Fig. 5.6. Binary Division Algorithm 167

Fig. 5.7a. MODIS Band 1 of the month of February (d1) 174

Fig. 5.7b. MODIS Band 2 of the month of February (d1) 174

Fig. 5.8a. MODIS Band 1 of the month of November (d2) 175

Fig. 5.8b. MODIS Band 2 of the month of November (d2) 175

Fig. 5.9a. LISS band 2 (L1) 176

Fig. 5.9b. LISS band 3 (L1) 176

Fig. 5.10a. MODIS NDVI for the month of February (MODIS_ndvi_feb)	177
Fig. 5.10b. MODIS NDVI for the month of November (MODIS_ndvi_nov)	177
Fig. 5.11. LISS NDVI (LISS_ndvi)	178
Fig. 5.12. Hotspot and non-hotspot regions classified for the month of February 2004	180
Fig. 5.13. Hotspot and non-hotspot regions classified for the month of November 2004	180
Fig. 5.14a. MODIS most confident fire of February 2004(d3) of MOD14A2	181
Fig. 5.14b. MODIS most confident fire of November 2004 (d4) of MOD14A2	181
Fig. 6.1a. Simple cosine curve representative of the first harmonic	189
Fig. 6.1b. Curves for harmonic terms 1, 2, and 3	189
Fig. 6.1c. Curve produced by addition of curves in (6.1b)	189
Fig. 6.2a. Flow graph for NDVI harmonic analysis	190
Fig. 6.2b. Flow graph for NDWI harmonic analysis	191
Fig 6.3a. Subset raw MODIS Band 1 image of MOD09A1.A2001057.h24v06.005.2006365121813.hdf	193
Fig 6.3b. Subset raw MODIS Band 2 image of MOD09A1.A2001057.h24v06.005.2006365121813.hdf	193
Fig 6.3c. Subset raw MODIS Band 7 image of MOD09A1.A2001057.h24v06.005.2006365121813.hdf	194
Fig 6.3d. NDVI of fig 6.3a and 6.3b	194

Fig 6.3e. NDWI of fig 6.3b and 6.3c	195
Fig 6.4 NDVI Additive term( $A_0$ ) of the year 2008	195
Fig 6.5 NDWI Additive term( $A_0$ ) of the year 2008	196
Fig 6.6 NDVI Amplitudes ( $A_1$ ) of the year 2008	196
Fig 6.7 NDWI Amplitudes ( $A_1$ ) of the year 2008	197
Fig 6.8 NDVI and NDWI Additive term( $A_0$ ) with respect to Agricultural (NDVI <sub>R_</sub> $A_0$ ) and Water (NDWI <sub>R_</sub> $A_0$ ) ROIs	199
Fig 6.9 NDVI (NDVI <sub>A_</sub> $A_0$ ), NDWI (NDWI <sub>A_</sub> $A_0$ ) Additive term( $A_0$ )	199
Fig 6.10 NDVI and NDWI Amplitudes term( $A_1$ ) with respect to Agricultural (NDVI <sub>R_</sub> $A_1$ ) and Water (NDWI <sub>R_</sub> $A_1$ ) ROIs	200
Fig 6.11 NDVI (NDVI <sub>A_</sub> $A_1$ ), NDWI (NDWI <sub>A_</sub> $A_1$ ) Amplitudes term( $A_1$ )	200

# List of Tables

Table 1.1. MODIS band details	17
Table 1.2. ASTER band details	18
Table 1.3. LISS-III band details	21
Table 3.1. Image sets details for the fusion of Optical (MODIS and ASTER) images	51
Table 3.2. Classification Accuracy of MODIS and ASTER Images	76
Table 3.3. Classification Accuracy of fusion of MODIS (d2) and ASTER (as1) through curvelet transform	76
Table 3.4. Classification Accuracy of fusion of MODIS (d2) and ASTER (as1) through fuzzy transform	86
Table 3.5. Classification Accuracy of fusion of MODIS image d1 and ASTER through curvelet transform	95
Table 3.6. Classification Accuracy of fusion of MODIS image d3 and ASTER through curvelet transform	96
Table 3.7. Classification Accuracy	96
Table 3.8. Quality assessment indicators for fused image with respect to MOD12	102

Table 4.1. Classification Accuracy	132
Table 4.2. Classification Accuracy for curvelet based fusion	142
Table 4.3. Classification Accuracy for fuzzy based fusion	144
Table 4.4. Quality Assessment Indicators between MODIS Band 1 and resultant curvelet based fusion of PALSAR Bands with MODIS Band 1	151
Table 4.5. Quality Assessment Indicators between MODIS Band 2 and resultant curvelet based fusion of PALSAR Bands with MODIS Band 2	152
Table 4.6. Quality Assessment Indicators between MOD12 and resultant curvelet based fusion of PALSAR Bands with MOD12	152
Table 4.7. Quality Assessment Indicators between MODIS Band 1 and resultant fuzzy based fusion of PALSAR Bands with MODIS Band 1	152
Table 4.8. Quality Assessment Indicators between MODIS Band 2 and resultant fuzzy based fusion of PALSAR Bands with MODIS Band 2	152
Table 4.9. Quality Assessment Indicators between MOD12 and resultant fuzzy based fusion of PALSAR Bands with MOD12	152
Table 5.1. Latitude and longitude of important hotspots in Jharia coalfield	160
Table 5.2. Data details	160
Table 6.1. Data sets details	185

# Acronyms

ALOS:	Advanced Land Observing Satellite
ASAR:	Advanced Synthetic Aperture Radar
ASTER:	Advanced Spaceborne Thermal Emission and Reflection Radiometer
ATSR:	Along Track Scanning Radiometer
ATWT:	Atrous Wavelet
AWLP:	Proportional Additive Wavelet
AVHRR:	Advanced High Resolution Radiometer
BCCL:	Bharat Coking Coal Limited
BDA:	Binary Division Clustering Algorithm
BDC:	Binary Division Clustering
CIMFR:	Central Institute of Mining and Fuel Research
CORR:	Correlation coefficient
DF:	Data Fusion
DI:	Deviation Index
ENVISAT:	Environmental Satellite



ERS:	European Remote Sensing Satellite
ERGAS:	Relative Dimensionless Global Error
ERSDAC:	Earth Remote sensing Data Analysis Center
FBS:	Fine-beam Single
FBD:	Fine-beam dual
FIS:	Fuzzy Inference Systems
GCP:	Ground Control point
GIMMS:	Global Inventory Modeling and Mapping Studies
GOES:	Geostationary Operational Environmental Satellite
GPS:	Global Positioning System
H:	Entropy
HDA:	Hotspot detection accuracy
HH:	Transmitted horizontal polarization and received also in horizontal polarization
HV:	Transmitted horizontal polarization and received vertical polarization
IFQI:	Image Fusion Quality Index
IGSS:	Intragroup sum of squares
IHS:	Intensity Hue Saturation
IRT:	Inverse ridgelet transforms
IRS:	Indian Remote Sensing Satellite
ISODATA:	Iterative Self-Organizing Data Analysis Techniques
ISRO:	Indian Space Research Organization
JAXA:	Japan Aerospace Exploration Agency

LISS:	Linear Imaging Self-Scanner
MAE:	Mean Absolute Error
MBE:	Mean Bias Error
MF:	Membership Function
MODIS:	Moderate Resolution Imaging Spectroradiometer
MS:	Multi-Spectral
MSE:	Mean Square Error
NDVI:	Normalized Difference Vegetation Index
NDWI:	Normalized Difference Water Index
NIR:	Near Infrared
NOAA:	National Oceanic and Atmospheric Administration
Landsat:	Land Satellite
PALSAR:	Phased Array Type L-band SAR
PAN:	Panchromatic
PCA:	Principal Component Analysis
PLR:	Polarimetric
PPI:	Pixel Purity Index
PSNR:	Peak signal to noise ratio
RMD:	Relative Difference of Means
RMSE:	Root Mean Square Error
ROI:	Region of Interest
RVD:	Relative Variation Difference

SAR:	Synthetic Aperture Radar
SAM:	Spectral Angle Mapper
SD:	Standard Deviation
SDI:	Spectral Distortion Index
SPOT:	Système Pour l'Observation de la Terre (French remote sensing satellite)
SSE:	Sum Squared Error
SWIR:	Short Wave Infrared
TIR:	Thermal Infrared
TM:	Thematic Mapper
UQI:	Universal Image Quality Index
VH:	Transmitted vertical polarization and received horizontal polarization
VNIR:	Visible near infrared region
VV:	Transmitted vertical polarization and received vertical polarization
WB:	ScanSAR
WD:	Warping Degree
WGSS	within-group sum of squares

# Chapter 1

## Introduction

---

Since, the launch of the first Earth resource satellite, i.e., Landsat-1 in 1972, satellite image processing has become an increasingly important tool for the inventory, monitoring, management of earth resources and many other applications (Draeger et al. 1997). The increasing availability of information products generated from satellite images has added greatly to our ability to understand the patterns and dynamics of the earth resource systems at all scales of inquiry (Lambin et al. 2001, Goldewijk and Ramankutty 2004).

The applications of satellite imagery are very diverse and also most of the image sensors are designed for specific purposes; therefore, for some applications they are incomplete while for some others are redundant or complementary. For example the information contained in multispectral datasets provide a valuable basis for environmental studies while the low spatial resolution characteristics of these datasets reduce their performances in many applications. Data Fusion (DF) is a formal framework in which the means and tools for the alliance of data originating from different sources are summarized. It aims at obtaining information of enhanced quality where the exact definition of the term “quality” will depend upon the application of fused datasets (Wald 1999). The satellite instruments provide a huge number of diverse datasets. Therefore, it is important to use these dataset properly by which its application avenue can be extended. Nowadays scientist are paying special

attention for MODIS because its temporal as well as spectral capability. Therefore, in this thesis, our main concern is concentrated towards enhancing the use of MODIS image which is moderate or low resolution images. Therefore fusion of high resolution satellite image may enhance MODIS capability. For this purpose, we have tested to fuse higher resolution ASTER (Advanced Spaceborne Thermal Emission and Reflection Radiometer), LISS (Linear Imaging Self-Scanner) and PALSAR (Phased Array Type L-band SAR) with the MODIS image. The developed methodologies are multi-sensor frameworks of data fusion using two modalities of datasets: Multispectral (MS) and Synthetic Aperture Radar (SAR). Due to the nature of satellite imagery, it could be denoted that diverse physical properties of materials are measured by different sensors from different points of view. For instance ASTER images produce data at higher spatial resolution while they suffer from the lack of high temporal resolution and on the contrary MODIS sensors are providing images with lower spatial resolution but they have the advantages of higher temporal resolution. Similarly, the PALSAR provide information that is complementary to that of MODIS like its penetration capability is more than MODIS. In such circumstances, multi-sensor image fusion to make beneficiary from all available datasets is supposed to be an effective paradigm for increasing the usability of satellite imagery.

Data fusion is useful for several purposes such as land surface objects and phenomena detection, recognition, identification, tracking, classification and many other applications. These objectives maybe encountered in many fields of study like remote sensing, defense systems, robotics, medicine, space, environmental, urban, agricultural studies (Pohl and Van Genderen, 1998). Data fusion has been used in many aspects of satellite image analysis: multi sensor fusion (Pohl and Van Genderen, 1998); image processing and analysis (Mascle et al. 1998); classification (Chen et al. 2005a); image sharpen (Chavez et al. 1991); improve geometric corrections (Strobl et al. 1990); provide stereo-viewing capabilities for stereophotogrammetry (Bloom et al. 1988); land mapping applications (Wald et al. 1997); enhance certain features not visible in either of the single data alone (Leckie, 1990); complement datasets for improving classification accuracy (Schistad-Solberg et al. 1994); etc. Single data sources usually offer limited information due to their limited maneuver abilities in the

data collection. The ideal of data fusion is getting the highest potential of the fused images; the highest potential can be defined as any properties of dataset.

The applications of data fusion for civil purposes have a long history as the availability of the remotely sensed data. The reality of satellite imagery is the robustness for some applications and shortage in some others. For example hyperspectral imagers like EO-1/Hyperion have good spectral presentation but suffering from low spatial resolution and on the contrary the Quickbird / panchromatic satellite imagery suffering from the lack of high spectral resolution. For this reason, In any case of application if the different characteristics of images like high spectral and high spatial resolutions are simultaneously needed, data fusion is an alternate procedure.

The increasing human-based pressures that are the main causes to the environmental changes during last two centuries have introduced a couple of new needs for knowing and understanding of environmental phenomena (Parrt et al. 2003). The principal aspects of environmental investigations like biodiversity loss, atmospheric pollution, desertification, fire burning, land use changes, sustainable development, climate changes and many others. Rainfall estimation (Antonio Turiel et al. 2005, Jacopo et al. 2007 , Varma et al. 2003, Varma and Liu 2004, Varma and Liu 2006, Varma et al. 2006) is one of the application of environmental phenomena through satellite images. Thereby, satellite images have also been used extensively by several researchers for weather analysis (Galletti et al. 2005, Galletti et al. 2007, Galletti et al. 2008a, Galletti et al. 2008b, Grazzini et al. 2002, Grazzini et al. 2003) and also the overview of oceans by satellite images was carried by several researchers (Pandey and Hariharan 1984, Kumar et al. 1999, Lohani et al. 2004, Luis and Pandey 2005, Pandey et al. 1986, Pandey and Kakar 1982, Lohani and Mason 2005, Gohil et al. 1994). Overview of satellite images with respect to geological applications are presented in Nagarajan and Venkataraman 1988, Madhavan et al. 1997, Venkataraman et al. 2000. Recent advances in satellite images have expanded opportunities to characterize the seasonal and interannual dynamics of natural and managed Land use/ land cover communities. Studies have shown that the temporal domain of multispectral data frequently provides more information about land cover and land use than the spatial, spectral, or radiometric domains (Briggs and Nellis

1991, Kremer and Running 1993, Eastman and Fulk 1993, Samson 1993, Reed et al. 1994). As an important agent of climate change and major disturbance to ecosystems, sub-surface fire (hotspot) is drawing increased attention from both scientists and the general public alike. Satellite images play an important role in obtaining quick and complete information on the occurrence and development of sub-surface fires (Li et al. 2001). Huang 2005, states that approximately 320 remotely sensed sensors are available for studying the Earth including land, ocean, atmosphere, etc. This high number of sensors will provide a tremendous volume of data; the combination of them in a proper way will cause a lot of advantages. Of course they will include some few disadvantages as well. The high dimensionality of multi-sensor datasets will introduce a more complete view of the environmental phenomena. For example Haack and Bechdol 2000, offered a good insight in the multi-sensor image fusion. Some very useful recipes in the environmental applications of data fusion are given by Simone et al. 2002 and Kalluri et al. 2003.

Desertification as the process of land degradation in arid, semi-arid and dry environments could be caused by climatic variations and human activities. With reference to this fact that desertification is one of the most pressing environmental issues affecting human life, therefore studying this phenomenon on local, regional and global scales is one of the most important aspects for environmental studies (Collado et al. 2002). The fusion of remotely sensed data providing a framework that we can extend the obtained results of field investigations to higher levels of regional and probably global scales. The fused data has enough spatial information needed for local scale analysis of the relationships between climate change, land degradation and desertification processes. Too many fusion procedures for combining the remotely sensed and the field collected data have been developed that mostly are in multitemporal data combination. This multi-temporality characteristic of satellite image is more useful than other aspects like multi-resolution, multi-frequency, etc for the monitoring desertification procedures. (Verbyla 1995, Tucker et al. 1994). Another aspect of data fusion is return to the vegetation monitoring in the dry environments that is very crucial. Sellers 1989 and Bannari et al. 1995, studied these phenomena using the combination red and infrared reflectance of vegetation land covers.

The application of data fusion in agricultural is a very broad field of study. Ostermeier et al. 2007, developed a data fusion methodology that high resolution SPOT (Système Pour l'Observation de la Terre)-XS is used to provide spatial information at the parcels level and very low spatial resolution NOAA-AVHRR which outputs images of large areas every day. Both datasets were fused to make the possibility to daily estimate reflectance of main cultivations at the parcels level.

Due to the high number of sensors most of the natural disastrous phenomena like flood can be monitored and probably predict. In this outlook, the costal planning also is considered by the researchers (Lucas et al. 2002, Madhavan et al. 1999 and Sanjeevi 1996). Singh et al. 2007, introduced a multi sensor remote sensing image fusion procedure after the Sumatra tsunami and earthquake of 26 December 2004. In this work multi-sensors datasets were analyzed to study the changes in ocean, land, meteorological and atmospheric parameters. Based on the prior and after phenomenon comparison using a data fusion framework it has been cleared that changes in ocean, atmospheric and meteorological parameters, as useful signs for disaster monitoring, are detectable. Another example is about the Geometric modeling of buildings in urban areas, which helps to detecting and interpreting their changes to obtain fast damage information after earthquakes. This information is valuable inputs for a disaster management system. For instance in Voegtle and Steinle 2005, airborne laser scanning data fusion was carried out for earthquake studies. Flood forecasting and monitoring is of very important in evaluation all aspects of damages from the human and non-human viewpoints. Almost due to the large size, remoteness and dynamic nature of the flood phenomenon, this procedure can mostly be carried out using remote sensing. As an example Temimi et al. 2005, introduced an approach that a combination of microwave data and discharge observations presents a high potential in flood and discharge prediction. Toyra et al. 2002, evaluated the usefulness of radar and visible/infrared satellite imagery for mapping the extent of flooded wetland areas. In their work the extent of standing water in the Peace–Athabasca Delta, Canada, during May 1996 and May 1998 was mapped using RADARSAT and SPOT imagery. The RADARSAT scenes and the SPOT scenes separately and in a combination mode of the two were classified. Using the fused datasets the results of classification has increased about 15%. Therefore they showed that the information from radar and



visible/infrared satellite imagery are complementary and that flood mapping can be achieved with higher accuracy if the two image types are used in combination.

Data fusion application in urban areas is one of the most practical and common cases. The fusion of spatial and spectral complementary datasets can facilitate human-based visual and machine-based automatic image interpretation. Numerous studies have demonstrated the usefulness of fused data for the study of urban areas (Couloigner et al. 1998). As the urban objects are always heterogeneous thus the high-quality of the fused spectral content of the MS images, when increasing the spatial resolution, allows further processing such as classification and image interpretation.

As the accessibility to military literature was limited, this paragraph is mostly based on Hall and Llinas 1997. One of the earliest and more common usages of data fusion is in military and defense operation systems. The main stresses on military applications, from the imagery viewpoint, are developing the techniques that can give out some information about the characterization and identification of dynamic entities such as emitters, platforms, weapons, high-level inferences for enemy situation and military units. For the mentioned cases the data fusion has an important role for combination different sensors like radar, sonar, electronic intelligence, observation of communications traffic, infrared, passive electronic support measures, infrared identification friend for sensors, electro-optic image sensors and visual (human) sightings and Synthetic Aperture Radar (SAR) observations. One of the main properties for this kind of data fusion is the dynamic nature of targets and fast changes and also the need for rapid decision making and potentially large combinations of target sensor pairings.

Battlefield intelligence, surveillance and target acquisition systems attempt to detect and identify potential ground targets. Examples include the location of land mines and automatic target recognition. Sensors include airborne surveillance via SAR, passive electronic support measures, photo reconnaissance, ground-based acoustic sensors, remotely piloted vehicles, electro-optic sensors and infrared sensors. The mentioned high numbers of data resources and the complexity of defense systems make high needs for using very sophisticated data fusion techniques. Multi-sensor

measurement which independently senses the physical properties of an object can be fused in a data fusion framework. In such circumstances the weaknesses of one sensor are alleviated by strengths of others. Consequently, a good performance of the complementary sensors is available for a wide variety of landmine detections. Sanjeev et al. 1999, introduced a framework for multi-sensor data fusion for the detection and identification of antipersonnel mines. They have developed hybrid architecture in order to integrate nonhomogeneous and dissimilar datasets from various sensors.

The goal of image fusion techniques is to combine and preserve all of the important visual information present in multiple input images in a single output image. In many applications, the quality of the fused images is of fundamental importance and is usually assessed by visual analysis subjective to the interpreter. In research publications, the widely used image fusion quality evaluation approaches can be included into two main categories:

- **Qualitative approaches**, which involve visual comparison of the colour between original MS and fused images, and the spatial detail between original high resolution and fused images.
- **Quantitative approaches**, which involve a set of pre-defined quality indicators for measuring the spectral and spatial similarities between the fused image and the original MS and/or high resolution images.

Because qualitative approaches—visual evaluations—may contain subjective factor and may be influenced by personal preference, quantitative approaches are often required to prove the correctness of the visual evaluation.

For quantitative evaluation, a variety of fusion quality assessment methods have been introduced by different authors. The quality indexes/indicators introduced include, for example, Standard Deviation (SD), Mean Absolute Error (MAE), Root Mean Square Error (RMSE), Sum Squared Error (SSE) based Index, Agreement Coefficient based on Sum Squared Error (SSE), Mean Square Error (MSE) and Root Mean Square Error, Information Entropy, Spatial Distortion Index, Mean Bias Error (MBE), Bias Index, Correlation Coefficient (CORR), Warping Degree (WD), Spectral Distortion Index (SDI), Image Fusion Quality Index (IFQI), Spectral Angle Mapper

(SAM), Relative Dimensionless Global Error (ERGAS), Q Quality Index and Q4 Quality Index (Wald et al. 1997, Buntikov and Bretschneider 2000, Li 2000, Wang and Bovik 2002, Piella and Heijmans 2003, Wang et al. 2004, Alparone et al. 2004, Willmott and Matsuura 2005, Wang et al. 2005 and Ji and Gallo 2006).

## **1.1. Motivation**

Earth observation is currently developing more rapidly than ever before. During the last decade the number of satellites has been growing steadily, and the coverage of the Earth in space, time, and the electromagnetic spectrum is increasing correspondingly fast and these earth observation satellites provide data at different spatial and spectral resolutions also. The increasing availability of information products generated from satellite images are extending the ability to understand the patterns and dynamics of the earth resource systems at all scales of inquiry. In which one of the most important application is the generation of land cover classification from satellite images for understanding the actual status of various land cover classes. The accuracy in classifying a scene can be increased by using images from several sensors operating at different wavelengths of the electromagnetic spectrum. The interaction between the electromagnetic radiation and the earth's surface is characterized by certain properties at different frequencies of electromagnetic energy. Sensors with different wavelengths provide complementary information about the surface. The merging of multi-source data can create a more consistent interpretation of the scene compared to an interpretation based on data from a single sensor. This development opens up for a potential significant change in the approach of analysis of earth observation data. Traditionally, analysis of such data has been by means of analysis of a single satellite image. The emerging exceptionally good coverage in space, time, and the spectrum opens for analysis of time series of data, combining different sensor types, combining imagery of different scales, and better integration with ancillary data and models. Thus, data fusion to combine data from several sources is becoming increasingly more important in many remote-sensing applications (Simone et al., 2002).

Satellite remote sensors can be divided into two major types of imaging systems: optical(optical and thermal) and radar imaging systems. Optical imaging

systems operate in the visible and IR (Infra Red) regions of the spectrum. Their operational use is weather dependent, since clouds are not transparent at visible/IR wavelengths (0.4-14  $\mu\text{m}$ ). Some of the satellite images working on optical and thermal images can be listed as AVHRR (Advanced Very High Resolution Radiometer), MODIS (Moderate Resolution Imaging Spectroradiometer), Landsat (land Satellite), LISS (Linear Imaging Self Scanner) and SPOT (Satellite Pour L'Observation de la Terra or earth observing satellites). On the other hand, radar imaging systems works in microwave region (1 GHz to 30 GHz), and are very much atmosphere and weather independent. ERS (European remote sensing satellite), JERS (Japanese earth remote sensing), ENVISAT (Environmental Satellite Advanced Synthetic Aperture Radar), RADARSAT (Radar Satellite), and PALSAR (Phased Array L-band Synthetic Aperture Radar) are some of the radar satellite sensors available for various applications.

These two sensor types are very different in terms of the wavelength of their electromagnetic energy, sensor structure, and image product (Brisco and Brown, 1995, Harris et al., 1990, Raghavawamy et al., 1996, Welch and Ehlers, 1988). In regions with frequent cloud cover the number of suitable optical image is often limited. The all weather capability is one major advantage of radar systems with respect to optical systems. Furthermore, radar sensors provide information that is complementary to that of visible to infrared imagery. In the optical range of the electromagnetic spectrum the information depends on reflective and emissive characteristics of the Earth's surface, whereas the radar system generates image data by recording microwave signals that are backscattered towards the receiver. Because of the differences in their data acquisition processes, image data obtained using two sensor systems often provide dissimilar and unique information over the same surface target (John and Xiuping, 2005).

A particularly important application of satellite image processing is the generation of landuse/ land-cover maps from satellite imagery (Anderson et al. 1976) Compared to more traditional mapping approaches such as terrestrial survey and basic aerial photo interpretation, land-use mapping using satellite imagery has the advantages of low cost, large area coverage, repetitivity, and computitivity. Consequently, land-use information products obtained from satellite imagery such as

land-use maps, data and GIS layers have become an essential tool in many operational programs involving land resource management. Eventually maximum high resolution satellite image is expensive with some extent. Therefore, it is need of current research to explore some techniques by which utilization of freely available satellite image may be enhanced. The increasing availability of satellite imagery with significantly improved spectral and spatial resolution has offered greater potential for more detailed land cover classification. The availability of moderate resolution imaging Spectroradiometer (MODIS) image with greatly improved spectral, spatial, geometric, and radiometric attributes provides significant new opportunities and challenges for remote sensing-based land cover classification (Friedl et al. 2002). But, only the MODIS image has limited capability for classification of land cover. One of the main reasons for this is its spatial resolution. To increase the utilization of MODIS image for land cover classification, there is a need to explore the possibility to use of some other techniques like a fusion. Spectral and spatial resolutions of images are very important parameters for fusion. Spatial resolution is also important as spectral resolution because classification accuracy quite dependent upon it. Therefore, there is a need to fuse a high resolution image with low or moderate resolution image to increase the classification accuracy. Another important aspect is for development of a land cover monitoring system, where every time one needs a time series image of both sensor (i.e., low resolution and high resolution images). The high resolution image is not freely and easily available. Therefore, there is a need to develop such a methodology where high resolution image uses in fusion can be minimized for time series analysis.

Subsurface coal fires are a serious and widespread problem in coal producing countries such as India, China, Indonesia and other developing countries. India accounts for the world's greatest concentration of coal fires which cause several devastating environmental effects. Jharia Coal Field (JCF) in Jharkhand (India) alone contains nearly half of subsurface mine fires (hotspots) in Indian coalfields. Most of the fires take place due to spontaneous heating of coal and cause a local rise in the surface temperature, which depends on various mining, geological and coal factors. Mine fires apart from economic aspects give rise to devastating environmental effects. Therefore attention is required in this direction for mapping, monitoring and detecting

these hotspots with less cumbersome and more economic way. Satellite images can be one of the best solutions for these kinds of problems which offer a cost effective and time saving technology for mapping various geo-environmental features.

The MODIS instrument has been designed to provide improved monitoring for land, ocean, and atmosphere research. The design of the land imaging component combines characteristics of the Advanced Very High Resolution Radiometer (AVHRR) and the Landsat Thematic Mapper, adding spectral bands in the middle and long-wave infrared (IR) and providing a spatial resolution of 250 m, 500 m, and 1 km. Spectral channels for improved atmospheric and cloud characterization have been included to permit both the removal of atmospheric effects on surface observations and the provision of atmospheric measurements (Barnes et al. 1998). The MODIS instruments, which began collecting image in February 2000 (Terra) and June 2002 (Aqua), are being used to generate oceanic, atmospheric, and terrestrial data products (Kaufman et al. 1998, Masuoka et al. 1998).

Hence the aforementioned paragraphs initiated us for the critical analysis to be performed for following tasks:

- To maximize the use of low resolution i.e., Moderate Resolution Imaging Spectroradiometer (MODIS) image, which are freely available for various application like land cover classification, harmonic analysis and hotspot and non-hotspot classification.
- There is a lack of fusion coefficients by which each time of fusion computational, complexity should be minimized
- Less attention has been given to fuse the MODIS with fully polarimetric data
- MODIS has very high temporal resolution which may be useful for developing monitoring system using different indexes.
- Minimum application of soft-classification tools like fuzzy based approach for fusion

## 1.2. Problem Statement

The present dissertation work is an effort to maximize the use of MODIS images for the land cover classification, an attempt has been carried out to enhance the classification accuracy of MODIS image by fusion technique. For this purpose MODIS image is fused with high resolution optical image like ASTER as well as full polarimetric RADAR image like PALSAR. It is also attempted to use the MODIS image for classifying the hotspot and non-hotspot region, where MODIS image is fused with LISS image. Another landcover application to develop monitoring system for various land cover, vegetation and water, and to quantify the changes in different years. Therefore it is concluded and the following major goals have been defined for the present research work:

- Analysis of Fusion of Optical (MODIS and ASTER) images for land cover classification
- Study of Fusion of Optical (MODIS) and Radar (PALSAR) images for land cover classification
- Application of MODIS and LISS-III images for hotspot and non-hotspot regions classification.
- Multitemporal Harmonic Analysis of MODIS indexes

## 1.3. Study Area

In this thesis, three study areas have been selected for the application of various tasks undertaken. Roorkee region of India is chosen for landcover classification and Jharia region of India is chosen for the single class classification i.e., hotspot and non-hotspot regions classification and for the multitemporal harmonic analysis, western Utter Pradesh and part of Uttarakhand, India is considered.

### **1.3.1. Study area for fusion techniques**

Solani river catchment around Roorkee town in the state of Uttarakhand, India has been selected as the test site for landcover classification (fig. 1.1). The area is relatively flat with a maximum slope of 4° (elevations ranging from 245.5 m to 289.9 m above the sea level). The region extends from 29°77' N and 30° N, and its longitude ranges from 77°83'E and 78°01' E. The study area basically consists of agricultural, water and urban classes. The central region of the test site is covered by Upper Ganga canal which is the main source of water in the area. Urban class is mostly comprised of residential areas.

### **1.3.2. Study area for hotspot and non-hotspot classification**

The study was carried out in the Jharia Coal field in Jharkhand, state of India, bounded by latitudes 23° 22' 22" N and 23° 51' 18"N and longitudes 86° 5' 57"E and 86° 45' 50" E. Jharia Coalfield is located about 250 km NW of Kolkata and about 1150 km SE of Delhi (fig. 1.2). The Jharia coal field is sickle shaped in plane. The maximum length is about 38 km from E to W and 19 km from N to S. The area covered by the coal belt is approximately 450 km<sup>2</sup>.

### **1.3.3. Study area for multitemporal harmonic analysis**

The study for the multitemporal harmonic analysis was carried at western Uttar Pradesh and part of Uttarakhand, India as the study area that lies between latitudes 29° 8' 15" N and 29° 45' 30" N and longitudes 77°29' 3" E and 77° 58' 48" E and is depicted in fig. 1.3. Western Uttar Pradesh and part of Uttaranchal has a blend of urban, water and agriculture bodies.



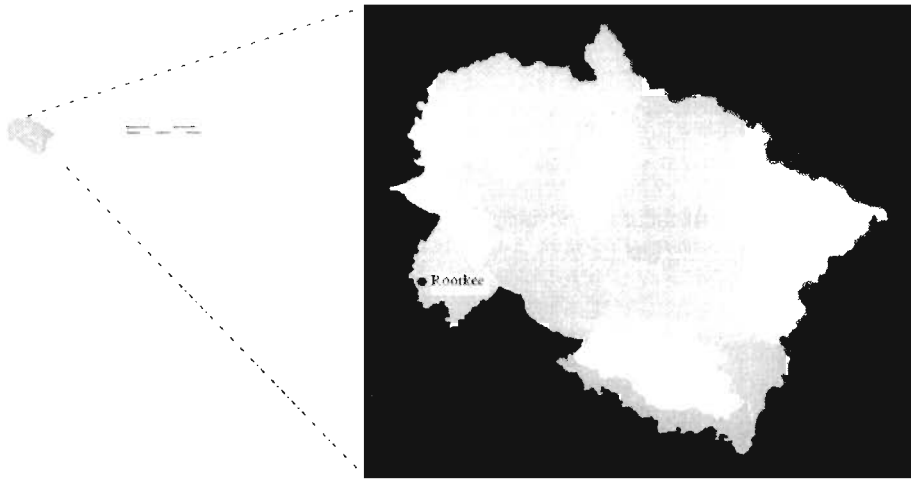


**Fig. 1.1.** Location of the study area (Roorkee region) for fusion techniques, in the Haridwar district, India.

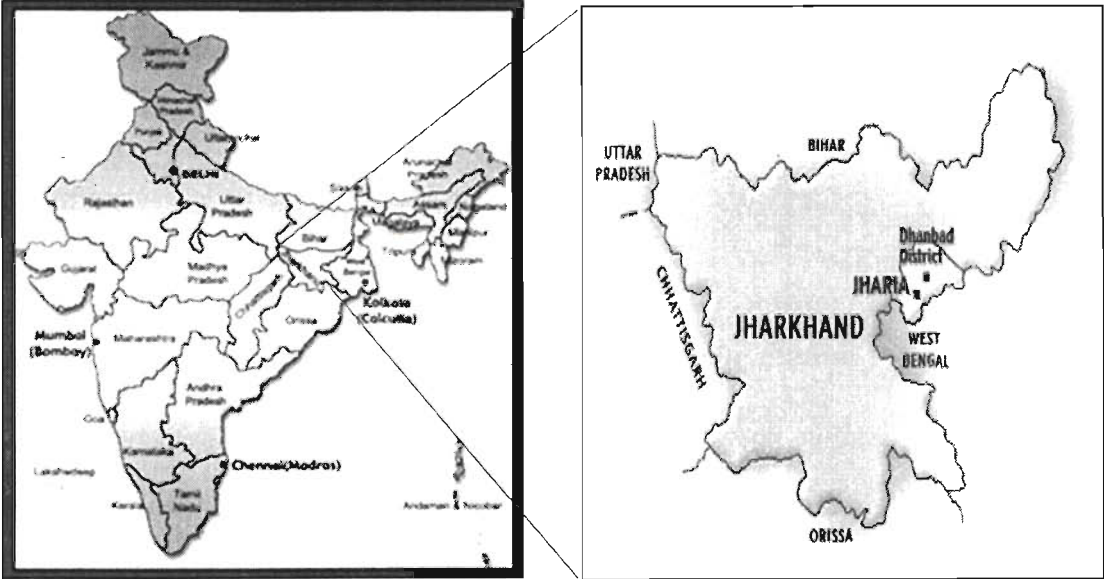


**Fig. 1.2.** Location of the study area (Jharia region) for hotspot and non-hotspot regions classification, in the Dhanbad district, Jharkhand state, India.

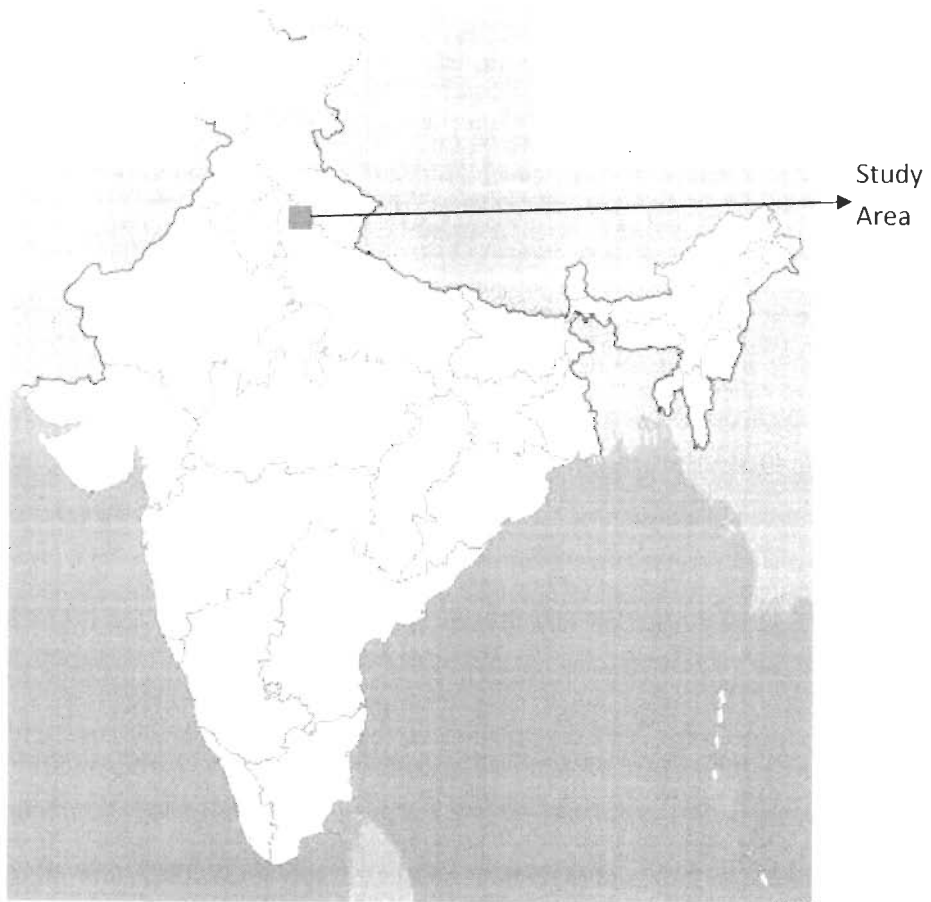


**Fig. 1.3.** Location of the study area for multitemporal harmonic analysis is indicated by the box in the top of the map

## **1.4. Satellite Data**

### **1.4.1. Satellite data used for land cover classification**

Three Satellite images are used for land cover classification purpose, and are listed as following

- MODIS
- ASTER
- PALSAR

### 1.4.1a. MODIS

Identical MODIS instruments are mounted on the Terra (formerly known as EOS AM-1) and Aqua (EOS PM-1) platforms, launched on December 18th, 1999 and on May 4th, 2002, respectively (Barnes et al. 1998, Barnes et al. 2003). While Terra operates on a descending orbit with a mean equatorial crossing time at 10:30 am (Justice et al. 2002), Aqua runs in an ascending mode and crosses the equator at 1:30 pm (Parkinson 2003). Although the orbit characteristics of both platforms are rather similar this study will focus on Terra, because of a longer availability of the data. Terra operates at an altitude of 705 km in a circular, sun-synchronous, near-polar orbit with  $98.1^\circ$  inclination (Justice et al. 2002, King et al. 2004). The repeat cycle at the same ground track is 16 days, with an orbit period of 98.9 minutes. Besides MODIS, four other instruments are onboard Terra including ASTER, CERES, MISR, and MOPITT. The scan angle of  $55^\circ$  yields a swath width of 2,340 km. Due to its wide swath the instrument provides daily global coverage above  $30^\circ$  latitude and two day coverage in the tropics.

MODIS has 36 bands and whose details have been listed in the table 1.1. The radiometric resolution of all bands is 12 bit. In this thesis, we have used MODIS band 1 and MODIS band 2 for the fusion techniques. The MODIS Band 1 is of spatial resolution 250m and bandwidth 620 - 670 nm, and Band 2, of spatial resolution of 250m and bandwidth 842 - 876nm. These bands are considered, as these bands have special features to identify the agriculture and other land covers.

The MODIS product considered for the fusion techniques is MODIS/Terra Surface Reflectance 8-Day L3 Global 250m SIN Grid (MOD09Q1). The MODIS Surface Reflectance products provide an estimate of the surface spectral reflectance as it would be measured at ground level in the absence of atmospheric scattering or absorption. MOD09Q1 provides Bands 1 and Band 2 in an 8-day gridded level-3 product in the Sinusoidal projection. Each MOD09Q1 pixel contains the best possible L2G (local to Global) observation during an 8-day period as selected on the basis of high observation coverage, low view angle, the absence of clouds or cloud shadow, and aerosol loading. Version-5 MODIS/Terra Surface Reflectance products are Validated Stage 2, meaning that accuracy has been assessed over a widely distributed

set of locations and time periods via several ground-truth and validation efforts. Therefore it is assumed that the product is geometrically and atmospheric corrected (www1 2008).

**Table 1.1. MODIS Band Details**

<b>Band</b>	<b>Wavelength (<math>\mu\text{m}</math>)</b>	<b>Resolution (m)</b>	<b>Band</b>	<b>Wavelength (<math>\mu\text{m}</math>)</b>	<b>Resolution (m)</b>
1	620 - 670	250	19	915 - 965	1000
2	841 - 876	250	20	3.660 - 3.840	1000
3	459 - 479	500	21	3.929 - 3.989	1000
4	545 - 565	500	22	3.929 - 3.989	1000
5	1230 - 1250	500	23	4.020 - 4.080	1000
6	1628 - 1652	500	24	4.433 - 4.498	1000
7	2105 - 2155	500	25	4.482 - 4.549	1000
8	405 - 420	1000	26	1.360 - 1.390	1000
9	438 - 448	1000	27	6.535 - 6.895	1000
10	483 - 493	1000	28	7.175 - 7.475	1000
11	526 - 536	1000	29	8.400 - 8.700	1000
12	546 - 556	1000	30	9.580 - 9.880	1000
13	662 - 672	1000	31	10.780 - 11.280	1000
14	673 - 683	1000	32	11.770 - 12.270	1000
15	743 - 753	1000	33	13.185 - 13.485	1000
16	862 - 877	1000	34	13.485 - 13.785	1000
17	890 - 920	1000	35	13.785 - 14.085	1000
18	931 - 941	1000	36	14.085 - 14.385	1000

### 1.4.1b. ASTER

The TERRA platform was launched in December 1999 with a total of five sensors as part of NASA's Earth Science Enterprise, USA. A key element of the Earth Observation System (EOS) mission is to develop synergy between the multiple sensors to improve understanding of land, ocean, and atmospheric processes. One of the Terra sensors, the Advanced Spaceborne Thermal Emission and Reflection Radiometer (ASTER), colloquially referred to as the zoom lens of the Terra platform since it has the highest spatial resolution of any sensor on the platform. ASTER has a 60-km swath width with 14 total bands in the visible and near infrared (VNIR), shortwave infrared (SWIR), and thermal infrared (TIR) (Yamaguchi et al. 1999) and the details of the bands have been listed in the table 1.2. The sensor also includes a backward pointing (3B) VNIR band that is used for stereo imaging to produce digital elevation models. The VNIR and SWIR sensors are pushbroom systems, whereas the TIR uses a spinning scan mirror for crosstrack coverage.

The Level 1B of ASTER image is considered and georeferenced. ASTER band 2 and ASTER band 3 are used for the fusion techniques. ASTER Band 2 is having a resolution of 15m and with bandwidth 630 to 690 nm and ASTER Band 3 is of resolution of 15m and bandwidth 760 – 860 nm. These bands are considered, as these bands have special features to identify the agriculture and other land covers.

**Table 1.2. ASTER Band Details**

Band	Label	Wavelength ( $\mu\text{m}$ )	Resolut ion(m)	Band	Label	Wavelength ( $\mu\text{m}$ )	Resolut ion(m)
1	VNIR	0.52 - 0.60	15	8	SWIR	2.295 - 2.365	30
2	VNIR	0.63 - 0.69	15	9	SWIR	2.36 - 2.43	30
3	VNIR	0.76 - 0.86	15	10	TIR	8.125 - 8.475	90
3B	VNIR	0.76 - 0.86	15	11	TIR	8.475 - 8.825	90
4	SWIR	1.60 - 1.70	30	12	TIR	8.925 - 9.275	90
5	SWIR	2.145 - 2.185	30	13	TIR	10.25 - 10.95	90
6	SWIR	2.185 - 2.225	30	14	TIR	10.95 - 11.65	90
7	SWIR	2.235 - 2.285	30				

### 1.4.1c. PALSAR

For the landcover classification, PALSAR product L1.0 CEOS which is acquired on 6th April 2009 is used. The PALSAR image has the incidence angle of 21.50 and approximately 30m resolution in full polarimetric mode has been used. PALSAR ground data system has been established in ERSDAC (Earth remote sensing data analysis center) since 1999 and was compiled at JAXA (Japan Aerospace Exploration agency). The development of PALSAR was a joint project between JAXA and the JAROS (Japan resources observation system organization). It was launched on 24th January 2006 as the first fully polarimetric SAR on the platform of ALOS (Advanced land observing satellite), a Japanese Earth Observation satellite, developed by JAXA. ALOS follows the Japanese Earth observing satellite-1(JERS-1) and the Advanced Earth observing satellite (ADEOS) and utilizes advanced land-observing technology. PALSAR is an active microwave sensor using L-band with a centre frequency of 1.27 GHz (wavelength  $\lambda=23.6$  cm) to achieve cloud free and all time land observation. In its experimental mode, it images a swath 20-65 km wide in full (quad) polarizations, with a resolution of 24-89 m. PALSAR image are provided by both JAXA and ERSDAC.

PALSAR can operate in several modes: the fine-beam single (FBS) polarization mode (HH (Transmitted horizontal polarization and received also in horizontal polarization)), fine-beam dual (FBD) polarization mode (HH / HV (Transmitted horizontal polarization and received vertical polarization) or VV (Transmitted vertical polarization and received vertical polarization)/VH (Transmitted vertical polarization and received horizontal polarization)), polarimetric (PLR) mode (HH/HV/VH/VV), and ScanSAR (WB) mode (HH/VV) (Rosenqvist et al., 2007). Depending on the different modes, PALSAR acquires image at spatial resolutions ranging from 6.25 to 50 m, with swath widths from 70 to 360 km, and off-nadir looking angles from 9.70 to 50.80 ((Rosenqvist et al., 2007). In overlapping areas, PALSAR could reach a temporal resolution higher than the satellite orbit repeat cycle of 46 days. These features, coupled with the regional observation strategy, make PALSAR imagery very attractive for spatially and temporally consistent monitoring system. The PALSAR, which is side-looking Radar will have distortion depends on

terrain. As the Roorkee region is coming under the flat region so the distortion due to terrain will not affect the PALSAR image.

#### **1.4.2. Satellite data for hotspot and non-hotspot region classification**

MODIS and LISS-III Satellite image of the year 2004 are used for single class classification. In 1.4.1a the MODIS satellite image is discussed. The MODIS product considered is MODIS/Terra Surface Reflectance 8-Day L3 Global 250m SIN Grid (MOD09Q1), and MODIS/Terra Thermal Anomalies/Fire 8-Day L3 Global 1km SIN Grid product (MOD14A2). The MOD14A2, is a gridded 1km composite of the most confident fire pixel detected in each grid cell over an eight-day interval, and which is used for comparison purpose. MODIS Band 1 and Band 2 are considered from the MOD09Q1 product and MOD14A2 product is used for most confident fire.

The Linear Imaging Self-Scanner (LISS) -III is a multispectral sensor in the Indian Remote Sensing Satellite (IRS) - P6. IRS - P6 is also called ResourceSat-1. The IRS-P6 is a three axis body-stabilized satellite. Launched on October 17, 2003, it has an operational life of five years, with a near-polar sunsynchronous orbit at a mean altitude of 817 km. The IRS-P6 payload consists of three sensors: LISS-III, AWiFS, and a highresolution multispectral sensor (LISS-IV). All three sensors work on the “pushbroom scanning” concept, using linear arrays of detectors. In this mode of operation, each line of image data is electronically scanned, and contiguous lines are imaged by the forward motion of the satellite (Gyanesh et al. 2008).

The LISS-III is operating in four spectral bands, three in the visible and near-infrared (VNIR) bands and one in the short-wavelength infrared (SWIR) region with 23.5-m spatial resolution and a ground swath of 141 km, and the details of the bands have been listed in the table 1.3. The P6 LISS-III sensor is a nadir-looking sensor with a 24-day revisit cycle. LISS Band 2 and LISS Band 3 are considered. The band 2 has the spectral bandwidth of 620 - 680 nm, and band 3 has the spectral bandwidth of 770 - 860 nm.

**Table 1.3.** LISS-III Band Details

<b>Band</b>	<b>Label</b>	<b>Wavelength (<math>\mu\text{m}</math>)</b>	<b>Resolution (m)</b>
1	VNIR	0.52 - 0.59	23.5
2	VNIR	0.62 - 0.68	23.5
3	VNIR	0.76 - 0.86	23.5
4	SWIR	1.55 - 1.70	23.5

It is supposed that there may be less or no vegetation near by the hotspots. So characterizing the vegetation in hotspots and non-hotspots region may be able to classify hotspot and non-hotspot region in satellite image.

### **1.4.3. Satellite data for multitemporal harmonic analysis**

Only MODIS Satellite image is used for multitemporal harmonic analysis. In 1.4.1a the MODIS satellite image is discussed. The MODIS product considered is MODIS/Terra Surface Reflectance 8-Day L3 Global 500m SIN Grid (MOD09A1). MOD09A1 provides Bands 1–7 at 500-meter resolution in an 8-day gridded level-3 product in the sinusoidal projection. Each MOD09A1 pixel contains the best possible L2G observation during an 8-day period as selected on the basis of high observation coverage, low view angle, the absence of clouds or cloud shadow, and aerosol loading. Science Data Sets provided for this product include reflectance values for Bands 1–7, quality assessment, and the day of the year for the pixel along with solar, view, and zenith angles. MODIS band 1, band 2 and band 7 is considered. The band 7 is having spectral resolution of 2105-2155 nm and the spectral resolution of the band 1 and band 2 is indicated in the section 1.4.1.

## **1.5. Framework of the Research**

The emphasis of this thesis is to enhance the use of low resolution satellite images. The tasks as mentioned in the subsection 1.1 are framed as following.



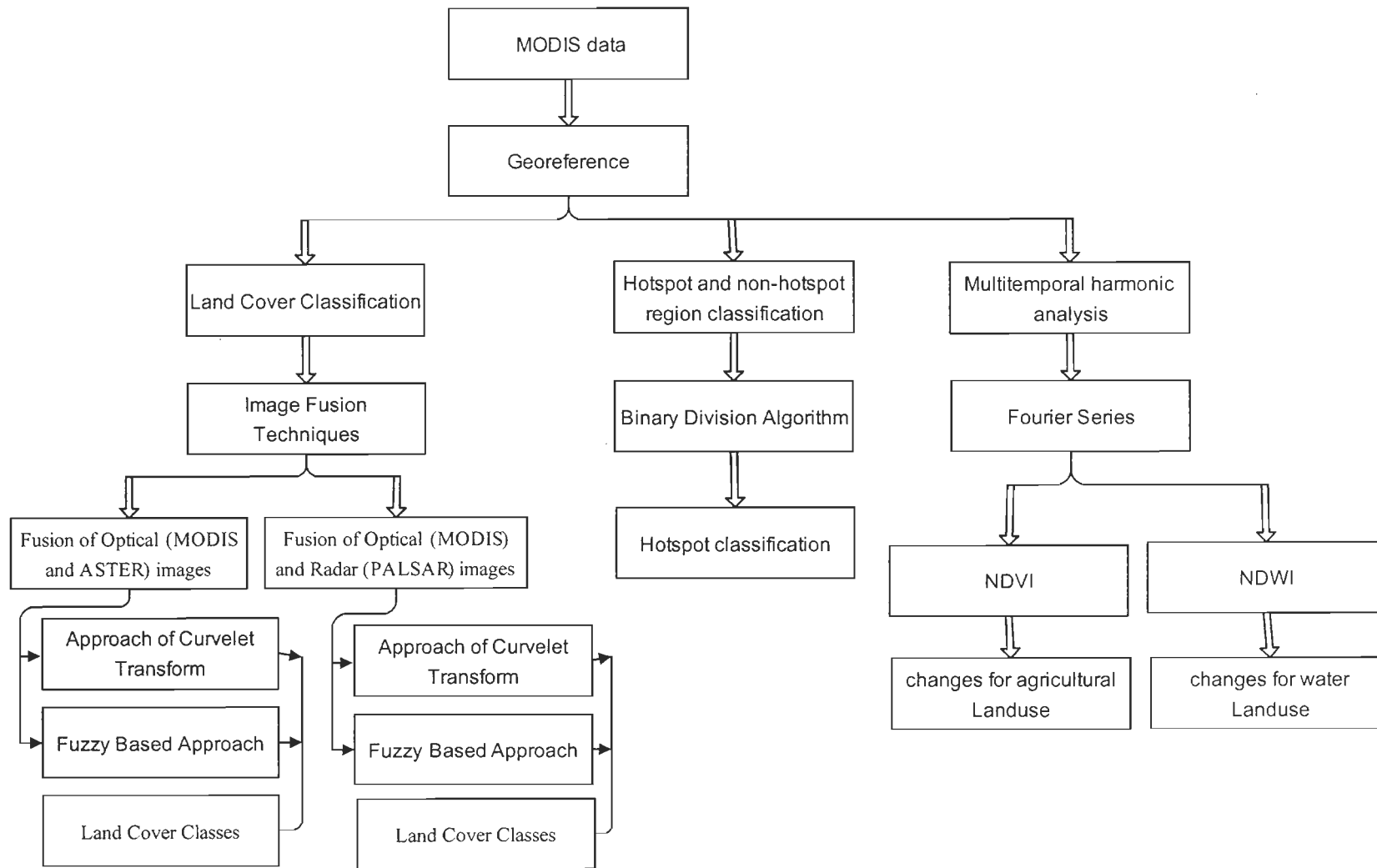


Fig. 1.4. Framework of the proposed research work

Framework of the research is shown in the form of a flow chart (fig. 1.4) which specifies the essential steps followed in the assessment of the aforementioned tasks of the subsection 1.1. The satellite images, whose details are previously discussed in the section 1.3 are considered. The flowchart clearly points the three main application of this thesis, which are land cover classification, hotspot and non-hotspot regions classification and multitemporal harmonic analysis. Different study area are selected for different task, for eq. Roorkee region is considered for major land cover classification using fusion techniques. The fusion of low and high resolution optical images such as MODIS and ASTER is carried out. Whereas it is also attempted to fuse optical image (MODIS) with radar image (PALSAR). MODIS image has a moderate resolution whereas ASTER (15m – 90m) and PALSAR (30m) have quite good resolution. The classification accuracy for fused images are computed as well as Quality index of fused images are checked. Jharia region is selected for classifying hotspot and non-hotspot region for which fusion of MODIS and LISS-III image is carried out. The temporal change analysis of NDVI and NDWI is carried out of the area of Uttarakhand and western Uttar Pradesh region of India and different bands of MODIS images are used. The land cover classification is accomplished by the fusion techniques, and thereby the approach of curvelet transform in one hand and in another hand the fuzzy based approach is considered and thereby land cover classes are obtained. Binary Division Algorithm is considered for the achievement of the hotspot and non-hotspot regions classification task. And Fourier Series is applied on NDVI and NDWI for the attainment of the Multitemporal harmonic analysis task, and thereby the changes of agricultural and water landuse are analyzed.

## **1.6. Organization of the Thesis**

The layout of the structure of the thesis is as follows: Chapter 2 gives a brief review of literature of the commonly used fusion techniques, followed by a brief review of literature of the fusion of optical images in one hand and in another hand the fusion of optical and radar images. This chapter also assembles the pertinent literature on the hotspot and non-hotspot classification and multitemporal harmonic analysis.

In Chapter 3, a methodology for the enhancement of overall classification accuracy of major landcover for the MODIS image is presented. It is extended to obtain fusion coefficient which reduces the computation complexity of fusion of images. The high resolution image (i.e., ASTER) is fused with moderate resolution image (i.e., MODIS) and the resultant fused image is analyzed in the viewpoint of land cover classification. The curvelet and fuzzy based fusion are used and compared. The new fusion coefficient is validated with respect to classification accuracy and quality assessment indicators (Correlation Coefficient, Root Mean squared error, Relative Mean Difference, Relative Variation Difference, Deviation Index, Peak signal-to-noise ratio (PSNR), Universal Image Quality Index). Chapter 4 is concerned with the curvelet transform and fuzzy based fusion is applied for various combination of PALSAR with MODIS image to assess the quality of fused image. The fused images are quantitatively analyzed by quality assessment indicators (Correlation Coefficient, Root Mean squared error, Relative Mean Difference, Relative Variation Difference, Deviation Index, Peak signal-to-noise ratio (PSNR), Universal Image Quality Index) in one hand and in another hand land cover classification accuracy is also compared with fused and without fused image. Chapter 5 is the occupied with the single class classification of hotspot and non-hotspot regions through binary division algorithm applied on LISS-III and MODIS image for the Jharia coalfield in Jharkhand, India. Chapter 6 is dealt with the study of multitemporal changes in the agriculture and water land use/land cover in western Uttar Pradesh and part of Uttarakhand of India from the year 2001 to 2008 through the use of NDVI and NDWI of MODIS images by the harmonic analysis. Such type of study is very helpful in near future to optimize the use of MODIS image in one hand and in another hand to observe the changes of vegetation and water during the particular month of every year for the selected area of interest.

Chapter 7 summarizes the obtained results and draws conclusion from a concise and comparative analysis. Thereupon, utilizing the findings it provides perspectives for future investigations.

## Chapter 2

# Brief Literature Survey

---

### 2.1. Introduction

Earth observation satellites provide data at different spatial, temporal and spectral resolutions. For the full exploitation of increasingly sophisticated multisource data advanced analytical or numerical data fusion techniques are being developed (Pohl and van Genderen 1998, Shen 1990). For many applications the information provided by individual sensors is incomplete, inconsistent, or imprecise (Varshney 1997, hall and Llinas 1997, Pohl and van Genderen 1998). Additional sources may provide complementary data, and fusion of different information can produce a better understanding of the observed site, by decreasing the uncertainty related to the single sources (Farina et al. 1996, Clément et al. 1993). Fused images may enhance the interpretation capabilities. The images used for fusion have different temporal and spatial resolution. Therefore, the fused image provides a more complete view of the observed objects. It is one of the main aims of image fusion to integrate different data in order to obtain more information that can be derived from each of the single sensor data alone. Various application of fusion in which classification accuracy is also one of the application. In this viewpoint, for classification task, the goal of fused data from different sensors is to reduce the classification error rate or increase the overall classification accuracy obtained by single source classification (Anne et al. 1994).

The fusion of these disparate data contributes to the increasing classification accuracy (Pohl and Van Genderen, 1998).

Wald (1999) proposed a general definition for data fusion in the context of earth data and is defined in the chapter 1. This definition equally emphasizes the tools for combining the data and the quality of the result. Merging, combination, data assimilation, and integration are other terms that are used to refer to data fusion. Image fusion is a sub domain of data fusion referring to the fusion of two or more images. Pohl and Van Genderen (1998) defined image fusion as: "the combination of two or more different images to form a new image by using a certain algorithm"

It can refer to any fusion process involving images from sensors of same satellites or different satellites having different spatial, spectral and temporal characteristics (e.g. SPOT (Système Pour l'Observation de la Terre (French remote sensing satellite)) PAN (Panchromatic) with Landsat (Land Satellite) TM (Thematic mapper), SPOT PAN and SPOT XS, ENVISAT (Environmental Satellite) ASAR (Advanced Synthetic Aperture Radar) with SPOT Vegetation).

## **2.2. Fusion Processing Levels**

Image fusion is generally performed at three different processing levels according to the stage at which the fusion takes place. Fusion can be either at the pixel, feature or decision level. The following description and illustrations of fusion levels (Shen 1990) are shown in the fig. 2.1 and in the following paragraph, is briefly explained.

Image fusion at pixel level means fusion at the lowest processing level referring to the merging of measured physical parameters. It uses the DN or radiance values of each pixel from different sources in order to derive the useful information. An illustration of the concept of pixel based fusion is visualized in fig. 2.1. It uses raster data that is at least co-registered but most commonly geocoded.

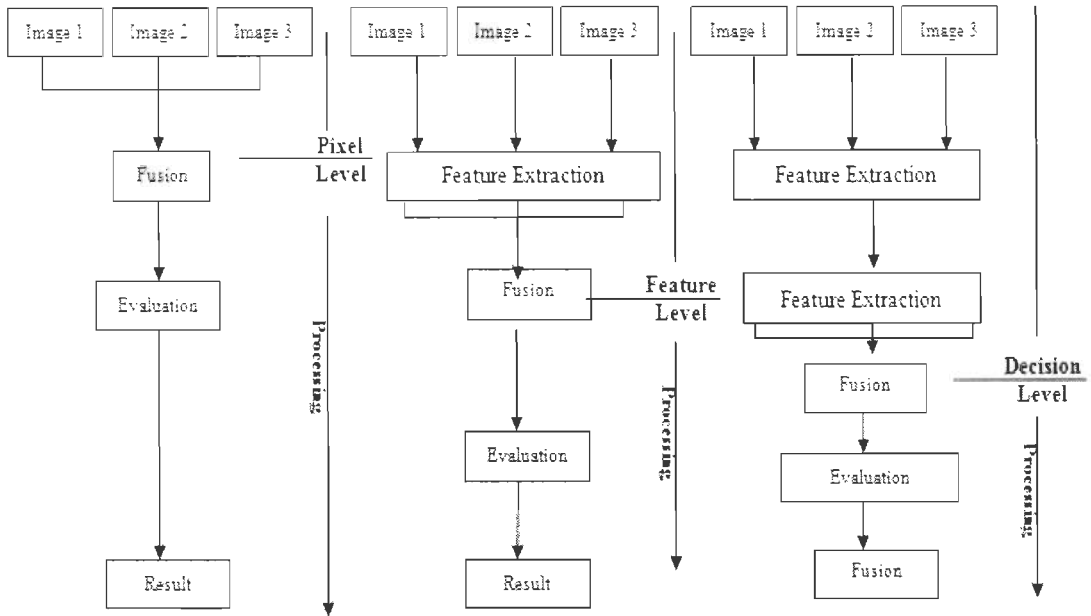


**Fig. 2.1.** Processing levels of image fusion (Shen 1990)

Fusion at feature level requires the extraction of objects recognized in the various data sources. Features correspond to characteristics extracted from the initial images which are depending on their environment such as extent, shape and neighbourhood. These similar objects from multiple sources are assigned to each other and then fused for further assessment using statistical approaches.

Decision- or interpretation level fusion represents a method that uses value-added data where the input images are processed individually for information extraction. The obtained information is then combined applying decision rules to reinforce common interpretation and resolve differences and furnishes a better understanding of the observed objects (Shen 1990).

Compared to feature or decision-level fusion, pixel level fusion can preserve more original information (Mitianoudis and Stathaki 2007). Feature-level algorithms typically fuse the source images using their various feature properties, such as regions

or boundaries (Piella, 2003). Thus, this kind of methods is usually robust to noise and misregistration. Decision level fusion algorithms combine image descriptions directly, for example, in the form of relational graphs (Williams et al. 1999). But the decision-level fusion methods are very much application dependent (Goshtasby and Nikolov 2007). Hence in this thesis, we only focus on the pixel-level image fusion technique.

## **2.3. Commonly used Fusion Techniques**

In this thesis, the referred word 'fusion' implies the pixel based fusion. Many image fusion methods have been proposed and developed, a detailed review on this issue was given by Pohl and Van Genderen, 1998. In which some methods, like intensity–hue–saturation (IHS), Brovey transform and principal component analysis, are elucidated in the following paragraphs.

### **2.3.1. Intensity Hue Saturation (IHS)**

IHS is a color space, hue is defined as the predominant wavelength of a color, saturation is defined as the purity or total amount of white light of a color and intensity relates to the total amount of light that reaches the eye (Harris et al., 1990). IHS largely explains the popularity of perceptual color space and overcomes the commonly used RGB color space drawbacks, which does not relate intuitively to the attribute of human color perception (Schetselaar, 2001).

Because of its simplicity and high sharpening ability, many applications using IHS transform in image fusion have been reported. Harris et al. 1990, described how to use IHS in integrating Radar with diverse types of image such as Landsat TM, airborne geophysical and thematic data. The use of IHS transform was also demonstrated for displaying the results of quantitative analyses such as change detection studies and comparison between images characterized by different sensing parameters. Chavez et al. 1991, compared IHS with PCA and other fusion methods by merging the information contents of the Landsat TM and SPOT panchromatic image. It was claimed that IHS method distorts the spectral characteristics of the data the

most. Grasso 1993, used the IHS transform for geologic mapping because the IHS transform could allow diverse forms of spectral and spatial landscape information to be combined into a single data set for analysis. Schetselarr 2001, modified the IHS transform and presented a new method, that preserves the spectral balance of the multispectral image data and modulates the IHS coordinate uniformly. The method takes the limits in the representation of color of the display device into account, which aids in compromising the amount and spatial distribution of the over-range pixels against contrast in intensity and saturation. There are other improvements about IHS such as using wavelet (Nuñez et al., 1999; King and Wang, 2001; Chibani and Houacine 2003, Bin et al. 2010). The main advantage of the IHS method is that it separates the spatial information as an intensity (I) component from the spectral information represented by the hue (H) and saturation (S) components. The spatial information can be manipulated independently to enhance the image while maintaining the overall colour balance of the original images (Carper et al. 1990). However, there exists color distortion in the fused image because IHS assumes that the intensity is formed by even contribution from the RGB bands; thus, all the details contained in the high resolution image are directly integrated into the intensity component. The color distortion will become worse when the panchromatic/ higher resolution image has a low correlation with the multispectral image. Another limitation of IHS is that it only processes three multispectral bands.

### **2.3.2. Brovey Transform**

The Brovey Transform is based on multiplying ratio images with the panchromatic/ higher resolution image. It was developed to visually increase contrast in the low and high ends of an image's histogram. The Brovey Transform is good for producing RGB images with a higher degree of contrast in the low and high ends of the image histogram and for producing visually appealing images. However, it should not be used if it is important to preserve the original scene radiometry (Erdas, 2002), because the Brovey Transform may cause color distortion if the spectral range of the intensity replacement image is different from the spectral range covered by the three bands used in the multispectral image. This limitation cannot be avoided in color composites



that do not use consecutive spectral bands. The spectral distortion incurred by this fusion technique is difficult to control and quantify, because the high resolution panchromatic image and the multispectral image are from different sensors or different dates (Alparone et al., 2004b).

### **2.3.3. Principal Component Analysis (PCA)**

The Principal Component Analysis (PCA) is a statistical technique that transforms a multivariate dataset of correlated variables into a dataset of new uncorrelated linear combinations of the original variables (Pohl and Van Genderen, 1998). PCA is widely used in signal processing, statistics, and many other applications.

Chavez et al. 1991, used principal component analysis to merge six Landsat TM bands and SPOT data and concluded that the color distortion in the fusion result of PCA method is less than the result acquired by IHS fusion method. Teggi et al. 2003, presented a fusion method which combines the principal component analysis and “à trous” wavelet and applied it to a pair of images acquired by Thematic Mapper (TM) and IRS-1C-PAN sensors. González-Audicana et al. 2004, presented a new fusion alternative, which uses the multiresolution wavelet decomposition to extract the details and principal component analysis to inject the spatial detail of the high resolution image into the low resolution multispectral image.

The main advantage of PCA method lies in the unlimited multispectral bands in the fusion process, unlike the IHS method, which uses only three multispectral bands. The PCA also distorts the spectral characteristics of the multispectral image, but distortions were less severe than those in the IHS results because the first component image is more similar to the high resolution than is the intensity image (Chavez et al., 1991). However, the PCA approach is sensitive to the choice of area to be analyzed. The correlation coefficient reflects the tightness of a relation for a homogeneous sample, while shifts in the band values due to markedly different cover types will influence the correlations and particularly the variances (Pohl and Van Genderen, 1998). There are other improvements about PCA such as integrating PCA with high pass filtering (Metwalli et al. 2010)

The above mentioned methods, intensity–hue–saturation (IHS), Brovey transform and principal component analysis provide superior visual high-resolution multispectral fused images, but have a limitation of the need of high-quality spectral information as input, while these methods are useful for visual interpretation. High-quality spectral information is very important for most satellite image applications especially in land cover classification (Liu, 2000). The importance of high-quality synthesis of spectral information is well suited and implemented for land cover classification (Garguet-Duport et al. 1996). More recently, an underlying multiresolution analysis employing the discrete wavelet transform has been used in image fusion. It was found that multisensor image fusion is a tradeoff between the spectral information from a low resolution multi-spectral images and the spatial information from a high resolution multi-spectral images. With the wavelet transform based fusion method, it is easy to control this tradeoff (Gonzalo Pajares and Jesus Manuel de la Cruz, 2004).

#### **2.3.4. Wavelet based fusion techniques**

The wavelet transform is an advanced mathematical tool developed in the field of signal processing. It can decompose a digital image into a set of multi-resolution images accompanied with wavelet coefficients for each resolution level. The wavelet coefficients for each level contain the spatial (detail) differences between two successive resolution levels.

Because the performance of the wavelet based image fusion technique outperforms the traditional image fusion method, it has caught a lot researchers' interest; thus, there are so many publications about this technique which cannot be listed at one time. Some typical wavelet based literature listed as following

Yocky 1995, proposed the two-dimensional discrete wavelet transform to image merging. The wavelet technique was compared with IHS transform by using multispectral and panchromatic/ higher resolution images. The comparison showed that the wavelet technique performs better in combining and preserving spectral-spatial information. Yocky 1996, proposed a new fusion method based on wavelet

transform technique, which is a kind of improvement of the method proposed by him in 1995. The method has been tested by SPOT and Landsat TM. Garguet-Duport et al. 1996, proposed a new method based on wavelet technique to merge a SPOT panchromatic image and its XS multispectral image. The method was compared with IHS and other methods; it has the least spectral characteristic distortion. The distortions are minimal and difficult to detect.

Zhou et al. 1998, presented a multiresolution orthogonal wavelet transform method to merge the SPOT PAN and TM reflective images. Two destination resolution levels, one quarter and one eighth of the original image resolution, were used for decomposition in evaluating the method. Nunez et al. 1999, developed a multiresolution wavelet decomposition image fusion method, which combines a higher resolution panchromatic image and a low-resolution multispectral image by the addition of some wavelet planes of the panchromatic/ higher resolution image to the intensity component of the low-resolution image. The discrete wavelet transform known as “a trous” algorithm, which provides a shift-invariant property that is not available with the orthonormal wavelet system, was used in the wavelet decomposition process. Ranchin and Wald 2000, designed the ARSIS concept based on a multiresolution modeling of the information, to improve the spatial resolution together with a high quality in the spectral content of the synthesized images.

King and Wang 2001, presented a wavelet based fusion method that combines IHS transformation and biorthogonal wavelet decomposition. The Landsat 7 image were used to evaluate the proposed fusion method. Chibani and Houacine 2003, investigated the use of the nonorthogonal (or redundant) wavelet decomposition in image fusion and concluded that this method is better for image fusion than the standard orthogonal wavelet decomposition. Zhu 2010, have presented image fusion based on wavelet and rough set.

### **2.3.5. Fuzzy based fusion techniques**

It's extremely important to explore new techniques for image fusion so as to meet the needs of industry. Fuzzy Logic is one of the approaches, which are finding

applications in object recognition, image analysis, automatic control, intelligent information processing and computer science, etc. Fuzzy approaches are used where there is uncertainty and no mathematical relations are easily available.

In 1965 Lotfi A. Zadeh published the first paper "Fuzzy Sets" as a novel way of characterizing non-probabilistic uncertainties by formally defining multi-valued or fuzzy, set theory. He extended traditional set theory by changing the two-valued indicator function to a multi-valued membership function. Fuzzy set theory (or Fuzzy logic) starts with and builds on a set of user-supplied human language rules. The fuzzy systems convert these rules to mathematical equivalents. This simplifies the job of the system designer and the computer, and results in much more accurate representations of the way systems behave in the real world. The consequences of the theory, however, have not been limited to set theory only. Almost immediately, the connection between fuzzy set theory and a form of logic was recognized, leading to the introduction of fuzzy logic: a logic based on fuzzy set theory. This relation is similar to the relation between the conventional set theory and binary logic.

The Fuzzy Logic approach is being utilized in different disciplines (Meitzler et al. 1996, Labib Arafeh et al. 1999) whereas, presently this approach is used for pixel level image fusion. This approach forms an alternative to a large number of conventional approaches, which are based on a host of empirical relations. Empirical approaches are time consuming and result in a low correlation. Fuzzy logic approach is based on simple rules, which are easy to apply and take less time. This approach is becoming more and more popular as is evidenced by a number of recent papers in this area.

Based on the fuzzy logic of Mamdani model, the medical image fusion algorithm for Infrared and CCD has been discussed (Singh et al. 2004) and CCD/SAR image fusion for navigation/guidance application through the fuzzy logic of Mamdani model was later on discussed (Long Zhao et al. 2005).

## 2.4. Fusion of Optical Images

In optical satellite images, with physical and technological constraints, some satellite sensors supply the spectral bands needed to distinguish features spectrally but not spatially, while other satellite sensors supply the spatial resolution for distinguishing features spatially but not spectrally. For many applications, the combination of image from multiple sensors provides more comprehensive information. Many image fusion methods have been proposed for combining high resolution images with low resolution multispectral images. A detailed review on this issue was given by Pohl and Van Genderen, 1998. The Researchers (Chavez and Bowell 1988, Carper et al. 1990, Edwards and Davis 1994, Schetselaar 1998, Liu 2000, Tu et al. 2001) have used the intensity–hue–saturation (IHS) methods and Brovey transform (BT) has been used by researchers (Gillespie et al. 1987, Zhou et al. 1998), and principal component analysis (PCA) (Zhou et al. 1998, Chavez and Kwarteng 1989). Currently used wavelet-based image fusion methods are mostly based on two computation algorithms: the Mallat algorithm (Zhou et al. 1998, Aiazzi et al. 2002, Mallat 1989, Yocky 1995, Yocky 1996, Ranchin and Wald 2000) and the à trous algorithm (Aiazzi et al. 2002, Shensa 1992, Nuñez et al. 1999, Murtagh and Starck 2000, Ranchin et al. 2003). Shi et al. 2003, used the Mallat algorithm and the  $M$  - band WT for the fusion of SPOT panchromatic and Landsat Thematic Mapper multispectral bands. Hong and Zhang 2003, integrated IHS and wavelet to fuse Quickbird images and IKONOS images, and obtained promising results. Jia and Xiao 2010, have used Contourlet transform for fusing IKONOS PAN image with IKONOS multispectral images.

The results of each implementation of image fusion algorithms are evaluated through a variety of quality indicators, both physical (statistical and similarity) based, which are explained in the chapter 1. Indicators that have previously been used to evaluate fusion results are the mean value and standard deviation (Choi et al. 2003, Shamshad et al. 2004), the mean gradient (Choi et al. 2003), the spectral and simple two-dimensional correlation (Bretschneider and Kao 2000, Sanjeevi et al. 2001, Dehghani 2003, Gungor and Shan 2004, Hong and Zang 2004), the root mean square error (RMSE) (Bretschneider and Kao 2000, Beaulieu et al. 2003), the universal quality index (Aiazzi et al. 2004), the peak signal-to-noise ratio (PSNR) (Li et al. 2004).

## **2.5. Fusion of Optical and Radar Images**

Multisource data fusion is probably the most difficult aspect in the integration of remote sensing image data products. In fact, while fusion is relatively straightforward when using data from the same satellite, the integration of imagery originating from different satellites carrying different sensors, is quite complicated. Various Researchers (Alparone et al. 2004b, Amarsaikhan and Douglas 2004, Hegarat-Mascle et al. 2000, Pal 2007, Yifang et al. 2010, Harish and Singh 2010) have demonstrated the benefit of combining optical and radar image for improved land cover mapping in several studies. With the availability of multifrequency and high-resolution spaceborne radar image, such as provided by the Advanced Land Observation Satellite (ALOS) Phase Array L-type Synthetic Aperture Radar (PALSAR) missions, an increased interest in tools to exploit the full information content of both image types is arising. Some of the researchers have used Polarimetric SAR image for various application like (Danklmayer et al. 2005, Gu et al. 2004, Kamran and Yang 2007, Yang et al. 2006, Yang et al. 2007)

## **2.6. Hotspot and non-Hotspot Classification**

Clustering is the unsupervised classification of patterns (observations, data items, or feature vectors) into groups (clusters). The clustering problem has been addressed in many contexts and by researchers in many disciplines; this reflects its broad appeal and usefulness as one of the steps in exploratory data analysis (Jain et al. 1999). However, clustering is a difficult problem combinatorially, and differences in assumptions and contexts in different communities have made the transfer of useful generic concepts and methodologies slow to occur (Jain et al. 1999). Eventually in this thesis, the clustering is used for one-class clustering or one class classification. This one single class classification, is to classify the hotspot (sub surface fires) and non-hotspot regions.

Several researchers have proposed methods for surface and subsurface fire monitoring based on satellite data acquired by different optical sensors, such as Along

Track Scanning Radiometer (ATSR) (Arino and Rosaz, 1999), LANDSAT (Brustet et al., 1991, Prakash et al., 1997, Prakash and Gupta, 1999, Saraf et al., 1995, Gupta and Prakash, 1998), Geostationary Operational Environmental Satellite (GOES) (Prins and Menzel, 1994), Advanced Very High Resolution Radiometer (AVHRR) aboard the National Oceanic and Atmospheric Administration's (NOAA) polar orbiting satellites (Flannigan and Vonder Haar, 1986, Kennedy et al., 1994, Flasse and Ceccato, 1996, Nakayama et al., 1999, Boles and Verbyla, 2000, Chrysoulakis et al. 2007, Yahia et al. 2007, Gautam et al. 2007a, Gautam et al. 2007b, Gautam et al. 2007c, Gautam et al. 2008a, Gautam et al. 2008b) and MODIS (Li et al., 2004), However, most of the algorithms have been designed for the problem of surface fires, but still uncertainties exist with respect to the subsurface fire problem. In addition, for subsurface fires, researchers have used Landsat TM, NOAA/AVHRR and other high resolution satellite images, and MODIS image is very less used for this purpose. A brief review has been provided below on few existing techniques which have been designed to solve the problem of subsurface fires.

The most frequently used sensor for fire monitoring is the Advanced Very High Resolution Radiometer (AVHRR) on board the National Oceanic Atmospheric Administration (NOAA) satellite series. Several algorithms have been proposed primarily for assessment of biomass burning and forest fire detection using NOAA/AVHRR image (Aguado et al. 2005, Cuomo et al. 2001, Flasse and Ceccato, 1996, Galindo et al. 2003, Giglio et al. 1999, Justice et al. 1996, Justice et al. 1993, Kennedy et al. 1994, Kucera et al. 2005, Li et al. 2001, Nakayama et al. 1999, Pozo et al. 1997, Pu et al. 2004, Gautam et al. 2007a, Gautam et al. 2007b, Gautam et al. 2007c, Gautam et al. 2008a, Gautam et al. 2008b). These algorithms can be classified broadly into two categories, fixed thresholding algorithms (Most of the classical AVHRR fire detection algorithms are based on fixed threshold values (Kennedy et al. 1994, Li et al. 2000, Rauste et al. 1997)). and contextual Algorithms (contextual algorithms were proposed by Lee and Tag 1990, Several authors have proposed this contextual approach (Boles and Verbyla 2000, Eva and Flasse 1996, Flannigan and Vonder Haar 1986, Flasse and Ceccato 1996, Giglio et al. 1999, Lee and Tag 1990, Nakayama et al. 1999). A number of studies have been proposed to detect subsurface fires with Landsat TM image (Chatterjee 2006, Chatterjee et al. 2007, Gupta and

Prakash 1998, Martha et al. 2005, Prakash and Gupta 1998, Prakash and Gupta 1999, Prakash et al. 1997, Prakash et al. 1999, Saraf et al. 1995, Zhang et al. 2004, Zhang et al. 1999). Prakash et al. 1997, proposed a solution to detect surface and subsurface coal fires using Landsat TM image in the Jharia coalfield. They used TM-6 image for subsurface fire detection as the surface temperature above subsurface fire is relatively high. Recently in 2007, Chatterjee et al. have presented a study on coal fire dynamics of Jharia Coalfield during the 1990s. They have used medium resolution satellite thermal IR image such as Landsat-5 TM and Landsat-7 ETM+ image for this purpose. The dynamics of coal fire was studied in terms of changes in spatial extent of fire affected areas and propagation of coal fire. Zhang 1998, showed that the spatial resolution of NOAA-AVHRR image (1km) in general is too low to detect underground coal fires in northwest China. However, with the partial failure of LANDSAT ETM+ in May 2003 (Kuenzer et al. 2008), coal fire research based on Moderate Resolution Imaging Spectroradiometer (MODIS) image is presently a highly required research area and recently very few researchers (Kuenzer et al. 2008, Ressler et al. 2009, Giglio et al. 2009) have used MODIS image for fire class classification.

Researchers have used LISS image for fusion with other optical and radar images for various other applications. Vani et al. 2001, have fused IRS -LISS III and PAN images at varying resolution ratios of the images and Sanjeevi et al. 2001 have also fused IRS -LISS III with PAN image with conventional and wavelet transform techniques, and compared the fused image results. Saraf 1999, also have fused IRS-1C-LISS-III image with PAN image data to improve visual interpretation. Venkataraman et al. 2004, fused IRS LISS-III image and Radarsat-1 SAR image using Bayesian formulation of data fusion to improve the classification accuracy of snow related features in Himalayan region, India. Pal et al. 2007 have fused ERS-2 SAR with IRS-1C LISS III image using Principal Component Analysis fusion technique to generate False Color Composite images, from which corresponding geological maps have been prepared and was used for change detection analysis for geological studies.



## 2.7. Multitemporal Harmonic Analysis of MODIS Indexes

Recent advances in satellite image processing have expanded opportunities to characterize the seasonal and interannual dynamics of natural and managed Land use/ land cover communities. Studies have shown that the temporal domain of multispectral data frequently provides more information about land cover and land use than the spatial, spectral, or radiometric domains (Brims and Nellis 1991, Kremer and Running 1993, Eastman and Fulk 1993, Samson 1993, Reed et al. 1994). Considerable progress has been made by classifying Land use/ land cover patterns at the state (Eve et al. 1997) and national (Craig 2001, Homer et al. 2004, Vogelmann et al. 2001) levels using multispectral, medium resolution image from the Landsat Thematic Mapper (TM) and Enhanced Thematic Mapper (ETM+) as a primary input. Similar advances in Land use/ land cover classification have also been made at national (Loveland et al. 1991, Lu et al. 2003) to global (DeFries et al. 1998, DeFries and Townshend, 1994; Hansen et al. 2000, Loveland and Belward 1997, Loveland et al. 2000) scales using multi-temporal, coarse resolution image (1 and 8 km) from the Advanced Very High Resolution Radiometer (AVHRR). Significant efforts are also devoted to address land cover characterization on a global scale by using ERS scatterometer data. These studies showed that the radar backscattering so was able to describe the vegetation cycle in a semi-arid region and in boreal forests (Schmullius 1997). A few significant studies for distinguishing land surfaces and estimating quantitative parameters with the use of spaceborne microwave radiometers were conducted and this research led to establishing empirical or semi-empirical rules for land surface classification (Judge et al 1996, Judge et al 1997a, Judge et al 1997b, Judge et al 1999, Judge et al 2001).

The development of a regional-scale monitoring procedure is challenging because it requires satellite images that have wide geographic coverage, high temporal resolution, adequate spatial resolution and minimal cost. Satellite images from traditional sources such as Landsat and AVHRR have some of these characteristics and are extensively used. In particular, the AVHRR instruments onboard the NOAA platforms have been widely used for terrestrial earth surface applications. Since 1981

they have been acquiring image in five spectral bands including a red and a near infrared band. The AVHRR instruments are the only long-term data source for environmental studies, for instance, of phenology (de Beurs and Henebry 2004), land-surface variability (Anyamba et al. 2002), and land-cover mapping (Hansen and deFries 2004). AVHRR image are provided as local area coverage (LAC) with 1.1 km resolution and global area coverage (GAC) with 4 km resolution. Frequently, image composites are generated to mitigate errors in the acquisition system, to minimize the influence of atmospheric constituents such as clouds or aerosols, and to eliminate product generation difficulties (Roy et al. 2002). The maximum value compositing (Holben 1986) has been the method of almost universal choice for AVHRR NDVI. Several global datasets have been derived (Townshend 1994), including Pathfinder AVHRR Land (PAL) at 8 km, (James and Kalluri 1994, Maiden and Greco 1994) and global vegetation index (GVI; Goward et al. 1994) with 25 km resolution. An overview of time series and approaches to time-series compilation is provided by Colditz et al. (2008). Recently, successful attempts have been made to generate a long-term data record for numerous products spanning from 1981 into the future. Disadvantages of the AVHRR instruments, such as insufficient cross-calibration, hard to estimate but known to exist deterioration of the charged coupled device, inaccurate geolocation, orbit-drifts, or inadequate and insufficient bands for a full atmospheric correction have been mitigated or eliminated. Having lessons learned from AVHRR and the long-term experiments of MODIS will continue time series for environmental applications of polar-orbiting systems (Townshend and Justice 2002).

In this regard, MODIS offers excellent possibilities, as MODIS 36 spectral bands allow for a full and automated atmospheric correction and detailed cloud masking. The spatial resolution ranges between 250 m and 1 km, and global coverage is achieved within two days. The fully operational product generation and a wide range of value added datasets for terrestrial applications following a standardized production process ensure long-term consistency of global products (Justice et al. 2002a). The MODIS offers an opportunity for detailed, large-area Land use/ land cover characterization by providing global coverage of science quality image with high temporal resolution (1–2 days) and intermediate spatial resolution (Justice and Townshend 2002). The MODIS image sets are available at no cost. The spatial,

spectral, and temporal components of the MODIS are appropriate for monitoring procedure. However, few studies have evaluated the potential of these data for detailed Land use/ land cover characterization (Hansen et al. 2002, Wessels et al. 2004). The researcher (Wessels et al. 2004, Zhan et al. 2002, Friedl et al. 2002) found that general land cover patterns could be successfully mapped with MODIS image. These results suggest that the MODIS image would be suitable for the multitemporal time series analysis.

Several time series have been generated from AVHRR data. Among global records of 1 km (Eidenshink and Faundeen, 1994), 4 km, and 8-km spatial resolution, products such as Pathfinder AVHRR Land (PAL) and Global Inventory Modeling and Mapping Studies (GIMMS) have been used for time-series studies (Townshend 1994). Initially time series have been generated by simply stacking composites. The GIMMS time series corrects for orbit drifts and its processing has been continued until today (Tucker et al. 1979). Often mathematical approaches such as harmonic analysis or filtering functions have been used to smooth the time series with remaining quality limitations. However, these approaches affect both, signal and noise (Jakubauskas et al. 2001, Jönsson and Eklundh 2002). The researchers (Jakubauskas et al. 2001, Jakubauskas et al. 2002, Westra and De 2007, Margarita Huesca et al. 2009) have used harmonic analysis for time series analysis. A automatic methods to generate training examples for the classification of multitemporal images was dealt by researchers (Feitosa et al. 2001, Feitosa et al. 2002, Jonathan et al. 2006, Mota et al. 2004, Mota et al. 2007).

After doing comprehensive study and critical analysis of the existing methodologies, following facts come up as conclusions:

- To maximize the use of low resolution i.e., MODIS which are freely available satellite images for land cover classification, harmonic analysis and hotspot and non-hotspot classification
- Focus on cost-effective solution for monitoring land cover changes i.e., harmonic analysis

- There are limited reported work for fusion of low and high resolution optical images as well as fusion of low resolution optical images with radar images
- Numerous studies have been carried out focusing on surface fire detection but less attention has given to use MODIS band 1 and band 2 for hotspot and non-hotspot region classification.

## Chapter 3

# Analysis of Fusion of Optical (MODIS and ASTER) Images for Land Cover Classification

---

### 3.1. Introduction

Generation of land cover classification from satellite images for understanding the status of various land cover classes is one of the most important application of satellite images. Land cover mapping using satellite imagery has a lot of advantages such as low cost, large area coverage, repetitively, and computability over the traditional mapping approaches like terrestrial survey and basic aerial photo interpretation. The prospect for the use of satellite images in land cover classification is an extremely promising one. The quality of satellite images available for land-use mapping is improving rapidly by development of advanced sensor technology. Particularly noteworthy in this regard is the improved spatial and spectral resolution of the images captured by satellite sensors like MODIS (Moderate Resolution Imaging Spectroradiometer), ASTER (Advanced Spaceborne Thermal Emission and

Reflection Radiometer), Landsat 7 (Land Satellite), and SPOT 5 (Système Pour l'Observation de la Terre (French remote sensing satellite)), LISS (Linear Imaging Self-Scanner), IKONOS, CARTOSAT etc. But, maximum high resolution satellite image is highly priced with some extent. Therefore, it is need of current research to explore some techniques by which utilization of freely available satellite image may be enhanced. The increasing availability of satellite imagery with significantly improved spectral and spatial resolution has offered greater potential for more detailed land cover classification. The availability of moderate resolution imaging Spectroradiometer (MODIS) image with greatly improved spectral, spatial, geometric, and radiometric attributes provides significant new opportunities and challenges for remote sensing-based land cover classification (Friedl et al. 2002). MODIS image has limited capability for classification of land cover. One of the main reasons for this is its spatial resolution. To increase the utilization of MODIS image for land cover classification, there is a need to explore the possibility to use of some other techniques like a fusion. Spectral and spatial resolutions of images are very important parameters for fusion. Spatial resolution is also important as spectral resolution because classification accuracy quite dependent upon it. Therefore, there is a need to fuse a high resolution image with low or moderate resolution image to increase the classification accuracy of low resolution images.

Fusion techniques are being developed for the full exploitation of increasingly sophisticated multisource data (Shen 1990). Fused images may enhance the interpretation capabilities. The images used for fusion have different temporal and spatial resolution. Therefore, the fused image provides a more complete view of the observed objects (Clement et al. 1993, Farina et al. 1996). It is one of the main aims of image fusion to integrate different data in order to obtain more information that can be derived from each of the single sensor data alone. A good example of this is the fusion of images acquired by different sensors having a different spatial resolution and of different spectral resolution. The fusion of these disparate data contributes to the increasing classification accuracy as stated by Pohl and Van Genderen 1998, and a detailed literature survey is carried out at the section 2.3

Many image fusion methods have been proposed and developed, a detailed review on this issue was given by Pohl and Van Genderen 1998. In which some

methods, like intensity–hue–saturation (IHS) (Edwards and Davis 1994 Schetselaar 1998), Brovey transform (Gillespie et al. 1987, Zhou et al. 1998), and principal component analysis (Chavez. P. S. and Kwarteng 1989, Zhou et al. 1998) have been discussed in the previous section 2.3, and these methods provide superior visual high-resolution multispectral fused images, but have a limitation of the need of high-quality spectral information as input, while these methods are useful for visual interpretation. High-quality spectral information is very important for most remote sensing applications especially in land cover classification (Liu 2000). The importance of high-quality synthesis of spectral information is well suited and implemented for land cover classification (Garguet-Duport et al. 1996). More recently, an underlying multiresolution analysis employing the discrete wavelet transform has been used in image fusion, and it is thoroughly discussed in the section 2.3. It was found that multisensor image fusion is a tradeoff between the spectral information from a low resolution multi-spectral images and the spatial information from a high resolution multi-spectral images. With the wavelet transform based fusion method, it is easy to control this tradeoff (Gonzalo Pajares and Jesus Manuel de la Cruz 2004). Ranchin et al. 2003 propose some successful implementation schemes for fusion using the spatial resolution enhancement by injection of structures (ARSIS) concept. Many researchers (Choi 2006, Wang et al. 2005, Alparone et al. 2007, Fasbender et al. 2008 and Thomas et al. 2008) focused on how to retain the spectral characteristics of the multispectral image after fusing with higher resolution images. Recently Ehlers et al. 2010, have fused multispectral remote sensing images with a panchromatic IKONOS image by proportional additive wavelet fusion (AWLP) technique.

The wavelet-transform fusion method provides a high spectral quality in fused satellite images. However, images fused by wavelets have much less spatial information than those fused by the intensity–hue–saturation, Brovey transform, principal component analysis (Yocky 1996, Gonza'les et al. 2004). For Land cover classification, the spatial information of a fused image is just as important as the spectral information. Therefore, there is a need to develop an advanced method of image fusion, so that fused images have the same spectral resolution as low resolution

image (i.e., MODIS image) and the spatial resolution as high resolution image (i.e., ASTER image).

Starck et al. 2002 has used a new transform that is curvelet transform. The curvelet transform is obtained by applying the ridgelet transform (Do and Vetterli 2003) to square blocks of detail frames of undecimated wavelet decomposition. Since the ridgelet transform possesses basis functions matching directional straight lines therefore, the curvelet transform is capable of representing piecewise linear contours on multiple scales through few significant coefficients. This property leads to a better separation between geometric details and background noise, which may be easily reduced by thresholding curvelet coefficients before they are used for fusion (Starck et al. 2002). Therefore, the curvelet transform represents boundaries better than wavelets and may be well suited for extracting detailed spatial information as well as spectral information from an image, and hence, can be very useful for clustering the various targets.

Fuzzy logic is a powerful problem-solving methodology with a myriad of applications in information processing (Zheru 1996). Fuzzy provides a remarkably simple way to draw definite conclusions from vague, ambiguous or imprecise information. In a sense, fuzzy logic resembles human decision making with its ability to work from approximate data and find precise solutions. Hence fuzzy approach is used where there is uncertainty and no mathematical relations are easily available (Zadeh L. A. 1965, proposed fuzzy logic approach). Recently, this approach is being utilized in different disciplines i.e., in the areas of robotics, automobiles and target detection (Meitzler et al. 1996, Bushra et al. 2007, Humayun et al. 2009 and Irina and Martina 2008). Based on the fuzzy logic approach, the medical image fusion algorithm for Infrared and CCD (Charge-Coupled Device) has been discussed by Singh et al. 2004 and Zhao et al. 2005. They have used the fuzzy logic based CCD/SAR image fusion in navigation/guidance application, whereas, in this thesis, this approach is used for pixel level image fusion i.e., for fusing high resolution satellite image with low or moderate resolution satellite image. Fuzzy approach has various advantages in which some of them are as following (Haci 2003):



- Fuzzy systems are able to blend different types of quantitative and qualitative information.
- Because of the ability of fuzzy logic to incorporate qualitative information, fuzzy systems are able to adequately model processes where human reasoning and decision-making are involved.
- Fuzzy systems can be built on top of the experience of experts.

Quality assessment is a key issue in the image fusion process in order to compare the quality of the fused images as well as the performance of the approach used. Attempts to establish a protocol for quality assessment have been published (Wald et al. 1997, Vrabel 2000; Wald and Ranchin 2002). Quality assessment Indicators that are most commonly used to evaluate fusion results are the mean value and standard deviation (Choi et al. 2003), the mean gradient i.e. the contrast between the detailed variation of pattern on the image and the clarity of the image (Choi et al. 2003), the spectral and simple two-dimensional correlation (Bretschneider and Kao 2000, Sanjeevi et al. 2001), the root mean square error (RMSE) (Bretschneider and Kao 2000, Beaulieu et al. 2003), the universal quality index (Aiazzi et al. 2004), and the peak signal-to-noise ratio (PSNR) (Li et al. 2004).

Ever since the first multispectral imagery became available from civilian remote sensing satellites in the early 1970s, considerable effort has been devoted to classification of image data with the aim of producing high-quality thematic maps and establishing accurate inventories of spatial classes. A significant proportion of the papers published over more than three decades in the field of satellite images concern classification in one way or another. Some papers have focused on the improvement of the classification process; others on the use of well-known classification methods in particular types of satellite image application. Classification is regarded as a fundamental process in remote sensing, which lies at the heart of the transformation from satellite image to usable geographic product. At present, there are different classification procedures used for different purposes by various researchers (Ozesmi

and Bauer 2002, Dean and Smith 2003, Liu et al 2002). In this thesis, the minimum distance classifier is used, as minimum distance classifier is more efficient when the number of training samples per class is limited, since it is based only on the use of the class mean vector, whose evaluation is more accurate with few samples (Richards and Jia 2006). Some of the researchers like Akgün et al. 2004, have used minimum distance classifier for classifying Landsat 7 ETM+ satellite image and Chavoshi et al. 2007 had used the Quickbird images for classifying using minimum distance has one of the classifiers

Another important aspect for the development of a land cover monitoring system, where every time one needs a time series data of both sensor (i.e., low resolution and high resolution images). The high resolution image is not freely and easily available. Therefore, there is a need to develop such a methodology where high resolution image uses in fusion can be minimized for time series analysis, as while doing the time-series analysis, where every low resolution image (i.e., MODIS image) may require the same number of high resolution image for fusion in one hand and in another hand every time one has to carry out the complex computation of fusion. So, it is another point of research to develop such a methodology by which use of high spatial resolution image (i.e., ASTER in our case) for fusion for time series analysis may be minimized and also develop some methodology by which computation complexity of fusion may be minimized. So that the freely available image like MODIS use can be enhanced.

Therefore, in this chapter, an attempt has been made to fuse a comparatively high resolution image (i.e., ASTER) with low or moderate resolution image (i.e., MODIS) using curvelet and fuzzy based fusion and the resultant fused image by both methods are analyzed in the viewpoint of land cover classification. The fused image is assessed by the quality indicators in one hand and in another hand we have attempted to explore some possible methodology to obtain some fusion coefficient by which high resolution image (i.e., ASTER image) use may be minimized and reduce the complexity of computation every time while analyzing time series data.

Although ASTER and MODIS are onboard on the same satellite platform and both are complementary in spatial and temporal resolutions. But, MODIS image is

freely and easily available whereas we have to pay for ASTER image. Another important aspect of MODIS image is that it is highly temporal (i.e., image is available twice a day). Therefore, the MODIS image may be very useful for time series analysis (i.e., for monitoring the land cover). The spatial resolution of ASTER image is 15m to 90 m while as the spatial resolution of MODIS image is 250 m to 1000 m.

This chapter is organized as following, image used for the study has been discussed in section 3.2. Section 3.3 deals the theoretical basis where a brief description of the curvelet based fusion and fuzzy based fusion, as well as the brief of Quality Assessment indicators which is used to assess the fused image is presented. Implementation and results of the used approach is given in section 3.4. In the subsequent section, i.e., in section 3.5 analysis of experimental results are carried out and finally this chapter is concluded in the section 3.6.

## **3.2. Data Used/Study Area**

Roorkee Region is located in the Hardwar district of the state of Uttarakhand, India, is depicted with fig. 1.1, and the details concerning the Roorkee region is given in the section 1.3.1. The Level 1B of ASTER image is considered and whose details are given in the section 1.4.1b. The date of acquisition of the aster image is listed in the table 3.1. In this chapter, ASTER Band 2 and ASTER Band 3 is considered. The MODIS image considered is MODIS/Terra Surface Reflectance 8-Day L3 Global 250m SIN Grid (MOD09Q1). The product details of product MOD09Q1 is given in the section 1.4.1a MOD09Q1 provides Band 1 and Band 2.

The Band 1 and Band 2 of MODIS and Band 2 and Band 3 of ASTER image is considered as these bands has special features to identify the agriculture and other land covers. Both satellite image covers approximate the same spectral range. Three image of MODIS (image ids d1 - d3, table 3.1) and one image of ASTER (as1) are used and details are given in Table 3.1.

### 3.3. Theoretical Basis

#### 3.3.1. Curvelet transform based fusion

The main feature of the curvelet transform is that it is sensitive to directional boundaries and capable of representing the highpass details of object contours at different scales through few sparse nonzero coefficients (Stark et al 2002). The different steps which is used for Curvelet fusion is discussed in the following subsections

Step 1: ATrous Wavelet Transform

Step 2: Ridgelet Transform

Step 3: Curvelet Transform

##### 3.3.1.1. Step 1: ATrous wavelet transform

The ATrous wavelet transform (ATWT) (Shensa 1992, Filippo *et al* 2007) is a nonorthogonal multiresolution decomposition defined by a filter bank  $\{h_n\}$  and  $\{g_n = \delta_n - h_n\}$ , with the Kronecker operator  $\delta_n$  denoting an all pass filter. The filter bank does not allow perfect reconstruction to be achieved if the output is decimated. In the absence of decimation, the low pass filter is up sampled by  $2^j$ , before processing the  $j$ th level; hence the name ‘‘ATrous’’ which means ‘‘with holes’’. In two dimensions, the filter bank becomes  $\{h_m h_n\}$  and  $\{\delta_m \delta_n - h_m h_n\}$  which means that the 2-D detail signals is given by the pixel difference between two successive approximations.

For  $J$ -level decomposition, the ATWT accommodates a number of coefficients  $J + 1$  times greater than the number of pixels. Due to the absence of decimation, the synthesis is simply obtained by summing details levels to the approximation, thereby the ATWT for the  $f(m, n)$  is given by

$$f(m, n) = c_j(m, n) + \sum_{j=1}^J d_j(m, n) \quad (3.1)$$

**Table 3.1.** Image sets Details for the fusion of Optical (MODIS and ASTER) images

Image id	Image set	Date of Acquisition
as1	Ast_11b_003_03172001054637_01082002073656.img	March 21 2001
d1	MOD09Q1.A2001057.h24v06.005.2006365121814.hdf	Feb 26 2001
d2	MOD09Q1.A2001081.h24v06.005.2007009180425.hdf	March 22 2001
d3	MOD09Q1.A2009081.h24v06.005.2009092060857.hdf	March 22 2009

Where,  $c_j(m,n)$  and  $d_j(m,n)$ ,  $j = 1, \dots, J$  are obtained through 2-D separable linear convolution with the equivalent lowpass and highpass filters, respectively.



### 3.3.1.2. Step 2: Ridgelet transform

The next step is finding a transformation capable of representing boundaries with different slopes and orientations. A possible solution is the ridgelet transform (Do and Vetterli 2003), which may be interpreted as the 1-D wavelet transform of the Radon transform. This is the basic idea behind the digital implementation of the ridgelet transform. The ridgelet basis function is given by (Filippo et al. 2007, Choi et al. 2004, Choi et al. 2005):

$$\psi_{a,b,\theta}(x_1, x_2) = a^{-\frac{1}{2}} \psi\left(\frac{x_1 \cos \theta + x_2 \sin \theta - b}{a}\right) \quad (3.2)$$

for each  $a > 0$ , each  $b \in R$  and each  $\theta \in [0, 2\pi)$ . This function is constant along lines  $x_1 \cos \theta + x_2 \sin \theta = \text{const}$ .

Thus, the ridgelet coefficients of an image  $f(x_1, x_2)$ , are represented by

$$R_f(a, b, \theta) = \int_{-\infty}^{\infty} \int_{-\infty}^{\infty} \psi_{a,b,\theta}(x_1, x_2) f(x_1, x_2) dx_1 dx_2 \quad (3.3)$$

This transform is invertible and the reconstruction formula is given by:

$$f(x_1, x_2) = \int_0^{2\pi} \int_{-\infty}^{\infty} \int_{-\infty}^{\infty} R_f(a, b, \theta) \psi_{a,b,\theta}(x_1, x_2) \frac{da}{a^3} db \frac{d\theta}{4\pi} \quad (3.4)$$

The Radon transform for an object  $f$  is the collection of line integrals indexed by  $\theta \in [0, 2\pi) \times R$  and is given by:

$$Rf(\theta, t) = \int_{-\infty}^{\infty} \int_{-\infty}^{\infty} f(x_1, x_2) * \delta(x_1 \cos \theta + x_2 \sin \theta - t) dx_1 dx_2 \quad (3.5)$$

Thus, the ridgelet transform can be represented in terms of the Radon transform as follows:

$$R_f(a, b, \theta) = \int_{-\infty}^{\infty} Rf(\theta, t) a^{\frac{-1}{2}} \psi\left(\frac{t-b}{a}\right) dt \quad (3.6)$$

The ridgelet transform is the application of the 1-D wavelet transform to the slices of the Radon transform where the angular variable  $\theta$  is constant and  $t$  is varying.

### 3.3.1.3. Step 3: Curvelet transform

The curvelet transform (Candès and Donoho, 1999, Starck et al., 2002, Starck et al., 2003) is given by filtering and applying multiscale ridgelet transform on each bandpass filters which is described as following in different steps

#### *i. Subband Decomposition*

The image is filtered into subbands

$$f \rightarrow (P_0 f, \Delta_1 f, \Delta_2 f, \dots) \quad (3.7)$$

where a filter,  $P_0$  deals with frequencies  $\xi \leq 1$  and the bandpass filter  $\Delta_s$  is concentrated near the frequencies  $[2^s, 2^{2s+2}]$ , e.g.,

$$\Delta_s = \psi_{2^s} * f, \Psi_{2^s}(\xi) = \Psi(2^{-2s} \xi) \quad (3.8)$$

#### *ii Smooth Partitioning*

Each subband is smoothly windowed into “squares” of an appropriate scale.

$$\Delta_s f \rightarrow (w_Q \Delta_s f)_{Q \in Q_s} \quad (3.9)$$

### iii Renormalization

Each resulting square is renormalized to unit scale

$$g_Q = (T_Q)^{-1}(w_Q \Delta_s f), Q \in Q_s \quad (3.10)$$

### iv Ridgelet Analysis

Each square is analyzed via the discrete ridgelet transform. For improved visual and numerical results of the digital curvelet transform, Starck et al, 2002 presented the following discrete curvelet transform algorithm:

iv-a) apply the ATWT algorithm with J scales as implied in Eq. (3.1)

$$\text{i.e., } f(m, n) = c_j(m, n) + \sum_{j=1}^J d_j(m, n)$$

iv-b) set  $B_1 = B_{min}$ ;

iv-c) for  $j=1, \dots, J$  do

A) partition the subband  $w_j$  with a block size  $B_j$  and apply the digital ridgelet transform to each block;

B) if  $j \bmod 2 = 1$  then  $B_{j+1} = 2B_j$  ;

else  $B_{j+1} = B_j$ .

iv-d) Apply the ridgelet transform to each block

Fig. 3.1, depicts the flow chart of Curvelet Transform which explains the decomposition of the original image into subbands followed by the spatial partitioning of each subband. The Ridgelet transform is then applied to each block (Starck et al, 2002 )

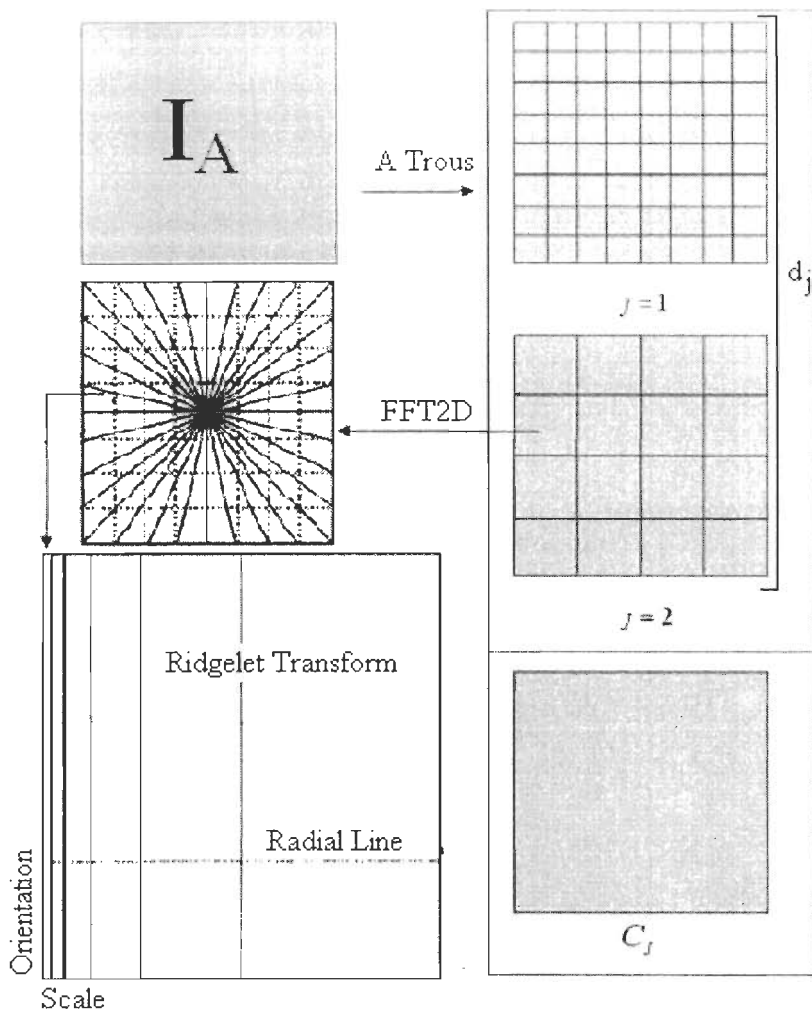


**Fig. 3.1.** Curvelet transform flowgraph. The figure illustrates the decomposition of the original image into subbands followed by the spatial partitioning of each subband (i.e., each subband is decomposed into blocks). The ridgelet transform is then applied to each block (Choi et al, 2005).

### 3.3.2. Fuzzy based fusion

#### 3.3.2.1. Fuzzy logic approach

Fuzzy logic is a powerful problem-solving methodology with a myriad of applications in information processing (Tizhoosh and Haußecker, 2000). Fuzzy provides a remarkably simple way to draw definite conclusions from vague, ambiguous or imprecise information. In a sense fuzzy logic resembles human decision making with



its ability to work from approximate image and find precise solutions. Hence fuzzy logic is used where there is uncertainty and no mathematical relations are easily available.

Fuzzy logic starts with the concept of a fuzzy set. A fuzzy set is a set without a crisp, clearly defined boundary (Klir and Folger, 1988). A fuzzy set admits the possibility of partial membership such as Friday is sort of a weekend day and the weather is rather hot. A classical set might be expressed as

$$\mu_A(x) = \begin{cases} 1, \forall x \in A \\ 0, \forall x \notin A \end{cases} \quad (3.11)$$

A fuzzy set is an extension of this classical set. If  $X$  is the universe of discourse and its elements are denoted by  $x$ , then a fuzzy set  $A$  in  $X$  is defined as a set of ordered pairs:

$$A = \{x, \mu_A(x) \mid x \in X\} \quad (3.12)$$

where  $\mu_A(x)$  is called the membership function (MF) of  $x$  in  $A$ .

Fuzzy logic models, called fuzzy inference systems (FISs), consist of a number of conditional "if-then" rules. For the designer who understands the system, these rules are easy to write, and as many rules as necessary can be supplied to describe the system adequately. Not only do the rule-based approach and flexible membership function scheme make fuzzy systems straightforward to create, but they also simplify the design of systems and ensure that one can easily update and maintain the system over time. Gradual transitions (i.e., from "belongs to a set" to "does not belong to a set") characterized by membership functions give fuzzy sets flexibility in modeling commonly used linguistic expressions, such as "the travel time is high."

Since the mid-1970s, fuzzy logic has become integrated within various fields and methodologies such as fuzzy graphs, calculus of fuzzy if-then rules, fuzzy interpolation, fuzzy topology, fuzzy inference system, fuzzy modeling, and fuzzy reasoning. The earliest applications, and perhaps still the most prevalent today, were led by the research of Mamdani 1974. Multi-disciplinary applications of fuzzy logic

include automatic control, electronics, pattern recognition, approximate reasoning, robotics, time-series prediction, information retrieval, database management and querying, data classification, natural language and image understanding, decision-making and machine learning (Zimmermann 1991, Meitzler et al. 1996, Bushra et al. 2007, Humayun et al. 2009 and Irina and Martina 2008)

Fuzzy set theory provides a formal system to make inferences about vague rules describing the relation between imprecise, qualitative linguistic expressions of the inputs and outputs of a system (Klir and Folger 1988). The control rules usually correspond to the knowledge of an expert and provide an easily comprehended pattern of knowledge representation. The major advantage of this approach is being able to introduce and use rules from experience, heuristics, intuition.

In this thesis, the fuzzy logic approach is used for pixel level image fusion i.e., for fusing high resolution satellite image with low or moderate resolution satellite image.

Some important steps of fuzzy set theory are as following

### **i. Fuzzy Membership Functions**

Designing membership functions is a key issue in fuzzy sets (Zadeh 1965). They should be suitable for the problem at hand and easy to calculate. The outcomes of fuzzy systems may yield different results by changing the parameters of the membership functions. The selection of appropriate membership functions is an important issue. A membership function (MF) is a curve that defines how each point in the input space is mapped to a membership value. The only condition a membership function must really satisfy is that it must vary between 0 and 1. Membership functions are built from several basic functions: piecewise linear function, Gaussian distribution function, sigmoid curve, and quadratic and cubic polynomial curves (McNeill and Freiberger 1993). Samples of fuzzy membership functions (Jang and Sun 1995) are Triangular, Trapezoidal, Gaussian and Bell. Conclusions about a certain phenomenon characterized by fuzziness are determined largely by the shape of its membership function. By using membership functions,

membership grade or truth-value of a member in a particular fuzzy set is determined. The simplest membership functions are formed using straight lines.

## ii. Fuzzy Inference Systems

Fuzzy inference systems (FISs) (Jang and Sun 1995; Wang 1994) are popular computing frameworks based on the concepts of fuzzy set theory, fuzzy if-then rules, and fuzzy reasoning. It is the process of deriving conclusions from a given set of fuzzy rules acting on fuzzified data. Basically, a FIS is composed of four functional blocks as shown in fig. 3.2.

Fuzzification maps crisp inputs into fuzzy sets, which are subsequently used as inputs to the inference engine. A fuzzy set  $U$  is characterized by a membership function (MF)  $\mu: U \rightarrow \{0,1\}$ . Membership functions are labeled by linguistic terms such as "small" or "large" (Mendel and Mouzouris 1997). Several classes of parameterized functions widely used to define membership functions such as Gaussian, Generalized bell, and Trapezoidal functions (Mendel and Mouzouris 1997).

A Fuzzy rule base is a set of fuzzy rules in the form of if-then clauses. For a multi input single output case, the  $i^{\text{th}}$  rule can be expressed by (Mendel and Mouzouris 1997)

$$R^i : \text{if } x \text{ is } A^i \text{ and } y \text{ is } B^i \text{ then } z \text{ is } C^i \quad (3.13)$$

where  $x$  and  $y$  are the input variables,  $z$  is the output variable, and  $A^i$  and  $B^i$  are the labels of membership functions associated to the input variables and  $C^i$  is the label of the membership function associated with the output variable,  $z$ , in the rule  $i$ .

A Fuzzy inference engine is a decision-making logic, which performs the inference operations on the rules and a given condition to derive a reasonable output or conclusion (Mathworks 2006). Thus fuzzy inference is the process of formulating the mapping from a given input to an output using fuzzy logic. The mapping then provides a basis from which decisions can be made, or patterns discerned. The process of fuzzy inference involves the Membership Functions (MF), Logical Operations like logical operation AND, OR, and NOT, and If-Then Rules (eq. 3.13).

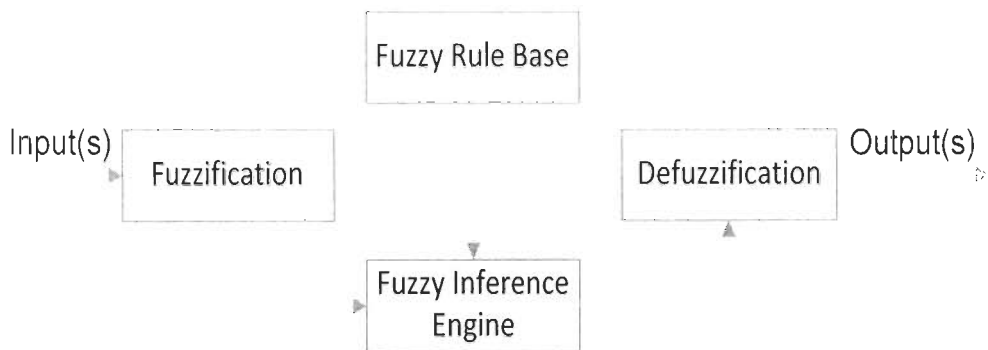


**Fig. 3.2.** Basic fuzzy inference system

Two types of FISs (Jang and Sun 1995): Mamdani fuzzy model and Sugeno fuzzy model, have been widely employed in various applications. These two types of inference systems vary somewhat in the way outputs are determined.

Mamdani's fuzzy inference method is the most commonly seen fuzzy methodology. Mamdani's method was among the first control systems built using fuzzy set theory. It was proposed in 1975 by Ebrahim Mamdani (Mamdani and Assilian 1975) as an attempt to control a steam engine and boiler combination by synthesizing a set of linguistic control rules obtained from experienced human operators. Mamdani's effort was based on Lotfi Zadeh's 1973 paper on fuzzy algorithms for complex systems and decision processes (Zadeh 1973). Mamdani-type inference, expects the output MF to be fuzzy sets. After the aggregation process, there is a fuzzy set for each output variable that needs defuzzification. It is possible, and in many cases much more efficient, to use a single spike as the output MF rather than a distributed fuzzy set. This type of output is sometimes known as a singleton output MF, and it can be thought of as a pre-defuzzified fuzzy set. It enhances the efficiency of the defuzzification process because it greatly simplifies the computation required by the more general Mamdani method, which finds the centroid of a two-dimensional function. Rather than integrating across the two-dimensional function to find the centroid, we use the weighted average of a few data points. Sugeno-type (Sugeno 1985) systems support this type of model. In general, Sugeno-type systems can be used to model any inference system in which the output MF are either linear or constant.

Defuzzification transforms the fuzzy results of the inference into a crisp output. The most popular defuzzification method is the centroid of area. Other defuzzification strategies arise for specific applications, which include bisector of area, mean of maximum, largest of maximum, and smallest of maximum (Jang and Sun, 1995). The essential part of a typical fuzzy system is formed by a knowledge base in which the process of the fuzzy system is explained as a set of fuzzy if-then rules. An inference mechanism compares the inputs of the system against the knowledge stored in the knowledge base and generates a system's output by using the given inputs and the available knowledge in the knowledge base. Conventional fuzzy systems are static; rules are acquired off-line and the system components do not change once operation begins.

### **3.3.3. Quality assessment indicators**

In order to assess the quality of the fused image by means other than simple visual inspection of the images, some quantitative assessment criteria have been defined by comparing the fused product and the low spatial resolution multispectral images (Wald et al. 1997). A series of indicators have been used for this purpose:

#### **i Correlation coefficient**

The correlation coefficient (Vijayaraj et al. 2004) of two images is often used to indicate their closeness between the images. Comparing the original image with the fused image, one can find the degree of differences. The correlation coefficient ranges from  $-1$  to  $+1$ . A correlation coefficient of  $+1$  indicates that the two images are highly correlated, i.e., very close to one another and a correlation coefficient of  $-1$  indicates that the two images are exactly opposite each other. The correlation coefficient is given by

$$corr(A, B) = \frac{\sum_{j=1}^n \sum_{i=1}^m (x_{i,j} - \mu(A))(x'_{i,j} - \mu(B))}{\sqrt{\sum_{j=1}^n \sum_{i=1}^m (x_{i,j} - \mu(A))^2 \sum_{j=1}^n \sum_{i=1}^m (x'_{i,j} - \mu(B))^2}} \quad (3.14)$$

where  $A$  and  $B$  are two images,  $x_{i,j}$  and  $x'_{i,j}$  the elements of the image  $A$  and the image  $B$ , respectively.  $\mu(A)$  and  $\mu(B)$  stand for their mean values. The fused image which will best preserve the spectral information of the original low resolution multispectral image is the one that has the maximum correlation with the initial low resolution multispectral image (Karathanassi et al. 2007).

### ii. Root Mean Square Error (RMSE)

The Root Mean Square Error (RMSE) (Li et al. 2002) measures the spectral fidelity between the original and the fused image. It measures the amount of change per pixel due to the processing and is described by

$$RMSE(A, B) = \sqrt{\frac{\sum_{j=1}^n \sum_{i=1}^m (x_{i,j} - x'_{i,j})^2}{n * m}} \quad (3.15)$$

where  $A$  and  $B$  are two images,  $x_{i,j}$  and  $x'_{i,j}$  the elements of the image  $A$  and the image  $B$ , respectively.

### iii. Relative Difference of Means (RMD)

The Relative Difference of Means (RMD) (Karathanassi et al. 2007) between the fused product and the original low spatial resolution multispectral image is given by

$$RMD(F, LR) = \frac{\overline{F} - \overline{LR}}{\overline{LR}} \quad (3.16)$$

Where  $\overline{F}$  is the mean value of the fused image and  $\overline{LR}$  is the mean value of the original low spatial resolution image.

The fused image which will best preserve the spectral information of the original low resolution multispectral image is the one that has the smallest possible relative difference of means.

#### iv. Relative Variation Difference (RVD)

The Relative Variation Difference (RVD) (Karathanassi et al. 2007) between the fused product  $\sigma_F^2$  and the original low spatial resolution multispectral image  $\sigma_{LR}^2$

$$RVD(F, LR) = \frac{\sigma_F^2 - \sigma_{LR}^2}{\sigma_{LR}^2} \quad (3.17)$$

$$\text{Where } \sigma_F^2 = \frac{1}{N-1} \sum_{i=1}^N (F_i - \bar{F})^2, \sigma_{LR}^2 = \frac{1}{N-1} \sum_{i=1}^N (LR_i - \bar{LR})^2$$

Where  $N$  = number of pixels in the image and  $\bar{F}$  is the mean value of the fused image and  $\bar{LR}$  is the mean value of the original low spatial resolution image.  $F$  is the fused image and  $LR$  is the original low spatial resolution image. The fused image which will best preserve the spectral information of the original low resolution multispectral image is the one that has the smallest possible relative variation difference.

#### v. Deviation Index(DI)

The Deviation Index (DI) (De Bethune et al. 1998), measuring the normalized global absolute difference of the fused image ( $F$ ) with the low spatial resolution multispectral image ( $LR$ ):

$$DI(F, LR) = \frac{1}{N * N} \sum_{i=1}^N \sum_{j=1}^N \frac{|F_{i,j} - LR_{i,j}|}{LR_{i,j}} \quad (3.18)$$

The fused image which will best preserve the spectral information of the original low resolution multispectral image is the one that has the smallest possible deviation index.

## vi. Peak signal to noise ratio (PSNR)

The peak signal to noise ratio (PSNR) (Li and Hu 2004) index reveals the radiometric distortion of the final image compared to the original.

$$PSNR = 20 \log_{10} \frac{peak}{\sqrt{MSE}} \quad (3.19)$$

$$\text{Where } MSE = \frac{1}{N} \sum_{i=1}^N (F_i - LR_i)^2$$

where  $F_i$  is the fused image pixel  $i$  value,  $LR_i$  is the low spatial resolution image pixel  $i$  value,  $N$  is the number of non-null image pixels, Peak is the maximum possible pixel value. The fused image which will best preserve the spectral information of the original low resolution multispectral image is the one that has the highest possible PSNR.

## vii. Universal Image Quality Index (UQI)

The Universal Image Quality Index (UQI) [34] introduced by

$$UQI = \frac{4\sigma_{F.LR} \overline{FLR}}{\sigma_F^2 + \sigma_{LR}^2 \left[ \left( \overline{F} \right)^2 + \left( \overline{LR} \right)^2 \right]} \quad (3.20)$$

$$\text{Where } \overline{F} = \frac{1}{N} \sum_{i=1}^N F_i, \quad \overline{LR} = \frac{1}{N} \sum_{i=1}^N LR_i, \quad \sigma_F^2 = \frac{1}{N-1} \sum_{i=1}^N (F_i - \overline{F})^2,$$

$$\sigma_{LR}^2 = \frac{1}{N-1} \sum_{i=1}^N (LR_i - \overline{LR})^2, \quad \sigma_{F.LR} = \frac{1}{N-1} \sum_{i=1}^N (F_i - \overline{F})(LR_i - \overline{LR})$$

Where  $N$  implies the number of image pixels. The fused image which will best preserve the spectral information of the original low resolution multispectral image is the one that has the highest possible UQI.



### 3.3.4. Minimum distance classification technique

The minimum distance technique uses the mean vectors of each end member and calculates the Euclidean distance from each unknown pixel to the mean vector for each class. All pixels are classified to the nearest class unless a standard deviation or distance threshold is specified, in which case some pixels may be unclassified if they do not meet the selected criteria. An image data can be commonly represented in the form of a column vector as;

$$X = \begin{bmatrix} x_1 \\ x_2 \\ \vdots \\ x_n \end{bmatrix} \quad (3.21)$$

Where  $x_1, x_2, x_3, \dots, x_n$  are the spectral values of the pixel vector  $X$  in bands 1 to  $n$  respectively. Discriminant function for minimum distance classifier is defined from the expression of the squared Euclidean distance between the position of the generic pixel  $X$  to be classified and the mean value  $m_i$  of  $i^{\text{th}}$  class (Richards and Jia 2006):

$$d(X, m_i)^2 = (X, m_i)' (X, m_i) \quad (3.22)$$

Classification is performed on the basis of:

$$X \in w_i \text{ if } d(X, m_i)^2 > d(X, m_j)^2 \quad \forall j \neq i \quad (3.23)$$

Minimum distance algorithm is more efficient when the number of training samples per class is limited, since it is based only on the use of the class mean vector ' $m$ ' whose evaluation is more accurate with few samples. The main disadvantage of the classifier lies with the fact that it can model only symmetric classes in multi-spectral space (i.e., assumes distribution of samples about the centre of mass in a spherical manner).

## 3.4. Implementation and Results:

### 3.4.1. Curvelet based fusion

The basis of curvelet transform used for the fusion of ASTER and MODIS image is shown in the fig. 3.1 whereas fig. 3.3 shows the flowchart of the applied methodology for the curvelet fusion of ASTER image and MODIS image. MODIS and ASTER image are subsetting to Roorkee region for this study and the care is taken so that area of sub-set region of both satellite images should be approximately equal. Therefore, MODIS has 87\*87 pixels and ASTER has 1186\*1186 no of pixels after subsetting, by which both are acquiring approximately the same area. The flowchart, fig. 3.3 is deciphered in the following steps

#### i. Fusion of MODIS band 1 and Band 2

MODIS Band 1 and Band 2 are considered initially. The Band 1 is fused with the Band 2, through the curvelet transform (For ATWT transform, eq. (3.1) is computed for Band 2, thereby Band 2 is decomposed into  $J + 1$  subbands, which includes  $C_j$  and  $d_j$ , where  $C_j$  is a coarse or smooth version of Band 2, and  $d_j$  is the details of Band 2 at scale  $2^j$ , here  $j=2$ .  $C_j$  is replaced by Band 1 and then the Ridgelets transform (eq. 3.2 to eq. 3.6) is applied to all the decomposed subbands i.e.,  $d_j$  bands, thereby obtained ridgelet coefficients are hard-thresholded in order to enhance boundaries in the fused image and inverse ridgelet transforms (IRT) is carried out to obtain a new image which reflects the fused image (MOD12) of Band 1 and Band 2 i.e., the resultant fused image MOD12 of 87\*87 pixels. This MOD12 image is interpolated through bi-linear interpolation technique (Thomas et al. 1999) to the scale of the ASTER image of 1186\*1186 pixels. The commonly used linear methods, such as bilinear interpolation and bicubic convolution interpolation, have advantages in simplicity and fast implementation (Vrcelj B. and Vaidyanathan 2001). Muhammad et al. 2008, have used non-linear interpolation technique for increasing the spatial resolution of Quickbird multispectral image to the spatial resolution of Quickbird panchromatic image.

## ii. Fusion of ASTER band 2 and Band 3

Similarly subsetting ASTER image of Band 2 and Band 3 are considered. It is georeferenced and it is also subset to the Roorkee region and hence the numbers of pixels are  $1186 \times 1186$  pixels. The Band 2 is fused with the Band 3, through the curvelet transform as shown in fig. 3.3. Similar fusion process as discussed above has been applied for fusion of ASTER band 2 and band 3. ATWT transformation is applied for band 3 and  $C_j$  is replaced by band 2. Here  $j$  is 2, as the number of pixels of ASTER image is  $1186 \times 1186$  pixels. Then ASTER fused image is obtained as AST23 which has  $1186 \times 1186$  pixels.

## iii. Fusion of AST23 and MOD12

The AST23 is the fused image of the ASTER bands of  $1186 \times 1186$  pixels and MOD12 is the bilinear interpolated fused image of MODIS bands of  $1186 \times 1186$  pixels. AST23 and MOD12 are considered for the fusion through curvelet transform as shown in fig. 3.3. Similar fusion process has been applied for fusion of AST23 and MOD12. ATWT transformation is applied for AST23 and  $C_j$  ( $j=2$  for present case) is replaced by MOD12 which gives the resultant fused image AS\_MO that has  $1186 \times 1186$  pixels.

### 3.4.2. Fuzzy based fusion

Fuzzy Inference System (FIS) based Mamdani Model is a computing process by using fuzzy logic from input space to output space is being used in this thesis, because Mamdani FIS has advantages (Abdelwahab and Nicolas 2008) like Expressive power, easy formalization and interpretability, reasonable results with relatively simple structure, intuitive and interpretable nature of the rule base and Output can either be fuzzy or a crisp output. For this reason Mamdani FIS is widely used in particular for decision support application

Fuzzy Inference System Editor for the fusion of ASTER and MODIS image is emphasized in fig. 3.4. Fig. 3.5 shows the selection of Membership Fusion (MF) plots using Membership Fusion Editor and fig. 3.6 indicates the Rule Editor, for

accentuating the rules that are used for the fusion of ASTER image with the MODIS image.

Fig. 3.7 shows the flowchart of the proposed methodology for the fuzzy based fusion of ASTER image and MODIS image for analyzing the classification of the MODIS image before and after the fusion. MODIS and ASTER image are subsetted to Roorkee region for this study and the care is taken so that area of sub-set region of both satellite images should be approximately equal. The flowchart fig. 3.7 is deciphered in the following steps

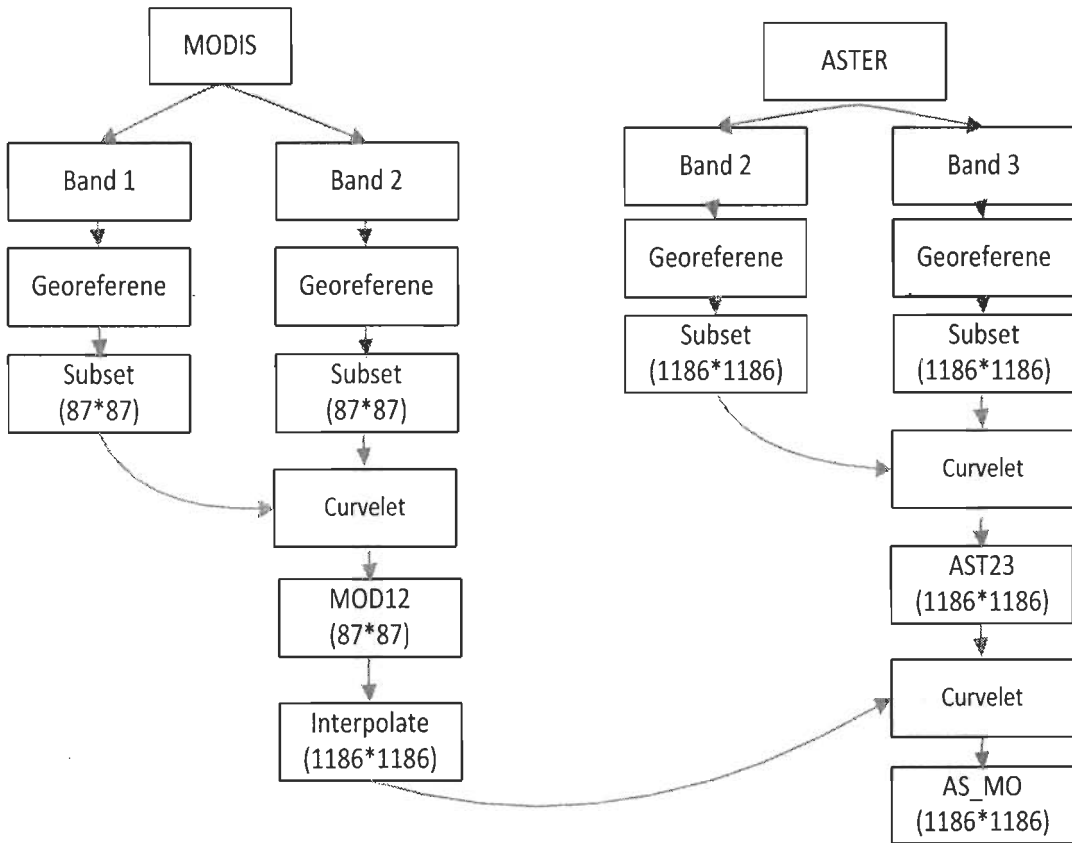


**Fig. 3.3.** Flowchart for fusion of ASTER and MODIS image through curvelet based fusion

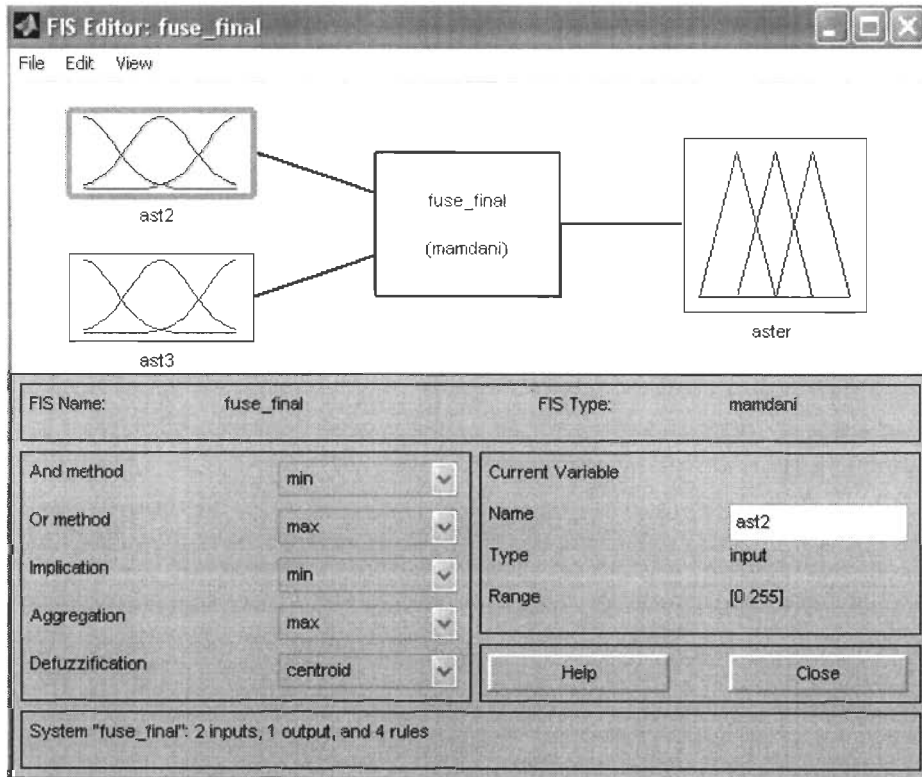


Fig. 3.4. Fuzzy Interference System Editor for the fusion of ASTER and MODIS images

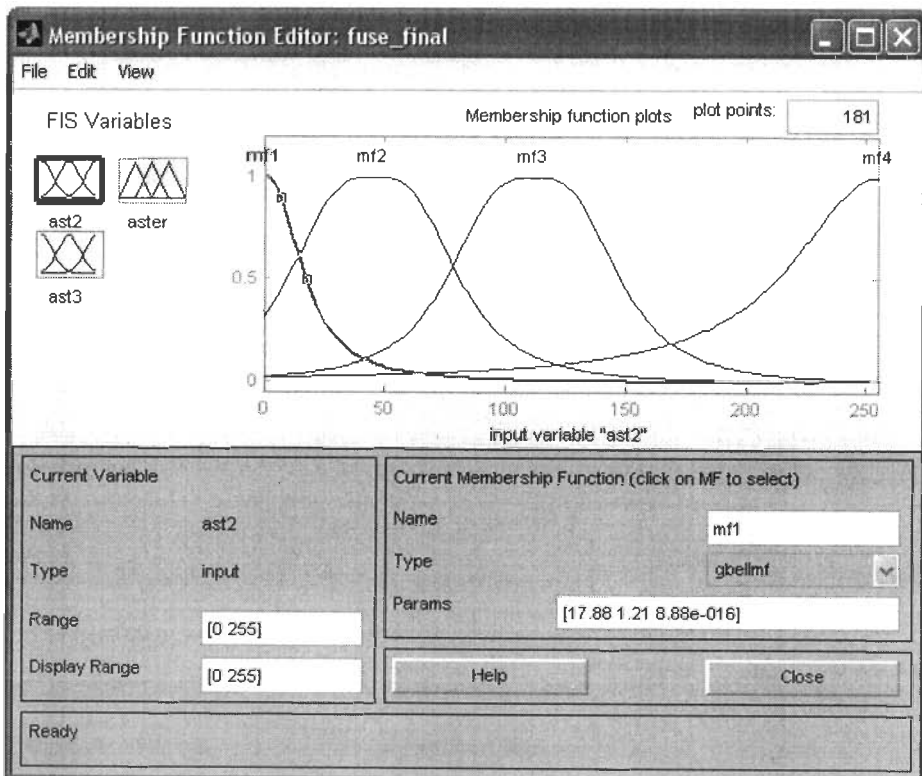


Fig. 3.5. Membership Fusion Editor implying the Membership Fusion(MF) for the ASTER and MODIS images

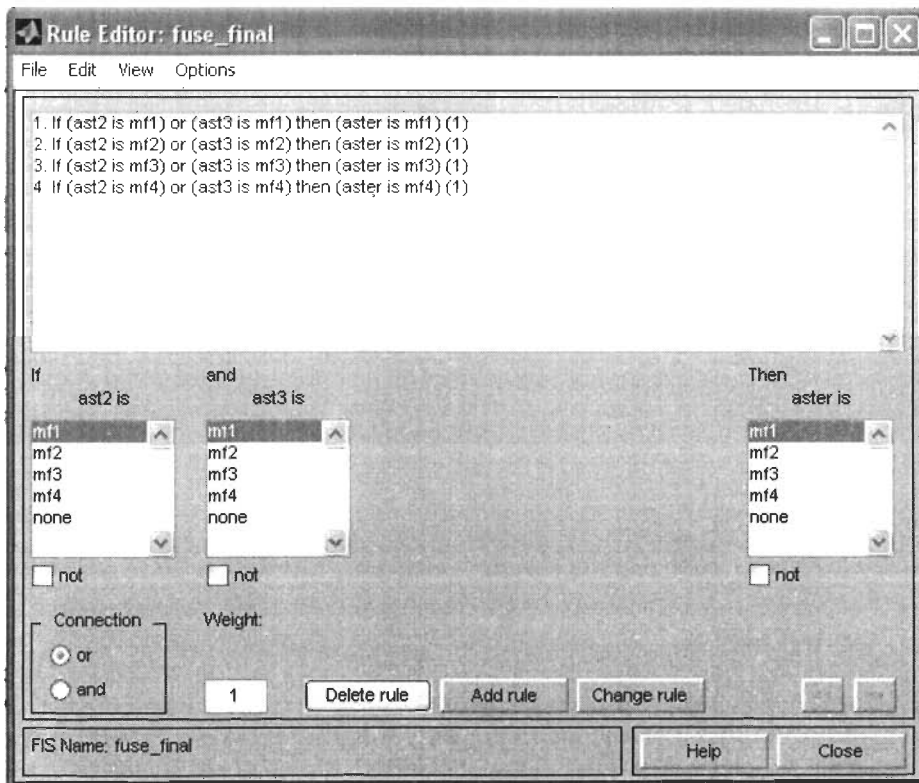


Fig. 3.6. Rule Editor for the fusion of ASTER and MODIS images

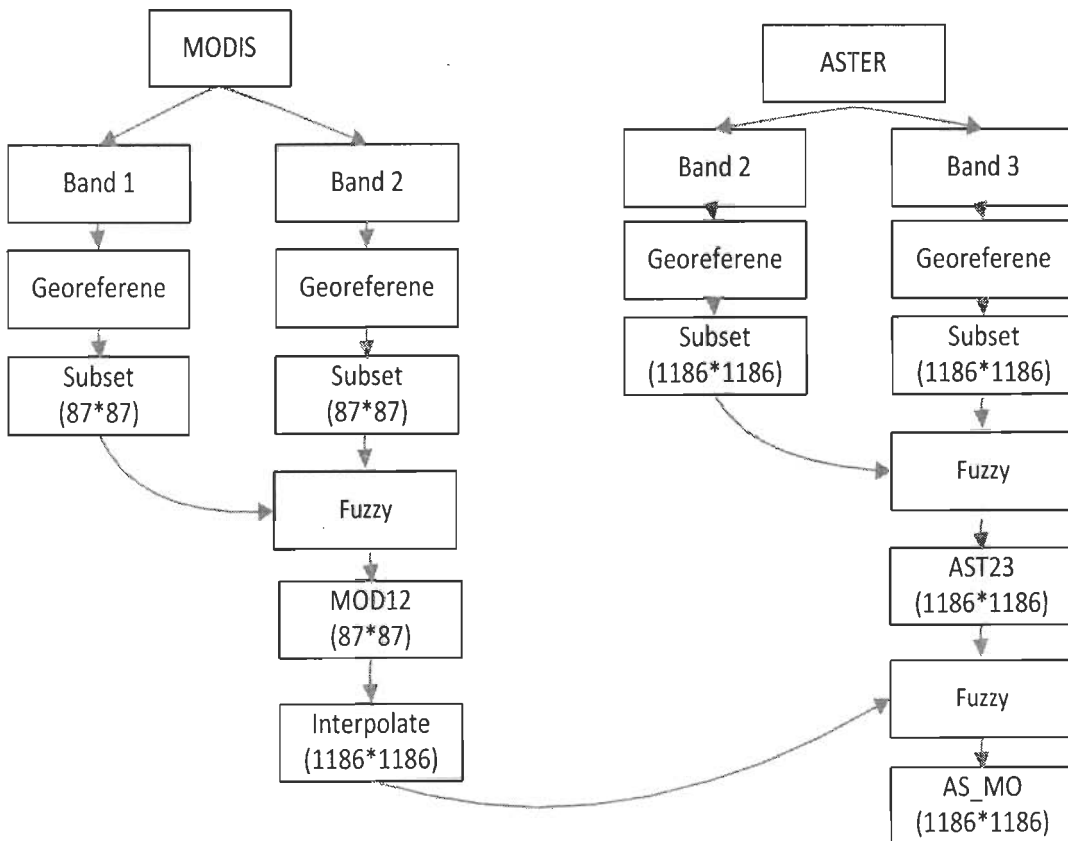


Fig. 3.7. Flowchart for the fusion of ASTER and MODIS image through fuzzy based fusion

### **i. Fusion of MODIS band 1 and Band 2**

MODIS Band 1 and Band 2 are considered initially. The Band 1 is fused with the Band 2, through the fuzzy based fusion. The FIS of the matlab is used for fusion, and fig. 3.4, 3.5 and 3.6 are used for the fusion. A new image which reflects the fused image (MOD12) of Band 1 and Band 2 i.e., the resultant fused image MOD12 of 87\*87 pixels. This MOD12 image is interpolated through bi-linear interpolation technique to the scale of the ASTER image of 1186\*1186 pixels.

### **ii. Fusion of ASTER band 2 and Band 3**

Simultaneously subsetted ASTER image of Band 2 and Band 3 are considered. It is georeferenced and it is also subset to the Roorkee region and hence the number of pixels are 1186\*1186 pixels. The Band 2 is fused with the Band 3, through the FIS of the matlab and fig. 3.4, 3.5 and 3.6 are used for the fusion, then ASTER fused image is obtained as AST23 which has 1186\*1186 pixels.

### **iii. Fusion of AST23 and MOD12**

The AST23 is the fused image of the ASTER image of 1186\*1186 pixels and MOD12 is the interpolated fused image of bilinear interpolated MODIS image of 1186\*1186 pixels. AST12 and MOD12 are considered for the fusion through the FIS of the matlab and fig. 3.4, 3.5 and 3.6 are used for the fusion, and thereby gives the resultant fused image AS\_MO that has 1186\*1186 pixels.

## **3.4.3. Fusion coefficients**

### **3.4.3.1. Methodology for deriving the Fusion coefficient**

The use of fusion coefficient may avoid procuring the high resolution image every year. So, this chapter is the first step in that direction where MODIS and ASTER image will be fused for improvement of classification accuracy of MODIS image and also attempted to obtain the fusion coefficient (eq. 3.24). This fusion coefficient has

been obtained by averaging the d1 and d2 image of the year 2001 and obtained coefficient is validated with image id d3 of the year 2009 and quite encouraging result is obtained.

The obtained fusion coefficient may be the season specific. Therefore we have considered the image of month March only. The following steps have been carried out to derive the Fusion coefficient

**Step 1:** ASTER averaged (AST\_avg) is computed first, and is derived as shown in the eq. 3.24. To accomplish this, we need to fuse the MODIS image d1 and d2 (table 3.1) with ASTER image. AS\_MO\_d1 and AS\_MO\_d2, is the resultant fused image AS\_MO with respect to MODIS image d1 and d2 (table 3.1) respectively

$$AST\_avg = (AS\_MO\_d1 + AS\_MO\_d2) / 2 \quad (3.24)$$

**Step 2:** Eq. 3.1 is applied for the AST\_avg (eq. 3.24). The derived  $d_j$  the ridgelet transformation (as shown in the dotted rectangle of fig. 3.8) is applied and the resultant  $d_j$  is proposed as fusion coefficient. This fusion coefficient  $d_j$  is then further used for fusion of MODIS image as shown in fig 3.8. This fusion coefficient is reducing the computation complexity, because now, we can directly use this fusion coefficient for fusing the MODIS image as stated by eq. 3.1. Only we have to replace the  $C_j$  by image d1 and d2 respectively.

To test our methodology, the sections 3.4.1. i. - iii. are applied for image d1, and d2 (table 3.1) and the corresponding resultant fused images are AST\_avg\_d1, and AST\_avg\_d2 respectively. The d3 image is considered to validate the proposed fusion coefficient. The sections 3.4.1 ( i. - iii.) are carried for d3. Here, we have compared the result with fusion of MODIS image to real ASTER image which resultant is AS\_MO\_d3 and fusion of MODIS image with AST\_avg (derived from eq. 3.24) image which resultant is AST\_avg\_d3.



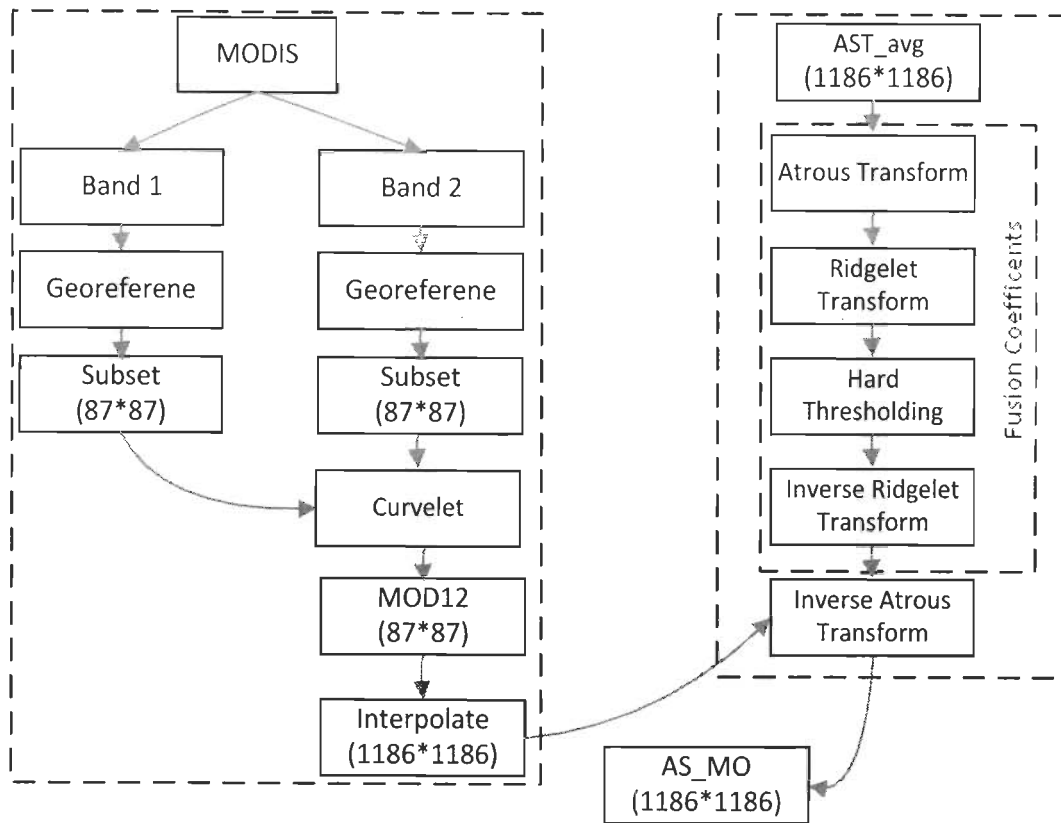


**Fig. 3.8.** The flowchart implying the fusion of the MODIS image with the AST\_avg

### 3.5. Analysis of Experimental Results

The ASTER band 2 and ASTER band 3 which is georeferenced and subset to the Roorkee region is shown in the fig. 3.9a and 3.9b. MODIS band 1 and MODIS band 2 images of image d2 are shown in Fig. 3.10a 3.10b respectively which is georeferenced and subset to the Roorkee region.

#### 3.5.1. Classification Accuracy

The Minimum Distance classification technique has been applied for obtaining the major type of land cover classification i.e. urban, agriculture and water. ENVI 4.3 and MATLAB 7.0 are used for whole processing and algorithm implementation.

We have identified 235 Ground Control points (GCP) for agriculture, 216 GCP for urban and 255 GCP for water bodies from Toposheet of Roorkee region (Fig.



**Fig. 3.9a.** ASTER band 2 image of asl image

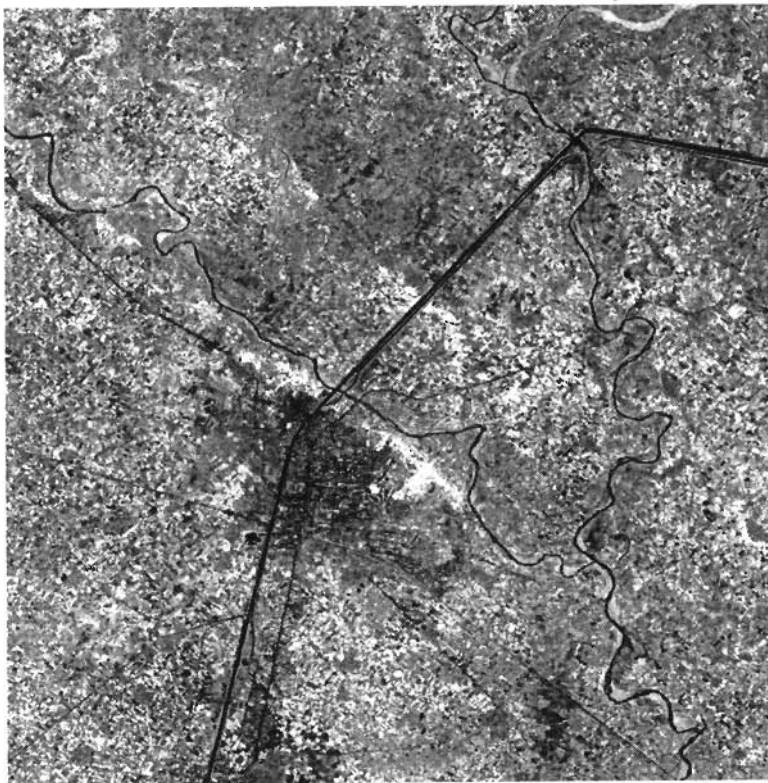


**Fig. 3.9b.** ASTER band 3 image of asl image

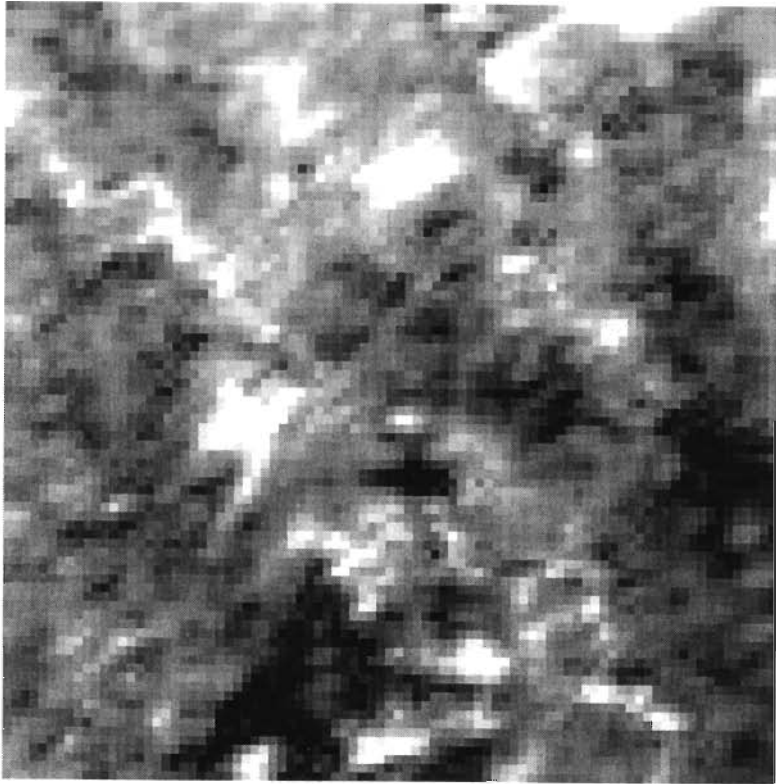


**Fig. 3.10a.** MODIS band 1 image of d2 image

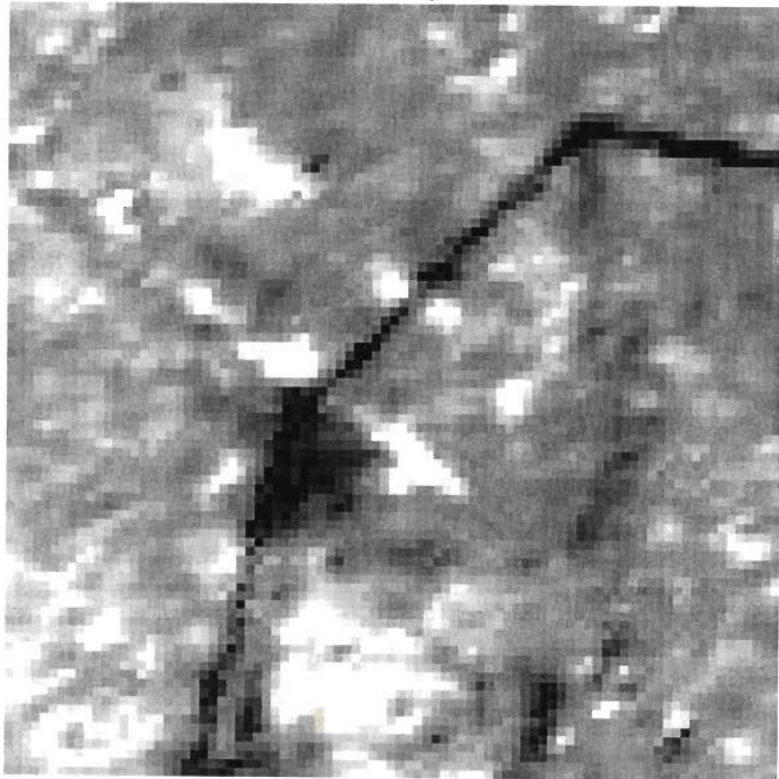


**Fig. 3.10b.** MODIS band 2 image of d2 image

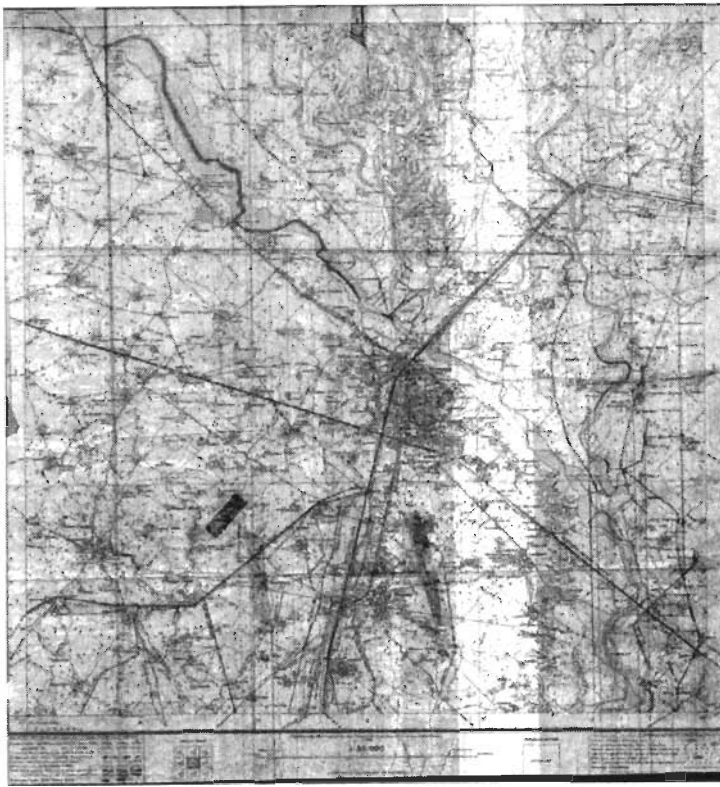


**Fig. 3.11.** Toposheet of the study area (Roorkee region) in the Haridwar district, India

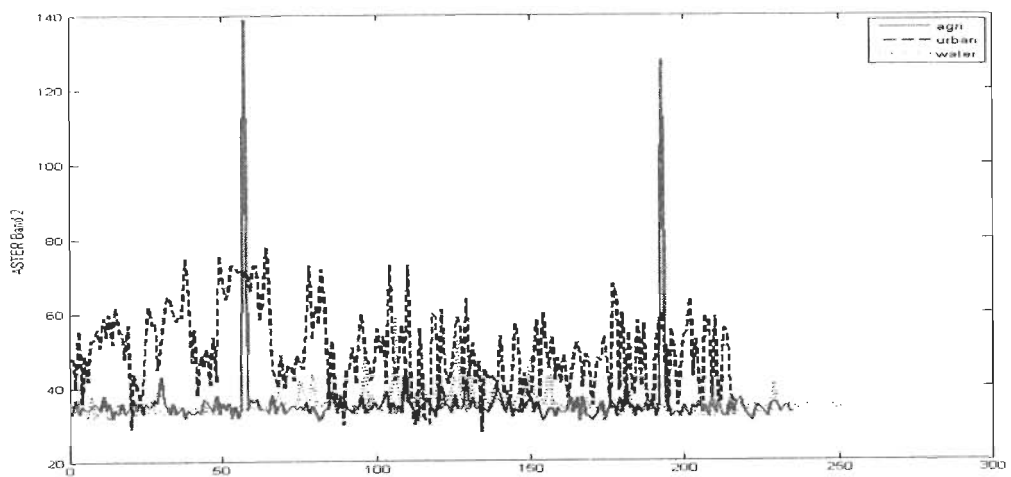


**Fig. 3.12a.** Spectral Response of ASTER Band 2 (as1) for different class

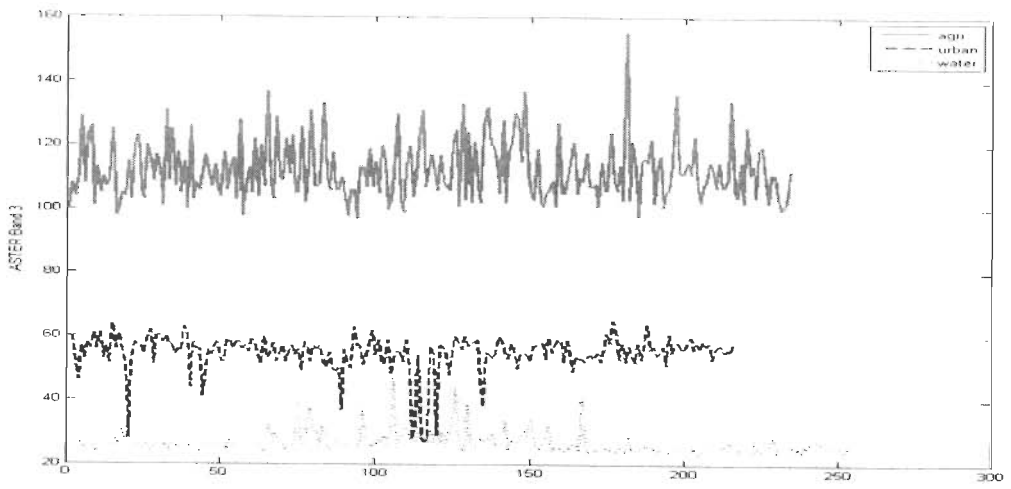


**Fig. 3.12b.** Spectral Response of ASTER Band 3 (as1) for different class

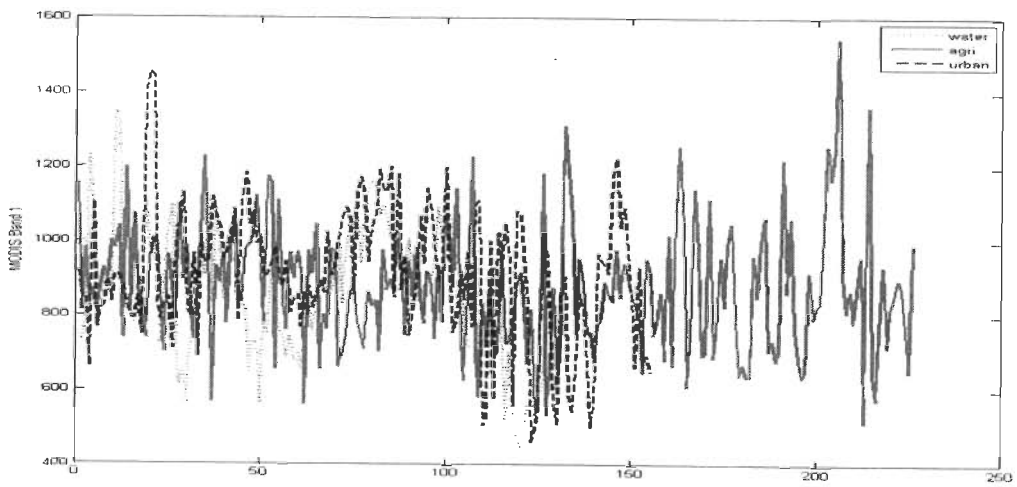


**Fig. 3.13a.** Spectral Response of MODIS Band 1 (d2) for different class

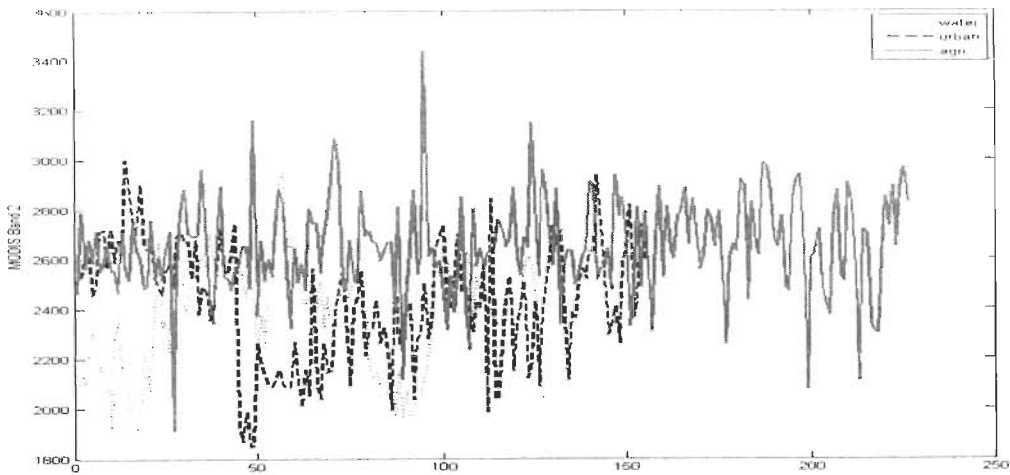


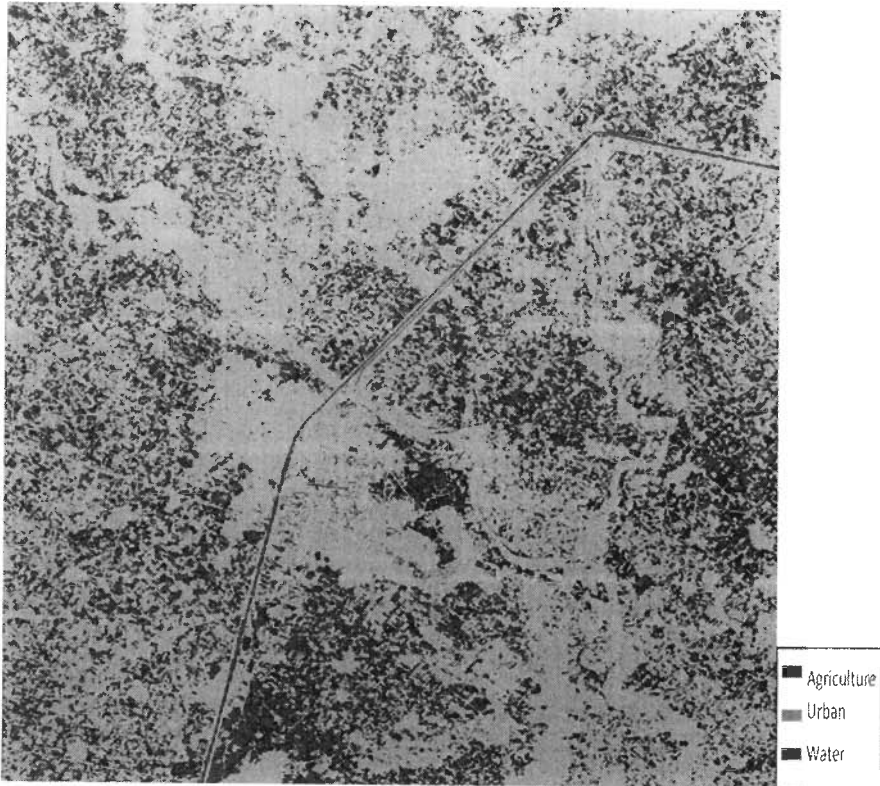
Fig. 3.13b. Spectral Response of MODIS Band 2 (d2) for different class

Table 3.2. Classification Accuracy for ASTER and MODIS Images

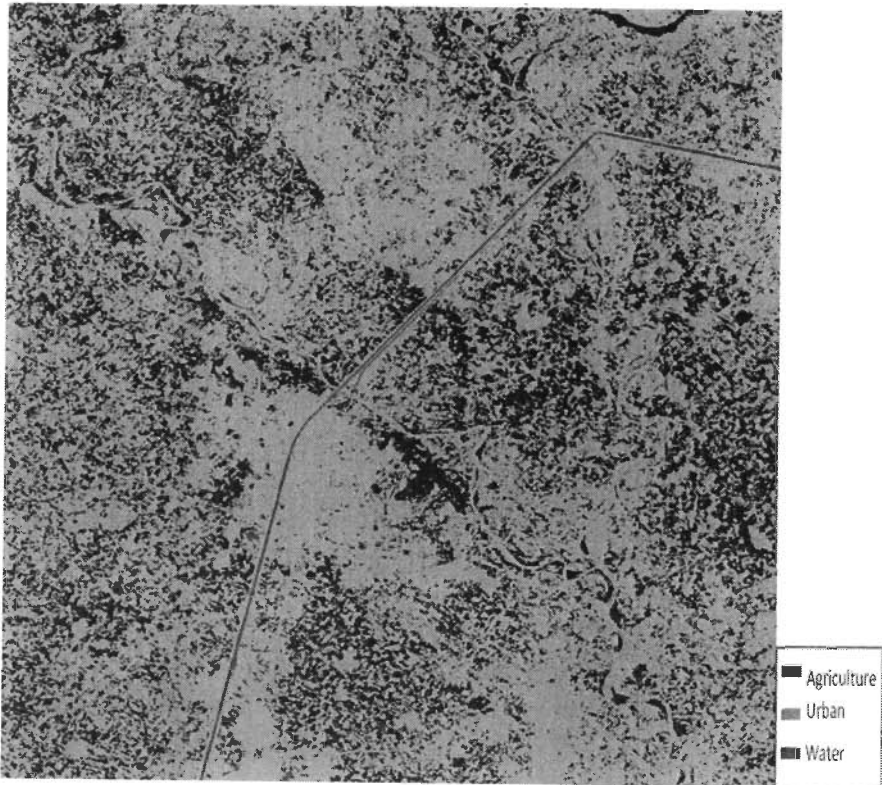
Image id	Images	Users Accuracy (%)			Producers Accuracy(%)			Overall Classification Accuracy (%)
		Agric ulture	Urban	Water	Agric ulture	Urban	Water	
as1	ASTER band 2	19.16	84.97	84.66	27.23	68.06	80.94	72.02
	ASTER band 3	99.85	94.09	99.29	99.67	95.83	98.98	98.73
d2	MODIS band 1	61.76	37.50	26.86	9.29	56.13	51.18	34.06
	MODIS band 2	65.23	34.58	42.07	73.89	23.87	48.03	52.17

Table 3.3. Classification Accuracy of fusion of MODIS (d2) and ASTER (as1) through curvelet transform

Images	Users Accuracy (%)			Producers Accuracy (%)			Overall Classification Accuracy (%)
	Agric ulture	Urban	Water	Agric ulture	Urban	Water	
MOD12	51.90	38.46	31.02	54.42	6.45	59.84	41.14
AST23	99.57	98.56	96.18	99.74	95.37	98.82	98.17
AS_MO	47.65	11.69	88.24	82.13	29.17	54.12	54.81



**Fig. 3.14a.** Minimum distance classified image of ASTER band 2 image of asl



**Fig. 3.14b.** Minimum distance classified image of ASTER band 3 image of asl

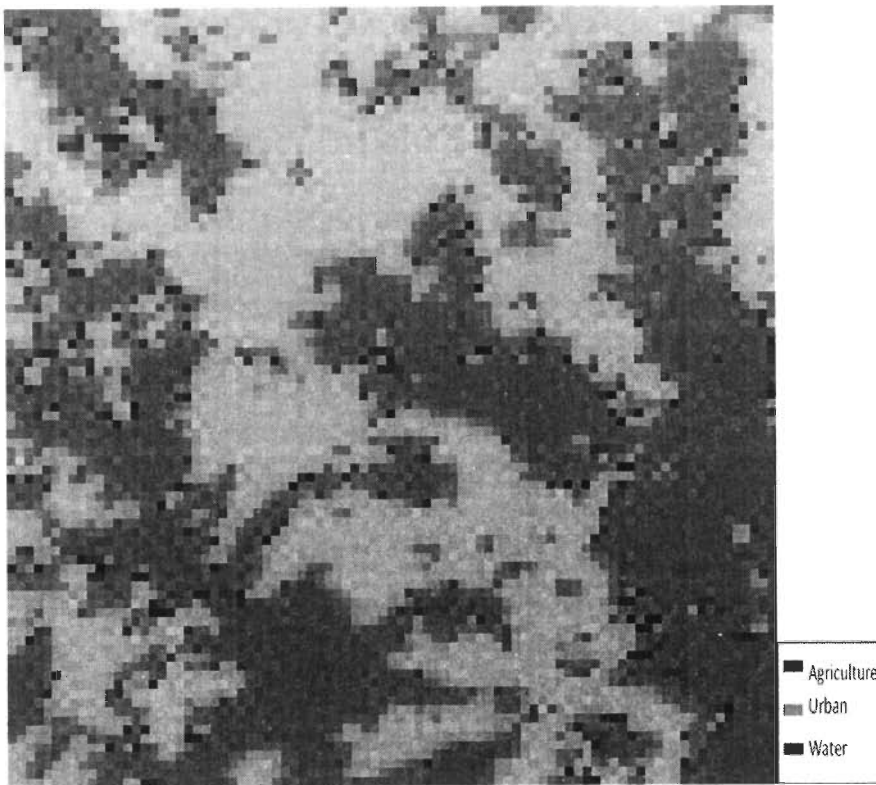


**Fig. 3.15a.** Minimum distance classified image of MODIS band 1 image of d2

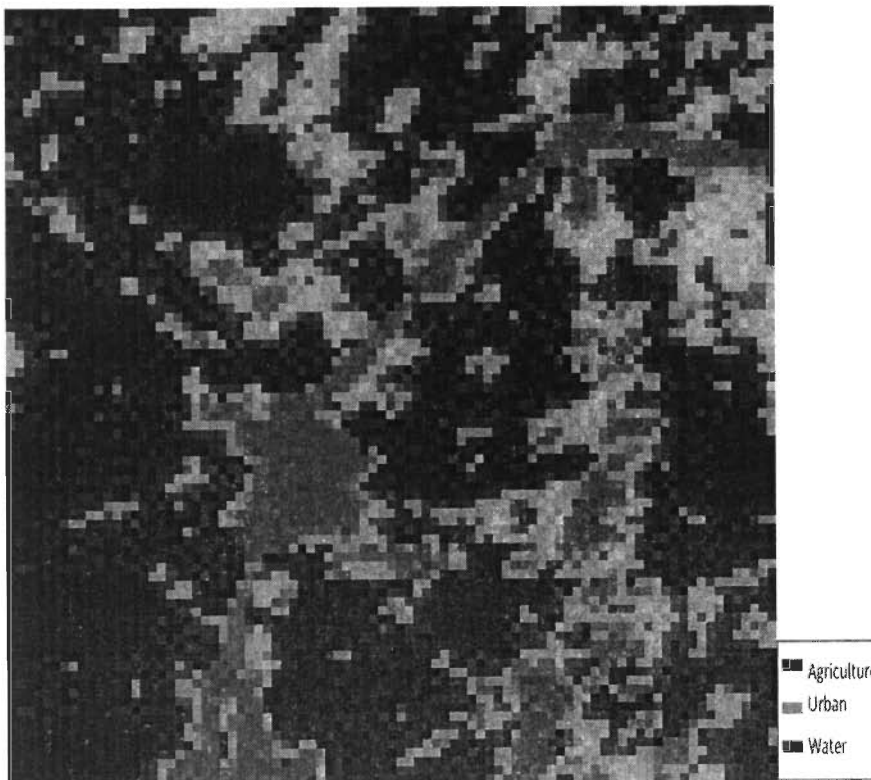


**Fig. 3.15b.** Minimum distance classified image of MODIS band 2 image of d2



3.11), Google earth, and ground survey points. The control points were basically collected by ground survey with the use of GPS and more than 100 points were separately collected for each classes, and these points were overlapped on Google Earth and Toposheet for visual interpretation of the points. On the basis of these GCPs, we have computed the classification accuracy. The Spectral response for this GCP for ASTER band 2, band 3 and MODIS band 1 and 2 are shown in the fig. 3.12a, fig. 3.12b, fig. 3.13a and fig. 3.13b respectively (x-axis represents the GCPs considered and y-axis represents the surface reflectance values of corresponding bands).

The Minimum Distance classified image of ASTER band 2 and ASTER band 3 i.e., fig. 3.9a and 3.9b are shown in the figs. 3.14a and 3.14b respectively. Similarly the minimum distance classified image of MODIS band 1 and band 2 i.e., fig. 3.10a and 3.10b are shown in the figs. 3.15a and 3.15b respectively. The producers and users classification accuracies of these classes for MODIS band 1, MODIS band 2, ASTER Band 2, ASTER Band 3 have been tabulated in Table 3.2. The overall classification accuracy for MODIS band 1, MODIS band 2 for d2 image is 34.06% and 52.17% respectively. In other hand ASTER band 2, ASTER band 3 of as1 image has overall accuracy of 72.02% and 98.73% respectively. It is clear from fig. 3.12b (i.e., ASTER Band 3's spectral response) that GCPs have a distinct spectral response for agriculture, urban and water bodies. Hence the classification accuracy is good for ASTER band 3, whereas the same GCPs in ASTER Band 2 (which is shown in fig. 3.12a) have some overlap spectral response, and hence there is a reduction in the accuracy. In another hand, the spectral response of MODIS Band 1 and MODIS Band 2 (Fig. 3.13a and Fig. 3.13b), represents no clear distinction of different land cover. This may be one of the main reasons for having poor classification accuracy of MODIS 1 and 2 image.

#### **3.5.1.1. Curvelet based fusion**

The overall methodology of the fusion of MODIS and ASTER image, through the curvelet based fusion is shown in the flowchart fig. 3.3, and the experimental results concern to it is deciphered in the following steps



**Fig. 3.16a.** Resultant curvelet based fused MOD12 image of d2

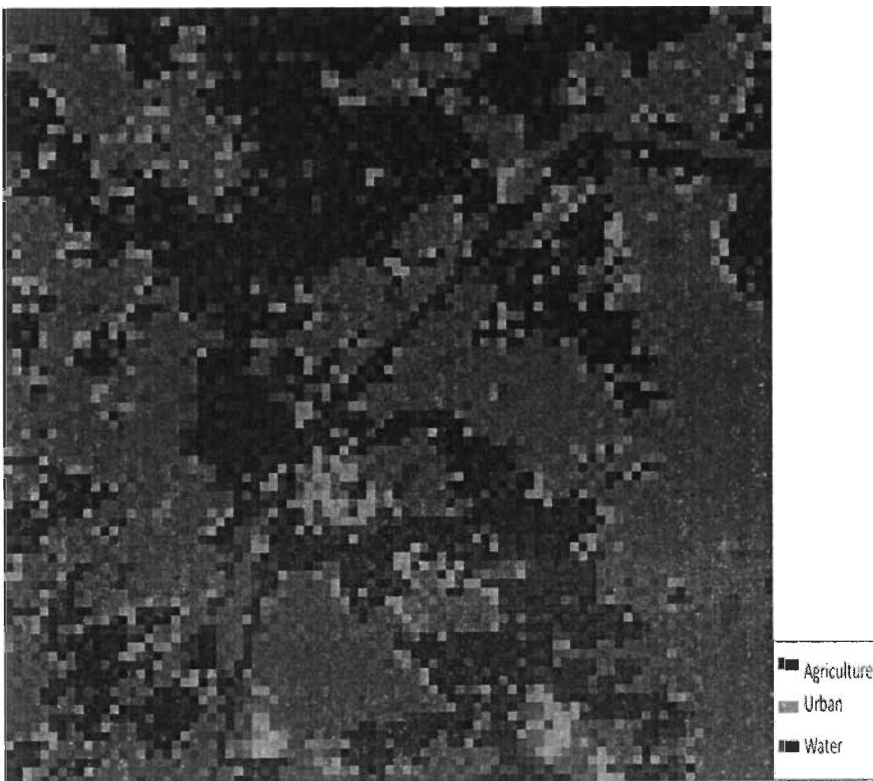


**Fig 3.16b.** Minimum distance classified of the resultant curvelet based fused MOD12 image of d2



**Fig. 3.17a.** Resultant curvelet based fused AST23 image of as l

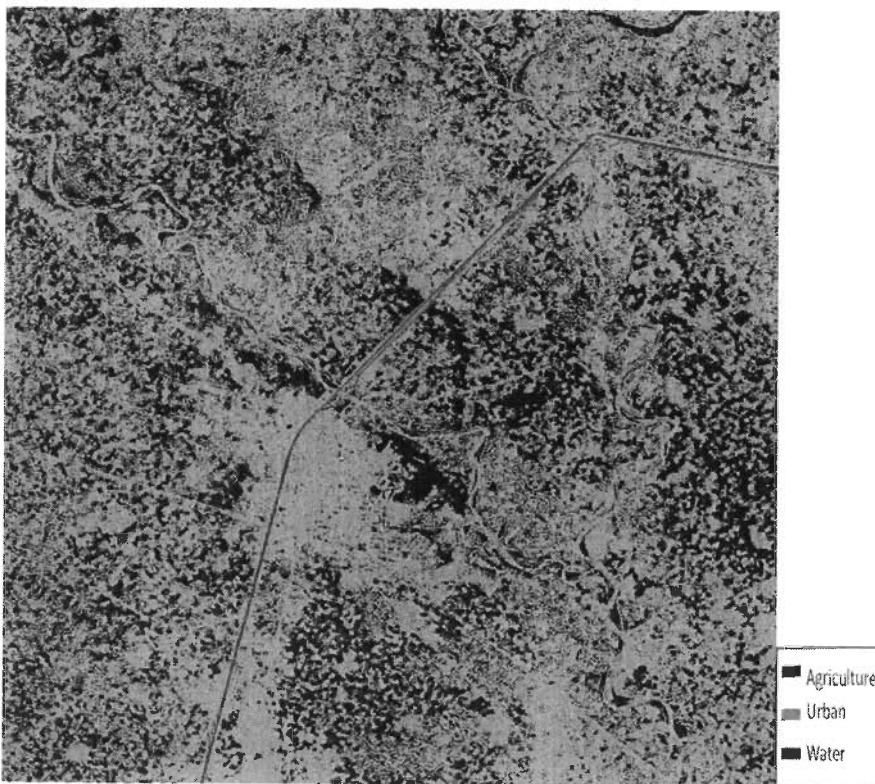


**Fig 3.17b.** Minimum distance classified of the resultant curvelet based fused AST23 image of as l

### **i. Fusion of MODIS band 1 and Band 2**

The resultant fused image of MODIS band 1 and band 2 of image d2 i.e., MOD12 is depicted in the fig. 3.16a, and MOD12 is classified by minimum distance classification technique and the minimum distance classified MOD12 is shown in the fig. 3.16b. It's classification accuracy is tabulated in the table 3.3 and its overall classification accuracy is 41.14%, and from the table 3.2, overall classification accuracy for MODIS band 1 and band 2 for d2 image is 34.06% and 52.17%.

### **ii. Fusion of ASTER band 2 and Band 3**

AST23, the resultant fused image of ASTER band 2 and band 3 is depicted in the fig. 3.17a, and it is classified by the application of minimum distance classification technique, and the minimum distance classified AST23 is shown in the fig. 3.17b, and it's classification accuracy is tabulated in the table 3.3, and it implies that the overall classification accuracy is 98.17%, and whereas the overall classification accuracy for ASTER band 2, ASTER band 3 is 72.02% and 98.73% respectively, and is tabulated in the table 3.2.

### **iii. Fusion of AST23 and MOD12**

The resultant fused image AST23 (fig. 3.17a) and MOD12 (fig. 3.16a, and it is interpolated to the size of ASTER. That is MOD12, is of size 87\*87, it is interpolated to the size of 1186\*1186, and it is depicted in the fig. 3.18a) is considered and it is fused by curvelet based transform, and the resultant fused image is AS\_MO and it is depicted in the fig. 3.18b and it is classified by the application of minimum distance classification technique, and the minimum distance classified AS\_MO is shown in the fig. 3.18c, and it's classification accuracy is tabulated in the table 3.3, and it implies that the overall classification accuracy is 54.81%, and whereas the overall classification accuracy for AST23 and MOD12 is 98.17% and 41.14% respectively.

It is observed that the resultant fused image i.e., AS\_MO has better accuracy than the MODIS image of band 1 and 2. It is also observed that the fused image has

enhanced the classification accuracy in comparison to MODIS band 1 image where as with MODIS band 2 it is moderately enhanced the classification accuracy. Overall as well as individual classification of each considered land cover has enhanced in the fused image.

### 3.5.1.2. Fuzzy based fusion

The overall methodology of the fusion of MODIS and ASTER image, through the fuzzy based fusion is shown in the flowchart fig. 3.7, and the experimental results concern to it is deciphered in the following steps



**Fig. 3.18a.** Interpolated resultant curvelet based fused MOD12 (1186\*1186) image of d2

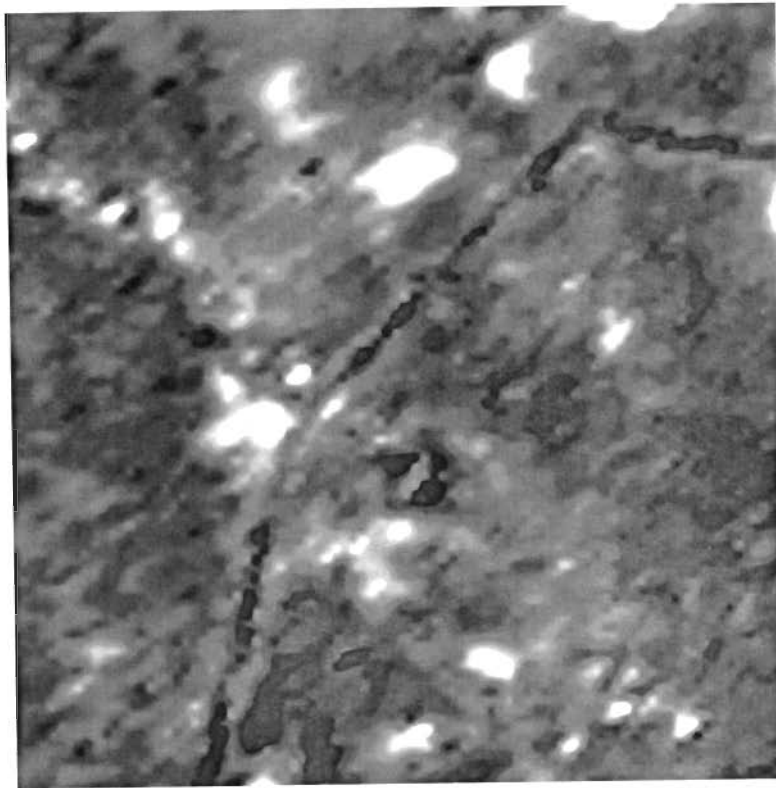


Fig. 3.18b. Resultant curvelet based fused AS\_MO

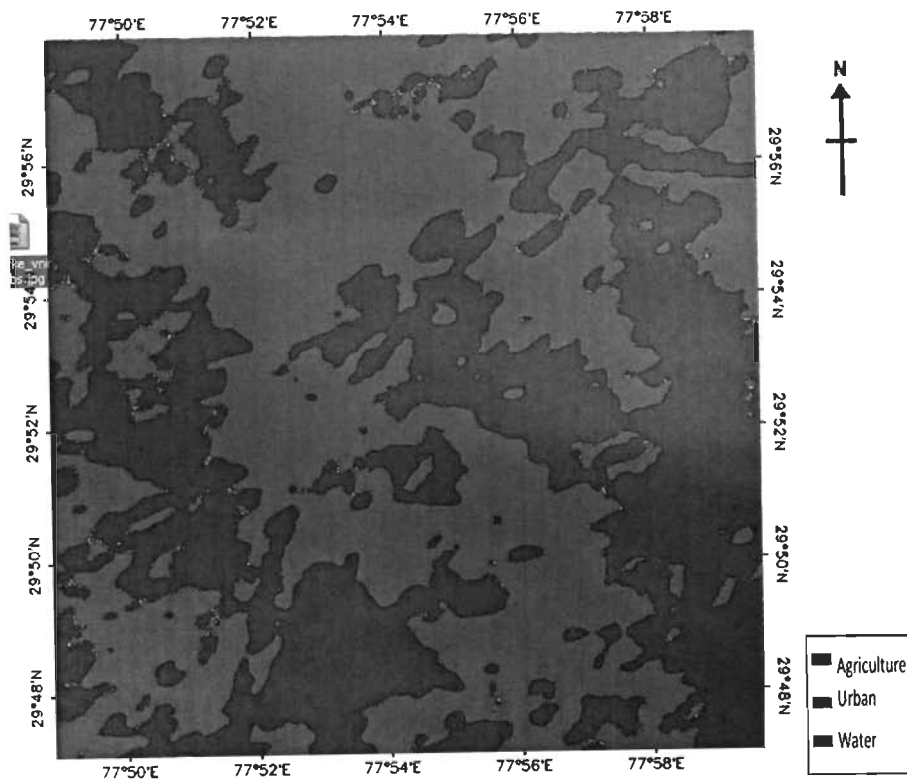


Fig. 3.18c. Minimum Distance classified of the resultant curvelet based fused AS\_MO

### **i. Fusion of MODIS band 1 and Band 2**

The resultant fuzzy based fused image of MODIS band 1 and band 2 of image d2 i.e., MOD12 is depicted in the fig. 3.19a, and MOD12 is classified by the application of minimum distance classification technique, and the minimum distance classified MOD12 is shown in the fig. 3.19b, and its classification accuracy is tabulated in the table 3.4, and it implies that the overall classification accuracy is 41.70, and whereas the overall classification accuracy for MODIS band 1, MODIS band 2 for d2 image is 34.06% and 52.17% is tabulated in the table 3.2.

### **ii. Fusion of ASTER band 2 and Band 3**

AST23, the resultant fuzzy based fused image of ASTER band 2 and band 3 is depicted in the fig. 3.20a, and it is classified by the application of minimum distance classification technique, and the minimum distance classified AST23 is shown in the fig. 3.20b, and its classification accuracy is tabulated in the table 3.4, and it implies that the overall classification accuracy is 96.89, and whereas the overall classification accuracy for ASTER band 2, ASTER band 3 is 72.02% and 98.73% respectively, and is tabulated in the table 3.2.

### **iii. Fusion of AST23 and MOD12**

The resultant fuzzy based fused image of AST23 (fig. 3.20a) and MOD12 (fig. 3.19a), and it is interpolated to the size of ASTER. That is MOD12, is of size 87\*87, it is interpolated to the size of 1186\*1186, and its depicted in the fig. 3.21a) is considered and it is fused and the resultant fused image is AS\_MO and its depicted in the fig. 3.21b, and it is classified by the application of minimum distance classification technique, and the minimum distance classified AS\_MO is shown in the fig. 3.21c, and its classification accuracy is tabulated in the table 3.4, and it implies that the overall classification accuracy is 85.71%, and whereas the overall classification accuracy for AST23 and MOD12 is 96.89% and 41.70% respectively.

The Resultant Fused image AS\_MO, has an enhancement of 51.65% overall

classification accuracy with respect to MODIS Band 1, and 33.54% overall classification accuracy with respect to MODIS Band 2. The Producers accuracy of fused Image has an increase of 89.02%, 23.5% and 28.04% of agriculture, urban and water classes respectively with respect to MODIS Band 1 and 24.42%, 55.76% and 31.19% of agriculture, urban and water classes with respect to MODIS Band 2. The Users accuracy of fused Image has been enhanced i.e., of 37.39%, 37.94% and 55.59% of agriculture, urban and water classes with respect to MODIS Band 1 and 33.92%, 40.86% and 40.38% of agriculture, urban and water classes with respect to MODIS Band 2.

It is observed in the classified images of MODIS Band 1, Band 2 and MOD12 (resultant MODIS Band 1 fused with MODIS band 2) and as well as the fused classified images of MODIS and ASTER image that it is difficult to classify the different major classes (agriculture, water and urban) accurately it may be due to the reason as MODIS images have quite low resolution as compared with ASTER image. A graph is plotted in the fig. 3.22, for the comparison of the classification accuracy of MODIS band 1, MODIS band 2, curvelet based fusion and fuzzy based fusion and also it infers from tables 3.2, 3.3 and 3.4 that the overall classification accuracy for the fused image (fuzzy and curvelet based) is better than the MODIS band 1 and band 2 and as well as with MOD12. It is also observed that the overall classification accuracy for the fuzzy based fusion is more than the curvelet based fusion.

**Table 3.4.** Classification Accuracy of fusion of MODIS (d2) and ASTER (as1) through fuzzy transform

Images	Users Accuracy			Producers Accuracy			Overall Classification Accuracy
	Agric ulture	Urban	Water	Agric ulture	Urban	Water	
<b>MOD12</b>	55.11	34.38	34.89	42.92	14.19	70.80	41.70
<b>AST23</b>	98.74	97.09	95.04	100.00	92.59	97.65	96.89
<b>AS_MO</b>	99.15	75.44	82.45	98.31	79.63	79.22	85.71





**Fig. 3.19a.** Resultant fuzzy based fused MOD12 image of d2

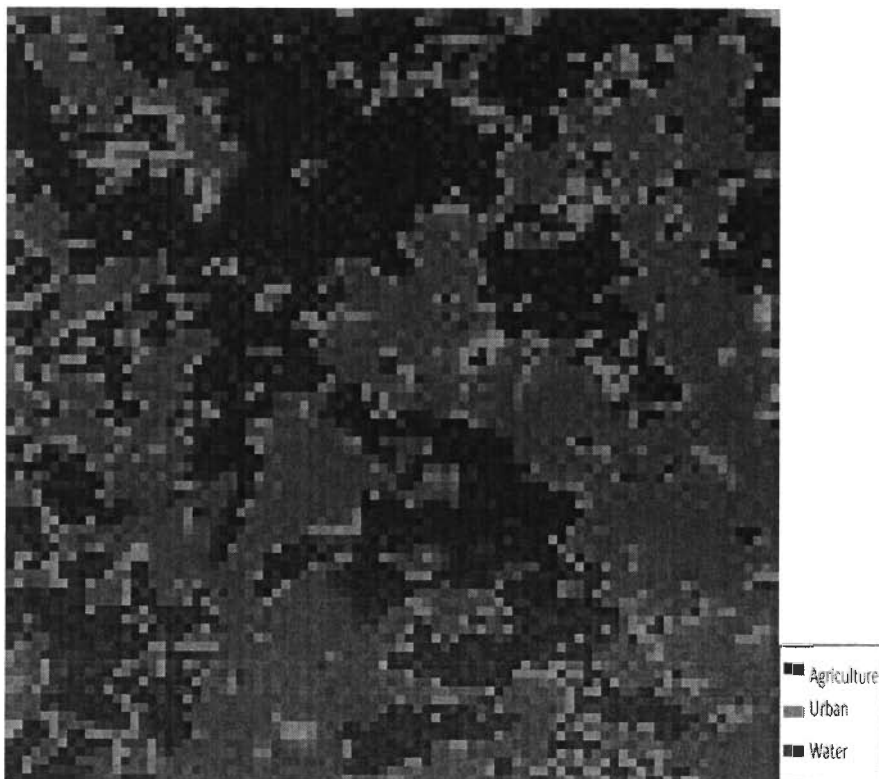


**Fig. 3.19b.** Minimum distance classified of the resultant fuzzy based fused MOD12 image of d2

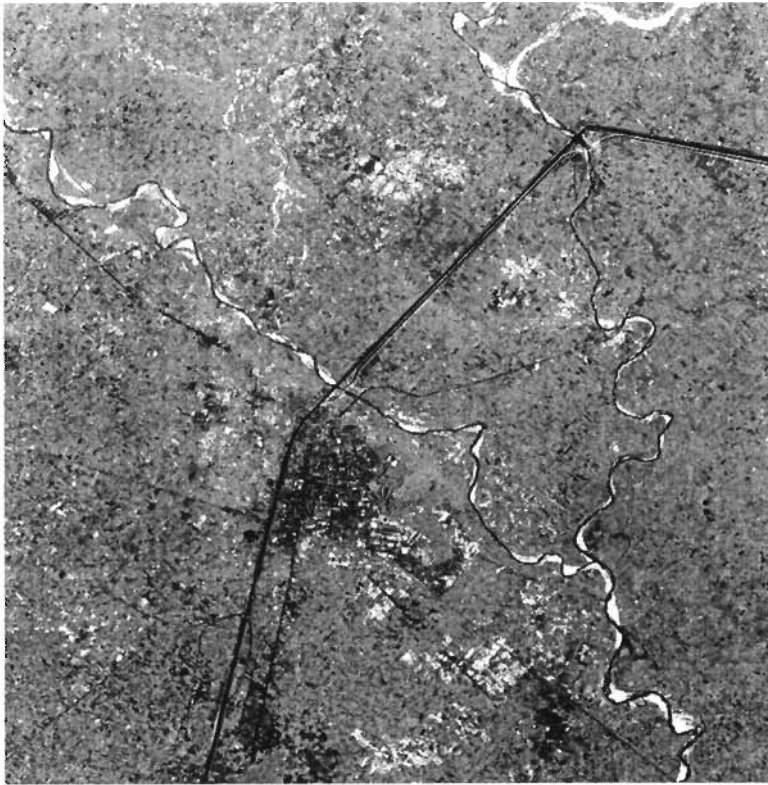


**Fig. 3.20a.** Resultant fuzzy based fused AST23 image of asl

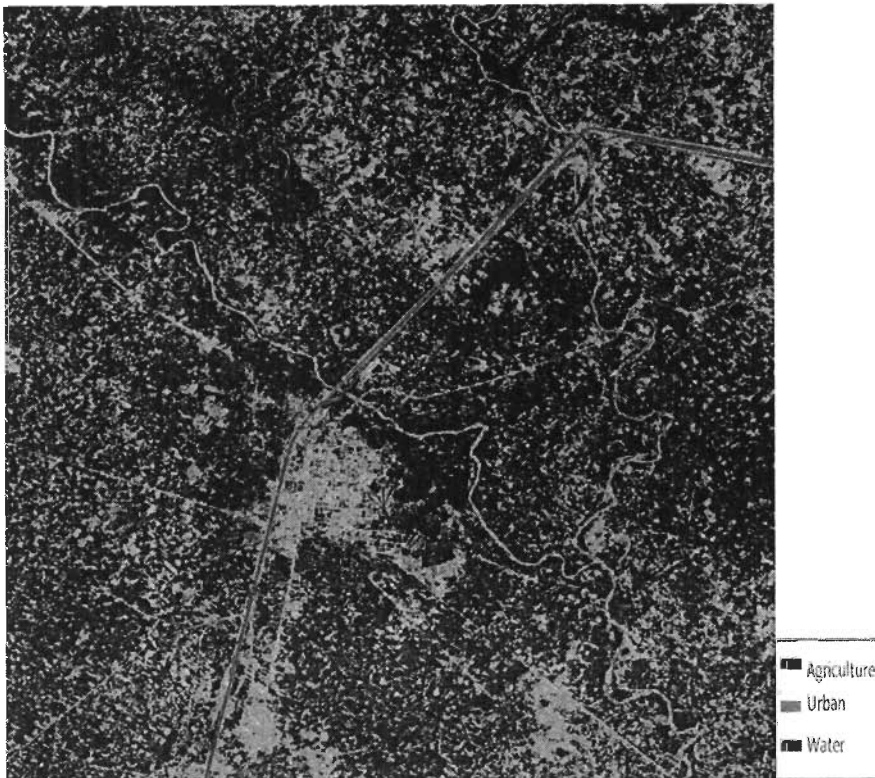


**Fig. 3.20b.** Minimum distance classified of the resultant fuzzy based fused AST23 image of asl

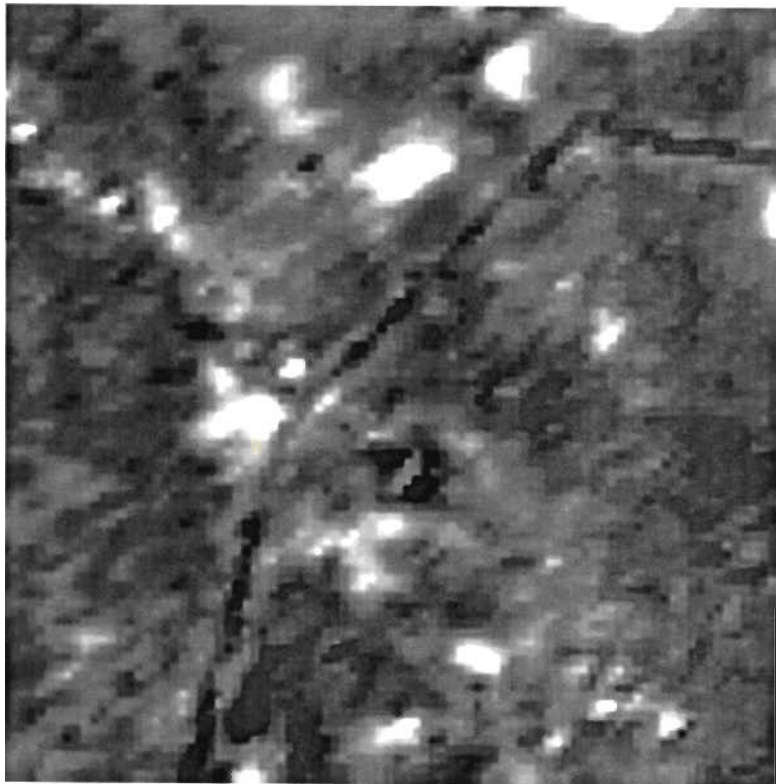


**Fig. 3.21a.** Interpolated resultant fuzzy based fused MOD12 (1186\*1186) image of d2

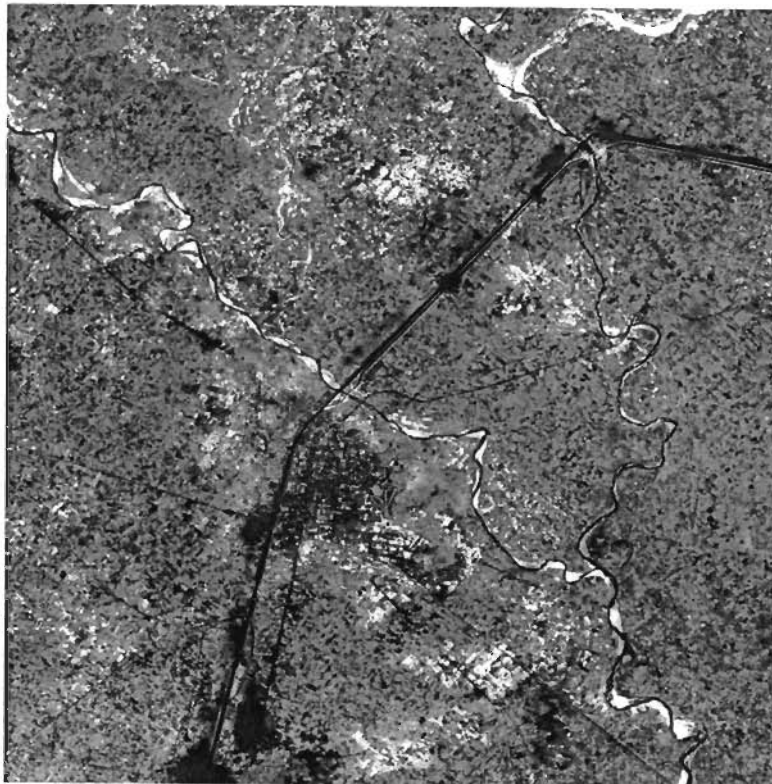


**Fig. 3.21b.** Resultant fuzzy based fused AS\_MO

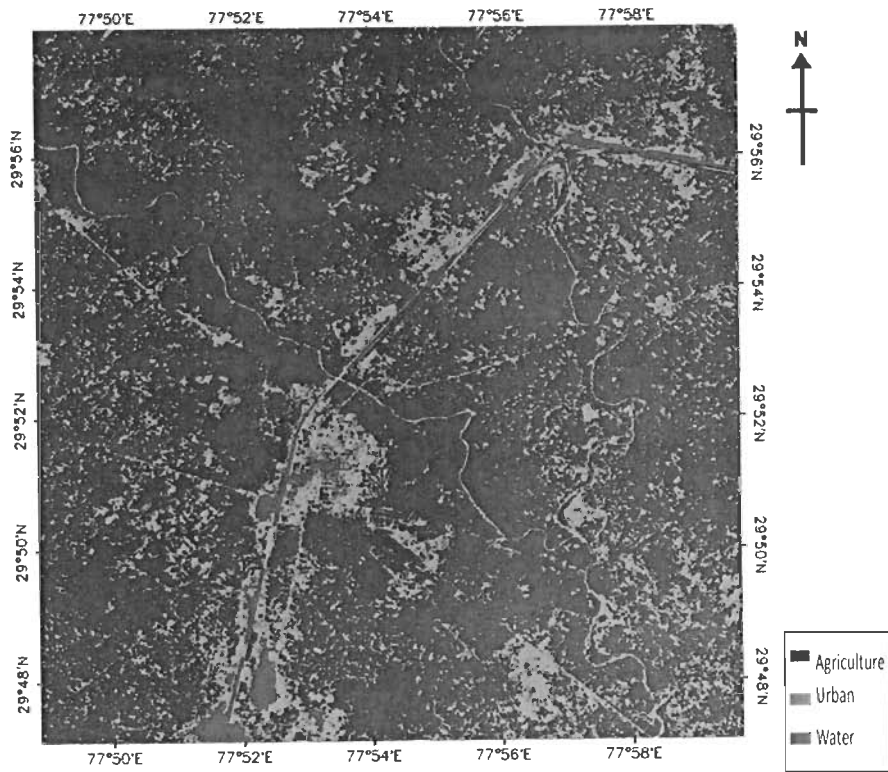


**Fig. 3.21c.** Minimum Distance classified of the resultant fuzzy based fused AS\_MO

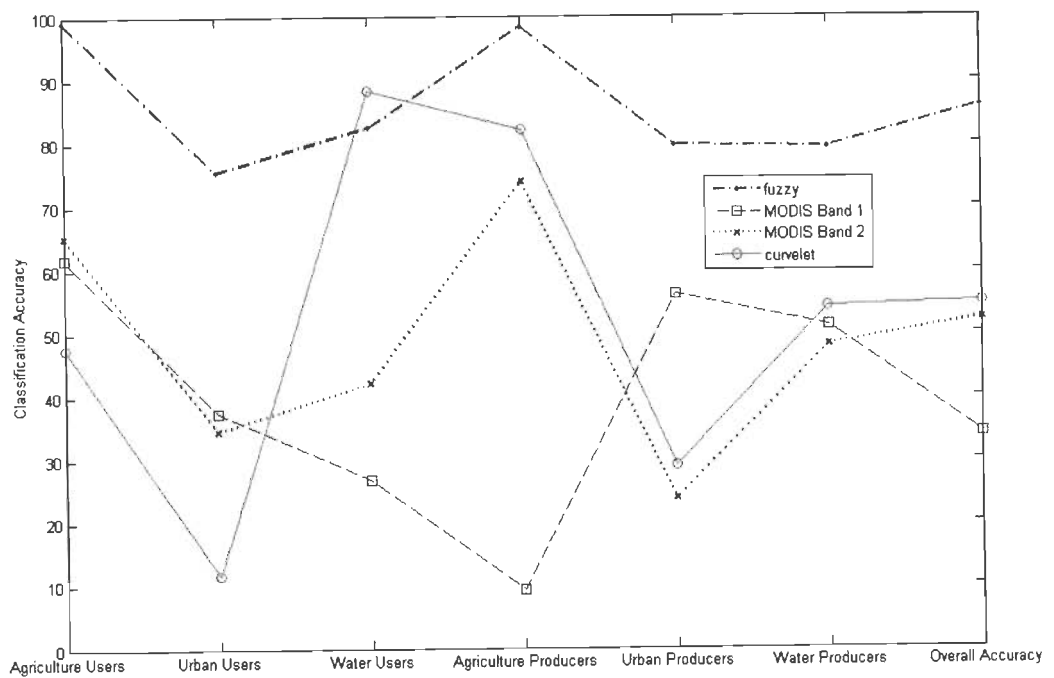


**Fig. 3.22.** Fuzzy vs Curvelet

### 3.5.1.3. Fusion coefficients

Eq. 3.24 indicates the computation of fusion coefficients, which is the average of the resultant fused image of AS\_MO\_d1 and AS\_MO\_d2. AS\_MO\_d1 and AS\_MO\_d2 has to be computed first as given in the section 3.5.1.1, the computation of AS\_MO\_d2 is shown in the fig. 3.18b. For the computation of AS\_MO\_d1, the MOD12 of image d1 has to be fused with the AST23 image. The MOD12 of image d1 is shown in the fig. 3.23a, and its minimum distance classified image is shown in the fig. 3.23b, and its classification accuracy is tabulated in the table 3.5, and it implies that the overall classification accuracy is 44.40%, and whereas the overall classification accuracy for MODIS band 1, MODIS band 2 for d1 image is 34.06% and 52.17%. The MOD12 (fig. 3.23a, and it is interpolated to the size of ASTER. i.e., MOD12, is of size 87\*87, it is interpolated to the size of 1186\*1186), is fused with AST23 (fig. 3.17a), and their resultant fused image is AS\_MO\_d1, and its depicted in the fig. 3.24a, and it is classified by the application of minimum distance classification technique, and the minimum distance classified AS\_MO\_d1 is shown in the fig. 3.24b, and it's classification accuracy is tabulated in the table 3.5, and it implies that the overall classification accuracy is 56.23%, and whereas the overall classification accuracy for AST23 and MOD12 is 98.17% and 44.40% respectively.

The resultant fused image AS\_MO\_d1, has an enhancement of 22.17% overall classification accuracy with respect to MODIS Band 1, and 4.06% overall classification accuracy with respect to MODIS Band 2. The producers accuracy of fused image has an increase of 76.24% and 2.15% of agriculture and water classes with respect to MODIS Band 1 and 11.64%, 3.91% and 5.3% of agriculture, urban and water classes with respect to MODIS Band 2. The users accuracy of Fused Image has an enhancement of 8.52% and 28.65% of agriculture and water classes with respect to MODIS Band 1 and 5.05% and 13.44% of agriculture and water classes with respect to MODIS Band 2.

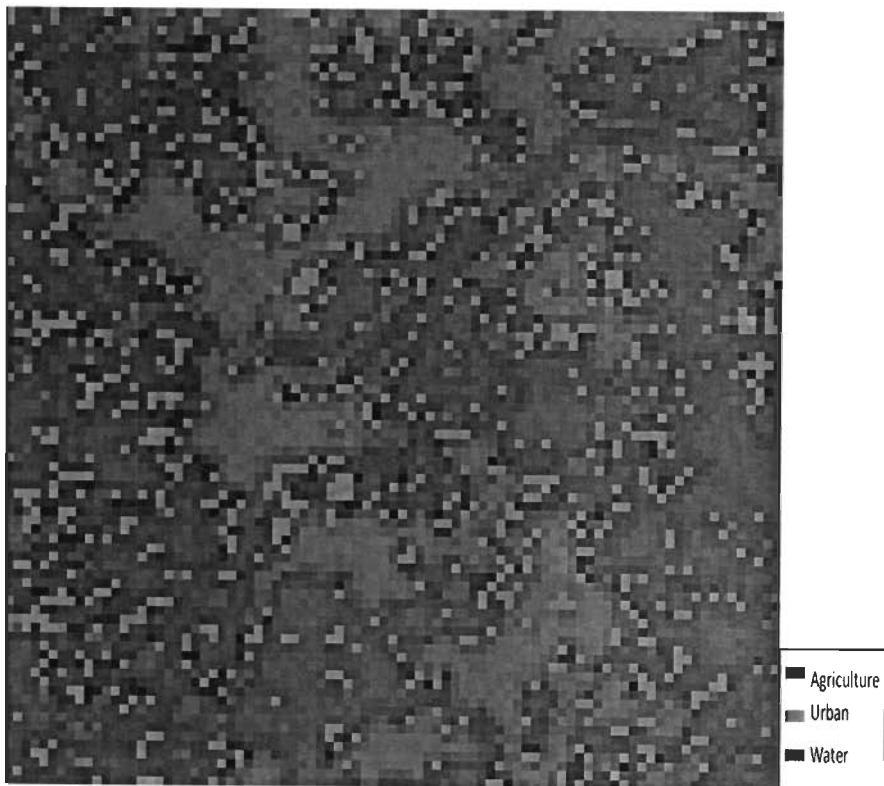
Once the AS\_MO\_d1 and AS\_MO\_d2 are computed, the fusion coefficients is computed by eq. 3.24, and the resultant fusion coefficient is shown in the fig. 3.25. Once the fusion coefficients is computed, it is again fused with the MODIS image d1 and d2, and its corresponding classification accuracy is computed. The resultant fused

image AST\_avg\_d1, of the fusion of fusion coefficients with MODIS d1 image, is shown in the fig. 3.26a, and its minimum distance classified image is shown in the fig. 3.26b, and their classification accuracy is tabulated in the table 3.7.

Similarly, image d2, is fused with fusion coefficients, and resultant fused image AST\_avg\_d2 is shown in the fig. 3.27a, and its minimum distance classified image is shown in the fig. 3.27b, and their classification accuracy is tabulated in the table 3.7.



**Fig. 3.23a.** Resultant curvelet based fused MOD12 of image d1



**Fig. 3.23b.** Minimum distance classified of the resultant curvelet based fused MOD12 of image d1

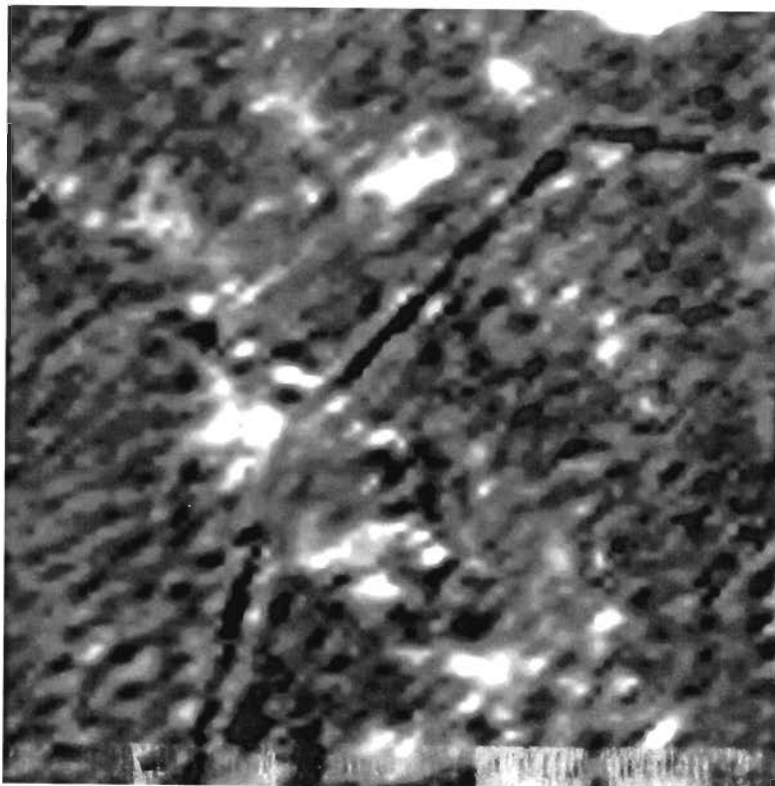


**Fig. 3.24a.** Resultant curvelet based fused AS\_MO of image d1

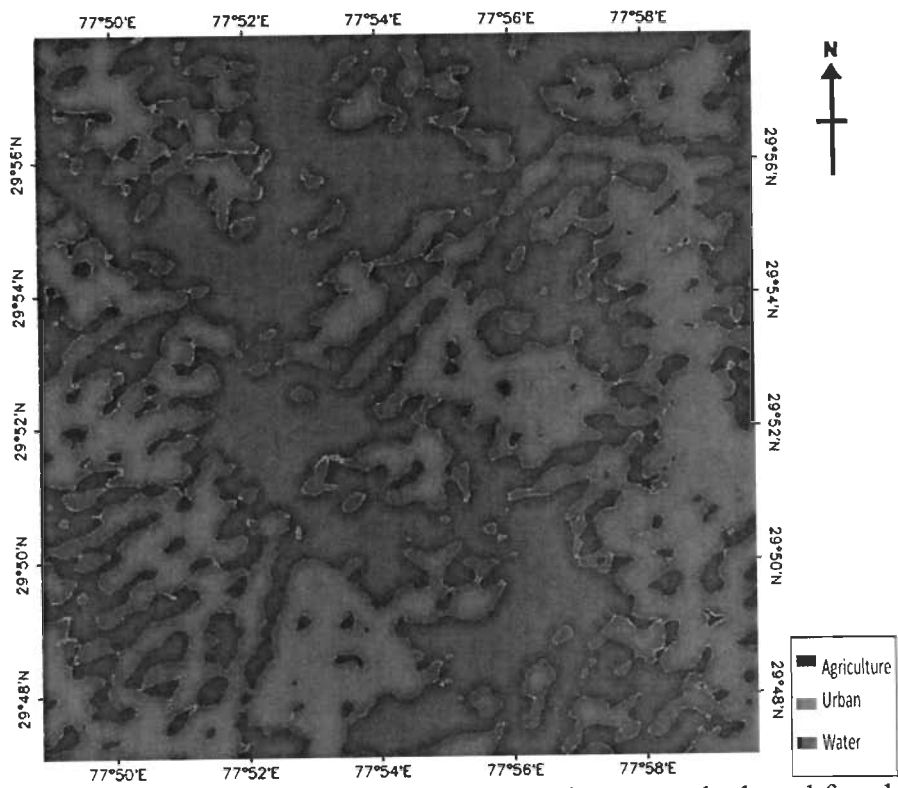


**Fig. 3.24b.** Minimum distance classified of the resultant curvelet based fused AS\_MO of image d1

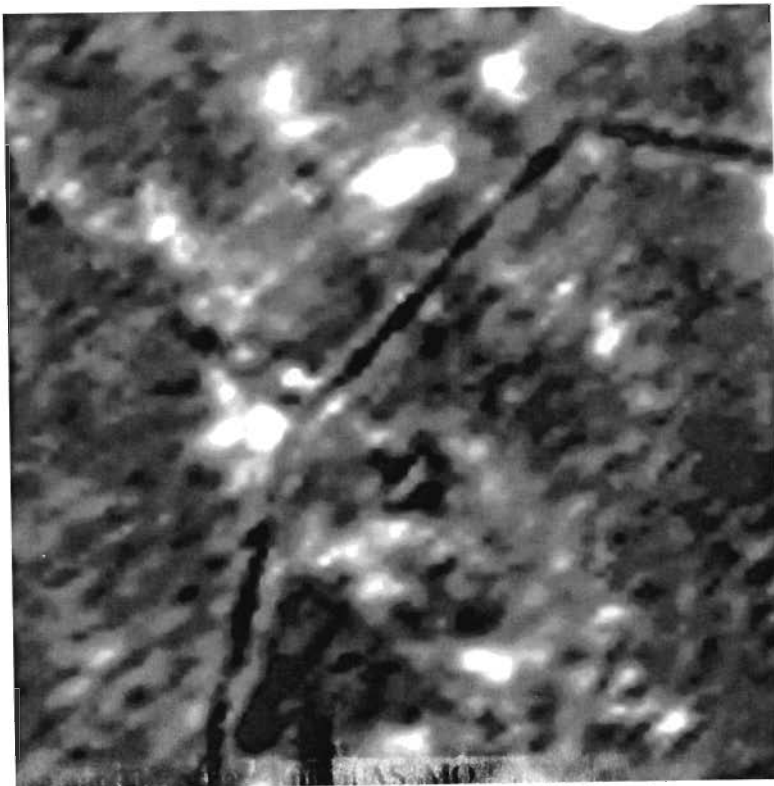


**Fig. 3.25.** AST\_avg (fusion coefficients)



**Table 3.5.** Classification Accuracy of fusion of MODIS image d1 and ASTER through curvelet transform

Image id	Images	Users Accuracy			Producers Accuracy			Overall Classification Accuracy
		Agriculture	Urban	Water	Agriculture	Urban	Water	
d1	MODIS band 1	61.76	37.50	26.86	9.29	56.13	51.18	34.06
	MODIS band 2	65.23	34.58	42.07	73.89	23.87	48.03	52.17
	MOD12	57.08	26.51	38.43	55.31	14.19	60.58	44.40
	AS_MO	70.28	34.29	55.51	85.53	27.78	53.33	56.23

A different year is considered for testing the fusion coefficients, that is the MODIS d3 (i.e., year 2009) image is fused with the ASTER image and also with the fusion coefficients. The MOD12 of image d3 is shown in the fig. 3.28a, and its minimum distance classified image is shown in the fig. 3.28b. Its classification accuracy is tabulated in the table 3.6 which implies that the overall classification accuracy is 42.77%, and whereas the overall classification accuracy for MODIS band 1, MODIS band 2 for d3 image is 38.65% and 52.53%. MOD12 of image d3 is fused with AST23 (fig. 3.17a) which resultant fused image is AS\_MO\_d3 (fig. 3.29a). It is classified by the application of minimum distance classification technique and the minimum distance classified AS\_MO\_d3 is shown in the fig. 3.29b. Its classification accuracy is tabulated in the table 3.6 which implies that the overall classification accuracy is 55.52% whereas the overall classification accuracy for AST23 and MOD12 is 98.17% and 42.77% respectively.

Simultaneously the MODIS image d3 is also fused with the fusion coefficients and resultant fused image AST\_avg\_d3 is shown in the fig. 3.30a, and its minimum distance classified image is shown in the fig. 3.30b, and their classification accuracy is tabulated in the table 3.7.

Fig. 3.31 shows the graph implying the classification accuracy of fused MODIS image d1, d2 and d3 with ASTER image in one hand in another hand it is fused with AST\_avg (fusion coefficients). The classification accuracy obtained by both approaches of fusion (i.e., directly with ASTER and ASTER\_avg) is quite encouraging which focus that the proposed methodology of fusion coefficient may be

used in near future for analyzing time series MODIS image. The proposed methodology may reduce the computational complexity because we have to compute only once the fusion coefficient and after that this coefficient may be useful for fusion with MODIS image for year to year for the month March.

**Table 3.6.** Classification Accuracy of fusion of MODIS image d3 and ASTER through curvelet transform

Image id	Images	Users Accuracy			Producers Accuracy			Overall Classification Accuracy
		Agric ulture	Urban	Water	Agric ulture	Urban	Water	
d3	MODIS band 1	55.41	36.85	37.12	33.63	55.16	28.88	38.65
	MODIS band 2	63.68	42.15	36.10	73.23	39.36	33.14	52.53
	MOD12	54.49	32.49	34.73	54.87	10.32	60.21	42.77
	AS_MO	58.97	22.99	71.88	83.83	28.48	53.73	55.52

**Table 3.7.** Classification Accuracy

Image id	Images	Users Accuracy			Producers Accuracy			Overall Classification Accuracy
		Agric ulture	Urban	Water	Agric ulture	Urban	Water	
d1	AS_MO_d1	70.28	34.29	55.51	85.53	27.78	53.33	56.23
	AST_avg_d1	70.03	34.29	55.33	85.53	27.78	52.94	56.09
d2	AS_MO_d2	47.65	11.69	88.24	82.13	29.17	54.12	54.81
	AST_avg_d2	66.10	29.56	52.78	82.98	21.76	52.16	53.12
d3	AS_MO_d3	58.96	22.99	71.87	83.83	28.47	53.72	55.52
	AST_avg_d3	56.87	20.62	70.51	82.55	25.46	53.14	53.96

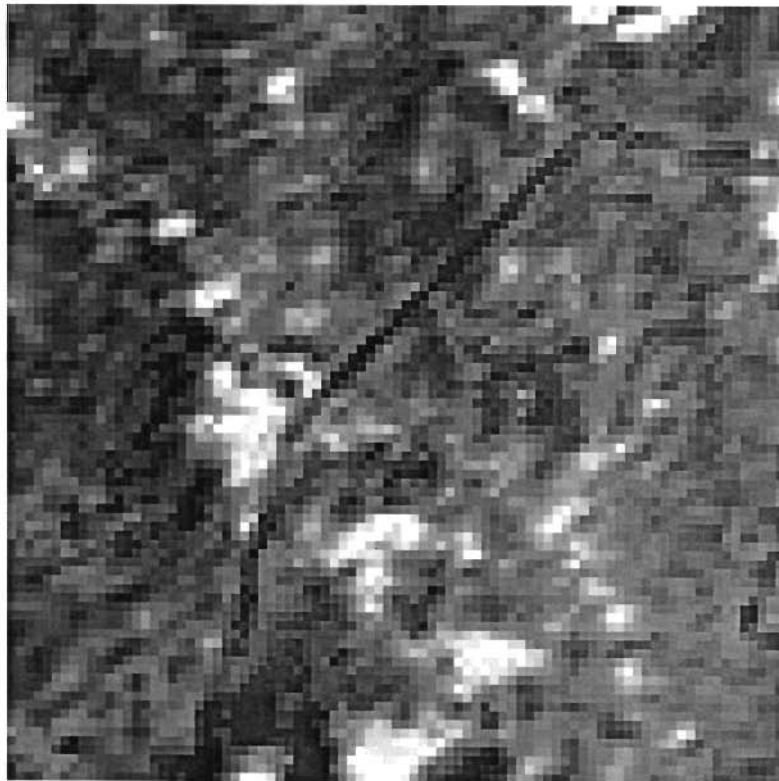


Fig. 3.26a. AST\_avg curvelet based fused with MOD12 of image d1 (i.e., AST\_avg\_d1)

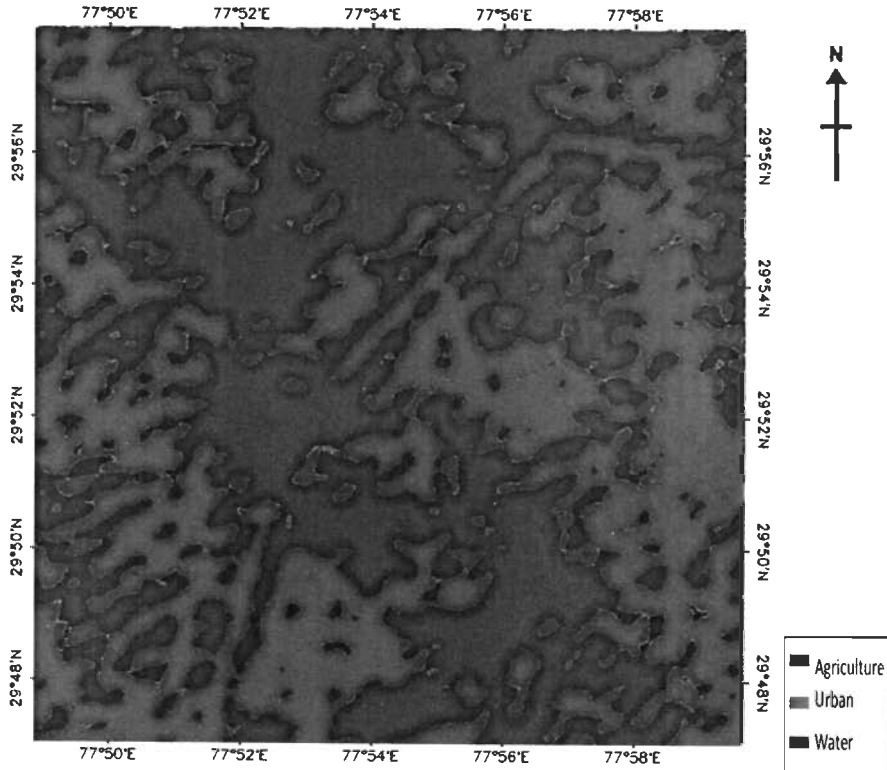
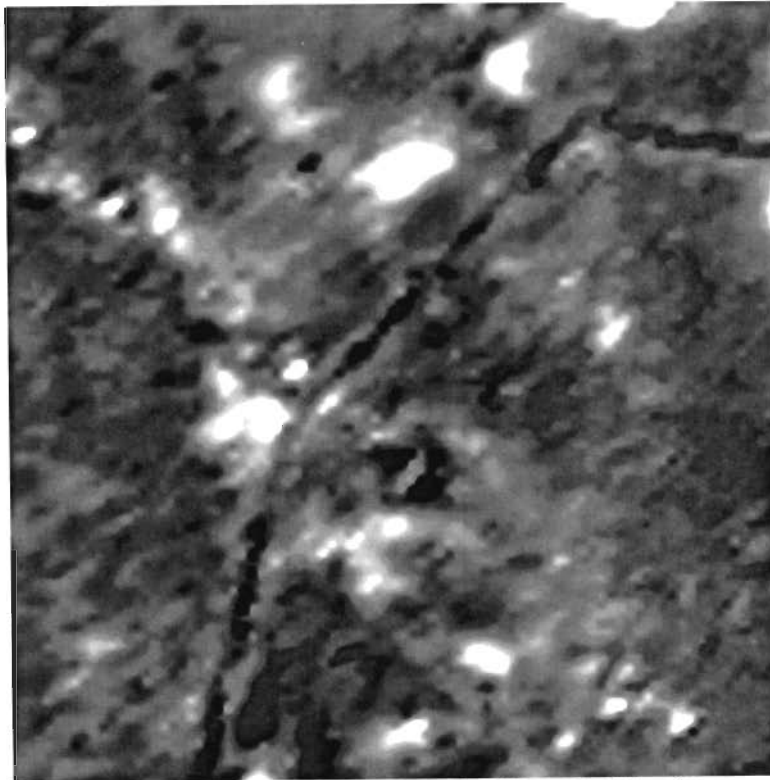
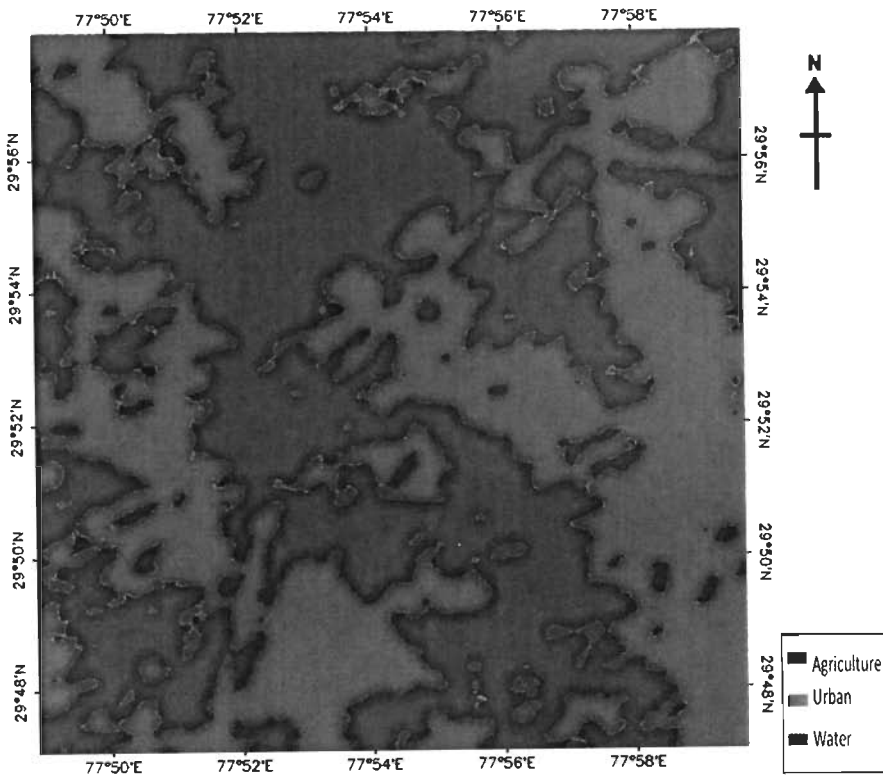


Fig. 3.26b. Minimum distance classified AST\_avg\_d1



**Fig. 3.27a.** AST\_avg curvelet based fused with MOD12 of image d2 (i.e., AST\_avg\_d2)



**Fig. 3.27b.** Minimum distance classified AST\_avg\_d2

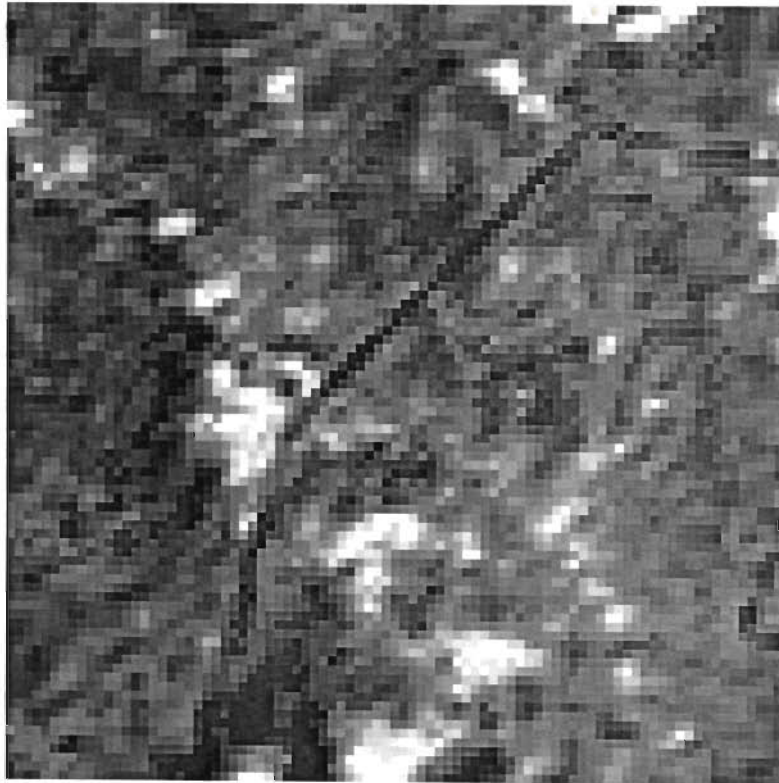


**Fig. 3.28a.** Resultant curvelet based MOD12 of image d3

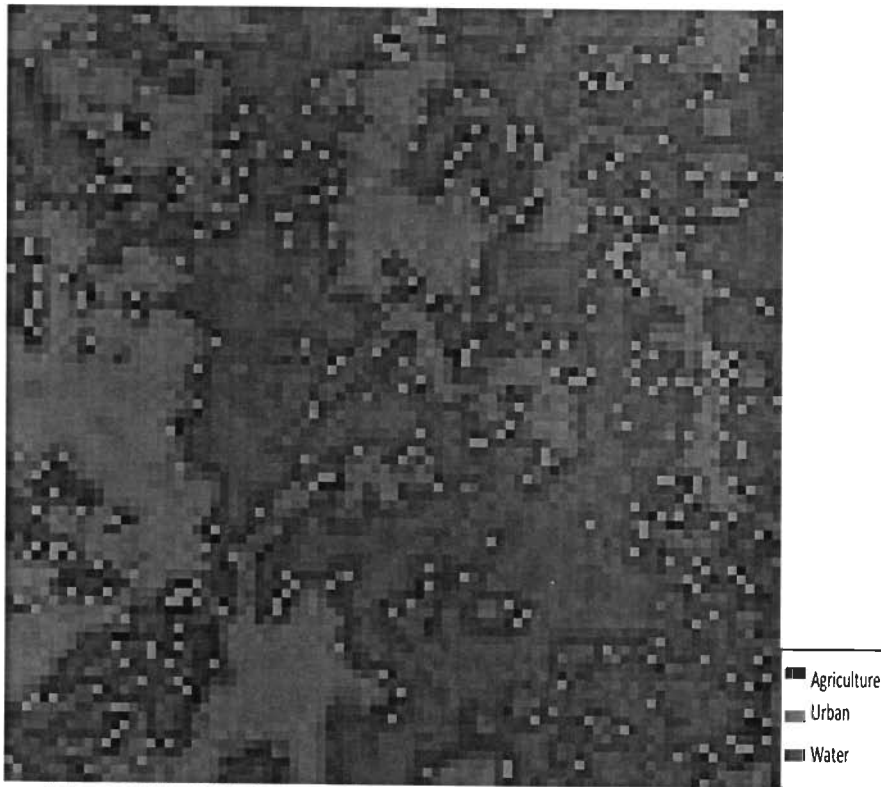


**Fig. 3.28b.** Minimum distance classified MOD12 of image d3

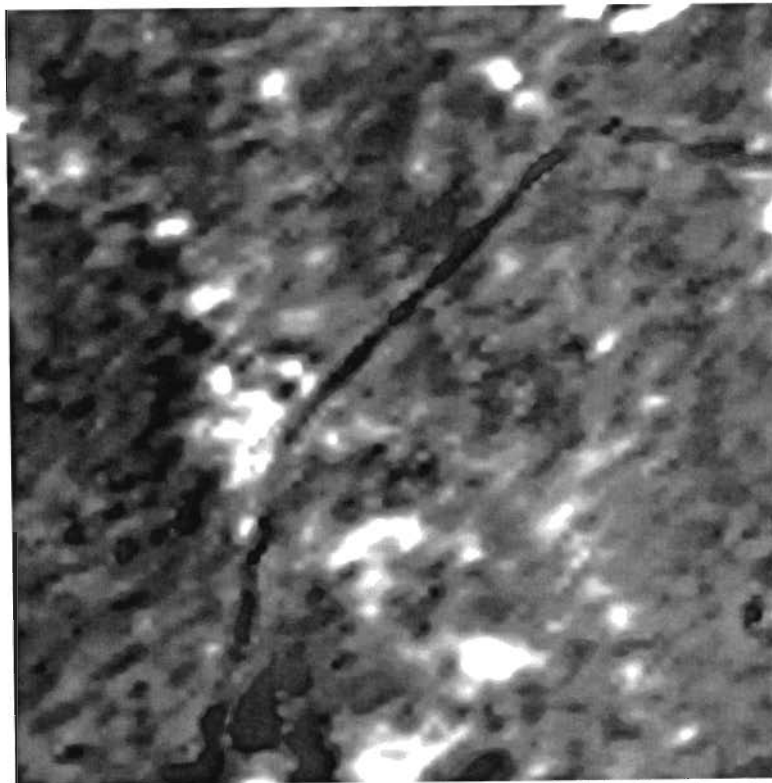


**Fig. 3.39a.** AS\_MO of image d3 (i.e., MOD12 of d3 is fused with AST23)

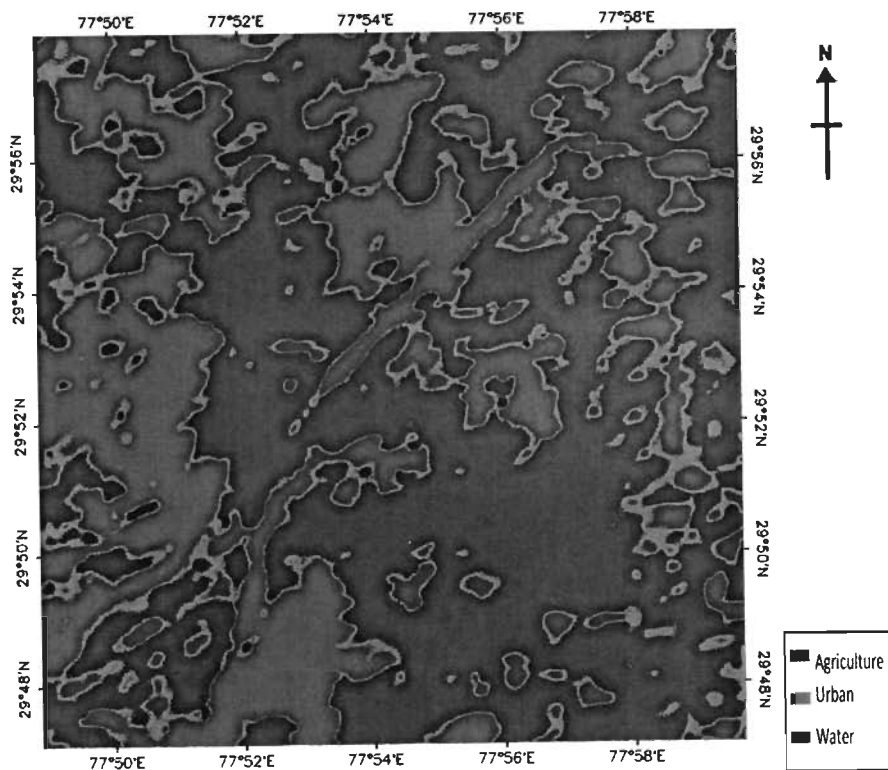


**Fig. 3.29b.** Minimum distance classified AS\_MO of image d3

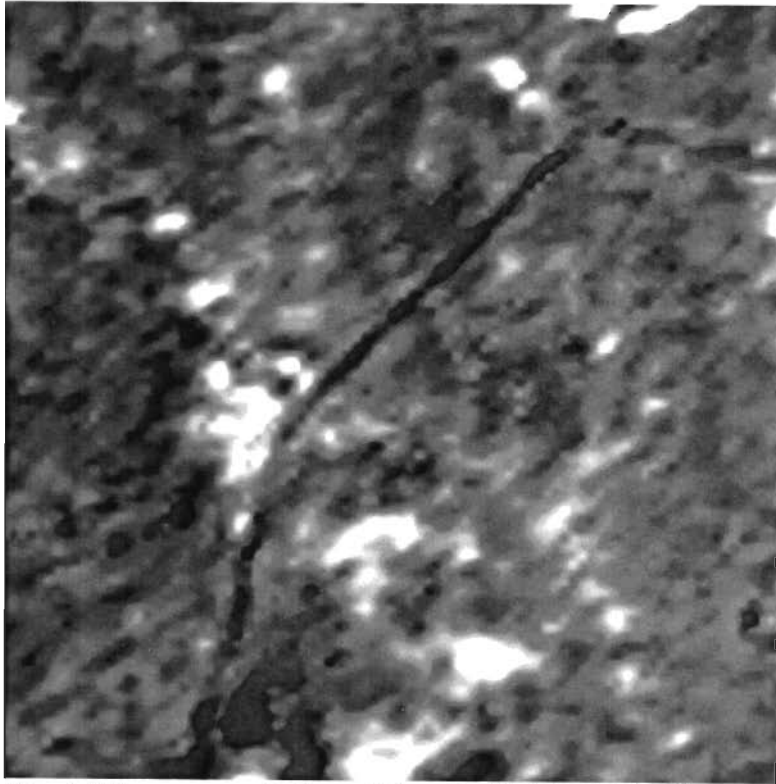


**Fig. 3.30a.** AST\_avg curvelet based fused with MOD12 of image d3 (i.e., AST\_avg\_d3)

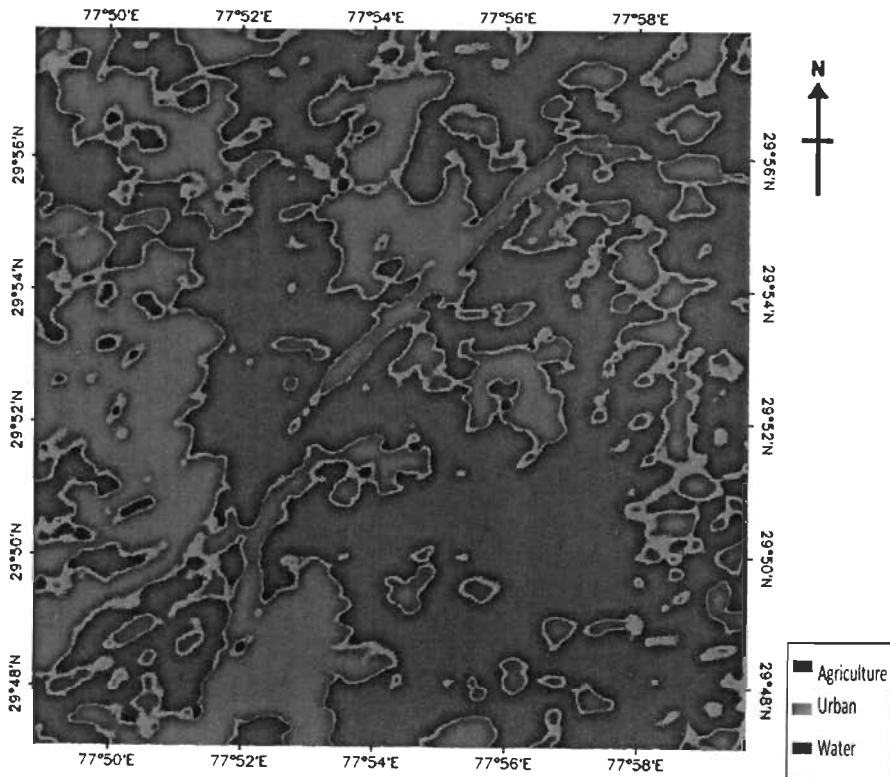


**Fig. 3.30b.** Minimum distance classified AST\_avg\_d3

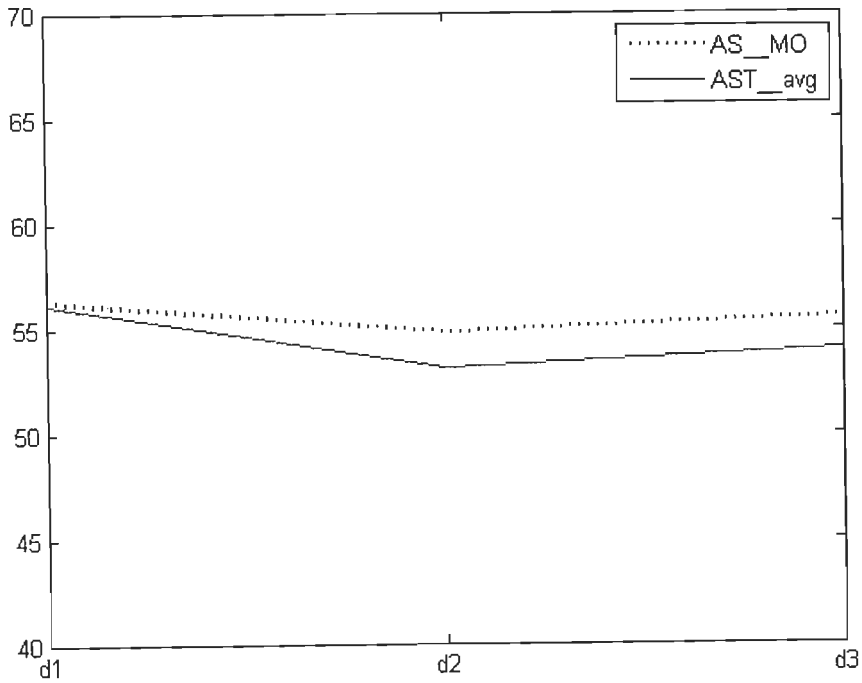


**Fig. 3.31.** Graph implying the classification accuracy of fused MODIS image with ASTER image and MODIS image with AST\_avg (fusion coefficients)

**Table 3.8.** Quality assessment indicators for fused images with respect to MOD12

	MOD12						
	Corr	RMSE	RMD	RVD	DI	PSNR	UQI
AS_MO d1	0.9656	49.6871	-1.4090e-004	0.1129	0.0523	14.2059	5.0348e-005
AS_MO d2	0.9805	34.9941	-2.2529e-004	0.0615	0.0280	17.2509	6.0104e-005
AS_MO d3	0.9780	27.5457	-2.0349e-004	0.0681	0.0219	19.3297	1.0889e-004
AST_av g d1	0.9657	49.6473	-1.4090e-004	0.1128	0.0522	14.2129	5.0359e-005
AST_av g d2	0.9806	34.9365	-2.2529e-004	0.0614	0.0279	17.2652	6.0119e-005
AST_av g d3	0.9779	27.5776	-2.0349e-004	0.0683	0.0220	19.3197	1.0887e-004



### 3.5.2. Quality assessment

The correlation coefficient, RMSE, RMD, RVD, DI, PSNR and UQI is computed as by the eq. 3.14, 3.15, 3.16, 3.17, 3.18, 3.19 and 3.20 respectively. These quality assessment indicators have been calculated for the fused images with respect to ASTER and fusion Coefficients. In Table 3.8 the quality assessment indicators are tabulated for the fused images AS\_MO\_d1, AS\_MO\_d2, AS\_MO\_d3, AST\_avg\_d1, AST\_avg\_d2 and AST\_avg\_d3 with respect to the MOD12 of the corresponding MODIS image i.e., for the AS\_MO\_d1, and AST\_avg\_d1 the quality assessment indicators are calculated with respect to the MODIS image d1 and similarly with respect to MODIS image d2 and image d3 the quality assessment indicators are calculated for AS\_MO\_d2, AS\_MO\_d3, AST\_avg\_d2 and AST\_avg\_d3 respectively. From the table 3.8 it clearly points out that there exists a high closeness between MOD12 of image d1 and AS\_MO\_d1, AST\_avg\_d1. Similarly there exists a higher closeness of MOD12 of image d2 and AS\_MO\_d2, AST\_avg\_d2 and also there exists a higher closeness of MOD12 of image d3 and AS\_MO\_d3, AST\_avg\_d3. Similarly, for the quality assessment indicators RMSE, RMD, RVD, DI, PSNR and UQI also implies that there doesn't exist more differences for the fused images of AS\_MO\_d1, AST\_avg\_d1 for the image d1 and for the fused images of AS\_MO\_d2, AST\_avg\_d2 for the image d2 and also for the fused images of AS\_MO\_d3, AST\_avg\_d3 for the image d3. Approximately the value of different quality indicators are same once we are computing these indicators with respect to AS\_MO with MOD12 and AST\_avg with MOD12. It infers that fusion coefficients may be alternative choice for reducing the computational complexity of the fusion processing for classification purpose.

### 3.6. Conclusion

A methodology for the enhancement of overall classification accuracy for the MODIS image is presented in one hand and in another hand a fusion coefficient is derived which reduces the computation complexity. The high resolution image (i.e., ASTER) is fused with low or moderate resolution image (i.e., MODIS) and the resultant fused image is analyzed in the viewpoint of land cover classification through the curvelet

based and fuzzy based fusion. The classification accuracy implies that the overall classification accuracy for the fuzzy based fusion is more than the curvelet based fusion, and also it points that the overall classification accuracy for the fused image is better than the MODIS band 1 and MODIS band 2. We have also attempted to obtain a fusion coefficient for the particular month (i.e., March) that may be useful for the further years. By this we can avoid to purchase the ASTER image or higher resolution every year. We have found that fusion coefficient may be obtained and that may be quite useful for the fusion of MODIS image. The new fusion coefficient is validated with respect to classification accuracy and quality assessment indicators (Correlation Coefficient, Root Mean squared error, Relative Mean Difference, Relative Variation Difference, Deviation Index, Peak signal-to-noise ratio (PSNR), Universal Image Quality Index). It implies the proposed methodology with fusion coefficient may be used to develop a land cover monitoring system with MODIS image (because it is free and temporal acquisition is high).

## Chapter 4

# Optical (MODIS) and Radar (PALSAR) Image Fusion for Land Cover Classification

---

In the previous chapter, analysis of fusion of optical images for land cover classification was dealt. In this chapter, analysis of fusion of optical and radar images in the viewpoint of land cover classification is carried out. For this purpose, we have considered the MODIS and PALSAR (Phased Array Type L-band SAR) images. Likewise the previous chapter, the fusion methodologies i.e., curvelet and fuzzy based fusion techniques are used in one hand and in another hand, Quality assessment indicators have been computed, in order to assess the quality of the fused image. Thereby we have attempted to analyze the fusion of optical and radar images, along with the inspection of the resultant fused image in terms of classification accuracy.

## 4.1. Introduction

Recent development in land-cover classification of satellite images was to a great extent driven by the increased availability of data from different, often complementary, sensors and sources. Richards, 2005 mentions the trend of enhanced numbers of bands and spectral resolution for optical sensors as well as the availability of multidimensional synthetic aperture radar (SAR) image at different wavelengths, polarizations, and incident angles as driving factors for the generation of land cover classification for understanding the actual status of various land cover classes. Land cover mapping using satellite imagery has a lot of advantages such as low cost, large area coverage, repetitively, and computability over the traditional mapping approaches like terrestrial survey and basic aerial photo interpretation which is well known fact nowadays.

Satellite remote sensors can be divided into two major types of imaging systems: optical and radar imaging systems. These two sensor types are very different in terms of the wavelength of their electromagnetic energy, sensor structure, and image product (Brisco and Brown, 1995, Harris et al., 1990, Raghavawamy et al., 1996, Welch and Ehlers, 1988), and the advantage of fusing optical and radar is explained in the section 1.1, and its literature survey is dealt in the section 2.5.

In this chapter, analysis of land cover classification is dealt after the fusion of optical and radar images. The curvelet and fuzzy based techniques have been used for fusion as discussed in the previous chapter 3. This chapter is structured as follows: image used for the study has been discussed in section 4.2. Section 4.3 briefly reviews the curvelet based fusion and fuzzy based fusion, as well as the quality assessment indicators for optical and radar images. Implementation and results of the used approach is given in section 4.4. In the subsequent section, i.e., in section 4.5 analysis of experimental results are carried out and finally this chapter is concluded in the section 4.6.

## **4.2. Data Used/Study Area**

Roorkee Region as discussed in the section 1.3.1 is considered for the fusion of optical and radar images. The MOD09Q1 product of the MODIS image is considered and whose details are given in the section 1.4.1a. In this chapter, the MODIS product MOD09Q1 of April 7<sup>th</sup> 2009 is used. The MODIS Band 1 and Band 2 are considered as these bands have special features to identify the agriculture and other land covers and radar image and PALSAR product L1.0 CEOS which is acquired on 6<sup>th</sup> April 2009 is used for fusion purpose. The PALSAR image has the incidence angle of 21.5<sup>0</sup> and approximately 30m resolution and details are give in section 1.4.1c.

## **4.3. Theoretical Basis**

### **4.3.1. Curvelet transform based Fusion**

The main feature of the curvelet transform is that it is sensitive to directional boundaries and capable of representing the highpass details of object contours at different scales through few sparse nonzero coefficients (Stark et al. 2002). The different steps which is used for Curvelet fusion is discussed in the section 3.3.1, and fig. 3.1 depicts the flow chart of Curvelet Transform.

### **4.3.2. Fuzzy based Fusion**

Fuzzy logic is a powerful problem-solving methodology with a myriad of applications in information processing (Tizhoosh and Haußecker, 2000). Fuzzy provides a remarkably simple way to draw definite conclusions from vague, ambiguous or imprecise information. In a sense, fuzzy logic resembles human decision making with its ability to work from approximate data and find precise solutions. The detailed descriptions of the fuzzy approach is elucidated in the section 3.3.2.

### **4.3.3. Quality assessment indicators**

In order to assess the quality of the fused product some quantitative assessment criteria have been defined by comparing the fused product and the low spatial resolution multispectral images (Wald et al., 1997). A series of indicators have been used for this purpose, and is thoroughly reviewed in the section 3.3.3.

## **4.4. Implementation and Results:**

The raw MODIS image is initially geo-referenced and the raw PALSAR image are also geo-referenced. The Wishart Gamma Map Filter is a polarimetric filter which is suitable for polarimetric image to remove the speckles. It performs well in the presence of regular texture and moderate relief. The filter operates under the assumption of target reciprocity (i.e.,  $HV=VH$ ) (SARSCAPE help document). This filter has ability of preserving polarimetric information after removing the speckle (Nezry and Yakam-Simen 1999). Hence, for the PALSAR image Wishart Gamma Map Filter is applied and three filtered images are obtained (HH, HV and VV). Consequently MODIS and PALSAR image are subsetting to Roorkee region and the care is taken so that area of sub-set region of both satellite images should be approximately equal. Therefore, MODIS has  $108*108$  pixels and PALSAR has  $1071*1071$  number of pixels after subsetting, by which both are acquiring approximately the same area.

### **4.4.1. Curvelet based fusion**

Fig. 4.1, fig. 4.2 and fig. 4.3 show the flowchart of the proposed methodology for the curvelet fusion of MODIS and PALSAR images for land cover classification.

#### **i. Fusion of MODIS band 1 and Band 2**

MODIS Band 1 and Band 2 is fused as discussed in the section 3.4.1 to obtain a new image which reflects the fused image (MOD12) of Band 1 and Band 2 i.e., the

resultant fused image MOD12 of 108\*108 pixels. The flowchart is depicted in the fig. 4.3. This MOD12 image is interpolated through bi-linear interpolation technique (Thomas et al., 1999) to the scale of the PALSAR image of 1071\*1071 pixels. The flowcharts for the fusion of PALSAR images with the MODIS images are deciphered in the following steps

**Step 1: Fusion of MODIS band 1 with the PALSAR images.** Fig. 4.1 implies the proposed methodology for the fusion of MODIS band 1 and PALSAR image. MODIS Band 1 and PALSAR image are considered initially and MODIS band 1 is interpolated through bi-linear interpolation technique to the scale of the PALSAR image of 1071\*1071 pixels. ATWT transformation is applied for PALSAR and  $C_j$  ( $j=3$  for present case) is replaced by MODIS band 1 and finally the resultant fused image MO1\_PA is obtained and has 1071\*1071 pixels. The PALSAR HH-Pol band is fused with the MODIS band 1 and the resultant fused is MO1\_PA(HH). Similarly we obtained the fused image of PALSAR HV-Pol band that is MO1\_PA(HV) and the fused image of PALSAR VV-Pol band i.e., MO1\_PA(VV).

**Step 2: Fusion of MODIS band 2 with the PALSAR images.** The proposed methodology for the fusion of MODIS band 2 and PALSAR image is shown in the fig. 4.2. MODIS Band 2 and PALSAR image are considered initially and MODIS band 2 is interpolated through bi-linear interpolation technique to the scale of the PALSAR image of 1071\*1071 pixels. ATWT transformation is applied for all the PALSAR bands and  $C_j$  ( $j=3$  for present case) is replaced by MODIS band 2 which gives the resultant fused image MO2\_PA that has 1071\*1071 pixels. The PALSAR HH-Pol band is fused with the MODIS band 2 and the resultant fused is MO2\_PA(HH). Similarly, we obtained the fused image of PALSAR HV-Pol band with MODIS band 2 i.e., MO2\_PA(HV) and the fused image of PALSAR VV-Pol band with MODIS band 2 i.e., MO2\_PA(VV).

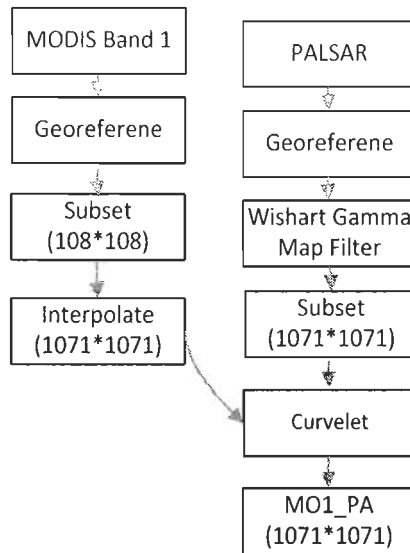


**Fig. 4.1.** Flowchart for fusion of MODIS (Band 1) on PALSAR images

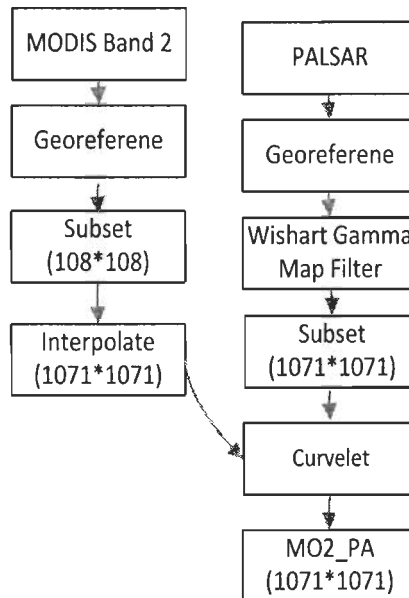


**Fig. 4.2.** Flowchart for fusion of MODIS (Band 2) on PALSAR images



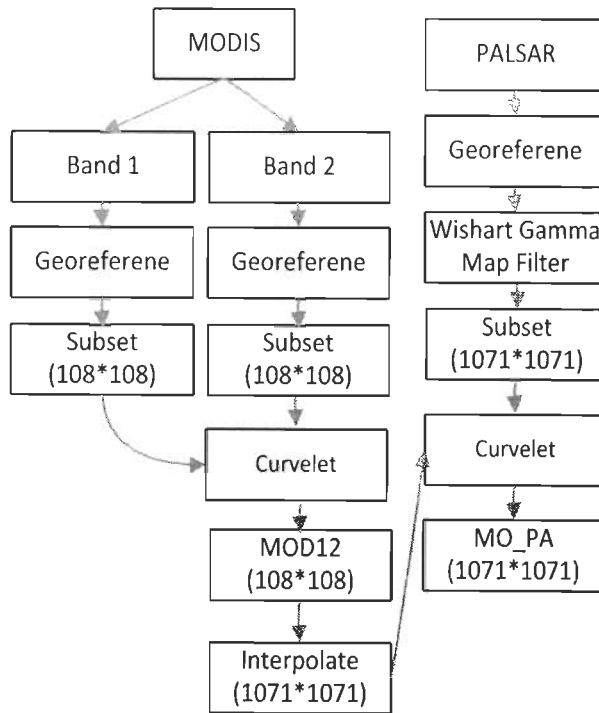


**Fig. 4.3.** Flowchart for fusion of MODIS (Band 1 and Band 2) on PALSAR images

**Step 3: Fusion of MOD12 image with the PALSAR images.** In the flowchart of fig. 4.3, the MOD12, the interpolated fused image of MODIS bands and PALSAR bands are considered for the fusion. ATWT transformation is applied for all the PALSAR bands and  $C_j$  ( $j=3$  for present case) is replaced by MOD12 which gives the resultant fused image MO\_PA that has 1071\*1071 pixels. The PALSAR HH-Pol band is fused with the MOD12 and the resultant fused is MO\_PA(HH). Similarly the fused image of MOD12 with PALSAR HV-Pol band is MO12\_PA(HV) and the fused image of PALSAR VV-Pol band is MO12\_PA(VV).

#### 4.4.2. Fuzzy based fusion

Fuzzy Inference System (FIS) Based Mamdani Model is a computing process by using fuzzy logic from input space to output space is being used in this chapter, as the advantages of using Mamdani FIS are described in the section 3.4.2

Fuzzy Inference System Editor for the fusion of MODIS and PALSAR image is emphasized in fig. 4.4. Fig. 4.5 shows the selection of Membership Fusion (MF) plots using Membership Fusion Editor and fig. 4.6 indicates the Rule Editor, for accentuating the rules that are used for the fusion of PALSAR image with the MODIS image.

Fig. 4.7, fig. 4.8 and fig. 4.9 shows the flowchart of the proposed methodology for the fuzzy based fusion of MODIS and PALSAR image for analyzing the classification of the MODIS image before and after the fusion. The subsetted MODIS has  $108 \times 108$  and PALSAR has  $1071 \times 1071$  pixels and the care is taken so that area of sub-set region of both satellite images should be approximately equal.

##### i. Fusion of MODIS band 1 and Band 2

MODIS Band 1 and Band 2 are considered initially. The Band 1 is fused with the Band 2, through the fuzzy based fusion. The FIS of the matlab is used for fusion and is deciphered by the figs. 4.4, 4.5 and 4.6. A new image which reflects the fused image (MOD12) of Band 1 and Band 2 i.e., the resultant fused image MOD12 of  $108 \times 108$  pixels. This MOD12 image is interpolated through bi-linear interpolation technique to the scale of the PALSAR of  $1071 \times 1071$  pixels.

The flowcharts for the fusion of PALSAR images with the MODIS images are deciphered in the following steps

**Step 1: Fusion of MODIS band 1 with the PALSAR images.** Fig. 4.7 implies the proposed methodology for the fusion of MODIS band 1 and PALSAR images. MODIS Band 1 and PALSAR image are considered initially and MODIS band 1 is

interpolated through bi-linear interpolation technique to the scale of the PALSAR image of 1071\*1071 pixels. The interpolated MODIS band 1 and PALSAR are considered for the fusion through the FIS of the matlab and fig. 4.4, 4.5 and 4.6 are used for the fusion, and thereby gives the resultant fused image MO1\_PA that has 1071\*1071 pixels. The PALSAR HH-Pol band is fused with the MODIS band 1 and the resultant fused is MO1\_PA(HH). Similarly the fused image of MODIS band 1 with PALSAR HV-Pol band is MO1\_PA(HV) and the fused image of MODIS band 1 with PALSAR VV-Pol band is MO1\_PA(VV).

**Step 2: Fusion of MODIS band 2 with the PALSAR images.** The proposed methodology for the fusion of MODIS band 2 and PALSAR image is shown in the fig. 4.8. MODIS Band 2 and PALSAR image are considered initially and MODIS band 2 is interpolated through bi-linear interpolation technique to the scale of the PALSAR image of 1071\*1071 pixels. The FIS of the matlab and fig. 4.4, 4.5 and 4.6 are used for the fusion, and thereby gives the resultant fused image MO2\_PA that has 1071\*1071 pixels. The PALSAR HH-Pol band is fused with the MODIS band 2 and the resultant fused is MO2\_PA (HH). Similarly the fused image of MODIS band 2 with PALSAR HV-Pol band is MO2\_PA(HV) and the fused image of MODIS band 2 with PALSAR VV-Pol band is MO2\_PA(VV).

**Step 3: Fusion of MOD12 image with the PALSAR images.** In the flowchart of fig. 4.11, the MOD12, the interpolated fused image of MODIS bands and PALSAR bands are considered for the fusion. The FIS of the matlab and fig. 4.4, 4.5 and 4.6 are used for the fusion, and thereby gives the resultant fused image MO\_PA that has 1071\*1071 pixels. The PALSAR HH-Pol band is fused with the MOD12 and the resultant fused is MO\_PA(HH). Similarly the fused image of MOD12 with PALSAR HV-Pol band is MO\_PA(HV) and the fused image of MOD12 with PALSAR VV-Pol band is MO\_PA(VV).

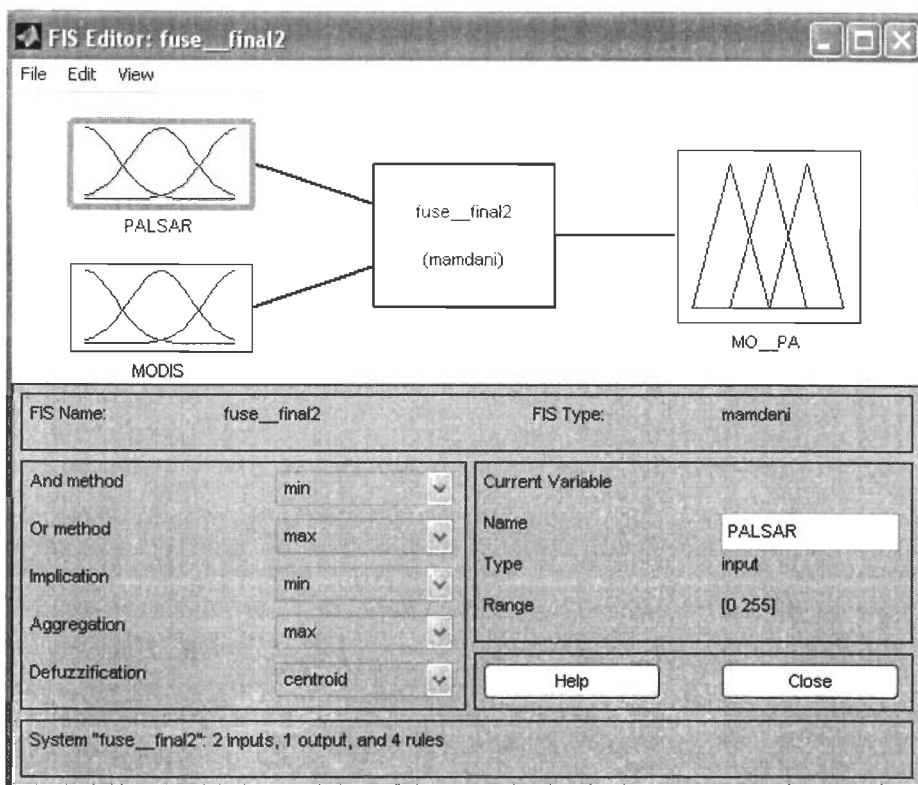


Fig. 4.4. Fuzzy Interference System Editor for the fusion of PALSAR and MODIS image

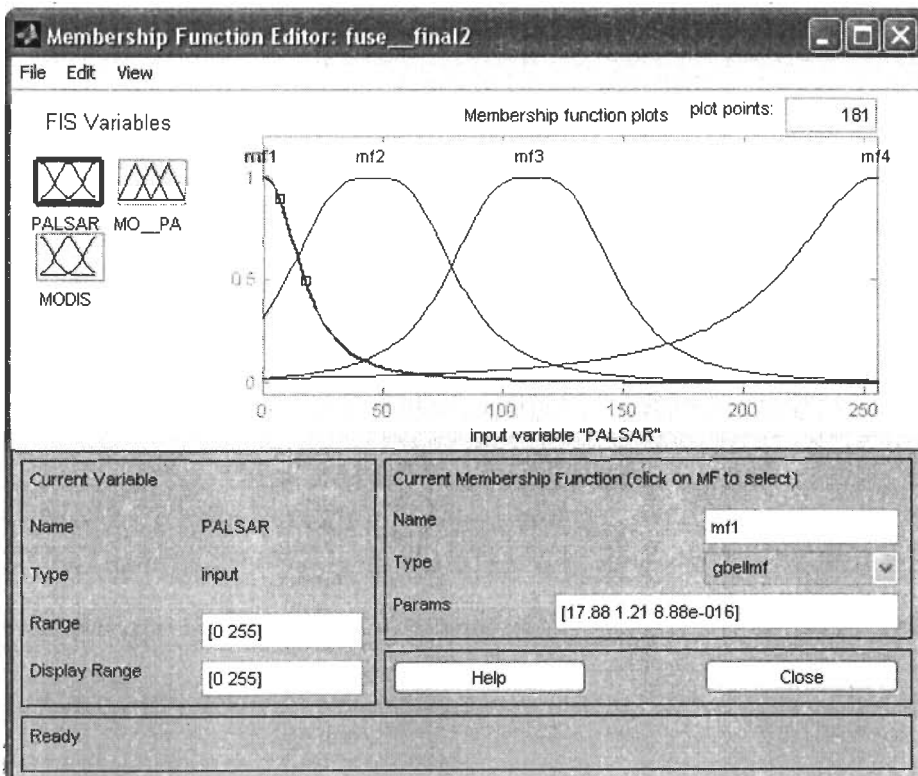


Fig. 4.5. Membership Fusion Editor implying the Membership Fusion(MF) for the PALSAR and MODIS image

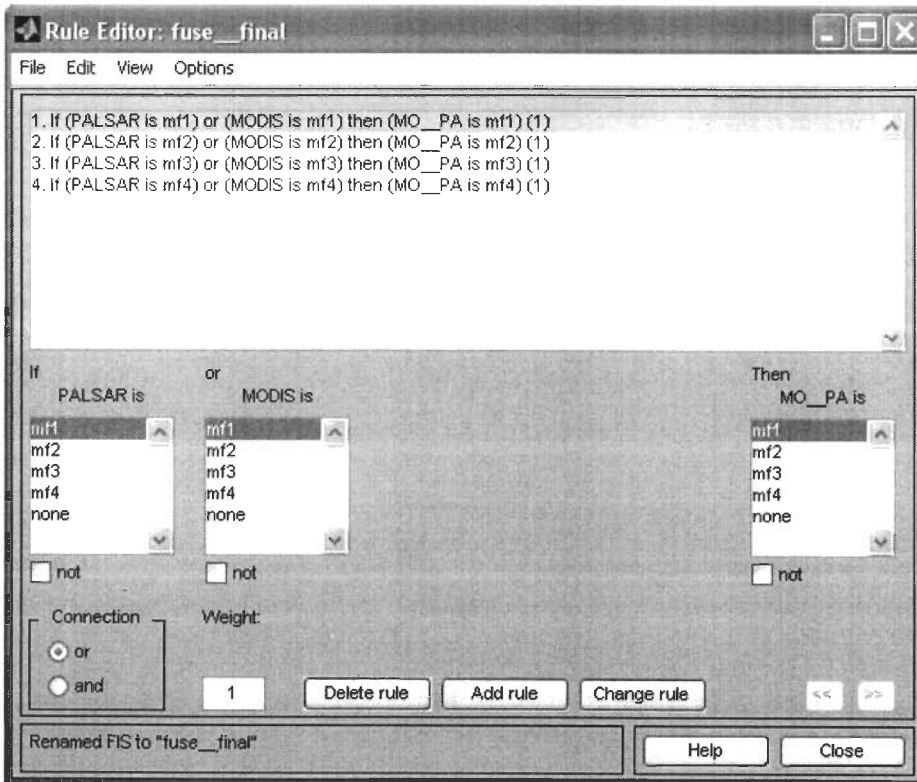


Fig. 4.6. Rule Editor for the fusion of PALSAR and MODIS image

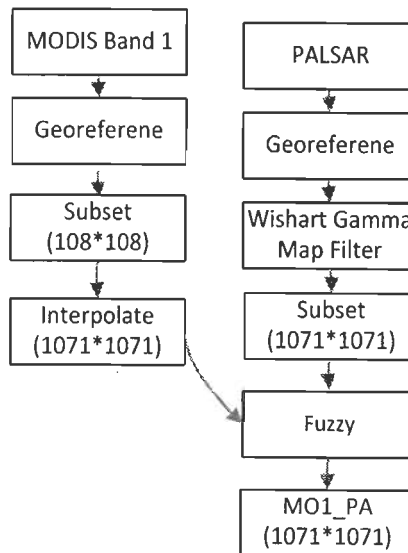
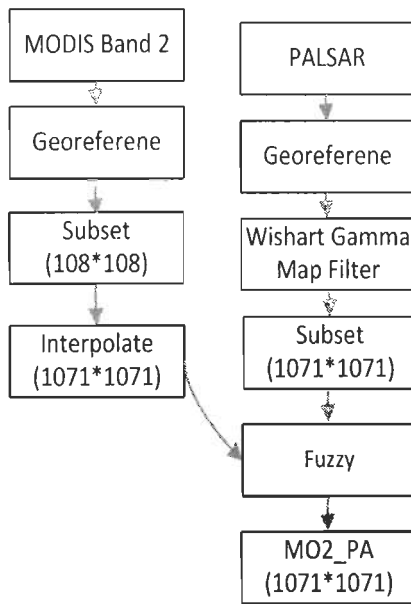
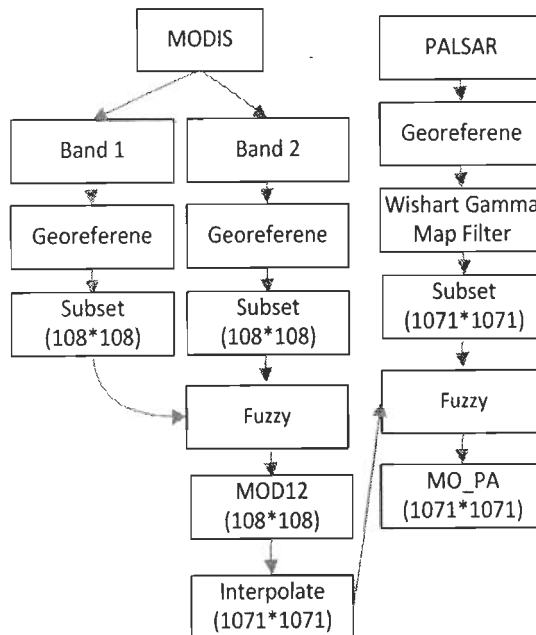


Fig. 4.7. Flowchart for fusion of MODIS(Band 1) on PALSAR images



**Fig. 4.8.** Flowchart for the fusion of MODIS(Band 2) on PALSAR images



**Fig. 4.9.** Flowchart for the fusion of MODIS(Band 1 and Band 2) on PALSAR images

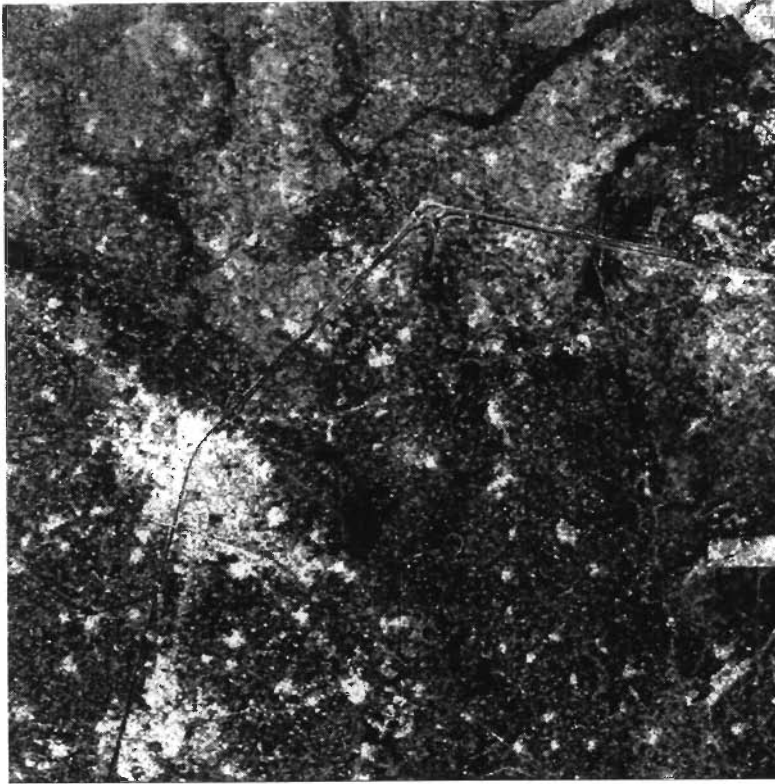


**Fig. 4.10a.** PALSAR HH-Pol image

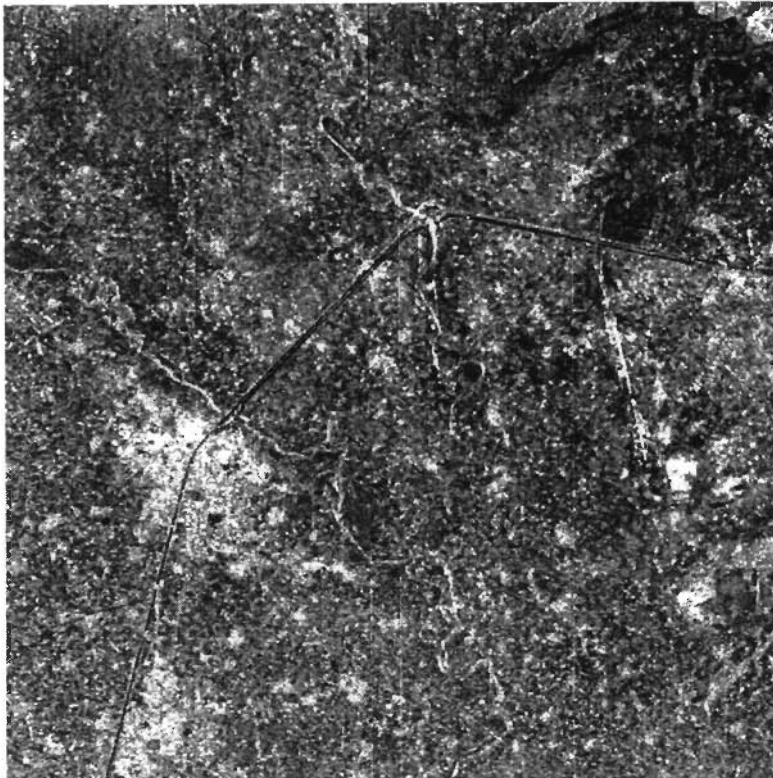


**Fig. 4.10b.** PALSAR HV-Pol image

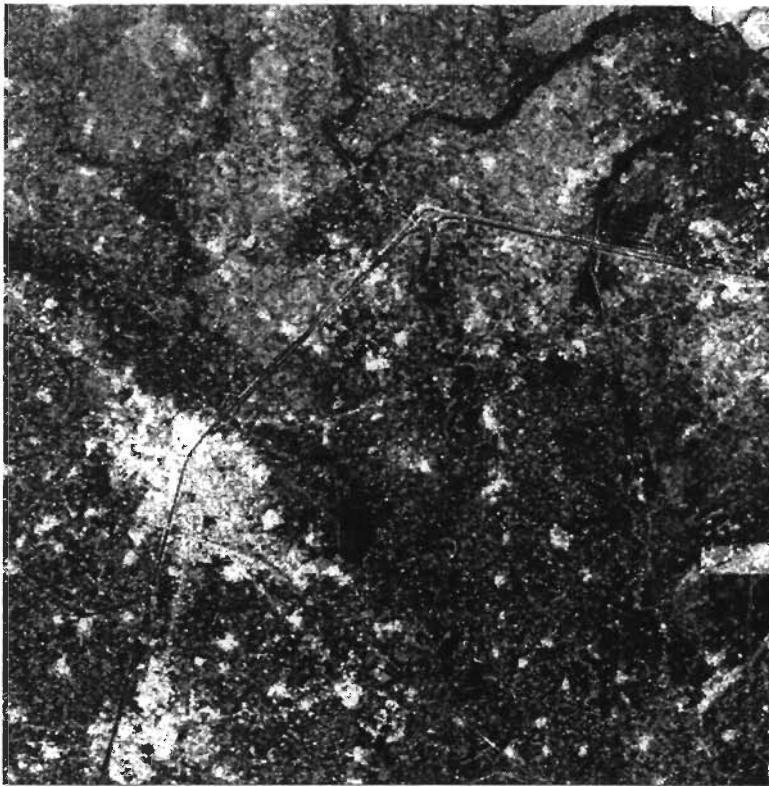


**Fig. 4.10c.** PALSAR VV-Pol image

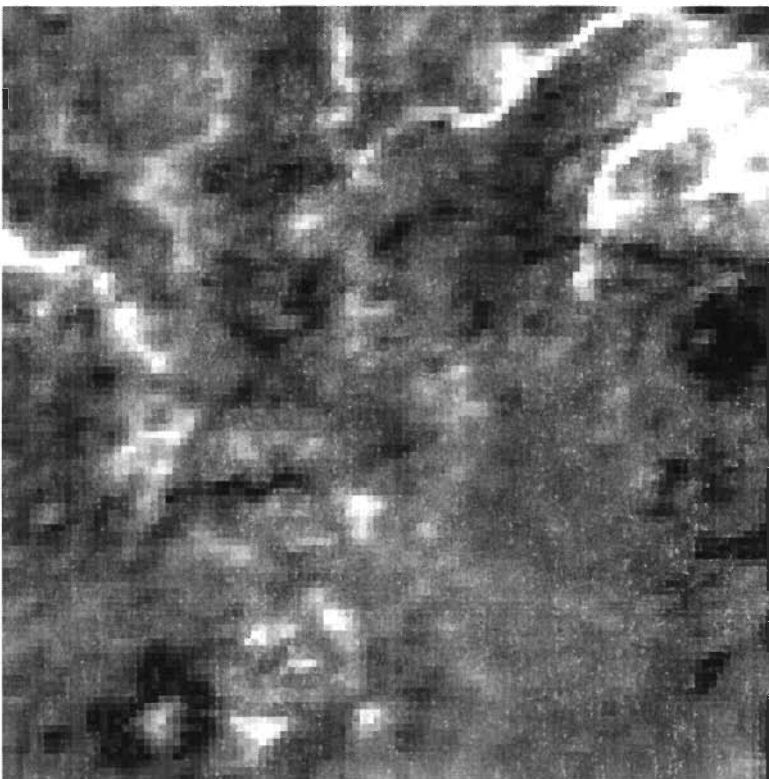


**Fig. 4.11a.** MODIS Band 1 image



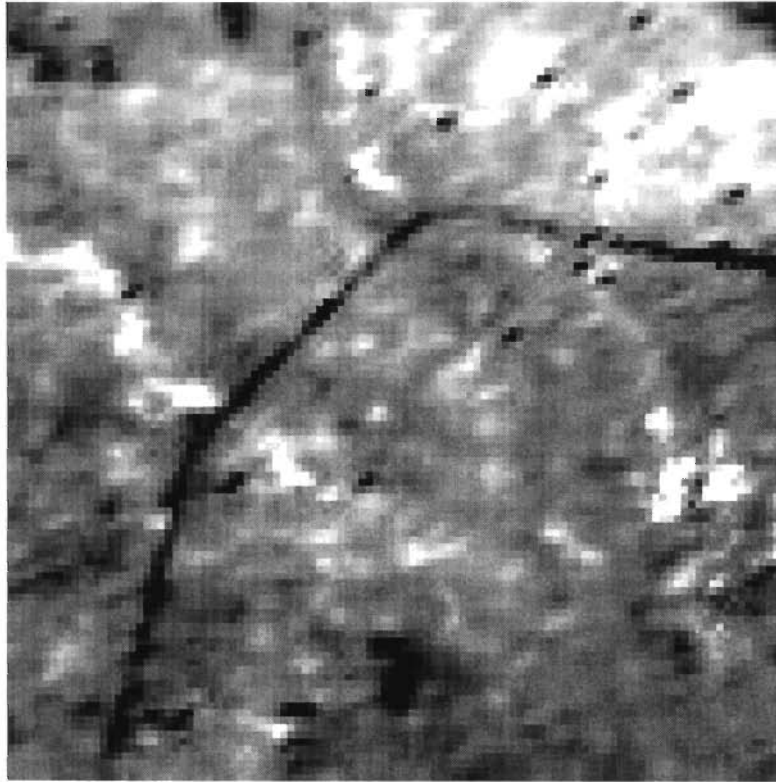


**Fig. 4.11b.** MODIS Band 2 image

## **4.5. Analysis of Experimental Results**

The subsetted PALSAR HH-Pol, HV-Pol and VV-Pol images are shown in the fig. 4.10a, fig. 4.10b and fig. 4.10c respectively and the subsetted MODIS band 1 and band 2 are shown in the fig. 4.11a and fig. 4.11b respectively. The toposheet for the Roorkee region is shown in the fig. 3.11.

### **4.5.1. Curvelet based fusion**

The proposed methodology for the fusion of MODIS and PALSAR image, through the curvelet based fusion is shown in the flowchart fig. 4.1, fig. 4.2 and fig. 4.3, and the concerned experimental results is deciphered in the following steps

**Step 1: Fusion of MODIS band 1 with the PALSAR images.** Fig. 4.1 implies the proposed methodology for the fusion of MODIS band 1 and PALSAR image. MO1\_PA(HH) is shown in the fig. 4.12a, and fig 4.12b, MO1\_PA(HV) is depicted and MO1\_PA(VV) is shown in fig. 4.12c.

**Step 2: Fusion of MODIS band 2 with the PALSAR images.** The proposed methodology for the fusion of MODIS band 2 and PALSAR image is shown in the fig. 4.2. MO2\_PA(HH) is shown in the fig. 4.13a, and fig 4.13b MO2\_PA(HV) is depicted and MO2\_PA(VV) is shown in fig. 4.13c.

**Step 3: Fusion of MOD12 image with the PALSAR images.** In the flowchart of fig. 4.3, the MOD12 (The resultant curvelet based fusion of MODIS band 1 and band 2 i.e., MOD12 is depicted in the fig. 4.14a) is bilinear interpolated and fused with PALSAR bands. MO\_PA(HH) is shown in the fig. 4.14b, and fig 4.14c, MO\_PA(HV) is depicted and MO\_PA(VV) is shown in fig. 4.14d.

#### **4.5.2. Fuzzy based fusion**

The proposed methodology for the fusion of MODIS and PALSAR images, through the fuzzy based fusion is shown in the flowchart fig. 4.7, fig. 4.8 and fig. 4.9, and the concerned experimental results is deciphered in the following steps

**Step 1: Fusion of MODIS band 1 with the PALSAR polarized images.** Fig. 4.7 implies the proposed methodology for the fuzzy based fusion of MODIS band 1 and PALSAR polarized image. MO1\_PA(HH) is shown in the fig. 4.15a, and fig 4.15b, MO1\_PA(HV) is depicted and MO1\_PA(VV) is shown in fig. 4.15c.

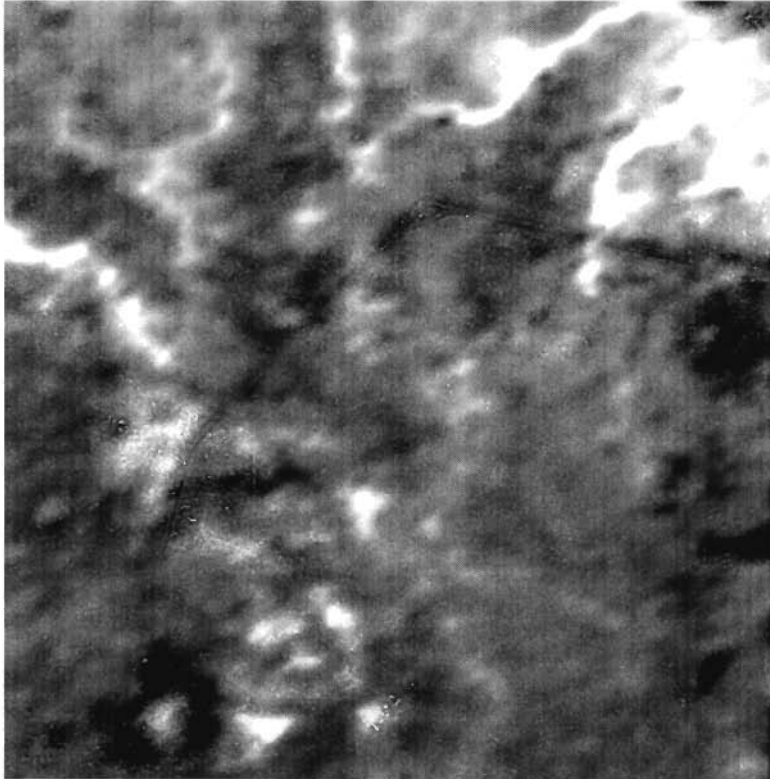


**Fig. 4.12a.** MO1\_PA(HH), the resultant fused image of MODIS Band 1 and HH-Pol image fused by curvelet based fusion .

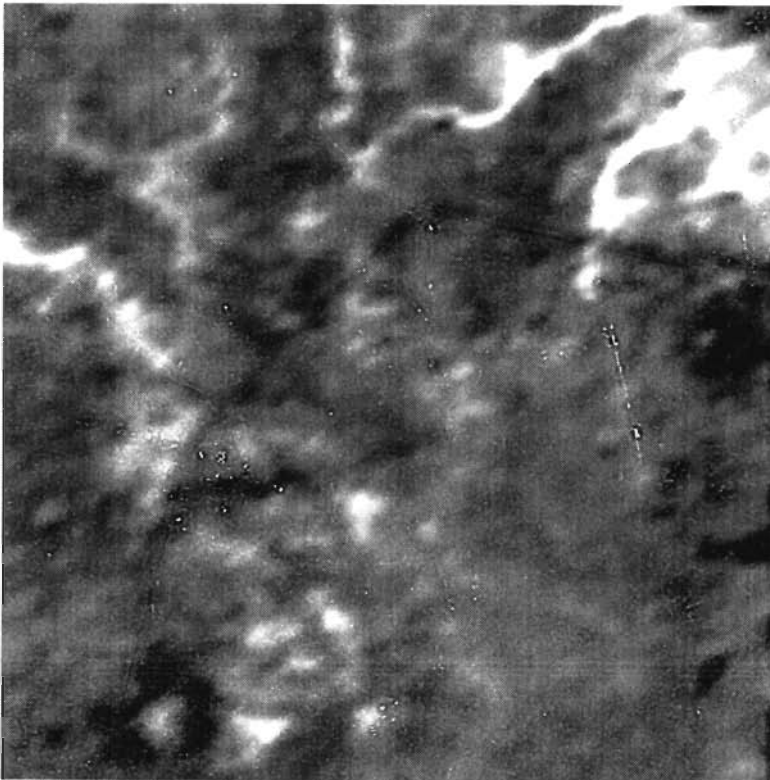


**Fig. 4.12b.** MO1\_PA(HV), the resultant fused image of MODIS Band 1 and HV-Pol image fused by curvelet based fusion.

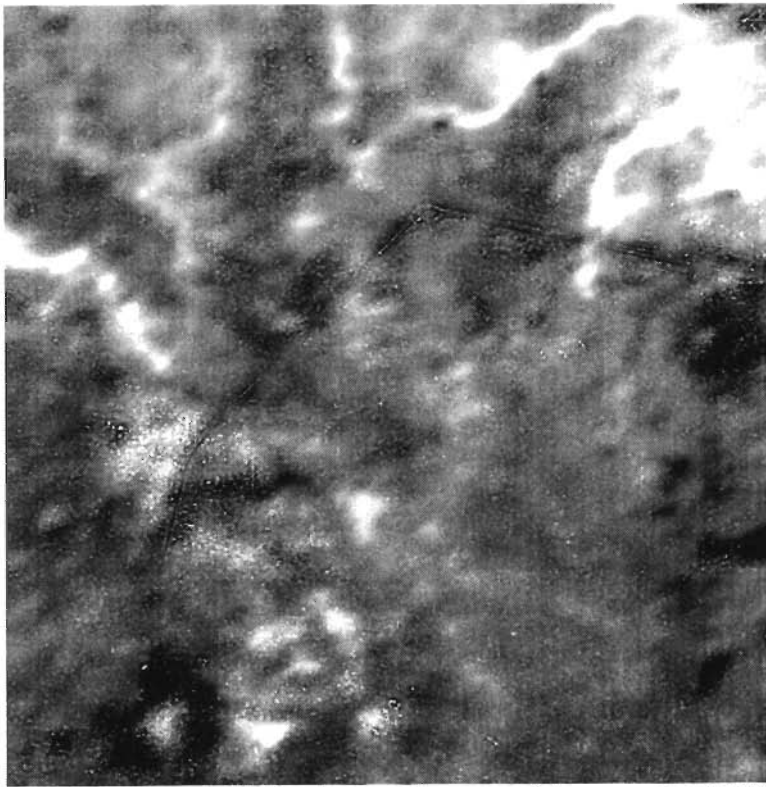


**Fig. 4.12c.** MO1\_PA(VV), the resultant fused image of MODIS Band 1 and VV-Pol image fused by curvelet based fusion.

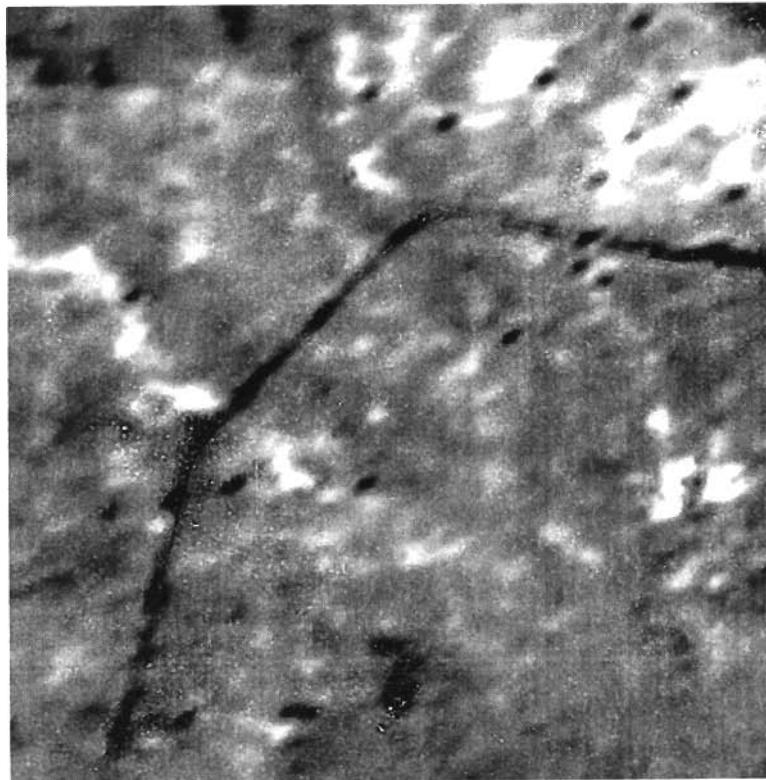


**Fig. 4.13a.** MO2\_PA(HH), the resultant fused image of MODIS Band 2 and HH-Pol image fused by curvelet based fusion.

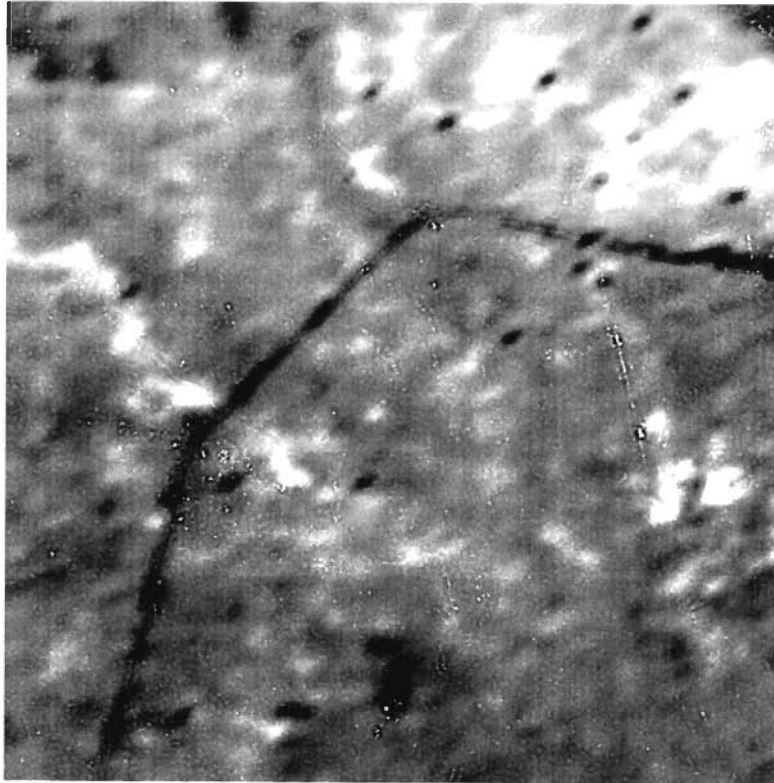


**Fig. 4.13b.** MO2\_PA(HV), the resultant fused image of MODIS Band 2 and HV-Pol image fused by curvelet based fusion.

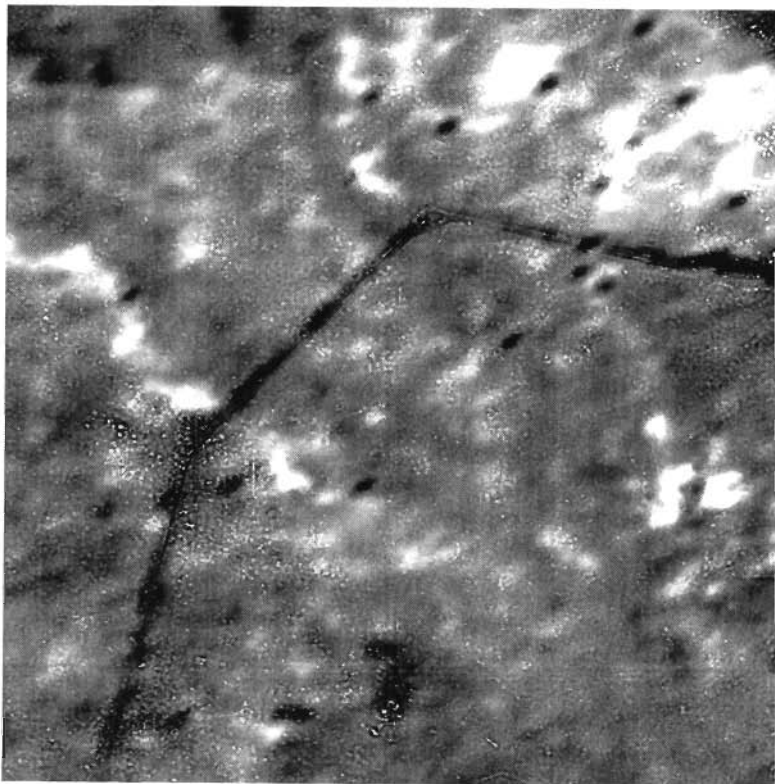


**Fig. 4.13c.** MO2\_PA(VV), the resultant fused image of MODIS Band 2 and VV-Pol image fused by curvelet based fusion.

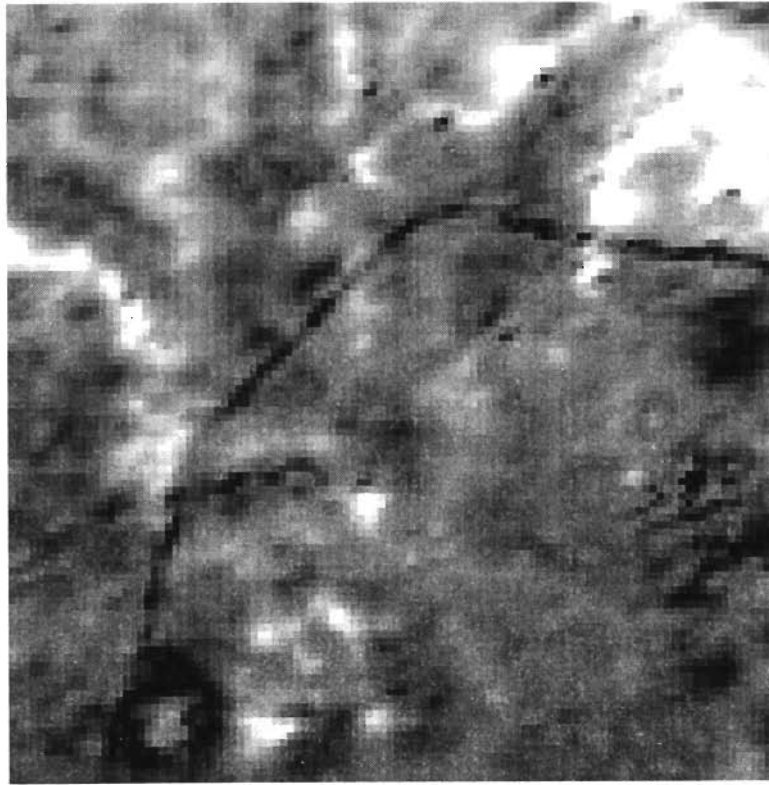


**Fig. 4.14a.** MOD12, the resultant fused image of MODIS band 1 and MODIS band 2 fused by curvelet based fusion.

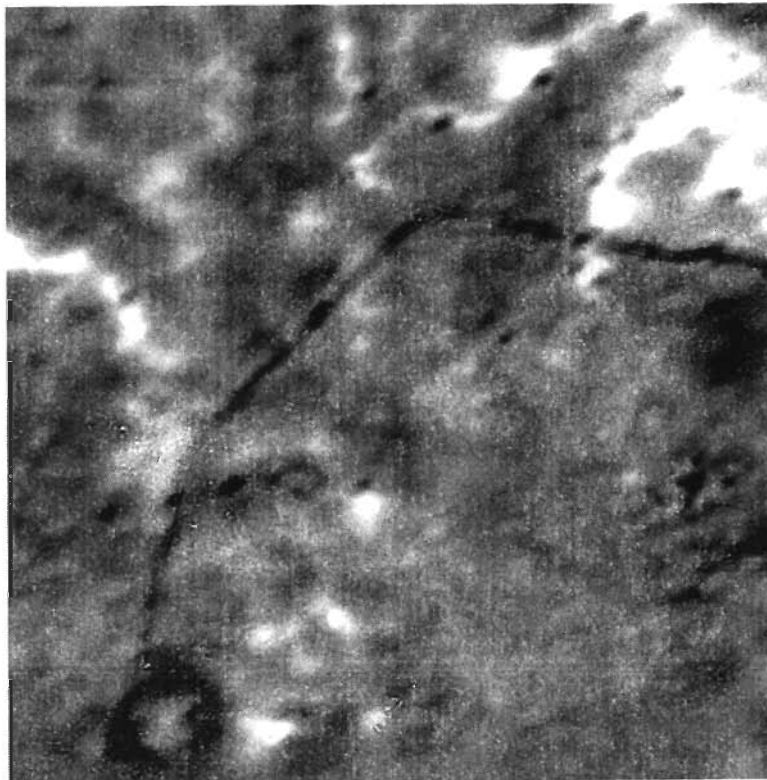


**Fig. 4.14b.** MO\_PA(HH), the resultant fused image of MOD12 and HH-Pol image fused by curvelet based fusion.

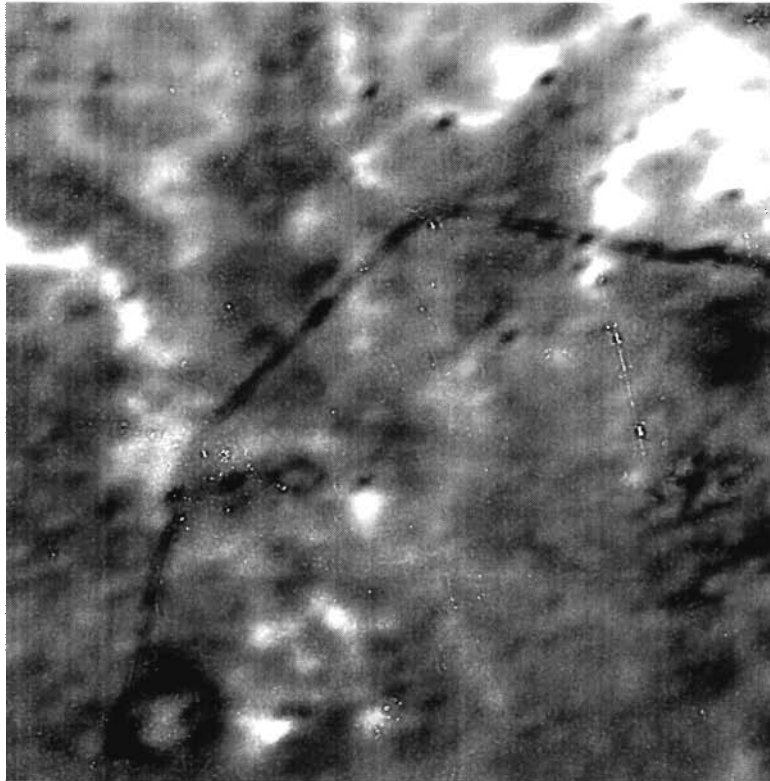


**Fig. 4.14c.** MO\_PA(HV), the resultant fused image of MOD12 and HV-Pol image fused by curvelet based fusion.

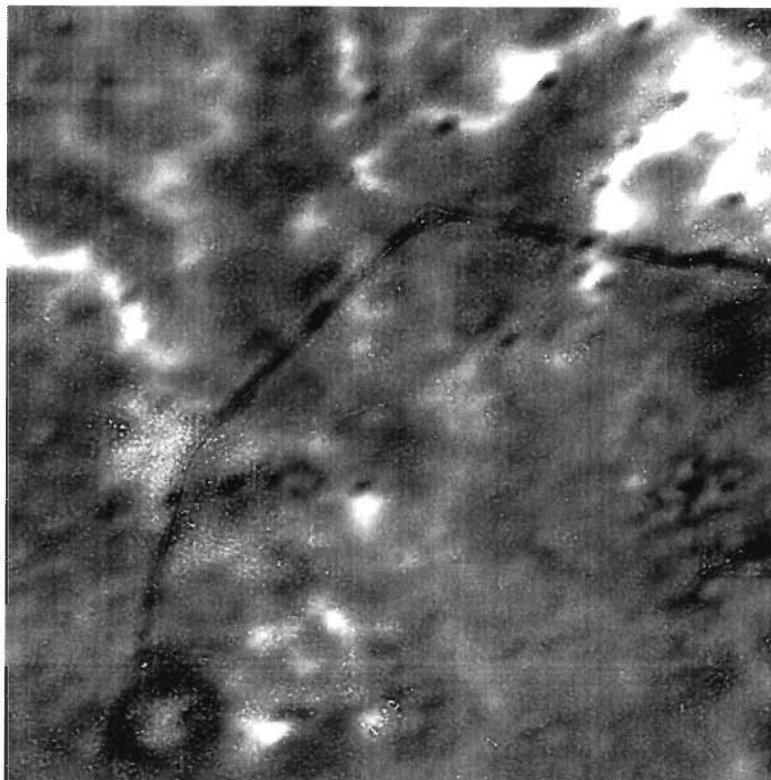


**Fig. 4.14d.** MO\_PA(VV), the resultant fused image of MOD12 and VV-Pol image fused by curvelet based fusion.

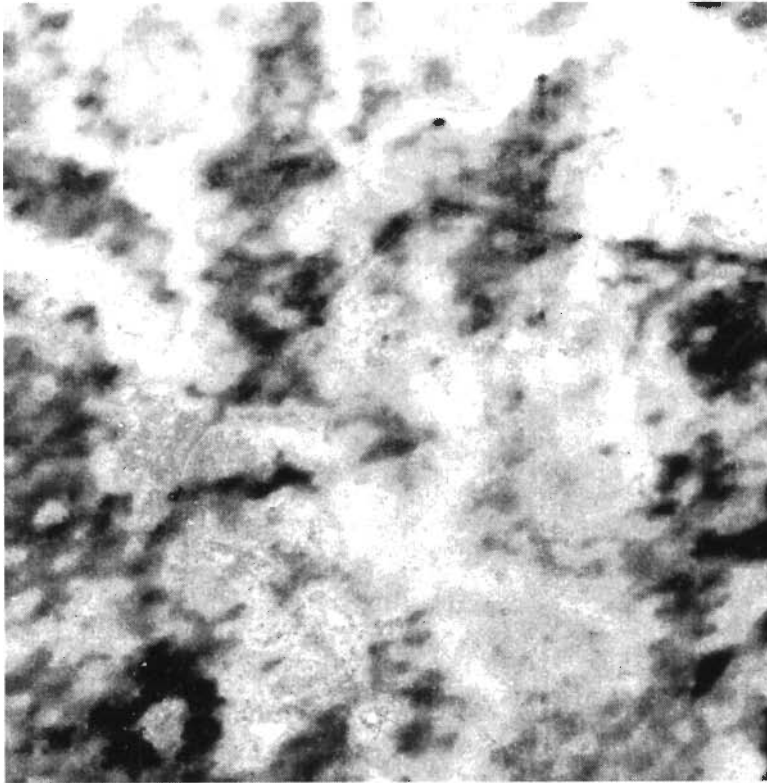


**Fig. 4.15a.** MOI\_PA(HH), the resultant fused image of MODIS Band 1 and HH-Pol image fused by fuzzy based fusion.

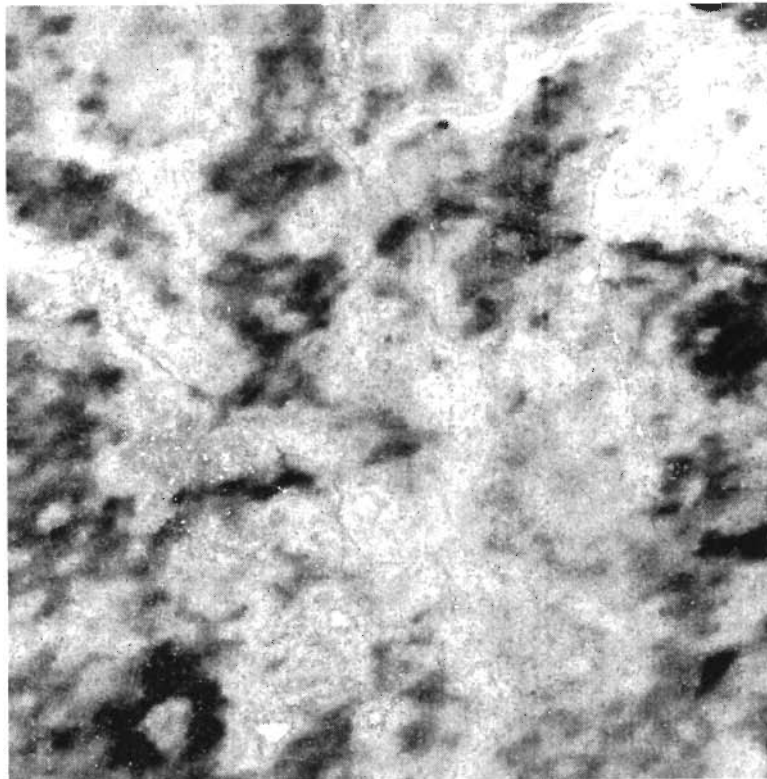


**Fig. 4.15b.** MOI\_PA(HV), the resultant fused image of MODIS Band 1 and HV-Pol image fused by fuzzy based fusion.



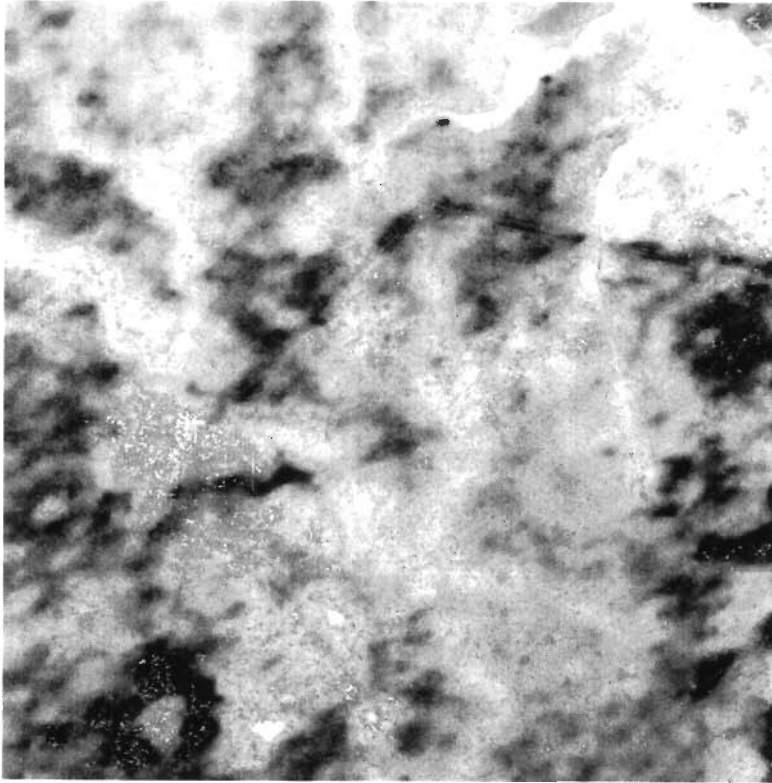


**Fig. 4.15c.** MO1\_PA(VV), the resultant fused image of MODIS Band 1 and VV-Pol image fused by fuzzy based fusion.

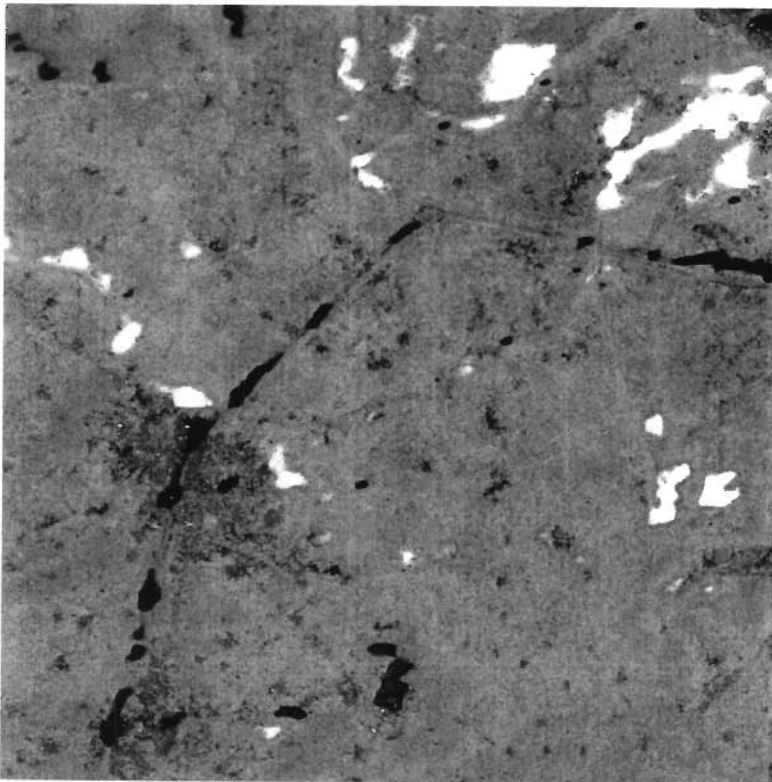


**Fig. 4.16a.** MO2\_PA(HH), the resultant fused image of MODIS Band 2 and HH-Pol image fused by fuzzy based fusion.



**Fig. 4.16b.** MO2\_PA(HV), the resultant fused image of MODIS Band 2 and HV-Pol image fused by fuzzy based fusion.

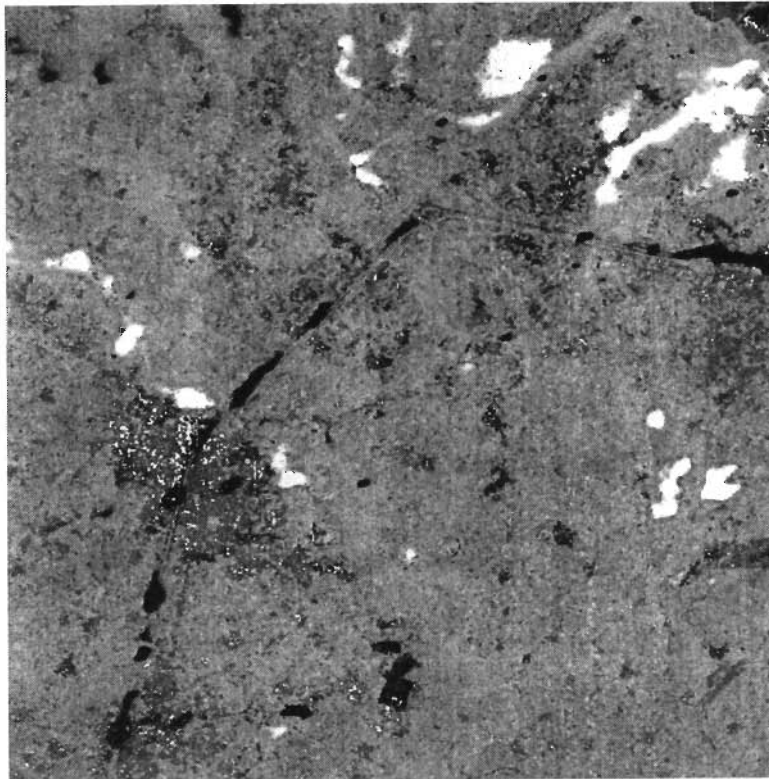


**Fig. 4.16c.** MO2\_PA(VV), the resultant fused image of MODIS Band 2 and VV-Pol image fused by fuzzy based fusion.

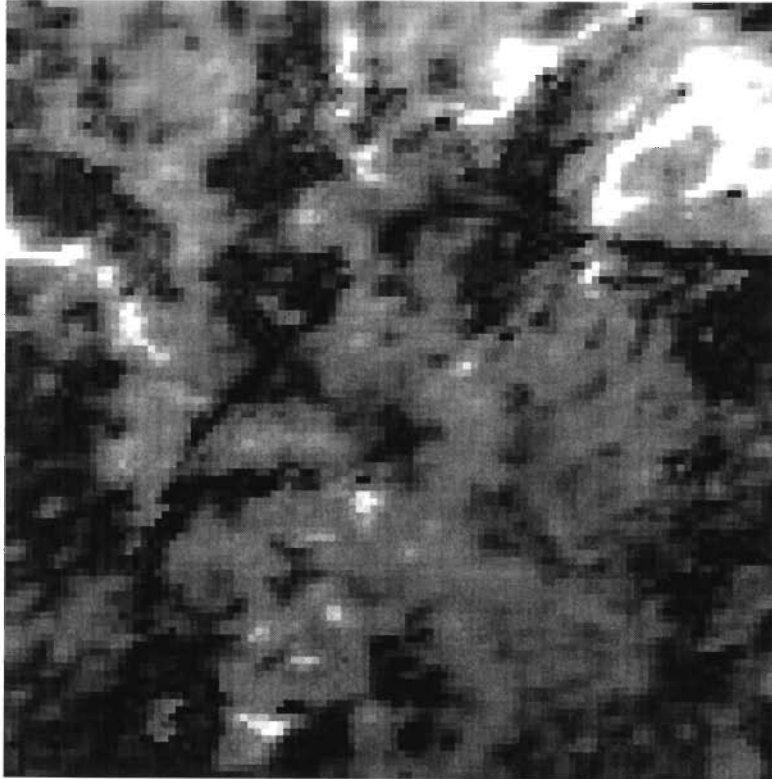


**Fig. 4.17a.** MOD12, the resultant fused image of MODIS band 1 and MODIS band 2 fused by fuzzy based fusion.



**Fig. 4.17b.** MO\_PA(HH), the resultant fused image of MOD12 and HH-Pol image fused by fuzzy based fusion.

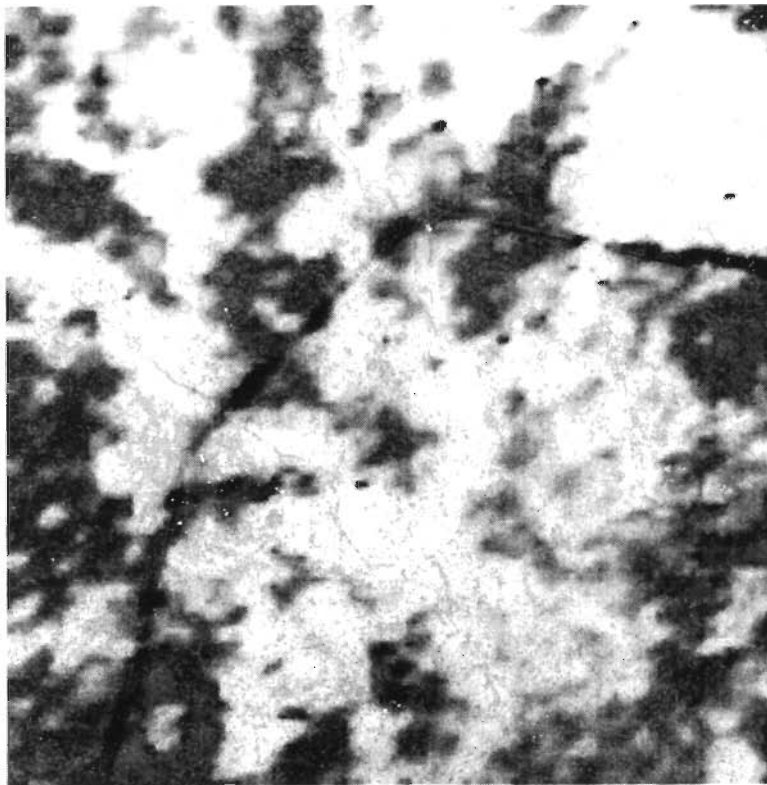


**Fig. 4.17c.** MO\_PA(HV), the resultant fused image of MOD12 and HV-Pol image fused by fuzzy based fusion.



**Fig. 4.17d.** MO\_PA(VV), the resultant fused image of MOD12 and VV-Pol image fused by fuzzy based fusion.

**Step 2: Fusion of MODIS band 2 with the PALSAR polarized images.**

Methodology for fuzzy fusion of MODIS band 2 and PALSAR images is shown in the fig. 4.8, and the resultant images MO2\_PA(HH), MO2\_PA(HV) and MO2\_PA(VV) are shown in figs. 4.16a, 4.16b and 4.16c respectively.

**Step 3: Fusion of MOD12 image with the PALSAR images.** In the flowchart of fig. 4.9, the MOD12 (The resultant fuzzy based fusion of MODIS band 1 and band 2 i.e., MOD12 is depicted in the fig. 4.17a) is bilinear interpolated and fused with PALSAR bands. MO\_PA(HH) MO\_PA(HV) and MO\_PA(VV) are shown in fig. 4.17b, 4.17c and 4.17d respectively.

In order to assess the quality of the fused image by some quantitative assessment criteria have been defined by comparing the fused product and the low spatial resolution multispectral images (Wald et al., 1997) in one hand and in another hand the classification accuracy is also computed to review the significance of the fused images in the direction of land cover classification. In the following paragraphs, the quantitative assessment criteria indicators, and classification accuracy are discussed.

**i. Classification Accuracy.**

The Minimum Distance classification technique has been applied for obtaining the major type of land cover classification, i.e., urban, agriculture and water. ENVI 4.3 software is used for georeferencing and classification purpose where as we have developed codes in MATLAB 7.0 for fusion methodology.

We have identified 392 GCPs for agriculture, 358 GCP for urban and 311 GCP for water bodies for training and for testing 209 GCP for agriculture, 318 GCP for urban and 223 GCP for water bodies from Toposheet of Roorkee region (Fig. 3.11), Google earth and Ground Survey points. The Control points were basically collected by ground survey with the use of GPS and more than 100 points were separately collected for each classes, and these points were overlapped on Google

Earth and Toposheet for visual interpretation of the points. On the basis of these GCPs, we have computed the classification accuracy for PALSAR Bands.

Similarly for MODIS bands, we have identified 35 GCP for agriculture, 22 GCP for urban and 30 GCP for water bodies for training and for testing 38 GCP for agriculture, 27 GCP for urban and 28 GCP for water bodies. It has resolution 250 m so less GCPs are considered in this study area. We have identified 355 GCP for agriculture, 309 GCP for urban and 333 GCP for water bodies for training and for testing 217 GCP for agriculture, 202 GCP for urban and 165 GCP for water bodies for fused image. On the basis of these GCPs, the Minimum Distance classification is applied and thereby classification accuracy is computed.

The minimum distance classified image of PALSAR HH-Pol, HV-Pol and VV-Pol Bands are shown in the figs. 4.18a, 4.18b and 4.18c respectively. In figs. 4.19a, 4.19b, shows the minimum distance classified image of MODIS Band 1 and Band 2 respectively. The producers, users, and overall classification accuracies of agriculture, urban and water classes for MODIS band 1, MODIS band 2, PALSAR HH-Pol, HV-Pol and VV-Pol bands has been tabulated in Table 4.1. The overall classification accuracy for MODIS band 1, MODIS band 2 is 47.31% and 67.74% respectively. In other hand PALSAR HH-Pol, HV-Pol and VV-Pol bands has overall accuracy of 66.27%, 85.47% and 65.07% respectively.

**Table 4.1.** Classification Accuracy

Images	Producers Accuracy			Users Accuracy			Overall Classification Accuracy
	Agric culture	Urban	Water	Agric culture	Urban	Water	
<b>MODIS Band 1</b>	23.68	44.44	82.14	42.86	48.00	48.94	47.31
<b>MODIS Band 2</b>	63.16	48.15	92.86	60.00	54.17	89.66	67.74
<b>HH</b>	28.71	79.87	82.06	36.59	100.0	55.12	66.27
<b>HV</b>	58.85	96.23	95.07	84.25	100.0	71.14	85.47
<b>VV</b>	31.58	80.50	74.44	35.68	100.0	53.72	65.07

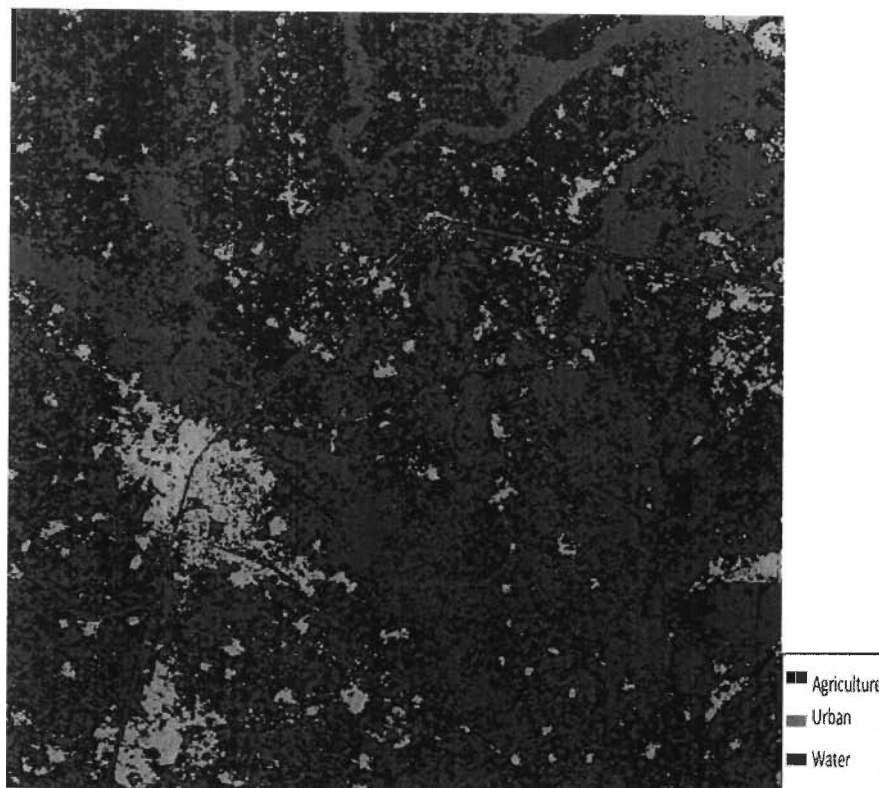


**Fig. 4.18a.** Minimum Distance classified PALSAR HH-Pol image.

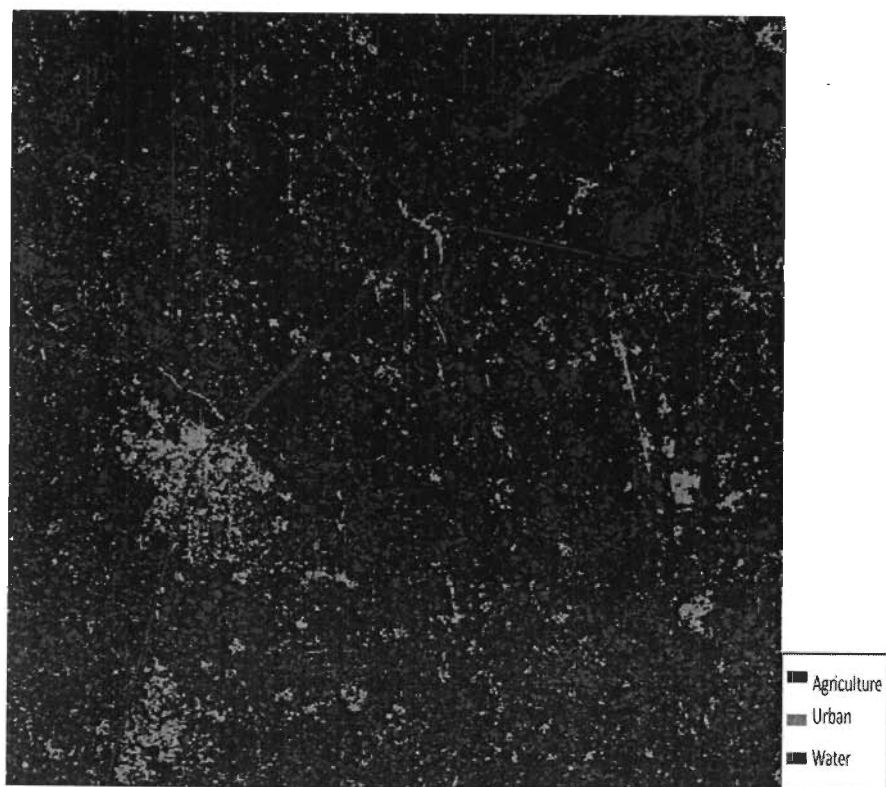


**Fig. 4.18b.** Minimum Distance classified PALSAR HV-Pol image.

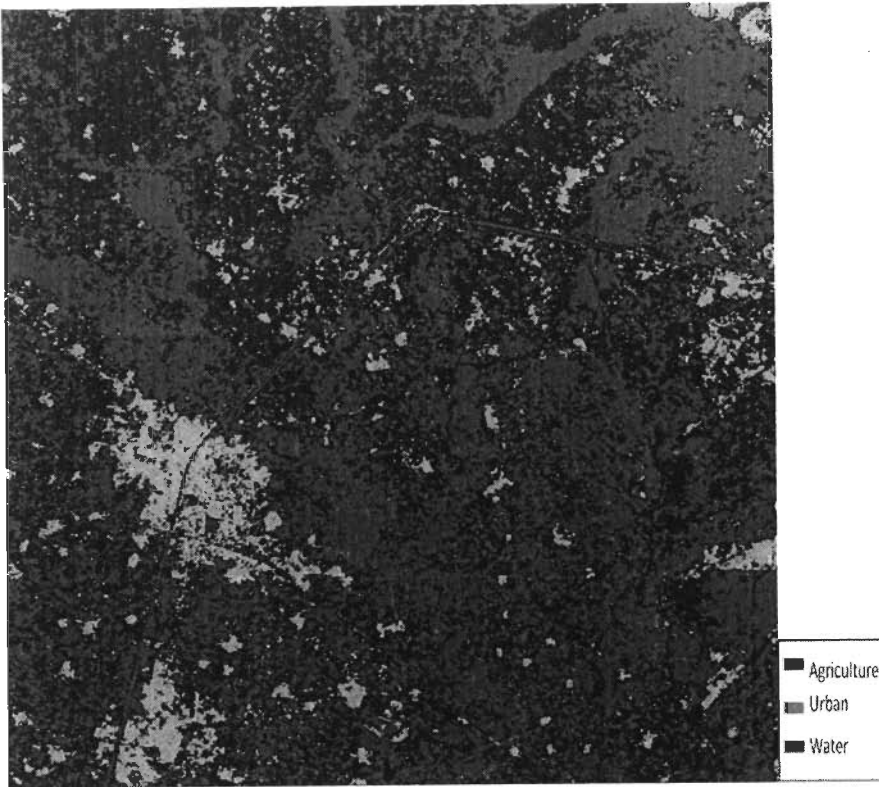


**Fig. 4.18c.** Minimum Distance classified PALSAR VV-Pol image.

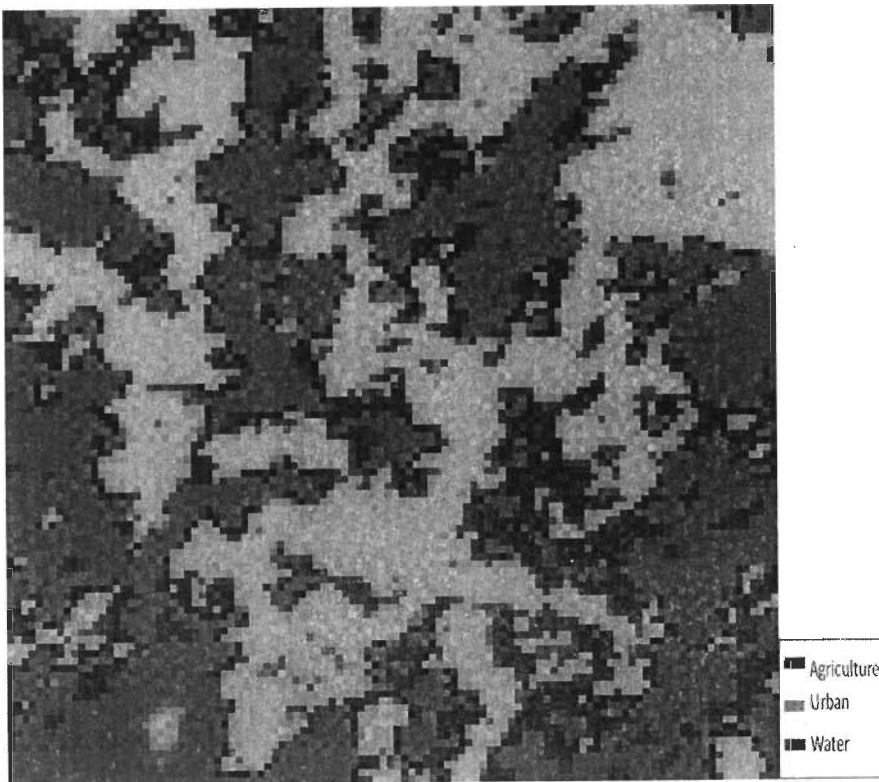


**Fig. 4.19a.** Minimum Distance classified MODIS band 1.



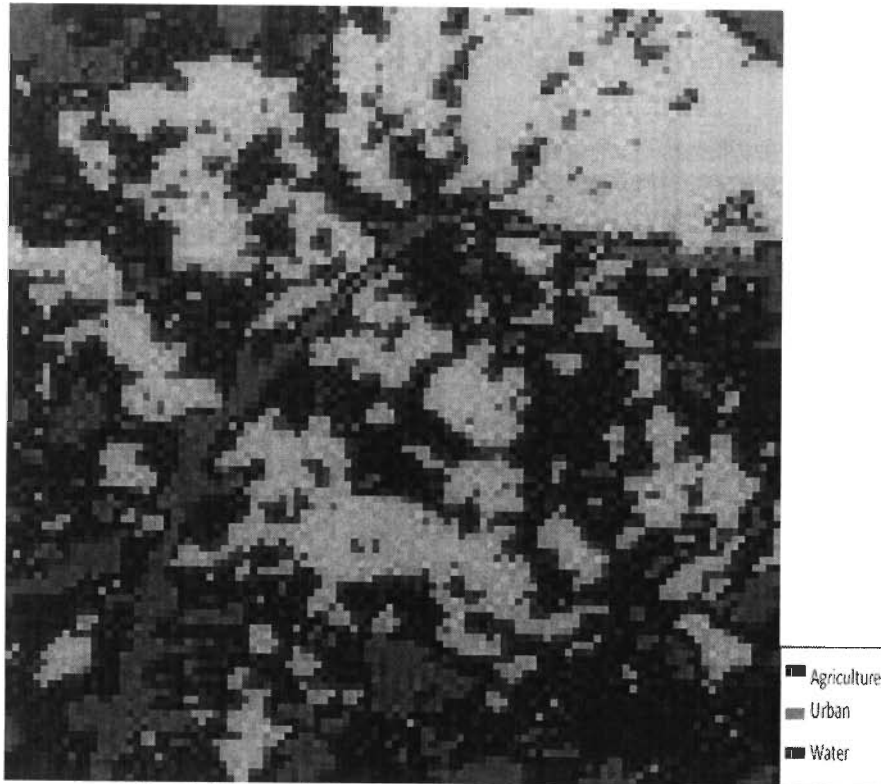


**Fig. 4.19b.** Minimum Distance classified MODIS band 2.

**Curvelet based Fusion.** The resultant minimum distance curvelet based classified image of MODIS band 1 and PALSAR bands i.e., MO1\_PA(HH), MO1\_PA(HV) and MO1\_PA(VV), is depicted in figs 4.20a, 4.20b and 4.20c respectively. In figs 4.21a, 4.21b and 4.21c shows the minimum distance classified image of MO2\_PA(HH), MO2\_PA(HV) and MO2\_PA(VV) respectively, the resultant fused image of PALSAR (HH, HV and VV) and MODIS band 2. The minimum distance classified image of MOD12, the resultant curvelet based fused image of MODIS band 1 and band 2, is depicted in fig 4.22a. The resultant fused image of MOD12 and PALSAR(HH, HV and VV) bands are MO\_PA(HH), MO\_PA(HV) and MO\_PA(VV), and its minimum distance classified image is depicted in the figs 4.22b, 4.22c and 4.22d respectively.

The classification accuracy for the curvelet based fusion is calculated and tabulated in the table 4.2. The fused image of MODIS band 1 and PALSAR bands are

MO1\_PA(HH), MO1\_PA(HV) and MO1\_PA(VV), and there overall classification accuracy are 78.60%, 77.40% and 78.08% respectively. MO2\_PA(HH), MO2\_PA(HV) and MO2\_PA(VV), the resultant fused image of MODIS band 2 and PALSAR bands, and there overall classification accuracy are 78.60%, 80.82% and 78.25% respectively. The fused image of MOD12 and PALSAR bands are MO\_PA(HH), MO\_PA(HV) and MO\_PA(VV), and there overall classification accuracy are 86.30%, 84.76% and 84.60% respectively. It is observed that the overall classification accuracy for the fused images of PALSAR with MOD12 is better than the overall classification accuracy for the fused images of PALSAR with MODIS band 2 or MODIS band 1.

From table 4.2, it is observed that the producers accuracy of agriculture for the images MO\_PA(HH), MO\_PA(HV) and MO\_PA(VV) are 96.31%, 94.47% and 96.31% respectively, and it is better than the producers accuracy of agriculture for MO2\_PA(HH), MO2\_PA(HV), MO2\_PA(VV) , MO1\_PA(HH), MO1\_PA(HV) and MO1\_PA(VV)

The producers accuracy of urban for the fused image with MODIS band 1 i.e., MO1\_PA(HH), MO1\_PA(HV) and MO1\_PA(VV) are 76.73%, 73.76% and 76.24% respectively (table 4.2) and it is better than the producers accuracy of urban for the fused image with MOD12 i.e., MO\_PA(HH), MO\_PA(HV) and MO\_PA(VV) and there producers accuracy are 72.77%, 71.29% and 71.78% respectively, and which is better than the producers accuracy of urban for the fused image with MODIS band 2 i.e., MO2\_PA(HH), MO2\_PA(HV) and MO2\_PA(VV) and there producers accuracy are 54.95%, 58.91% and 55.94% respectively.

The producers accuracy of water for the fused image with MODIS band 2 i.e., MO2\_PA(HH), MO2\_PA(HV) and MO2\_PA(VV) are 95.15%, 95.76% and 94.55% respectively (table 4.2), and it is better than the producers accuracy of water for the fused image with MOD12 i.e., MO\_PA(HH), MO\_PA(HV) and MO\_PA(VV) and there producers accuracy are 89.70%, 88.48% and 84.85% respectively, and which is better than the producers accuracy of water for the fused image with MODIS band 1 i.e., MO1\_PA(HH), MO1\_PA(HV) and MO1\_PA(VV) and there producers accuracy are 75.15%, 75.15% and 75.15% respectively.

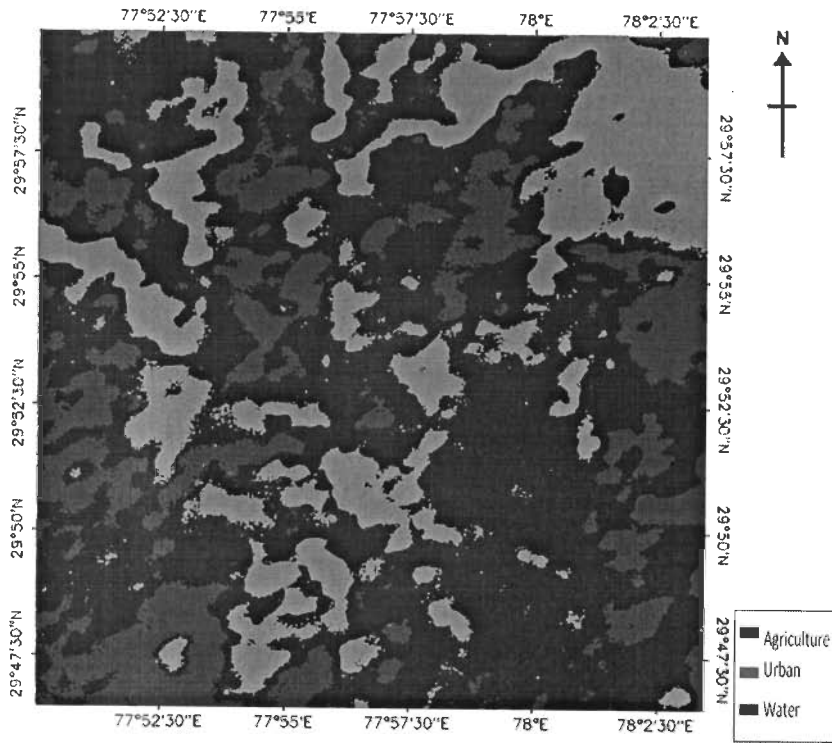


**Fig. 4.20a.** Minimum Distance classified of the curvelet based fused resultant MOI\_PA(HH).

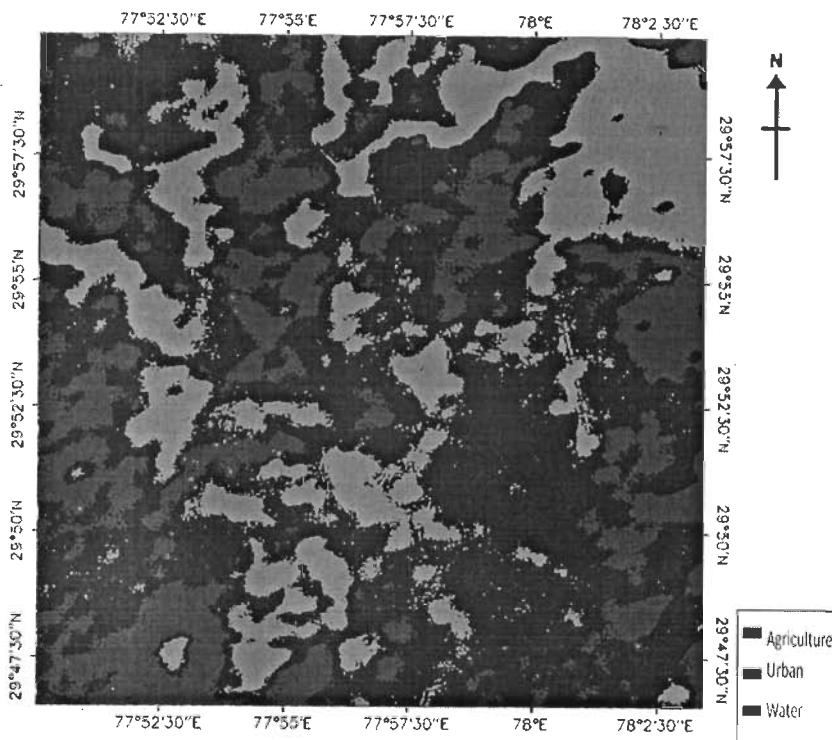


**Fig. 4.20b.** Minimum Distance classified of the curvelet based fused resultant MOI\_PA(HV).

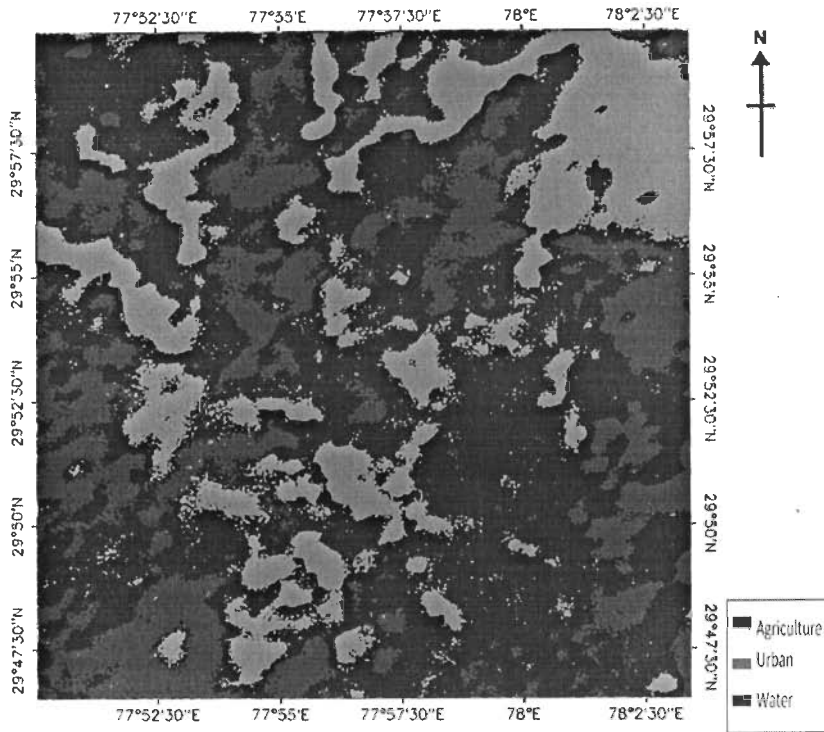


**Fig. 4.20c.** Minimum Distance classified of the curvelet based fused resultant MO1\_PA(VV).

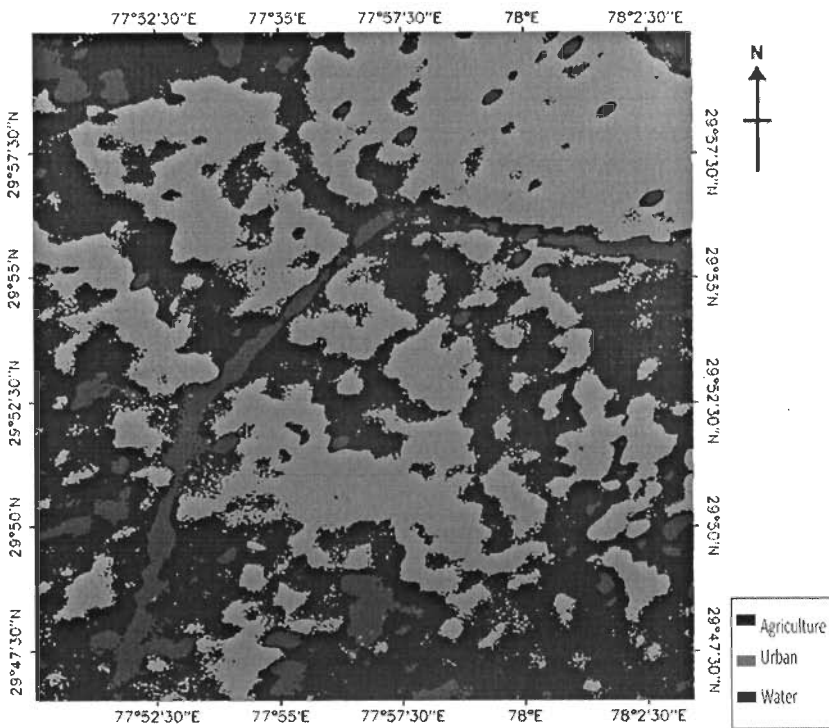


**Fig. 4.21a.** Minimum Distance classified of the curvelet based fused resultant MO2\_PA(HH).

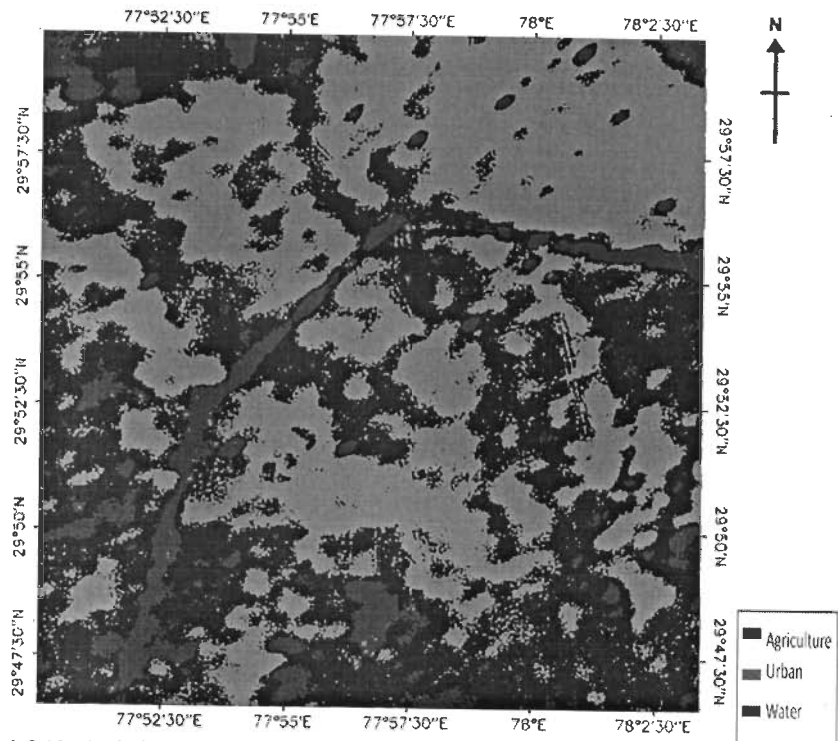


**Fig. 4.21b.** Minimum Distance classified of the curvelet based fused resultant MO2\_PA(HV).

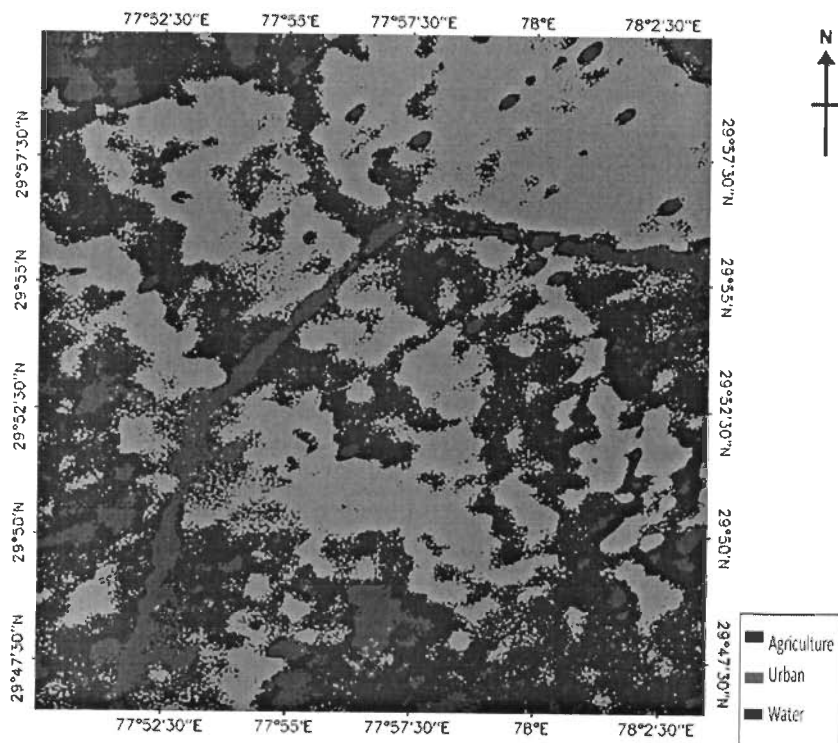


**Fig. 4.21c.** Minimum Distance classified of the curvelet based fused resultant MO2\_PA(VV).

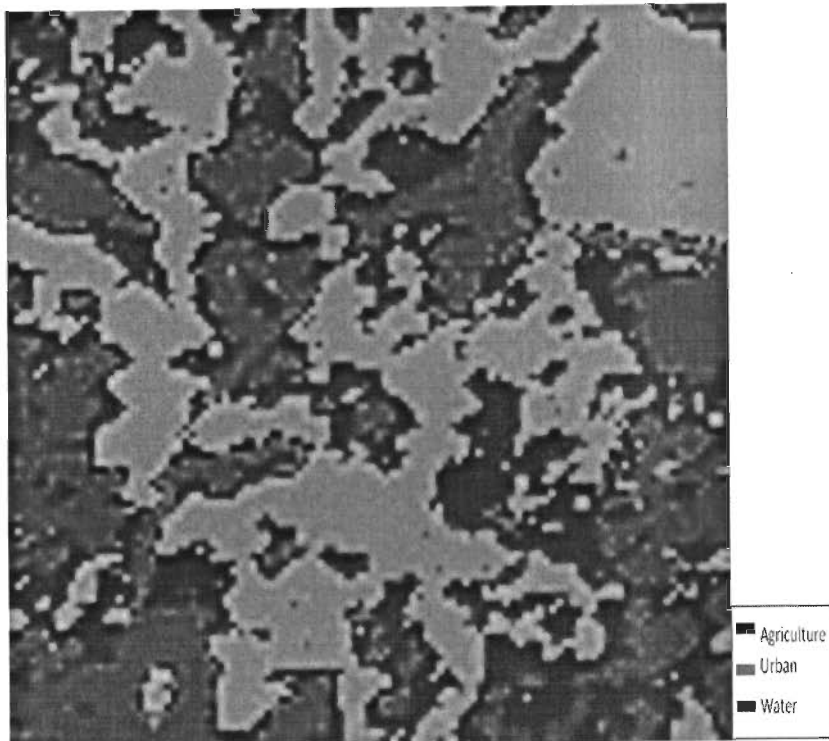


Fig. 4.22a. Minimum Distance classified of the curvelet based fused resultant MOD12

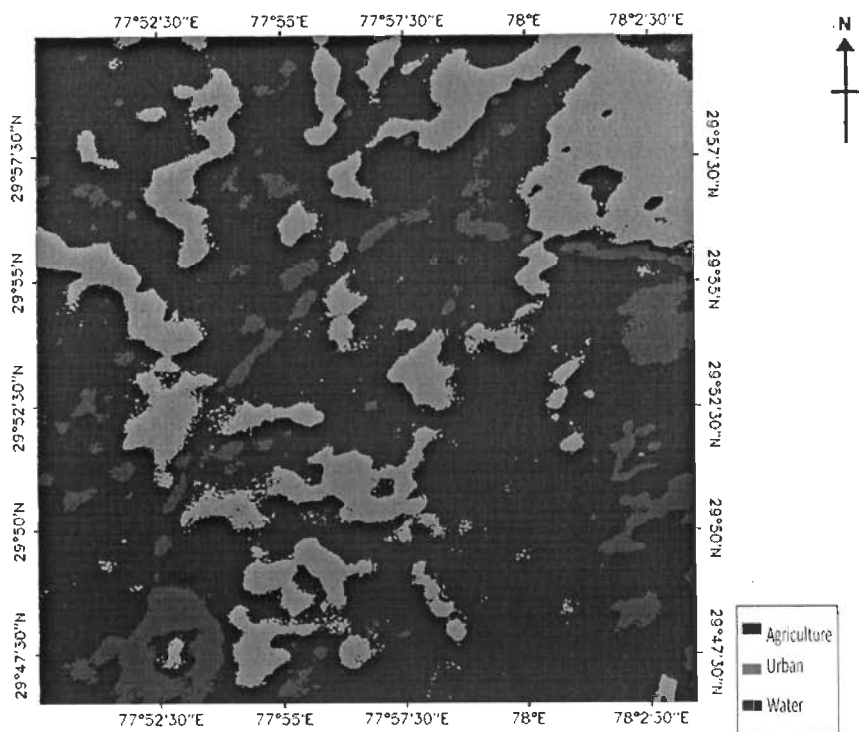
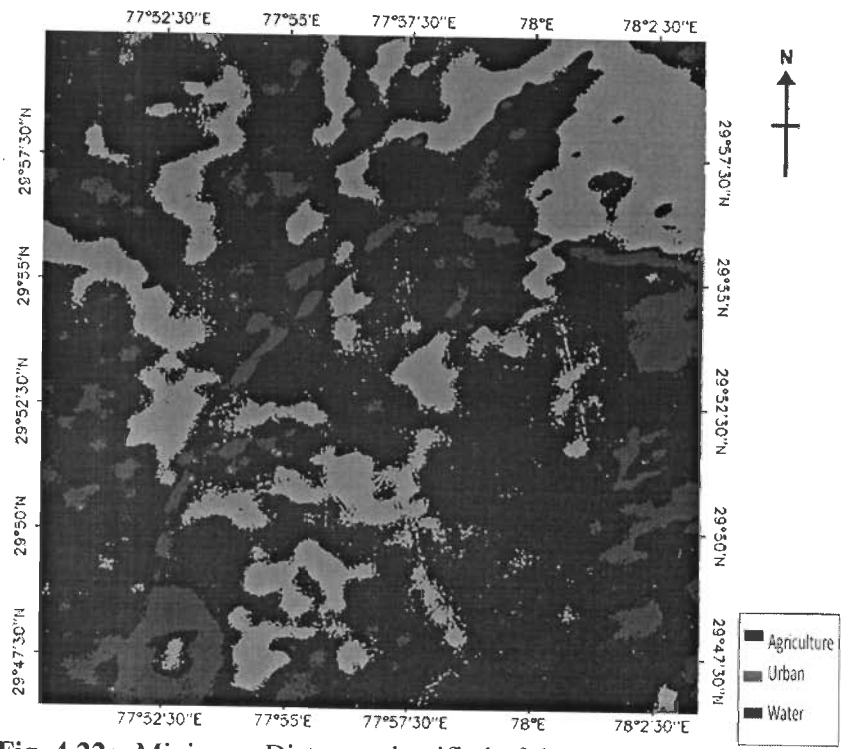
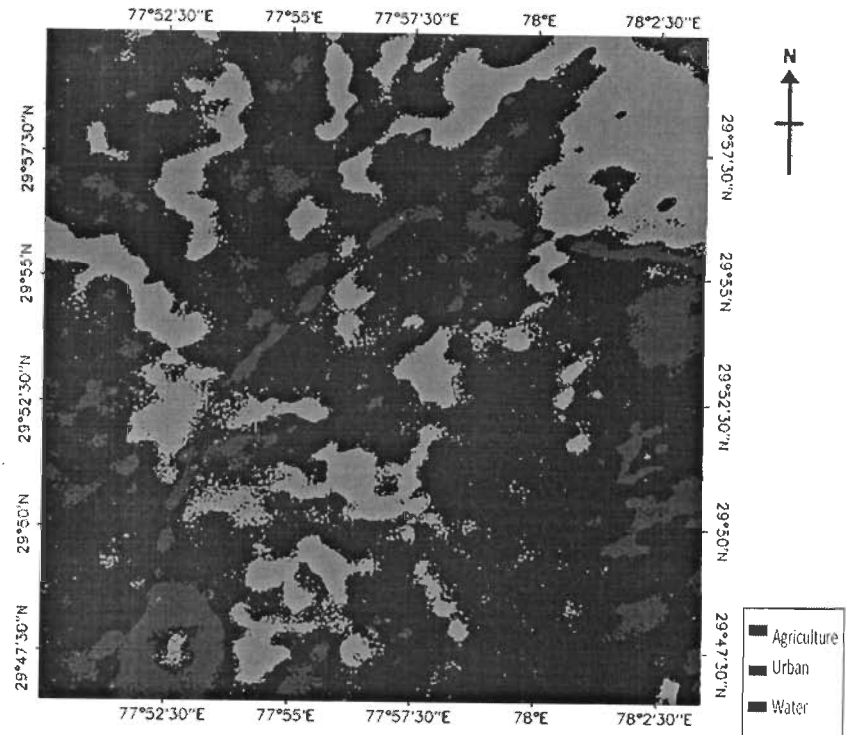


Fig. 4.22b. Minimum Distance classified of the curvelet based fused resultant MO\_PA(HH).



**Fig. 4.22c.** Minimum Distance classified of the curvelet based fused resultant MO\_PA(HV).



**Fig. 4.22d.** Minimum Distance classified of the curvelet based fused resultant MO\_PA(VV).

**Table 4.2.** Classification Accuracy for Curvelet based fusion

Images	Producers Accuracy			Users Accuracy			Overall Classification Accuracy
	Agric ulture	Urban	Water	Agric ulture	Urban	Water	
<b>MOD12</b>	39.47	59.26	82.14	57.69	53.33	62.16	58.07
<b>MO1_PA(HH)</b>	82.95	76.73	75.15	68.18	99.90	75.15	78.60
<b>MO1_PA(HV)</b>	82.49	73.76	75.15	66.79	98.75	74.25	77.40
<b>MO1_PA(VV)</b>	82.03	76.24	75.15	66.92	99.35	76.07	78.08
<b>MO2_PA(HH)</b>	88.02	54.95	95.15	66.55	82.84	96.32	78.60
<b>MO2_PA(HV)</b>	89.86	58.91	95.76	70.14	85.00	95.18	80.82
<b>MO2_PA(VV)</b>	86.64	55.94	94.55	66.67	82.48	94.55	78.25
<b>MO_PA(HH)</b>	96.31	72.77	89.70	74.38	98.92	94.87	86.30
<b>MO_PA(HV)</b>	94.47	71.29	88.48	72.70	99.80	92.41	84.76
<b>MO_PA(VV)</b>	96.31	71.78	84.85	71.82	99.55	94.59	84.60

The users accuracy of agriculture for the fused image with MOD12 i.e., MO\_PA(HH), MO\_PA(HV) and MO\_PA(VV) are 74.38%, 72.70% and 71.82% respectively (table 4.2), and it is better than the users accuracy of agriculture for the fused image with MODIS band 2 i.e., MO2\_PA(HH), MO2\_PA(HV) and MO2\_PA(VV) and there users accuracy are 66.55%, 70.14% and 66.67% respectively, and which is better than the users accuracy of agriculture for the fused image with MODIS band 1 i.e., MO1\_PA(HH), MO1\_PA(HV) and MO1\_PA(VV) and there users accuracy are 68.18%, 66.79% and 66.92% respectively.

The user accuracy for urban areas after fusion are quite good and it is observed from the table 4.2 that the MO\_PA(HH), MO\_PA(HV) and MO\_PA(VV) are giving better result than other fused image.

The users accuracy of water for the fused image with MODIS band 2 i.e., MO2\_PA(HH), MO2\_PA(HV) and MO2\_PA(VV) are 96.32%, 95.18% and 94.55% respectively (table 4.2), and it is better than the users accuracy of water for the fused image with MOD12 i.e., MO\_PA(HH), MO\_PA(HV) and MO\_PA(VV) and there users accuracy are 94.87%, 92.41% and 94.59% respectively, and which is better than the users accuracy of water for the fused image with MODIS band 1 i.e., MO1\_PA(HH), MO1\_PA(HV) and MO1\_PA(VV) and there users accuracy are 75.15%, 74.25% and 76.07% respectively.

MO\_PA(HH) the resultant image of fusion of MOD12 (Resultant image of



MODIS band 1 and band 2) and HH-Pal PALSAR band is exemplifying the highest overall classification accuracy of 86.30%.

**Fuzzy based Fusion.** The resultant minimum distance fuzzy based classified image of MODIS band 1 and PALSAR bands i.e., MO1\_PA(HH), MO1\_PA(HV) and MO1\_PA(VV), is depicted in figs 4.23a, 4.23b and 4.23c respectively. In figs 4.24a, 4.24b and 4.24c shows the minimum distance classified image of MO2\_PA(HH), MO2\_PA(HV) and MO2\_PA(VV) respectively. The minimum distance classified image of MOD12, the resultant fuzzy based fused image of MODIS band 1 and band 2, is depicted in fig 4.25a. The resultant fused image of MOD12 and PALSAR(HH, HV and VV) bands are MO\_PA(HH), MO\_PA(HV) and MO\_PA(VV), and its minimum distance classified image is depicted in the figs 4.25b, 4.25c and 4.25d respectively.

The classification accuracy for the fuzzy based fusion is calculated and tabulated in the table 4.3. The fused image of MODIS band 1 and PALSAR bands are MO1\_PA(HH), MO1\_PA(HV) and MO1\_PA(VV), and their overall classification accuracies are 69.18%, 69.35% and 71.75% respectively. MO2\_PA(HH), MO2\_PA(HV) and MO2\_PA(VV), the resultant fused image of MODIS band 2 and PALSAR bands, and their overall classification accuracies are 65.41%, 61.99% and 50.51% respectively. The fused image of MOD12 and PALSAR bands are MO\_PA(HH), MO\_PA(HV) and MO\_PA(VV), and their overall classification accuracies are 82.88%, 82.71% and 83.22% respectively. The overall classification accuracy for the fused images with MOD12 is better than the overall classification accuracy for the fused images with MODIS band 1, and which is better than the overall classification accuracy for the fused images with MODIS band 2.

The producer's accuracy of agriculture for the fused image with MOD12 i.e., MO\_PA(HH), MO\_PA(HV) and MO\_PA(VV) are 64.98%, 65.44% and 67.28% respectively (table 4.3), and it is better than the producer's accuracy of agriculture for the fused image with MODIS band 1 i.e., MO1\_PA(HH), MO1\_PA(HV) and MO1\_PA(VV) and their producer's accuracies are 52.07%, 53.46% and 56.68% respectively. Which is better than the producer's accuracy of agriculture for the fused

image with MODIS band 2 i.e., MO2\_PA(HH), MO2\_PA(HV) and MO2\_PA(VV) and there producers accuracy are 76.50%, 51.61% and 41.47% respectively.

The producers accuracy of urban for the fused image with MOD12 i.e., MO\_PA(HH), MO\_PA(HV) and MO\_PA(VV) are 96.04%, 95.54% and 95.54% respectively (table 4.3), and it is better than the producers accuracy of urban for the fused image with MODIS Band 1 i.e., MO1\_PA(HH), MO1\_PA(HV) and MO1\_PA(VV) and there producers accuracy are 80.69%, 79.21% and 83.66% respectively, and which is better than the producers accuracy of urban for the fused image with MODIS band 2 i.e., MO2\_PA(HH), MO2\_PA(HV) and MO2\_PA(VV) and there producers accuracy are 49.01%, 65.84% and 42.57% respectively.

The producers accuracy of water for the fused image with MOD12 i.e., MO\_PA(HH), MO\_PA(HV) and MO\_PA(VV) are 90.30%, 89.70% and 89.09% respectively (table 4.3), and it is better than the producers accuracy of water for the fused image with MODIS band 1 i.e., MO1\_PA(HH), MO1\_PA(HV) and MO1\_PA(VV) and there producers accuracy are 77.58%, 78.18% and 76.97% respectively, and which is better than the producers accuracy of water for the fused image with MODIS band 2 i.e., MO2\_PA(HH), MO2\_PA(HV) and MO2\_PA(VV) and there producers accuracy are 70.91%, 70.91% and 72.12% respectively.

**Table 4.3.** Classification Accuracy for fuzzy based fusion

Images	Producers Accuracy			Users Accuracy			Overall Classification Accuracy
	Agric ulture	Urban	Water	Agric ulture	Urban	Water	
<b>MOD12</b>	26.32	59.26	85.71	47.62	48.48	61.54	53.76
<b>MO1_PA(HH)</b>	52.07	80.69	77.58	61.41	72.44	73.14	69.18
<b>MO1_PA(HV)</b>	53.46	79.21	78.18	62.03	71.43	74.57	69.35
<b>MO1_PA(VV)</b>	56.68	83.66	76.97	64.74	75.45	74.71	71.75
<b>MO2_PA(HH)</b>	76.50	49.01	70.91	57.44	55.62	99.92	65.41
<b>MO2_PA(HV)</b>	51.61	65.84	70.91	57.44	48.90	99.80	61.99
<b>MO2_PA(VV)</b>	41.47	42.57	72.12	36.29	39.63	99.49	50.51
<b>MO_PA(HH)</b>	64.98	96.04	90.30	85.98	87.78	74.87	82.88
<b>MO_PA(HV)</b>	65.44	95.54	89.70	84.52	85.78	77.49	82.71
<b>MO_PA(VV)</b>	67.28	95.54	89.09	84.39	87.33	77.37	83.22

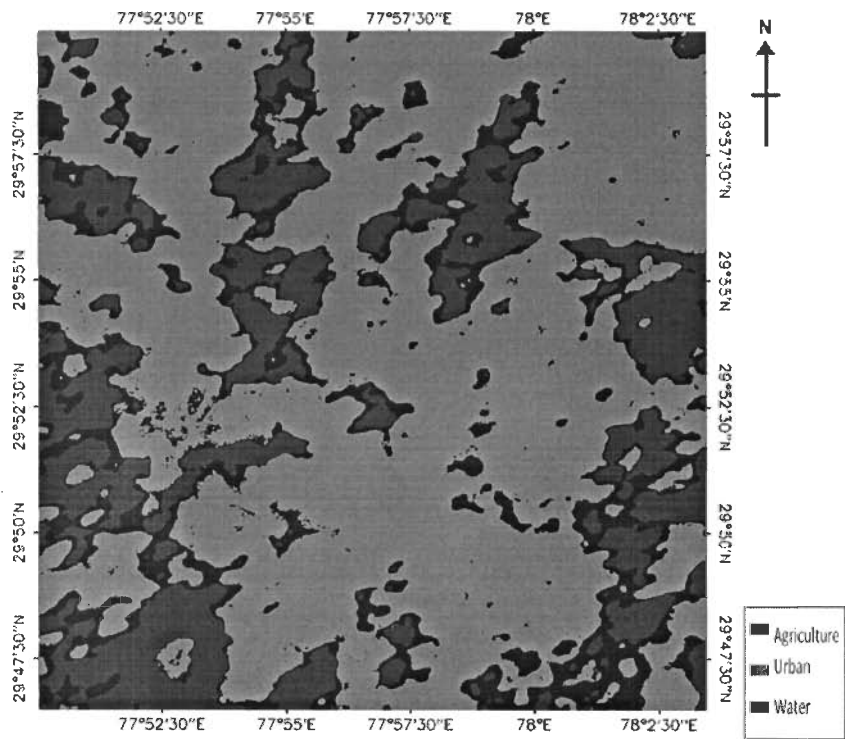


**Fig. 4.23a.** Minimum Distance classified of the fuzzy based fused resultant MO1\_PA(HH).

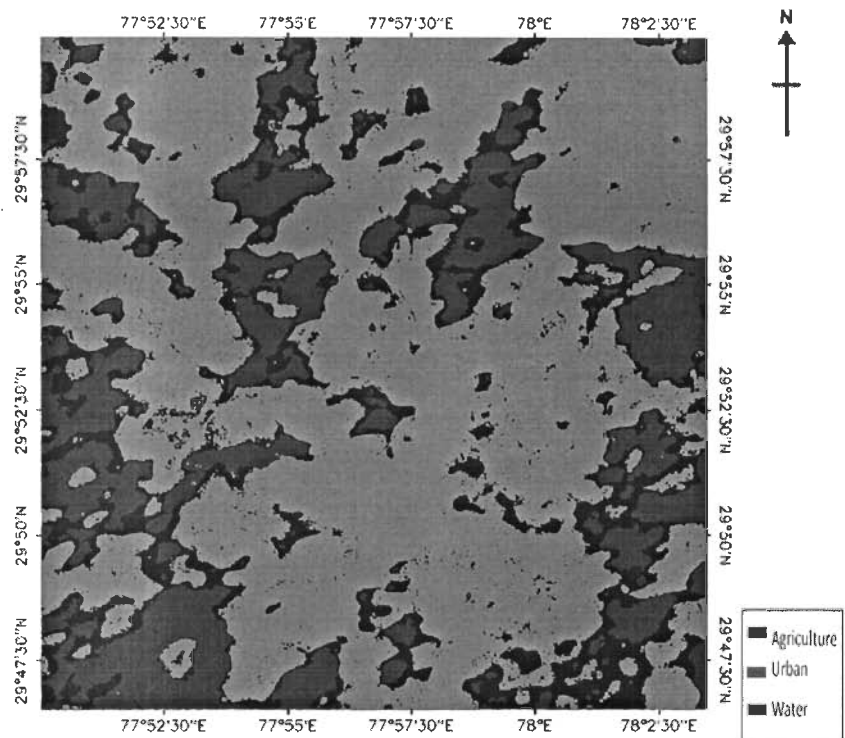


**Fig. 4.23b.** Minimum Distance classified of the fuzzy based fused resultant MO1\_PA(HV).

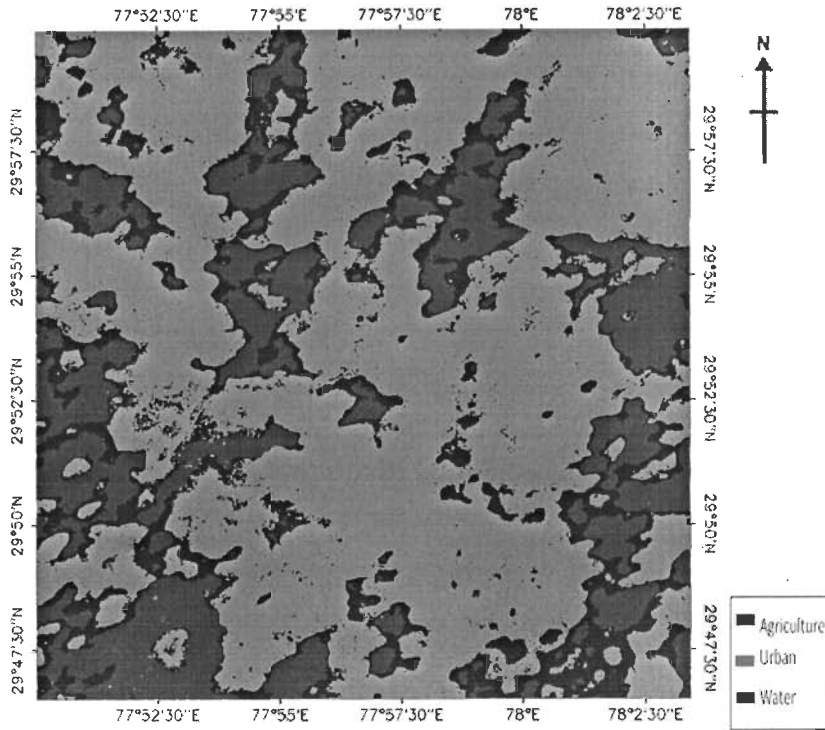


Fig. 4.23c. Minimum Distance classified of the fuzzy based fused resultant MO1\_PA(VV).

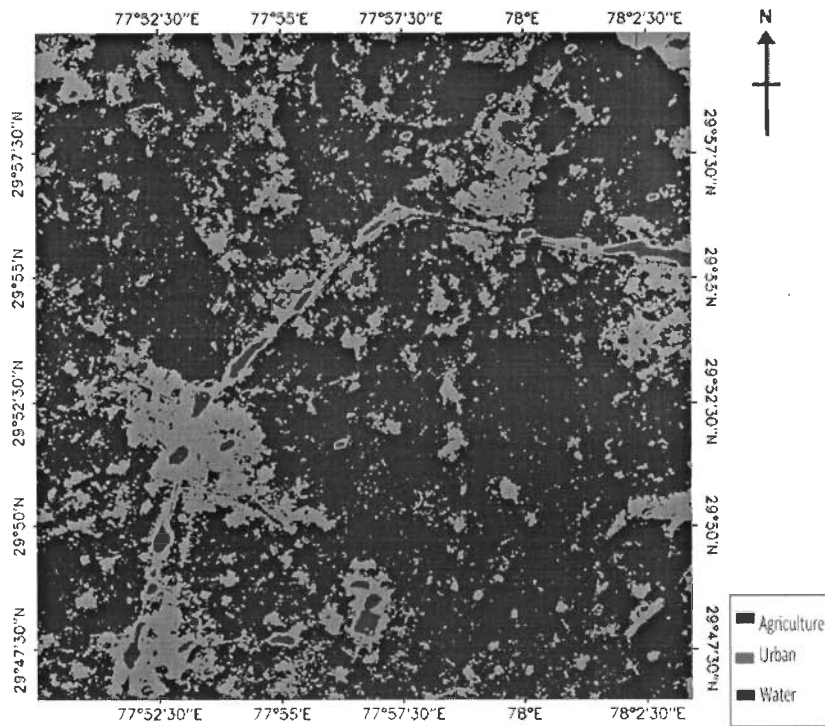


Fig. 4.24a. Minimum Distance classified of the fuzzy based fused resultant MO2\_PA(HH).

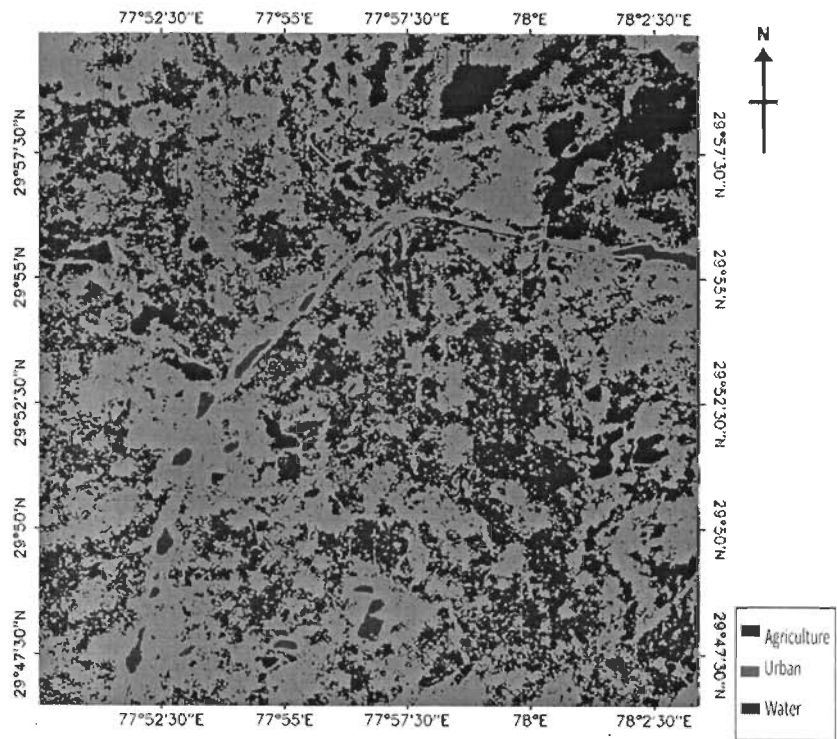


Fig. 4.24b. Minimum Distance classified of the fuzzy based fused resultant MO2\_PA(HV).

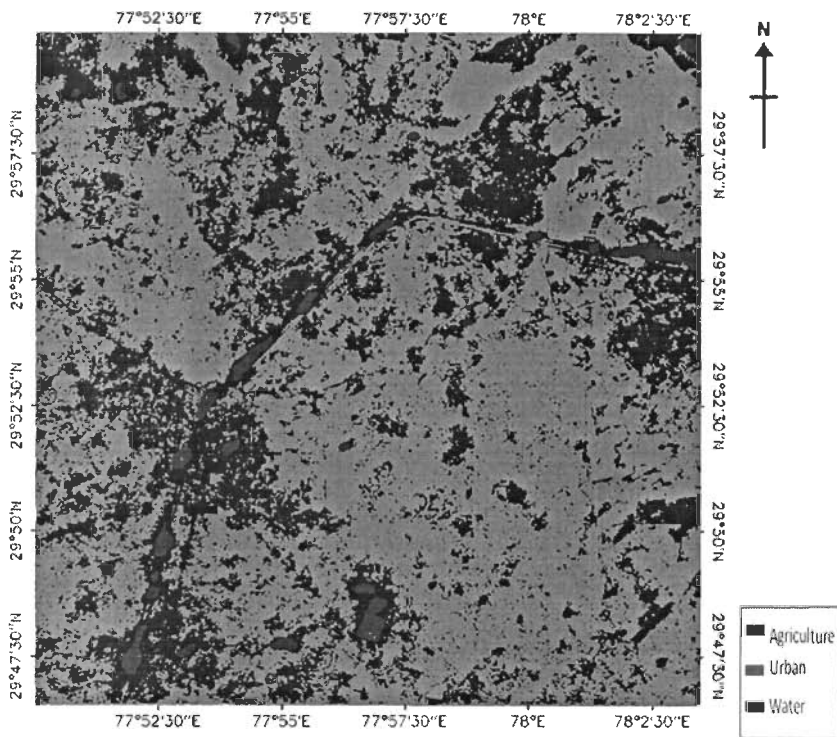


Fig. 4.24c. Minimum Distance classified of the fuzzy based fused resultant MO2\_PA(VV).

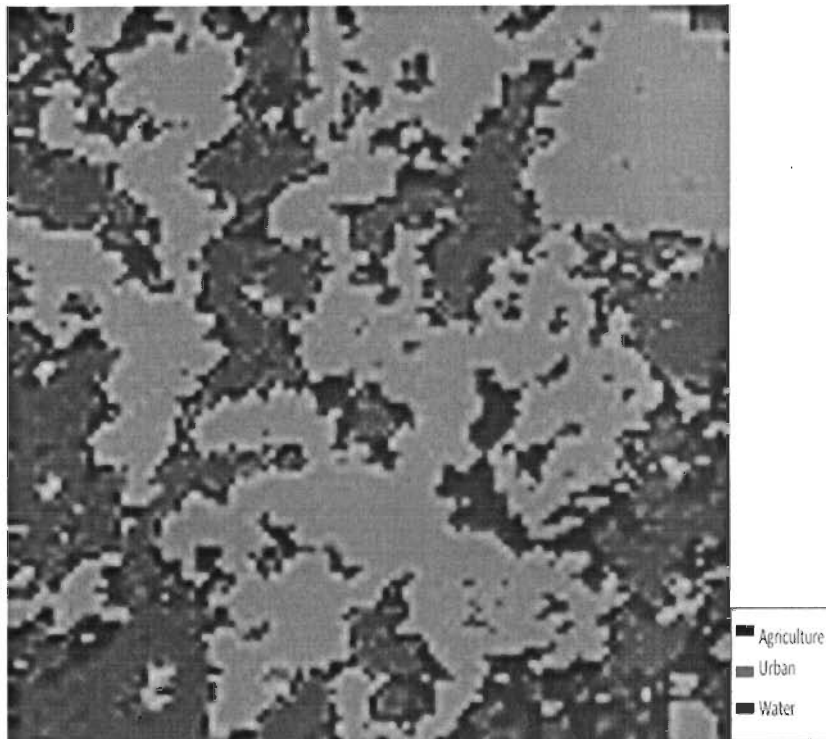


Fig. 4.25a. Minimum Distance classified of the fuzzy based fused resultant MOD12

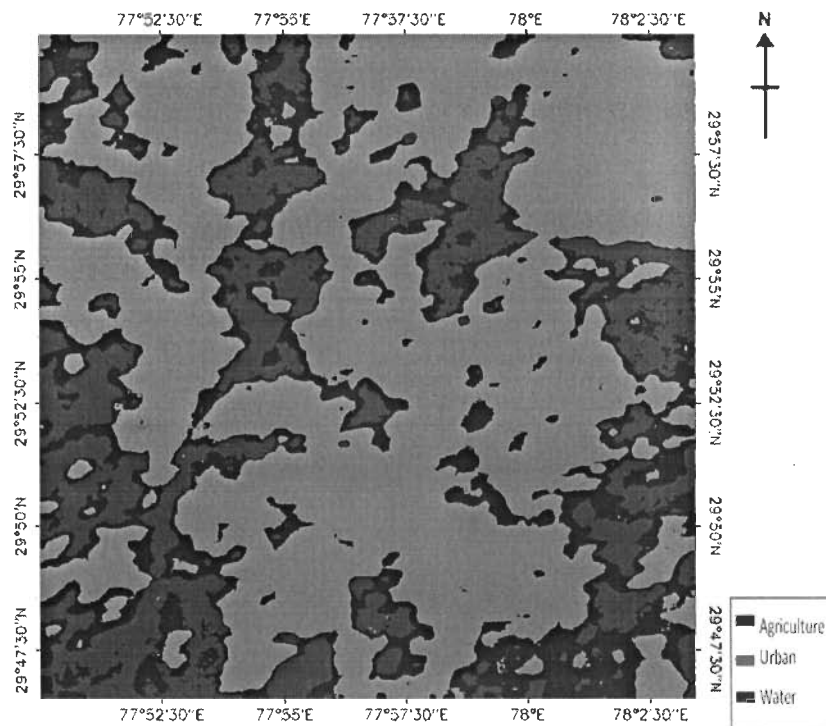
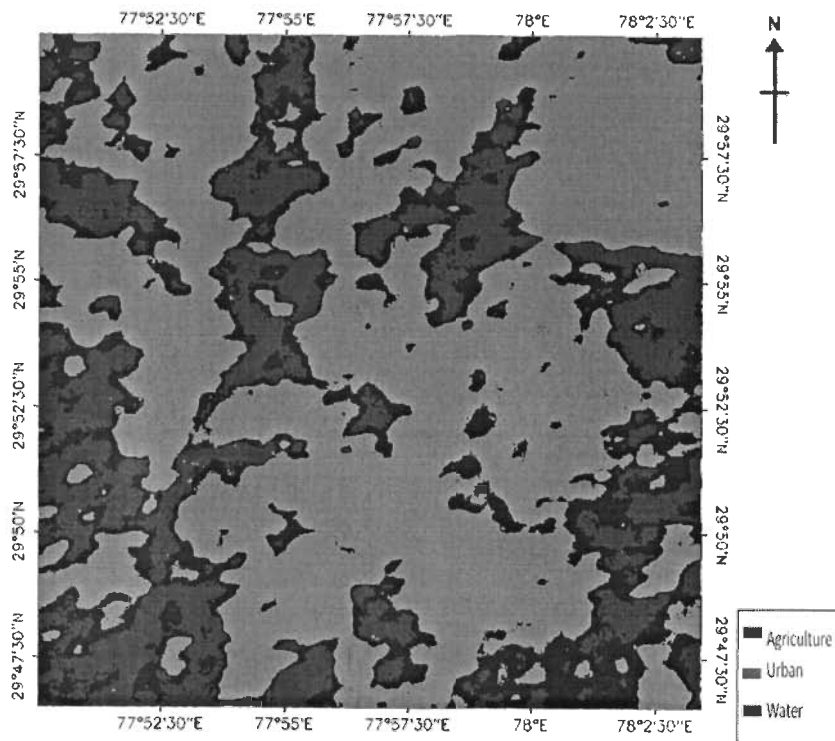
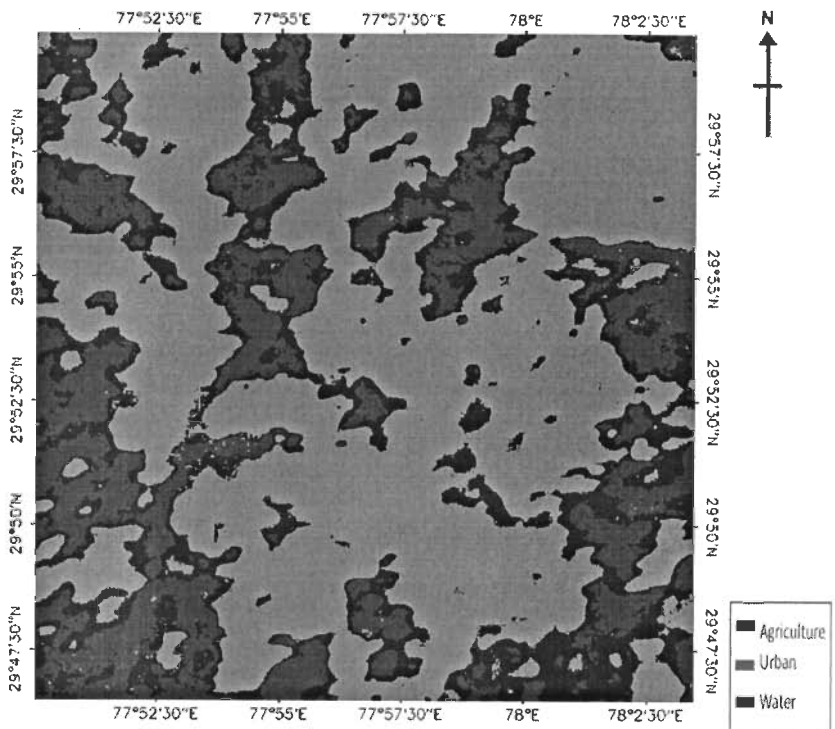


Fig. 4.25b. Minimum Distance classified of the fuzzy based fused resultant MO\_PA(HH).



**Fig. 4.25c.** Minimum Distance classified of the fuzzy based fused resultant MO\_PA(HV).



**Fig. 4.25d.** Minimum Distance classified of the fuzzy based fused resultant MO\_PA(VV).

It is observed from the table 4.3 that user accuracies for agricultural and urban are quite enhanced in the case of MO\_PA(HH), MO\_PA(HV) and MO\_PA(VV) images in comparison to the other fused image while as for the water class MO2\_PA(HH), MO2\_PA(HV) and MO2\_PA(VV) are giving the better result. But overall accuracy is certainly quite high for MO\_PA(HH), MO\_PA(HV) and MO\_PA(VV) in comparison to other fused images (table 4.3).

It is observed from the table 4.2 that the PALSAR images after curvelet based fusion with MODIS individual bands i.e., MODIS band 1 and band 2 and as well as MOD12 (resultant fused image of MODIS band 1 and band 2) are giving quite satisfactory classification accuracy and more than 75% overall classification accuracy for all the fused image. In another hand table 4.3 indicates that for fuzzy based fusion good classification accuracy is achieved for MOD12 and all individual PALSAR bands (HH-Pol, HV-Pol and VV-Pol)

## ii. Quality Assessment.

Quality assessment indicators represents that after fusion what is preserved information in the fused image with original image. The correlation coefficient, RMSE, RMD, RVD, DI, PSNR and UQI are computed as by the eq. 3.14, 3.15, 3.16, 3.17, 3.18, 3.19 and 3.20 respectively. These quality assessment indicators have been calculated for the fused images with respect to MODIS Bands.

**Curvelet based Fusion.** In table 4.4 the quality assessment indicators are tabulated for the curvelet based fused images MO1\_PA(HH), MO1\_PA(HV), MO1\_PA(VV), with respect to MODIS band 1. The quality assessment indicators for the curvelet fused images MO2\_PA(HH), MO2\_PA(HV), MO2\_PA(VV) with respect to MODIS band 2 is tabulated in the table 4.5, and in table 4.6 the quality assessment indicators are tabulated for the curvelet fused images MO\_PA(HH), MO\_PA(HV), MO\_PA(VV) with respect to MOD12(Resultant fused image of MODIS band 1 and band 2).



From the tables 4.4, 4.5 and 4.6, it is observed that there is a good closeness between resultant fused images i.e., MO\_PA(HH), MO\_PA(HV), MO\_PA(VV) with MOD12 and MO1\_PA(HH), MO1\_PA(HV), MO1\_PA(VV) with MODIS band 1 and MO2\_PA(HH), MO2\_PA(HV), MO2\_PA(VV) with MODIS band 2 (while as MO\_PA(HH) and MOD12 has higher closeness in comparison to other fused images). Similar results have been obtained with other quality indicators like RMSE, RMD, RVD, DI, PSNR and UQI. This type of analysis resembles the advantages of fusion with curvelet based technique.

**Fuzzy based Fusion.** The quality assessment indicators for the fuzzy based fused images MO1\_PA(HH), MO1\_PA(HV), MO1\_PA(VV), with respect to MODIS band 1 are tabulated in table 4.7 and in table 4.8, the quality assessment indicators for the fuzzy based fused images MO2\_PA(HH), MO2\_PA(HV), MO2\_PA(VV) with respect to MODIS band 2 are tabulated. The quality assessment indicators are tabulated for the fused images MO\_PA(HH), MO\_PA(HV), MO\_PA(VV) with respect to MOD12(Resultant fused image of MODIS band 1 and band 2) in table 4.9.

Fuzzy based fusion is giving some different result in comparison to the curvelet based fusion from the tables 4.7, 4.8 and 4.9. The correlation coefficient for MO1\_PA(HH), MO1\_PA(HV), MO1\_PA(VV) with MODIS band 1 and MO\_PA(HH), MO\_PA(HV), MO\_PA(VV) with MOD12 are quite high in comparison to MO2\_PA(HH), MO2\_PA(HV), MO2\_PA(VV), while as a good correlation coefficient in all combination in case of curvelet based fusion from the tables 4.4, 4.5 and 4.6. it is noticed that other quality indicators are strengthening the interference obtained by correlation coefficient value. It clearly indicates that these type of fusion may be used for various application.

**Table 4.4.** Quality Assessment Indicators between MODIS Band 1 and resultant curvelet based fusion of PALSAR Bands with MODIS Band 1

	MODIS Band 1						
	Corr	RMSE	RMD	RVD	DI	PSNR	UQI
<b>MO1_PA(HH)</b>	0.9917	4.0861	-0.3044	-0.6249	0.2965	16.6188	0.0080
<b>MO1_PA(HV)</b>	0.9802	6.3747	-0.2434	-0.5399	0.3691	16.5318	0.0060
<b>MO1_PA(VV)</b>	0.9722	7.6103	-0.1974	-0.5933	0.3222	19.4116	0.0072

**Table 4.5.** Quality Assessment Indicators between MODIS Band 2 and resultant curvelet based fusion of PALSAR Bands with MODIS Band 2

	<b>MODIS Band 2</b>						
	<b>Corr</b>	<b>RMSE</b>	<b>RMD</b>	<b>RVD</b>	<b>DI</b>	<b>PSNR</b>	<b>UQI</b>
<b>MO2_PA(HH)</b>	0.9838	4.0841	-0.2739	-0.5428	0.1932	16.2280	0.0078
<b>MO2_PA(HV)</b>	0.9620	6.3744	-0.2758	-0.5174	0.2748	14.8443	0.0062
<b>MO2_PA(VV)</b>	0.9471	7.6093	-0.1917	-0.5070	0.3036	15.9705	0.0075

**Table 4.6.** Quality Assessment Indicators between MOD12 and resultant curvelet based fusion of PALSAR Bands with MOD12

	<b>MOD12</b>						
	<b>Corr</b>	<b>RMSE</b>	<b>RMD</b>	<b>RVD</b>	<b>DI</b>	<b>PSNR</b>	<b>UQI</b>
<b>MO_PA(HH)</b>	0.9920	4.0749	-0.3717	-0.6388	0.1896	20.8267	0.0118
<b>MO_PA(HV)</b>	0.9807	6.3681	-0.3246	-0.5753	0.2373	17.9525	0.0106
<b>MO_PA(VV)</b>	0.9728	7.6042	-0.3098	-0.6250	0.2724	19.7172	0.0104

**Table 4.7.** Quality Assessment Indicators between MODIS Band 1 and resultant fuzzy based fusion of PALSAR Bands with MODIS Band 1

	<b>MODIS Band 1</b>						
	<b>Corr</b>	<b>RMSE</b>	<b>RMD</b>	<b>RVD</b>	<b>DI</b>	<b>PSNR</b>	<b>UQI</b>
<b>MO1_PA(HH)</b>	0.8333	26.7137	-0.2239	-0.9139	0.2980	19.5961	0.0517
<b>MO1_PA(HV)</b>	0.8234	27.1745	-0.2260	-0.9200	0.3008	19.4476	0.0551
<b>MO1_PA(VV)</b>	0.8415	26.0684	-0.2241	-0.9000	0.2894	19.8085	0.0441

**Table 4.8.** Quality Assessment Indicators between MODIS Band 2 and resultant fuzzy based fusion of PALSAR Bands with MODIS Band 2

	<b>MODIS Band 2</b>						
	<b>Corr</b>	<b>RMSE</b>	<b>RMD</b>	<b>RVD</b>	<b>DI</b>	<b>PSNR</b>	<b>UQI</b>
<b>MO2_PA(HH)</b>	0.4507	46.7041	-0.1111	-0.5441	0.2213	14.7437	0.0208
<b>MO2_PA(HV)</b>	0.4479	47.1527	-0.1147	-0.5763	0.2231	14.6607	0.0230
<b>MO2_PA(VV)</b>	0.5469	45.5941	-0.1089	-0.4746	0.2226	14.9526	0.0171

**Table 4.9.** Quality Assessment Indicators between MOD12 and resultant fuzzy based fusion of PALSAR Bands with MOD12

	<b>MOD12</b>						
	<b>Corr</b>	<b>RMSE</b>	<b>RMD</b>	<b>RVD</b>	<b>DI</b>	<b>PSNR</b>	<b>UQI</b>
<b>MO_PA(HH)</b>	0.8837	25.4357	-0.3108	-0.9699	0.1820	20.0219	0.0595
<b>MO_PA(HV)</b>	0.8789	25.7404	-0.3140	-0.9730	0.1830	19.9185	0.0567
<b>MO_PA(VV)</b>	0.8911	25.3167	-0.3027	-0.9756	0.1711	20.0627	0.0712

## 4.6. Conclusion

A curvelet transform and fuzzy based fusion is applied for various combination of PALSAR with MODIS image to assess the quality of fused image. The fused images are quantitatively analyzed by quality assessment indicators (Correlation Coefficient, Root Mean squared error, Relative Mean Difference, Relative Variation Difference, Deviation Index, Peak signal-to-noise ratio (PSNR), Universal Image Quality Index) in one hand and in another hand land cover classification accuracy is computed and compared with fused and without fused image. It is clearly observed that, the resultant curvelet fused image of HH-Pol PALSAR image with MOD12 (Resultant fused image of MODIS Band 1 and Band 2), i.e., MO\_PA(HH) is providing maximum classification accuracy in comparison to other combination of fused images with the curvelet based fusion, and it is supported with the quality assessment indicators with also indicate MO\_PA(HH) has the better fused image in comparison with other combination of PALSAR and MODIS fusions. And thereby it is observed that the overall classification accuracy of fused image is quite enhanced in comparison to the classification accuracy of individual MODIS images, i.e., MODIS Band 1 and MODIS Band 2. Similarly in the outline of fuzzy based fusion it is observed that, the resultant curvelet fused image of VV-Pol PALSAR image with MOD12 (Resultant fused image of MODIS Band 1 and Band 2), i.e., MO\_PA(VV) is providing maximum classification accuracy in comparison to other combination of fused images. This type of fusion may be helpful in near future to maximize the use of MODIS images.

## Chapter 5

# MODIS Image Application for Hotspot and non-Hotspot Region Classification

---

### 5.1. Introduction

MODIS has 36 bands and each band has their own individual characteristic which are useful for particular application. In this thesis, we are very much interested to enhance the use of MODIS images for various applications. Therefore, in this chapter we have taken a task to classify the landcover in a single class and this single class we have taken as a subsurface fire (i.e., hotspot) region. So, an attempt has been made to classify the single class i.e., subsurface fire with MODIS image especially using MODIS band 1 and MODIS band 2 using Binary Division Algorithm.

Subsurface coal fires are a serious and widespread problem in coal producing countries such as India, China, Indonesia and other developing countries. India accounts for the world's greatest concentration of coal fires which cause several devastating environmental effects. Jharia Coal Field (JCF) in Jharkhand (India) alone contains nearly half of subsurface mine fires (hotspots) in Indian coalfields. Most of the fires take place due to spontaneous heating of coal and cause a local rise in the

surface temperature, which depends on various mining, geological and coal factors. Mine fires apart from economic aspects give rise to devastating environmental effects. Therefore attention is required in this direction for mapping, monitoring and detecting these hotspots with less cumbersome and more economic way (Agarwal et al.,2006). Satellite images can be one of the best solutions for these kinds of problems which offer a cost effective and time saving technology for mapping various geo-environmental features.

As discussed in the review section (i.e., section 2.6) that several researchers proposed various methodologies to detect hot spots. MODIS has also the one special product i.e., MOD14A2 for fire product which is also not providing satisfactory results. But still uncertainties exist. Because, we are interested to increase the use of MODIS images, so we have made an attempt to classify hotspots and non hotspot regions using MODIS as one of the data.

Humans learn from the past. We learn by experience, by mistakes or successes. But what is this experience and how can it be formalized to make machines to learn. Probably most important: how do we generalize from these experiences, and how do we make decisions and how can we build it into a machine. Pattern recognition is concerned with the learning from experience, learning from examples, and making decisions (Bishop 1995, Jain et al. 2000, Duda et al. 2001). Pattern Recognition has a long history within engineering, especially for military applications. But it has long been a rather specialized subject due to the cost of hardware for acquiring the image and to compute the answers. In recent years, the advances made in hardware, made the concerns of pattern recognition of much wider applicability. According to Jain et al. 2000, pattern recognition is a general term to describe a wide range of problems like recognition, description, classification, and grouping of patterns. These problems are important in a variety of engineering and scientific disciplines such as biology, psychology, medicine, marketing, artificial intelligence, computer vision and remote sensing.

Unsupervised clustering is a fundamental tool in image processing for geosciences and satellite imaging applications (Aplin et al. 1999, Stuckens et al. 2000, Franklin et al. 2002, Gallego 2004). For example, unsupervised clustering is often

used to obtain vegetation maps of an area of interest. This approach is useful when reliable training data are either scarce or expensive, and when relatively little a priori information about the data is available. Unsupervised clustering methods play a significant role in the pursuit of unsupervised classification (Richards and Jia 2006). Eventually this unsupervised clustering can be used for one-class clustering or one class classification. The unsupervised clustering is roughly divided into three groups : agglomerative, partitioning, and agglomerative-partitioning methods (Hanaizumi and Chino, 1995). The key point in clustering is efficiency as well as accuracy, because they have an enormous volume of data, as the clustering of satellite images involves enormous volume of data. For efficiency and accuracy point of view, the methods proposed still need more attention. The agglomerative methods have high efficiency but have low accuracy. On the other hand, the partitioning methods are accurate and efficient, but they require huge memory and much time. The agglomerative-partitioning methods, such as ISODATA (Ball and Hall, 1965), improve the performance in accuracy by using iterative processing, which makes the method inefficient. Hanaizumi et al. 1995 developed an algorithm with high speed and high accuracy for clustering remotely sensed multispectral images with a partitioning method which is known as Binary Division Clustering (BDC) for clustering. This method has a binary division process and image data are repeatedly divided into two groups until the group consists of a single cluster.

The main objective of this chapter is to classify hotspots and non-hotspots region using MODIS image. Generally researcher (Boles and Verbyla, 2000, Kennedy et al., 1994, Nakayama et al., 1999) are using thermal bands for classifying hotspot and non- hotspot regions. MODIS has also a separate product i.e., MOD14A2 for the fire detection, but we have observed this product has limited capability to classify hotspot such as subsurface fire and non-hotspots regions. Another problem of MODIS image is its resolution therefore there is a need of research by which we may able to use MODIS images for classification of hotspot and non-hotspot regions. Therefore in this chapter, an attempt has been made to develop such an technique by which MODIS can be useful for these type of classification. For this purpose, to enhance the spatial resolution of MODIS image, we have fused the MODIS image with the LISS (Linear Imaging Self-Scanner) image which have quite good resolution. For selection

of the bands which may be useful for separating hotspots and non-hotspots, we have checked some bands of MODIS. After exhaustive study, we found that MODIS band 1 and MODIS band 2 may be useful to classify hotspots and non-hotspots regions. It may be due to the reason that these bands represents the vegetation or greenness of the particular region and it is known factor that in the hotspots region the possibility of greenness i.e., vegetation is very minimum. So, these bands may be helpful to classify the hotspot and non-hotspot regions. The spectral response of hotspot and non-hotspot regions in the MODIS Band 1 is shown in the fig. 5.1a and the spectral response for the MODIS Band 2 is shown in the fig. 5.1b. It infers that the hotspot and non-hotspot regions can be easily classified as there is a distinct spectral response of hotspot and non-hotspots regions. Similarly, the spectral response of hotspot and non-hotspot regions for the LISS Band 2 is shown in the fig. 5.2a, and the spectral response for the LISS Band 3 is shown in the fig. 5.2b, and it also implies that the hotspot and non-hotspot regions can be easily classified because there is a distinct spectral response of hotspot and non-hotspots regions. The NDVI (Normalized Difference Vegetation Index) is an important indicator which defines the presence of vegetation. So this may be also useful for classifying these hotspot and non-hot spot regions as the spectral response of the NDVI of MODIS (fig. 5.3) indicates the distinct response between hot spot and non-hot spot regions.

Another advantage of selecting these bands i.e., MODIS band 1 and MODIS band 2 is that these bands wavelength is quite similar to the LISS Band 2 and band 3 images. After selecting these bands for single class classification i.e., hotspot and non-hotspot region, a pattern recognition based technique BDA has been applied.

This chapter is structured as follows: data used for the study has been discussed in section 5.2. Section 5.3 briefly reviews the BDC Algorithm (BDA). Implementation and results of the used approach is given in section 5.4. In the subsequent section, i.e., in section 5.5 analyses of experimental results and finally this chapter is concluded in the section 5.6.

## 5.2. Data Used/Study Area

Jharia coal field is located in Jharkhand state, India and is named after the main mining area of Jharia. It is situated at the heart of the Damodar valley and is depicted with fig. 1.2, and the details concerning the Jharia coal field is clarified in the section 1.3.2.

The area covered by the coal belt is about 450 km<sup>2</sup>. The Jharia coal field is an exclusive storehouse of prime coke coal in the country, consisting of 23 large underground and nine large open cast mines (Agarwal et al. 2006). The mining activities in these coal fields started in 1894 and were intensified in 1925. The history of coal-mine fire in Jharia coal field can be traced back to 1916 when the first fire was detected. The Subsurface fire coordinates i.e., hotspots information are provided by BCCL (Bharat Coking Coal Limited, India) and by CIMFR (Central Institute of Mining and Fuel Research), Dhanbad, India and these coordinates are listed in the table 5.1 (Prakash, 1996, Prakash et al., 1997). The hotspot pixels were identified from the ground observations using location (Latitude, Longitude) information and therefore projected easily on georeferenced MODIS images.

MOD09Q1 is used to extract MODIS band 1 and MODIS band 2 information, where as MOD14A2 which is the fire product of MODIS is used for comparison purpose. IRS-P6 LISS-III is used to extract LISS band 2 and LISS band 3 information. The MOD09Q1 provides Band 1 of spatial resolution 250m and bandwidth 620 - 670 nm, and Band 2 of spatial resolution of 250m and bandwidth 842 - 876nm, and details of the product is covered in the section 1.4.1a. The IRS (Indian Remote-Sensing Satellite) - P6, LISS (Linear Imaging Self-Scanner) –III band 2 and band 3 are considered in this chapter. The Band 2 has the spectral bandwidth of 620 - 680 nm, and band 3 has the spectral bandwidth of 770 - 860 nm. The details of the data set used for this chapter is given in table 5.2.



**Table 5.1.** Latitude and longitude of important hotspots in Jharia coalfield (Prakash, 1996, Prakash et al., 1997)

Latitude	Longitude	Latitude	Longitude
23.80625	86.143752	23.752083	86.122918
23.80625	86.377086	23.752083	86.410419
23.797916	86.452086	23.74375	86.406252
23.797916	86.218752	23.735416	86.368752
23.797916	86.264585	23.735416	86.427086
23.79375	86.314585	23.73125	86.443752
23.79375	86.343752	23.714583	86.389586
23.789583	86.197919	23.710416	86.422919
23.789583	86.289585	23.710416	86.452086
23.785416	86.277085	23.70625	86.427086
23.785416	86.314585	23.702083	86.427086
23.777083	86.322919	23.689583	86.377086
23.772916	86.164585	23.689583	86.389586
23.76875	86.360419	23.660416	86.452086

**Table 5.2.** Data Details

Data id	Data set	Date of Acquisition
d1	MOD09Q1.A2004057.h25v06.005.2007251185548.hdf	February 26 <sup>th</sup> 2004
d2	MOD09Q1.A2004329.h25v06.005.2007337162720.hdf	November 24 <sup>th</sup> 2004
d3	MOD14A2.A2004057.h25v06.005.2007251151130.hdf	February 26 <sup>th</sup> 2004
d4	MOD14A2.A2004329.h25v06.005.2007337114507.hdf	November 24 <sup>th</sup> 2004
L1	IMAGERY.L-3(LISS)	February 25 <sup>th</sup> 2004

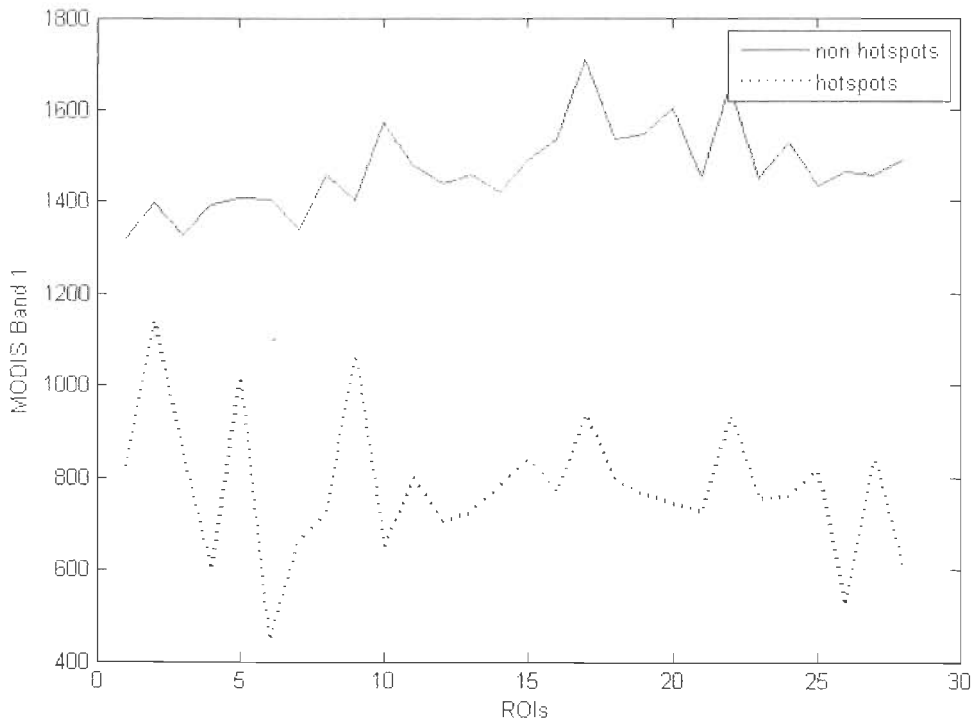


**Fig 5.1a.** Spectral response of hotspot and non-hotspot regions in the MODIS band 1(d1).

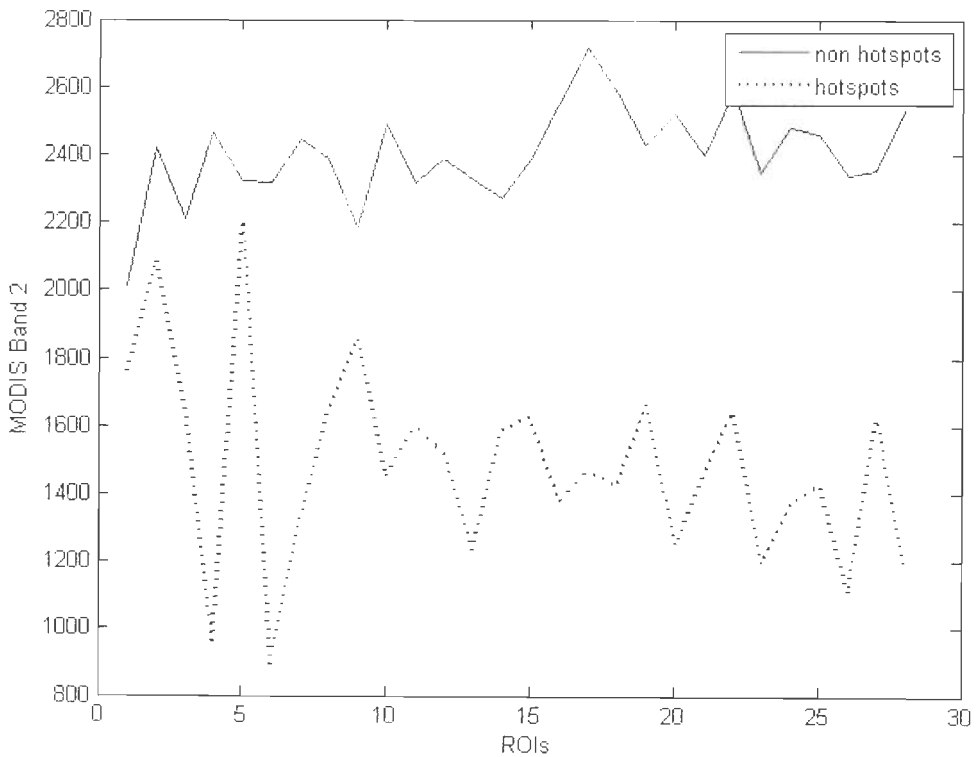


**Fig 5.1b.** Spectral response of hotspot and non-hotspot regions in the MODIS band 2 (d1).

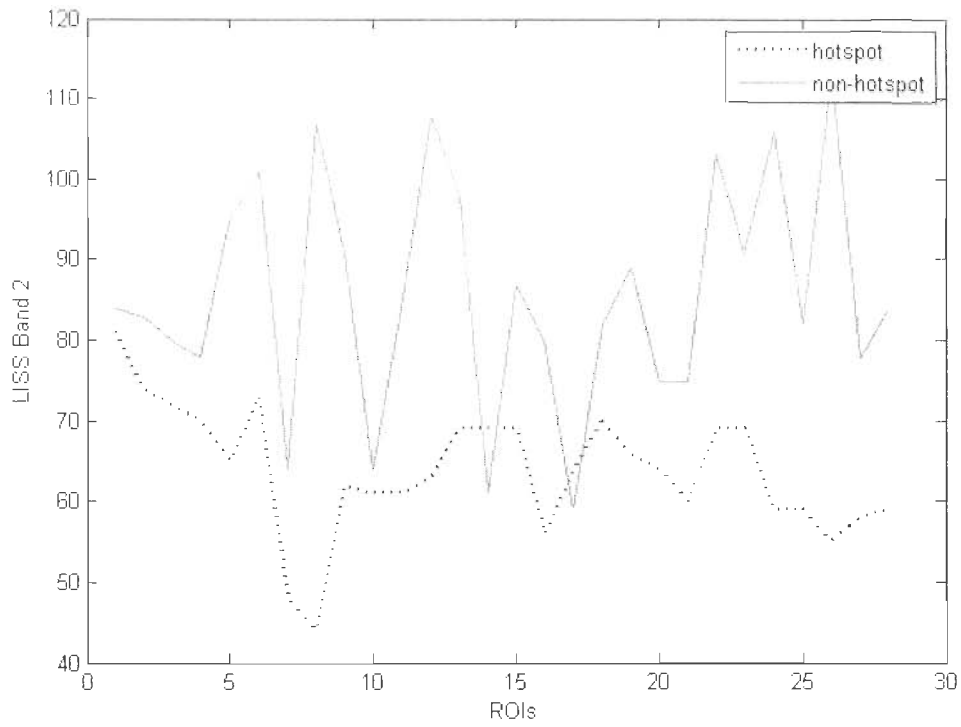


**Fig 5.2a.** Spectral response of hotspot and non-hotspot regions in the LISS band 2 (L1).

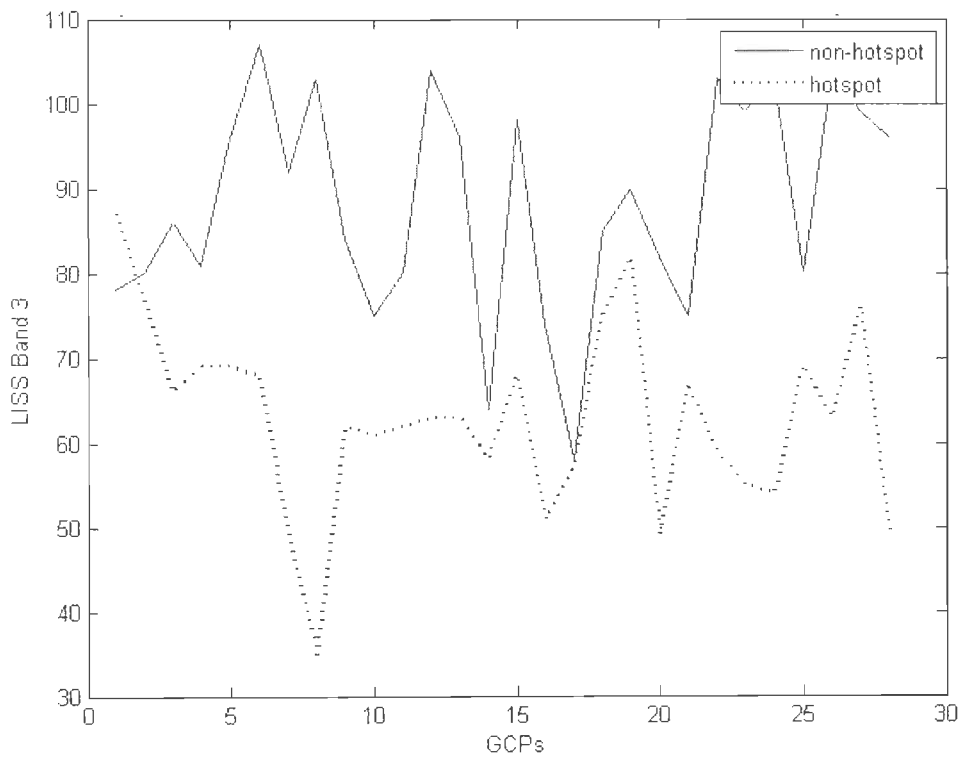


**Fig 5.2b.** Spectral response of hotspot and non-hotspot regions in the LISS band 3 (L1).

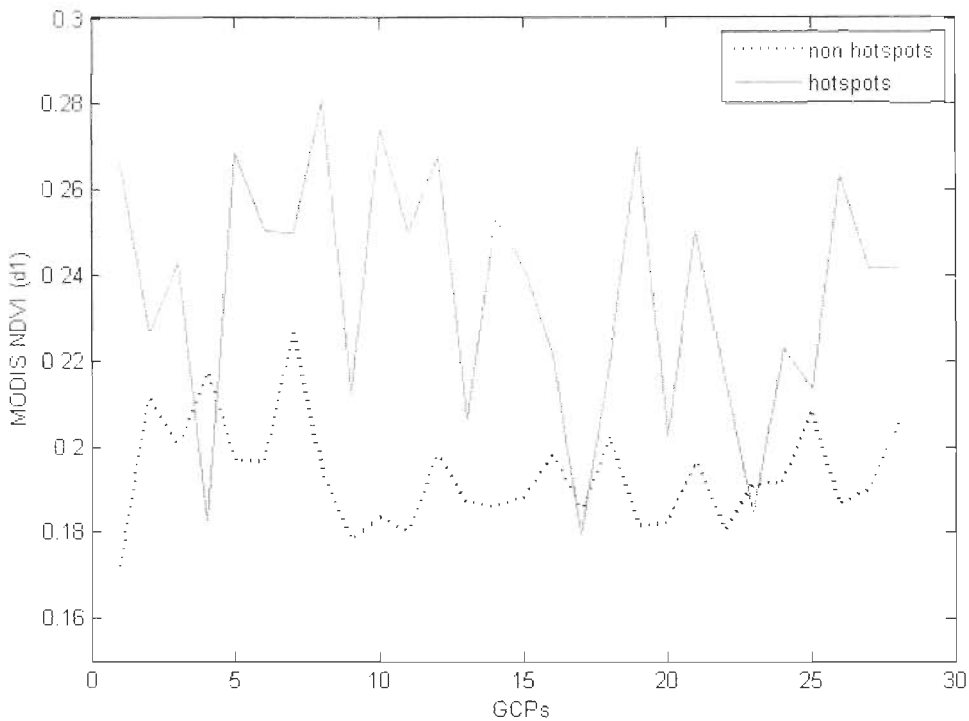


**Fig 5.3.** Spectral response of hotspot and non-hotspot regions in the MODIS NDVI (d1)

### 5.3. Theoretical Basis

It is introduced in the introduction that MODIS band 1, band 2 and corresponding LISS band 2 and band 3 may be useful for classification of hotspots and non-hotspot regions. It is also represented in the spectral response of hotspots and non-hotspots of fig. 5.1a, 5.1b, 5.2a, 5.2b. We have done fusion to enhance the information in spatial level. It is seen that MODIS band 2 (fig 5.1b) and LISS band 3 (fig 5.2b) have better separability to classify hotspots and non-hotspots in one hand, and in another hand NDVI of MODIS (fig 5.3) has also a good spectral response of hotspots and non-hotspots regions. We have done considerable amount of study like checking the spectral response in various images of different years. Therefore in this chapter, we have selected NDVI of MODIS and LISS image, LISS band 3 and MODIS band 2 for classification of hotspot and non-hotspot region. It is also assumed that nearby hotspot regions vegetation (i.e., greenness) possibility will be very less. Therefore the selected bands and NDVI values may classify the hotspot and non-hotspot regions. Flowchart of the proposed methodology is given in the fig. 5.4. Following steps have been

involved to implement the proposed methodology.

**Step 1:** MODIS band 1, band 2, LISS band 2, band 3 are geo-referenced and are subsetted to Jharia region.

**Step 2:** NDVI of MODIS and LISS images are calculated as given in the eq. 5.13.

**Step 3: Masking water bodies:** Firstly the computed MODIS NDVI image is considered for masking the water bodies in the image. For this purpose, the following criteria has been applied (Zhang et al. 2007)

- $NDVI < 0.04$
- $(MODIS\ Band\ 4 - MODIS\ Band\ 5) > 2.0$

with the above criteria, water bodies pixel are extracted for further processing. The product MOD09A1 are downloaded of the corresponding date, February 2004 (MOD09A1.A2004057.h25v06.005.2007251185548.hdf) and November 2004 (MOD09A1.A2004329.h25v06.005.2007337162719.hdf) for MODIS band 4 and MODIS band 5. The above mentioned criteria are applied in these images for extracting the water pixels and these pixels were masked in MODIS NDVI and MODIS band 3 images. Because the MODIS and LISS images has approximately the same area, so corresponding water pixels has been masked in LISS\_NDVI and LISS band 3 images. Then masked water pixel LISS NDVI images and MODIS NDVI images has been fused with curvelet fusion in one hand, and in another hand, the masked water pixel of LISS band 3 and MODIS band 2 are fused with curvelet fusion.

**Step 4:** BDA is applied for both the fused images to classify both hotspot and non-hotspot regions.

### 5.3.1. Curvelet transform

The main feature of the curvelet transform is that it is sensitive to directional boundaries and capable of representing the highpass details of object contours at

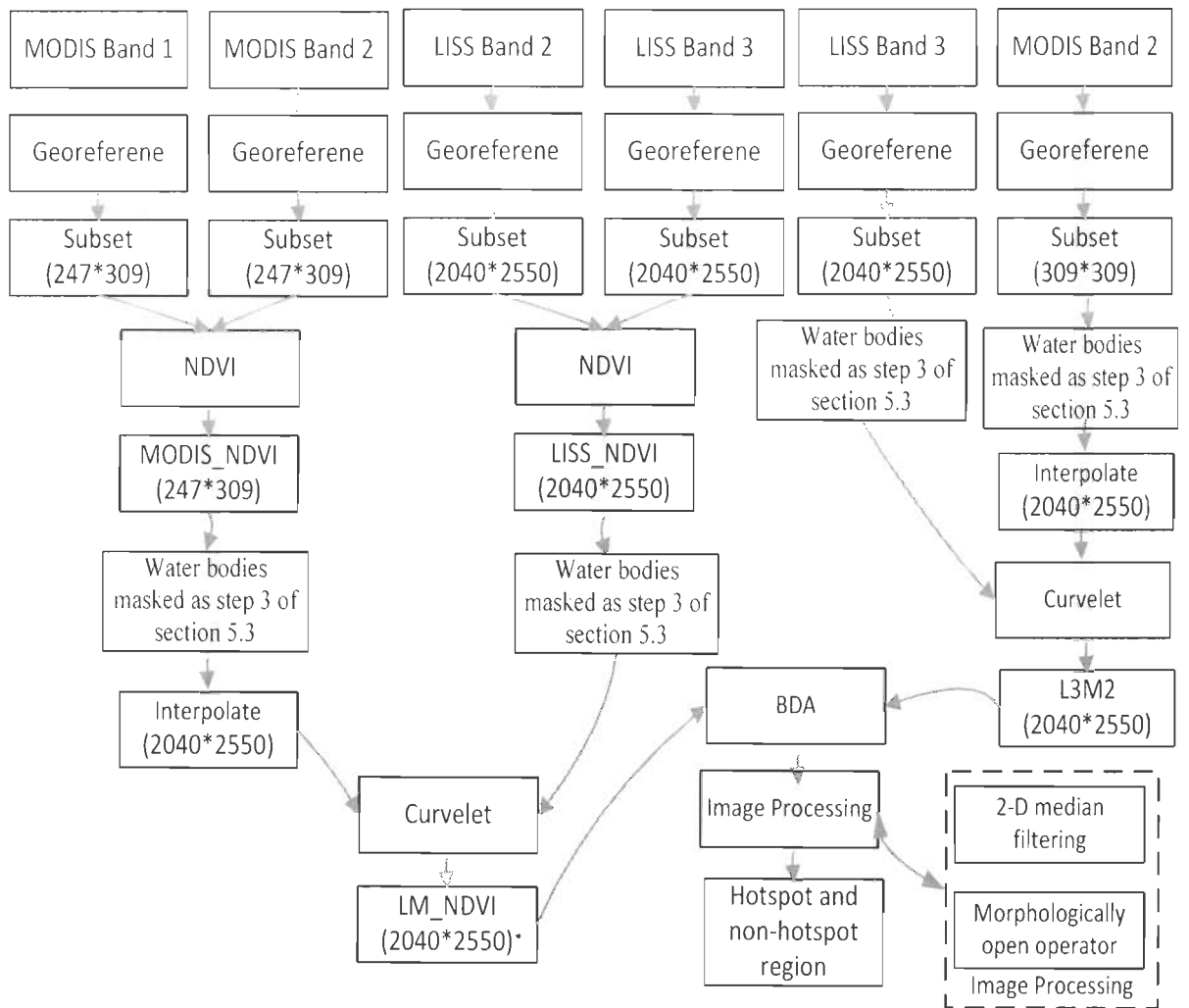


**Fig 5.4.** Proposed Methodology

different scales through few sparse nonzero coefficients (Stark et al. 2002). The different steps which is used for Curvelet fusion is discussed in the section 3.3.1. Fig. 3.1 depicts the flow chart of Curvelet Transform.

### 5.3.2. Binary Division Algorithm

In the binary division (Hanaizumi et al., 1995, Hanaizumi and Chino., 1995), it is essential to determine the cluster to be divided. The subset of the feature space to be used for the division and the division threshold in the subspace. These steps have been shown in the fig 5.5.

### i. Selection of Division Cluster:

The methodology by which the binary division Algorithm works is explained through an example and it is shown in the fig 5.6. In this example, image data are divided into clusters 1 and 2 at node  $n_0$ , and those in cluster 2 into clusters 3 and 4 at a node  $n_2$ . Cluster 3 is selected for the next division among all terminal clusters 1, 3, and 4.

Clustering in Binary division Algorithm is regarded as a minimization process of the total within-group sum of squares (WGSS) of the image data. In this Algorithm, image data are clustered so that the maximum reduction is obtained in the intragroup sum of squares (IGSS) among child clusters produced by the division. It is known that a mixed cluster  $c_0$  of clusters  $c_1$  and  $c_2$  has the variance (Hanaizumi et al. 1995)

$$Var(c_0) = Var(c_1) + Var(c_2) + [mean(c_1) - mean(c_2)]^2 \quad (5.1)$$

Using the same manner, we obtain the relation for the sum of squares in  $N$ -dimensional feature space as

$$S_{Parent} = S_{child1} + S_{child2} + S_{between} \quad (5.2)$$

where  $S_{Parent}$  is an  $N \times N$  matrix for the WGSS of a parent cluster,  $S_{child1}$  and  $S_{child2}$  are those for child clusters produced by the division, and  $S_{between}$  means the IGSS between the child clusters. We select the division cluster among all terminal clusters so that the WGSS efficiently falls to the minimum. We define a matrix  $D$  for evaluation of the reduction of the WGSS, as

$$D = S_{Parent} - (S_{child1} + S_{child2}) \quad (5.3)$$

The reduction  $D$ , however, depends on the sum of squares of the parent cluster. So we define the reduction rate  $A$  as a normalized index

$$A = trace(S_E^{-1/2} D S_E^{-1/2}) \quad (5.4)$$

where  $S_E$  is the total WGSS of all terminal nodes clusters, and is  $S_1 + S_3 + S_4$  in the example shown in fig. 5.6. Thus, next cluster among all terminal clusters is selected so that a maximum reduction rate is obtained. Next, algorithm for selecting the optimal subspace to divide the cluster into two subclusters are described and for determination of the threshold in the subspace.

**ii. Subsets of Feature Space and Boundary Search:** Search areas in which the optimal boundary will be selected become larger as the dimension (the number of spectral bands) increases. In order to achieve higher efficiency, we decrease the dimension by projecting image data onto a small number of the feature spaces. The first two canonical components  $p_1$  and  $p_2$  has to be adopted to form the two-dimensional subspace as canonical correlation analysis is useful in data compression

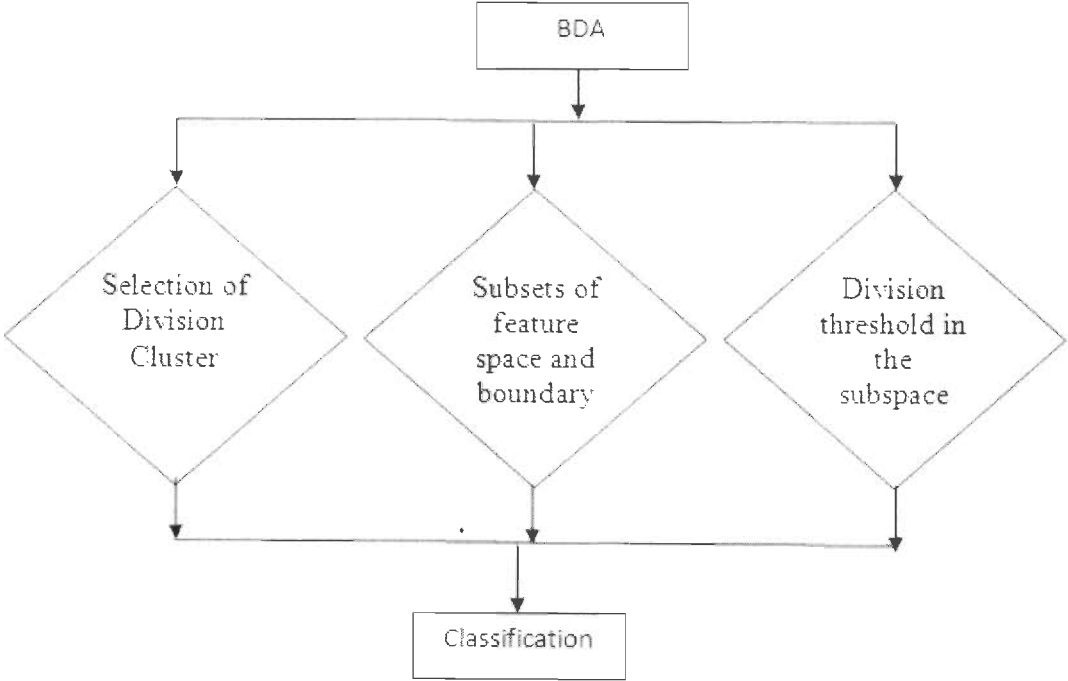


Fig 5.5. BDA flowgraph.

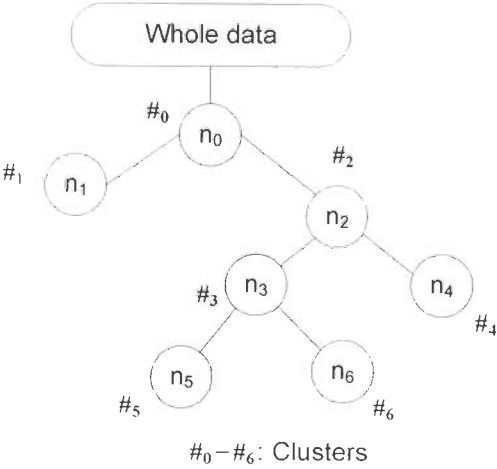


Fig 5.6. Binary Division Algorithm (Hanaizumi et al., 1995).



and in noise reduction. Then, following six projection functions defined on a two-dimensional subspace (Hanaizumi et al. 1995).

$$\begin{aligned} & f_1(p_1), & f_2(p_2) \\ & f_3(p_1 + p_2), & f_4(p_1 - p_2) \\ & f_5(p_1 \times p_2), & f_6(\tan^{-1}(p_1/p_2)) \end{aligned} \quad (5.5)$$

Let  $V_T$  be the variance-covariance matrix of data in a cluster and  $V_e$  be that of noise. Then compute the eigenvector matrix  $B$  which makes  $BV_TB$  and  $BV_eB$  diagonal matrices. The first two canonical components  $p_1$  and  $p_2$  are derived from eigenvectors related to the larger two eigenvalues. An element  $\sigma_{ij}^2$  of the matrix  $V_e$  is estimated from differential values

$$\sigma_{ij}^2 = \frac{1}{20\{(s-2)(t-2)-1\}} \sum_k \sum_l u_{kl}^i u_{kl}^j \quad (5.6)$$

$$u_{kl}^i = d_{k-1,l}^i + d_{k,l+1}^i + d_{k+1,l}^i + d_{k,l-1}^i - 4d_{k,l}^i \quad (5.7)$$

Where it is assumed that the image has  $s$  columns and  $t$  lines ( $s \times t = M$ ), and  $d_{k,l}^i$  means spectral density of a pixel at the position of the  $k^{\text{th}}$  column and the  $l^{\text{th}}$  line in an image of the  $i^{\text{th}}$  band. Next is the boundary search in the subspaces. Data projected onto the subspaces are reassigned to integer values from 0 to 255 for the following processing. The histogram of these values were used to search a candidate for the optimal boundary. For this purpose an index  $Q$  is employed which is a kind of pixel density, in a cluster for boundary search as

$$Q = \frac{L}{(V+1)} \quad (5.8)$$

Where  $L$  means the number of pixels in a cluster,  $V$  is variance of data in the cluster, and constant  $1$  is added to avoid the divergence of  $Q$ . The index changes from  $Q_{\text{parent}}$  to  $Q_{\text{child1}} + Q_{\text{child2}}$  with division. As the division decreases  $S_{\text{between}}$  in eq. 5.3, the density increases with division as

$$Q_{\text{parent}} \leq Q_{\text{child1}} + Q_{\text{child2}} \quad (5.9)$$

The equality holds when data in the parent cluster are uniformly distributed. The candidate for the optimal boundary is selected among all possible boundaries so that the sum of densities of child clusters has the maximum, that is

$$Q_1(X) + Q_2(X) = \max_x \{ Q_1(x) + Q_2(x) \} \quad (5.10)$$

Where, we suppose cluster 0 is divided into clusters 1 and 2,  $x$  is a boundary number, and  $X$  the selected boundary. The optimal boundary is selected among these candidates obtained from all the subspaces. The normalized density  $G$  is used for comparison as

$$G_i = \frac{Q_1(X_i) + Q_2(X_i)}{Q_{0i}} \quad (i=1\sim 6) \quad (5.11)$$

Where  $i$  specifies the subspace. The boundary  $X_j$  in the  $j^{\text{th}}$  subspace is the optimal boundary for division of a terminal cluster when

$$G_j = \max_i \{ G_i \} \quad (5.12)$$

**iii. Procedures for applying BDA:** The procedures of Binary Division Algorithm are summarized below and we have developed the code in MATLAB 7.0. As algorithm has no stopping rule yet, the algorithm is stopped when the number of clusters is equal to a specified number  $N_{ic}$ . (Here, in this chapter, the clusters are only 2, hotspot and non-hotspot regions).

- 1) Specify the number of clusters to be obtained.
- 2) Apply procedure 3) for all terminal clusters, and select a cluster for the next division.
- 3) Apply canonical correlation analysis to a terminal cluster and project the first two canonical components to the subspaces. Select the optimal boundary among all possible boundaries in the spaces.
- 4) Divide the cluster at the boundary.

- 5) Repeat procedures 2)-4) until the number of clusters is equal to  $N_{ic}$ .
- 6) Calculate the mean vectors of all terminal clusters, and replace the density of pixels with the mean vector.
- 7) Yield the resultant image.

**5.3.3. Normalized Difference Vegetation Index (NDVI).** NDVI values were computed using spectral reflectance values in the red (R) channel (620–670 nm) and the near-infrared (NIR) channel (841–876 nm) using the eq. 5.13.

$$NDVI = \frac{(NIR - R)}{(NIR + R)} = \frac{Band\ 2 - Band\ 1}{Band\ 2 + Band\ 1} \quad (5.13)$$

For the MODIS image the NIR channel corresponds to Band 2 and whose spectral resolution is 842 - 876nm and R indicates red channel corresponds to band 1, and whose spectral resolution is 620 - 670 nm. LISS image has NIR channel corresponds to Band 3, whose spectral resolution is 770 - 860 nm and R channel corresponds to band 2, whose spectral resolution is 620 - 680 nm. These bands are used to calculate the NDVI

## 5.4. Implementation and Results:

The raw data (d1, d2, d3, d4 and L1) are geo-referenced and are subsetted to Jharia region and the care is taken so that area of sub-set region of all the satellite images should be approximately equal. As discussed in the flowchart of the fig 5.4 and details of steps, it is applied on the data id d1, d3 and L1 for the February 2004 initially and consequently again it is applied on the id d2, d4 and L1 for the November 2004 (table. 5.2) in the following manner.

### **Step 1. MODIS NDVI (MODIS\_ndvi)**

The georeferenced and subset MODIS image (MOD09Q1) is considered initially. From this data, Band 1 and band 2 are considered and thereby the NDVI is computed using the eq. 5.13. The resultant NDVI is MODIS\_ndvi and from this MODIS\_ndvi the pixels that corresponds to water pixels are masked as step 3 of section 5.3.

### **Step 2. LISS NDVI (LISS\_ndvi)**

The georeferenced and subset LISS image is considered initially. From this image, the Band 2 and band 3 are considered and thereby the NDVI is computed using the eq. 5.13. The resultant NDVI is LISS\_ndvi, and from this LISS\_ndvi, the pixels that corresponds to water pixels are masked as step 3 of section 5.3.

### **Step 3. Curvelet based fusion of LISS band 3 with MODIS band 2**

The fusion process is given in flow chart fig. 5.4. MODIS Band 2 and LISS Band 3 are considered initially. Before fusion, from the MODIS band 2, the water pixels are masked as step 3 of section 5.3. Similarly for the LISS Band 3 also the water pixels are masked as step 3 of section 5.3. The masked water pixels MODIS band 2 and LISS Band 3 is fused, through the curvelet transform (LISS band 3 is decomposed into  $J + 1$  subbands by ATWT transform as eq. 3.1. The  $J+1$  subbands includes  $C_j$  and  $d_j$ , here  $j=4$ . Initially the MODIS band 2 has 247\*309 pixels and it is bilinear interpolated (Thomas et al., 1999) to the size of LISS image i.e., the MODIS band 2 is now having 2040\*2550 pixels and this interpolated MODIS band 2 replaces  $C_j$ . Consequently the Ridgelets transform (eq. 3.2 to eq. 3.6) is applied to all the decomposed subbands i.e.,  $d_j$  bands, thereby obtained ridgelet coefficients are hard-thresholded in order to enhance boundaries in the fused image and inverse ridgelet transforms (IRT) is carried out to obtain a new image which reflects the fused image (L3M2) of LISS Band 3 and MODIS Band 2.

#### **Step 4. Curvelet based fusion of LISS\_ndvi and MODIS\_ndvi**

In this step, computed LISS\_ndvi and MODIS\_ndvi are considered. Before fusion, the corresponding water pixels are masked as step 3 of section 5.3 from LISS\_ndvi and MODIS\_ndvi and are fused through the curvelet transform (LISS\_ndvi is decomposed into  $J + 1$  subbands by ATWT transform as eq. 3.1. The  $J+1$  subbands includes  $C_j$  and  $d_j$ , here  $j=4$ . Initially the MODIS\_ndvi has 247\*309 pixels and it is bilinear interpolated (Thomas et al., 1999) to the size of LISS image i.e., the MODIS\_ndvi is now having 2040\*2550 pixels, and this interpolated MODIS\_ndvi replaces  $C_j$ . Consequently the Ridgelets transform (eq. 3.2 to eq. 3.6) is applied to all the decomposed subbands i.e.,  $d_j$  bands, thereby obtained ridgelet coefficients are hard-thresholded in order to enhance boundaries in the fused image and inverse ridgelet transforms (IRT) is carried out to obtain a new image which reflects the fused image (LM\_ndvi) of LISS\_ndvi and MODIS\_ndvi.

#### **Step 5. BDA for hotspot and non-hotspot region classification**

The binary division algorithm is applied as discussed in section 5.3 on obtained LM\_ndvi and L3M2 images. On the resultant binary division image, the image processing techniques i.e., (Median filtering, Morphologically open operator) are applied which produce finally the hotspot and non-hotspot regions. The presence of noise enabled us to use Median filtering (Tong and Yrjö 1994) because median filtering is a nonlinear operation often used as it is more effective when the goal is to simultaneously reduce noise and preserve boundaries. Consequently to remove small objects from an image while preserving the shape and size of larger objects in the image, morphologically open operator (Maragos et al. 1996) is used. The classified hotspot were validated with the hotspots information provided by BCCL (Bharat Coking Coal Limited, India) and by CIMFR (Central Institute of Mining and Fuel Research), Dhanbad, India. Table 5.1 gives the latitude and longitude of hotspots observed from ground (Prakash 1996, CIMFR). Hotspot classification accuracy

(HCA) (eq. 5.14) were computed pixel by pixel with the help of location information of ground observations (Table 5.1).

$$\text{Hotspot Classification Accuracy} = \frac{\text{Correctly reported hotspots}}{\text{Total hotspots that exist}} \quad (5.14)$$

## 5.5. Analysis of Experimental Results:

We have checked the process for two different data sets, February and November 2004, approximately has the similar temperature. The MODIS Band 1 and Band 2 of data id d1 and d2 are georeferenced and subset to the Jharia region which is shown in the fig. 5.7a, 5.7b, 5.8a and 5.8b respectively. Concurrently the LISS band 2 and band 3 which is of the month of February 2004 is georeferenced and subset to the Jharia region (fig. 5.9a and 5.9b respectively). A region is encircled and is marked as a region A that is the Damodar river basin (figs. 5.7a, 5.7b, 5.8a, 5.8b, 5.9a and 5.9b).

### i. MODIS NDVI (MODIS\_ndvi)

The subsetted MODIS band 1 and band 2 of the month of February are considered to compute the NDVI, thereby, the computed NDVI is MODIS\_ndvi\_feb, and it is shown in the fig. 5.10a. Similarly for the month of November, MODIS band 1 and band 2 are considered to compute the NDVI, thereby, the computed NDVI is MODIS\_ndvi\_nov, and is shown in the fig. 5.10b. In these figs (5.10a and 5.10b) also the region is encircled and is marked as a region A, which indicates the Damodar river basin

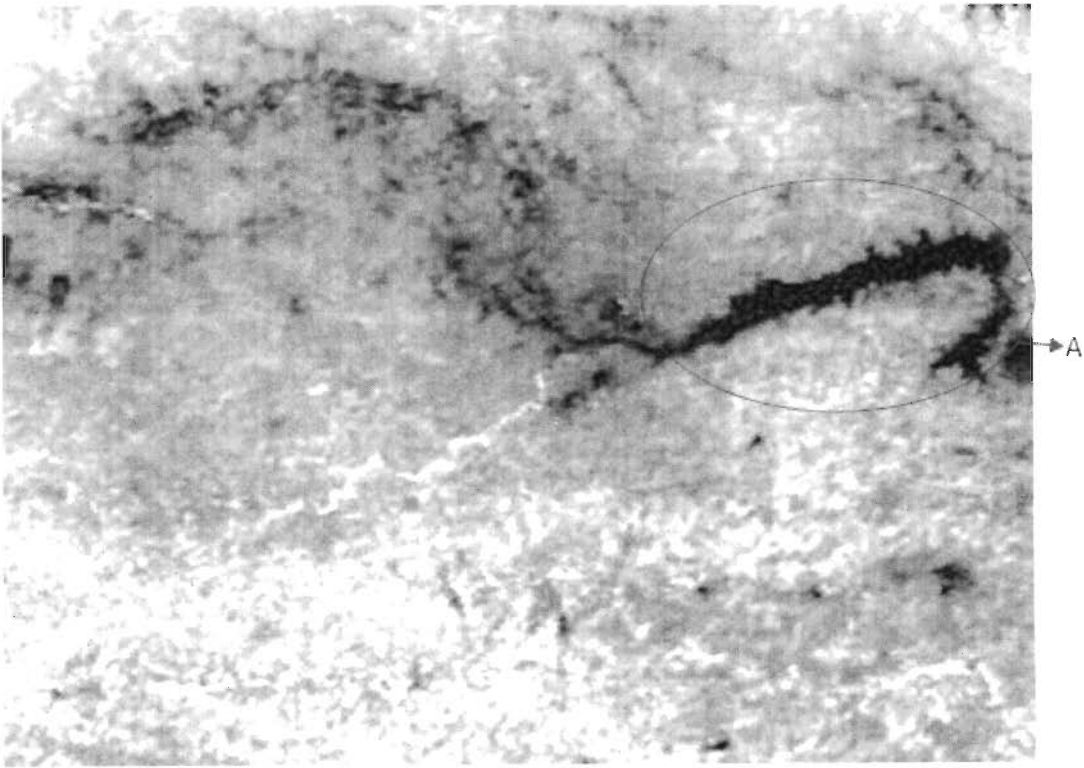


**Fig. 5.7a.** MODIS Band 1 of the month of February (d1)

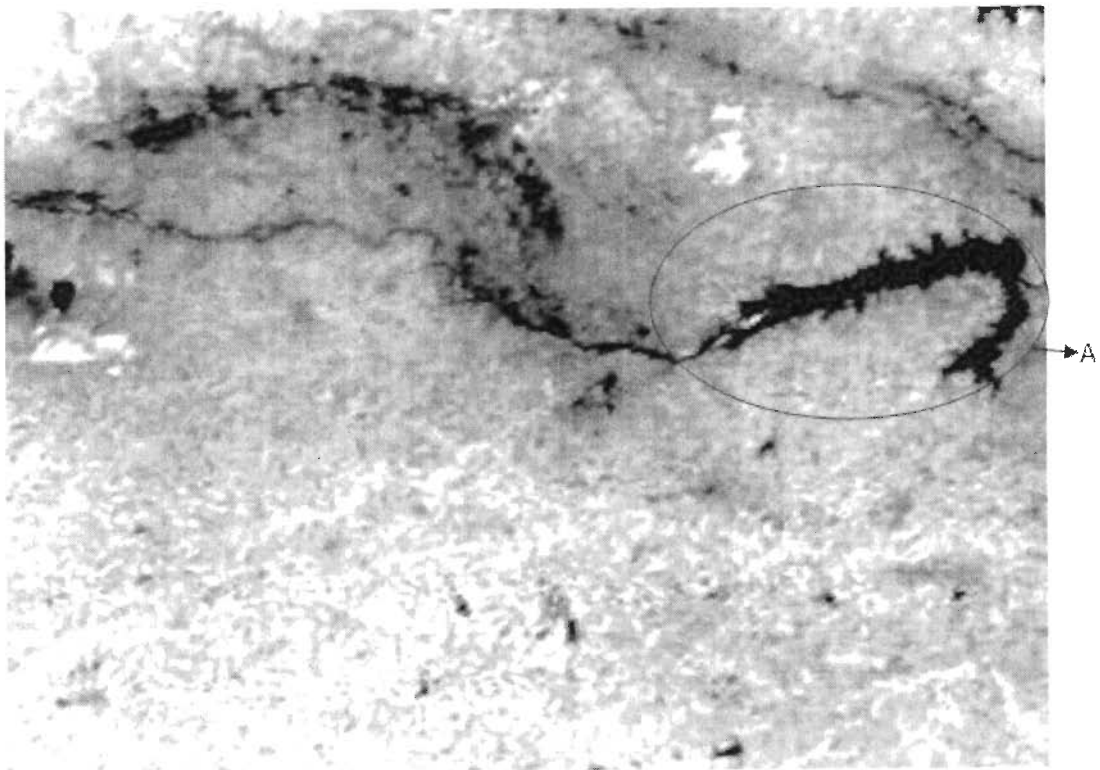


**Fig. 5.7b.** MODIS Band 2 of the month of February (d1)

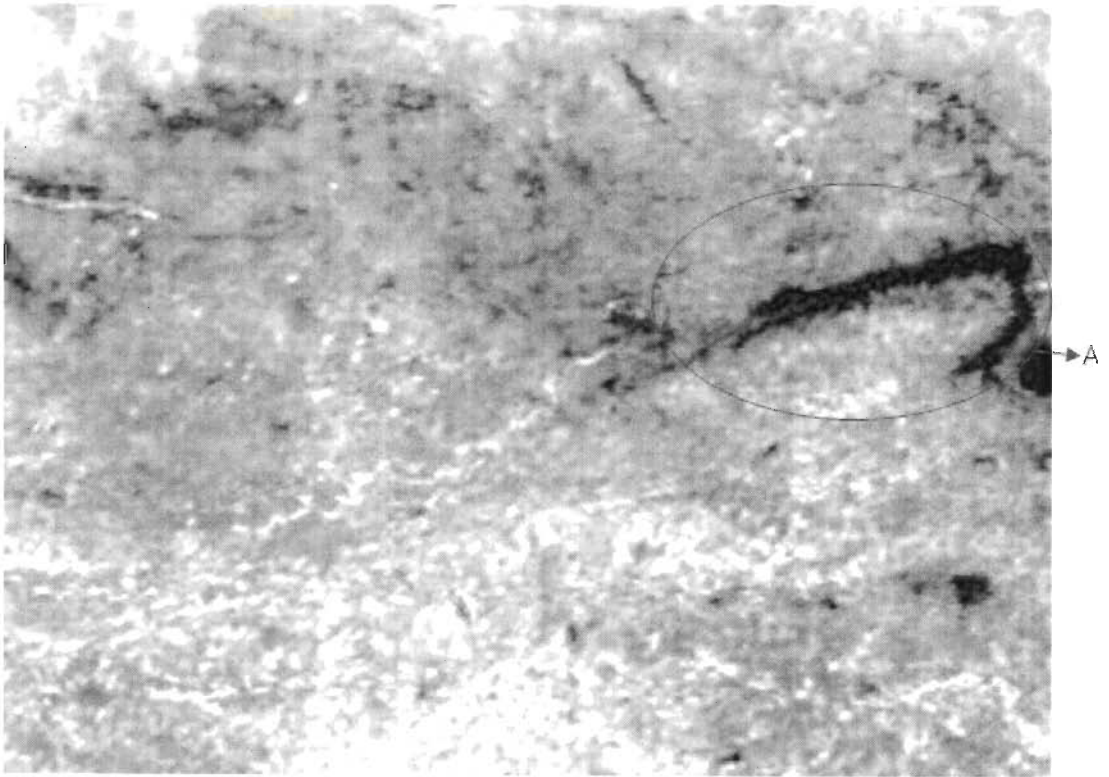


**Fig. 5.8a.** MODIS Band 1 of the month of November (d2)

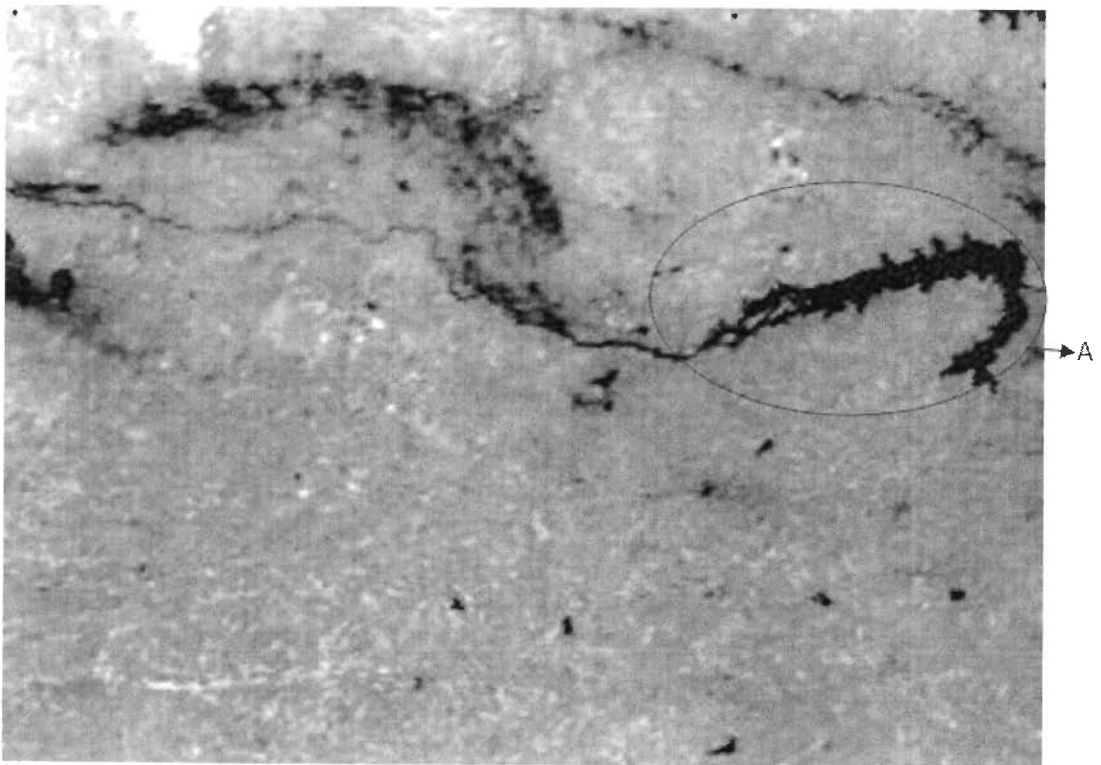


**Fig. 5.8b.** MODIS Band 2 of the month of November (d2)



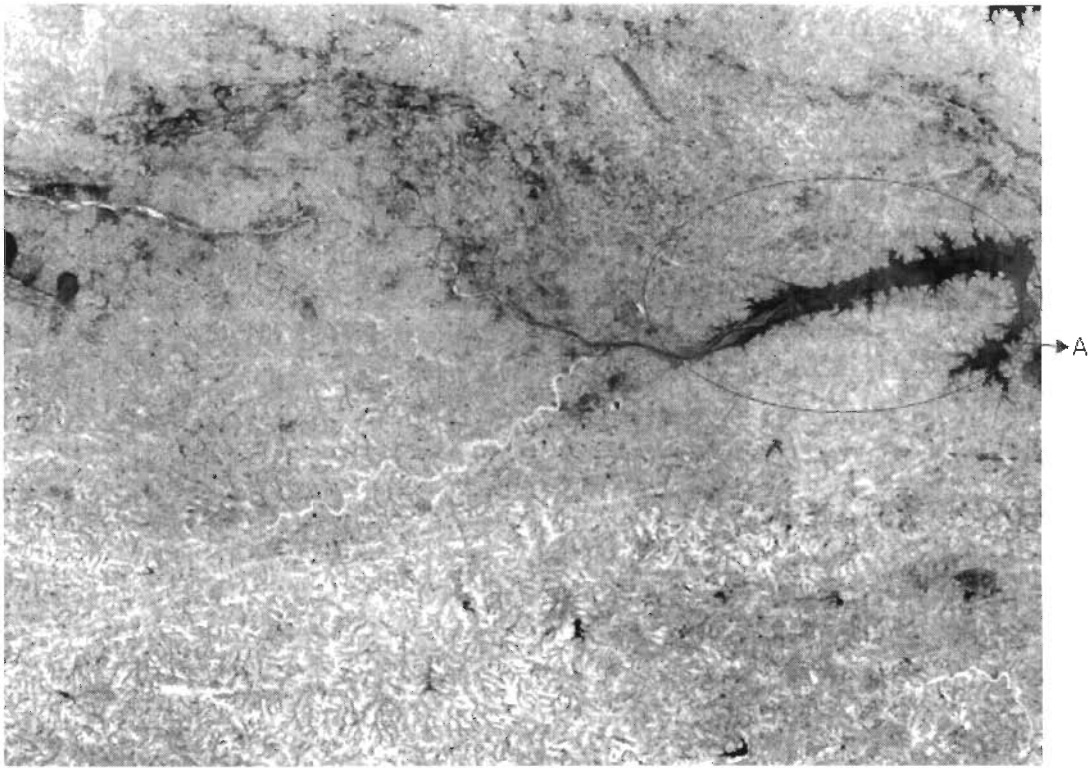


**Fig. 5.9a.** LISS band 2 (L1)

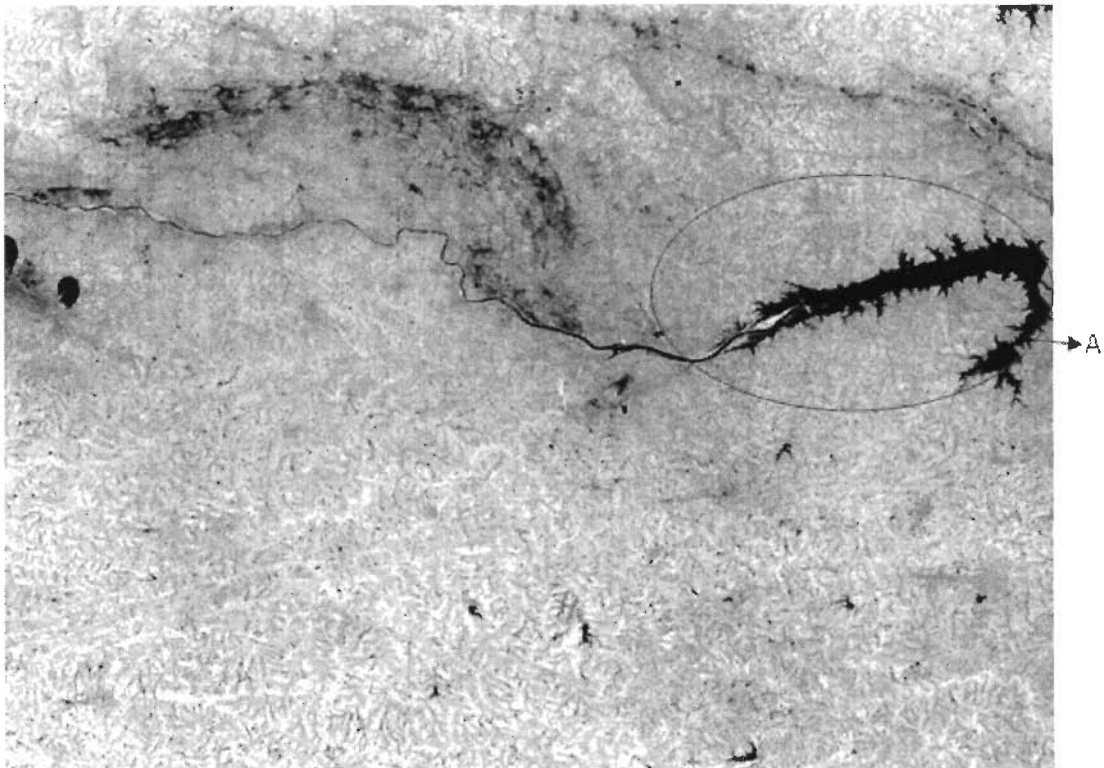


**Fig. 5.9b.** LISS band 3 (L1)

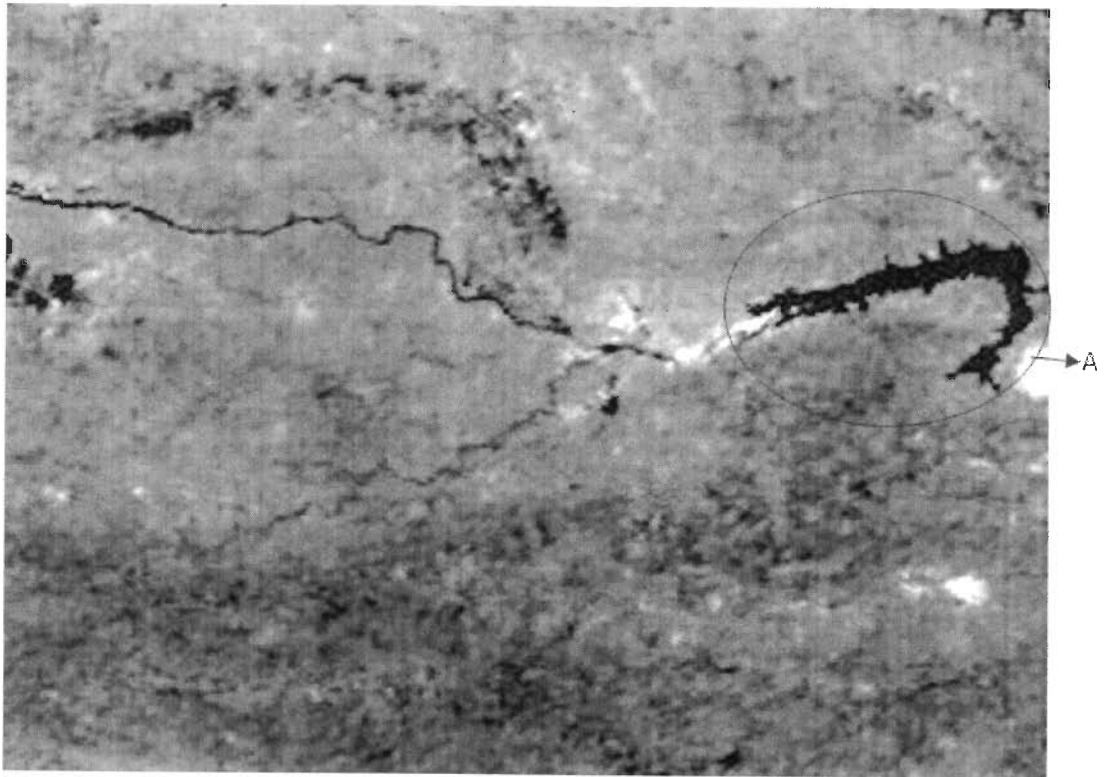


**Fig. 5.10a.** MODIS NDVI for the month of February (MODIS\_ndvi\_feb)

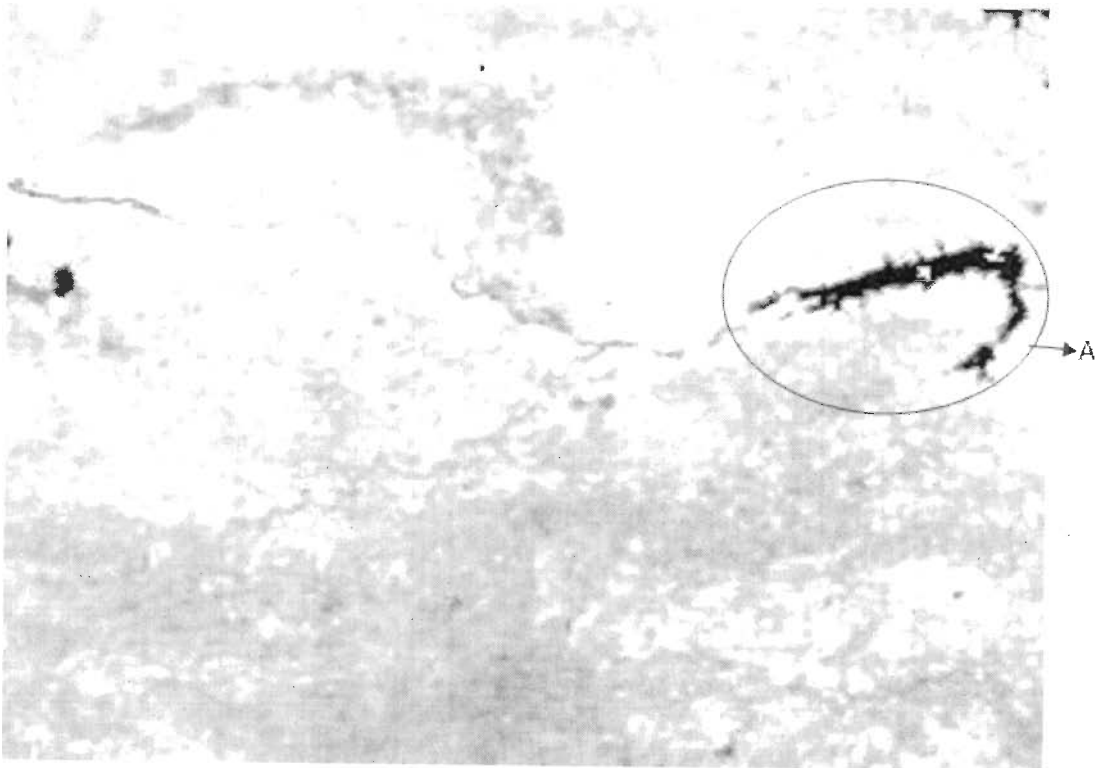


**Fig. 5.10b.** MODIS NDVI for the month of November (MODIS\_ndvi\_nov)

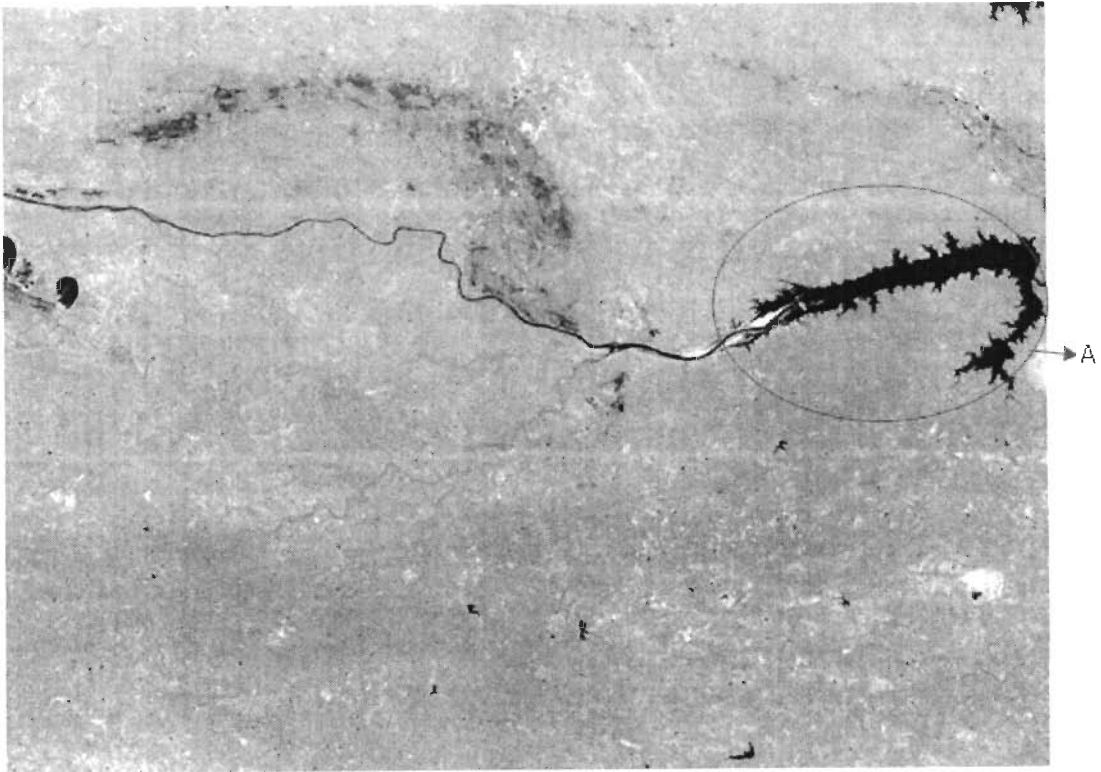


**Fig. 5.11.** LISS NDVI (LISS\_ndvi)

## **ii. LISS NDVI (LISS\_ndvi)**

The subsetting LISS image is considered and consequently the NDVI is computed from the LISS band 2 and band 3 image. The corresponding resultant LISS\_ndvi is shown in the fig. 5.11 and similarly a clear distinguished small region is identified and is encircled and marked as a region A, which is Damodar river basin.

## **iii. curvelet based fusion of LISS band 3 with MODIS band 2**

The subsetting MODIS band 2 of the month of February 2004 is considered along with the LISS band 3. Before fusion from the MODIS band 2 the water pixels are masked as step 3 of section 5.3. Similarly for the LISS Band 3 also the water pixels are masked as step 3 of section 5.3. The masked water pixels MODIS band 2 and LISS

Band 3 are fused through the curvelet based fusion, whose resultant fused image is L3M2\_feb. Likewise from the MODIS band 3 of the month of November the water pixels are masked as step 3 of section 5.3 and then it is fused with the masked water pixels LISS band 3 and the corresponding resultant fused image is L3M2\_nov.

#### **iv. curvelet based fusion of LISS\_ndvi with MODIS\_ndvi**

The computed MODIS\_ndvi\_feb of the month of February 2004 is considered along with the LISS\_ndvi. And these images are fused through the curvelet based fusion whose resultant fused image is LM\_ndvi\_feb. Likewise the computed MODIS\_ndvi\_nov of the month of November is fused with the LISS\_ndvi and the corresponding resultant fused image is LM\_ndvi\_nov.

#### **v. BDA for classification**

The LM\_ndvi\_feb and L3M2\_feb were considered. The Binary Division algorithm is applied on these images and the resultant image is BDA\_feb and consequently the image processing techniques (dashed line box labeled image processing in the fig. 5.4) are applied for the noise removal and final resultant image obtained as shown in the fig. 5.12 which classifies the hotspot and non-hotspot for the month of February. The Hotspot Classification Accuracy (HCA) is computed from the eq. 5.14, where in the eq. 5.14, for the "Total hotspots that exist", totally 28 hotspots were reported and which is tabulated in the table 5.1, and for the "correctly reported hotspot" for the month of February 2004, the classified hotspots are 24 and it is marked as red dots in the fig. 5.12. Thereby HCA is computed and it is 85.7%.

In the same way for the month of November, the hotspots are classified. Hence, in this scenario, the BDA is applied on LM\_ndvi\_nov and L3M2\_nov and the resultant image is BDA\_nov. Eventually on the BDA\_nov, the image processing techniques are applied. The final resultant image is shown in the fig. 5.13, and correctly reported hotspot are 22 and are marked as red dots in the fig. 5.13, hence the HCA is 75%.

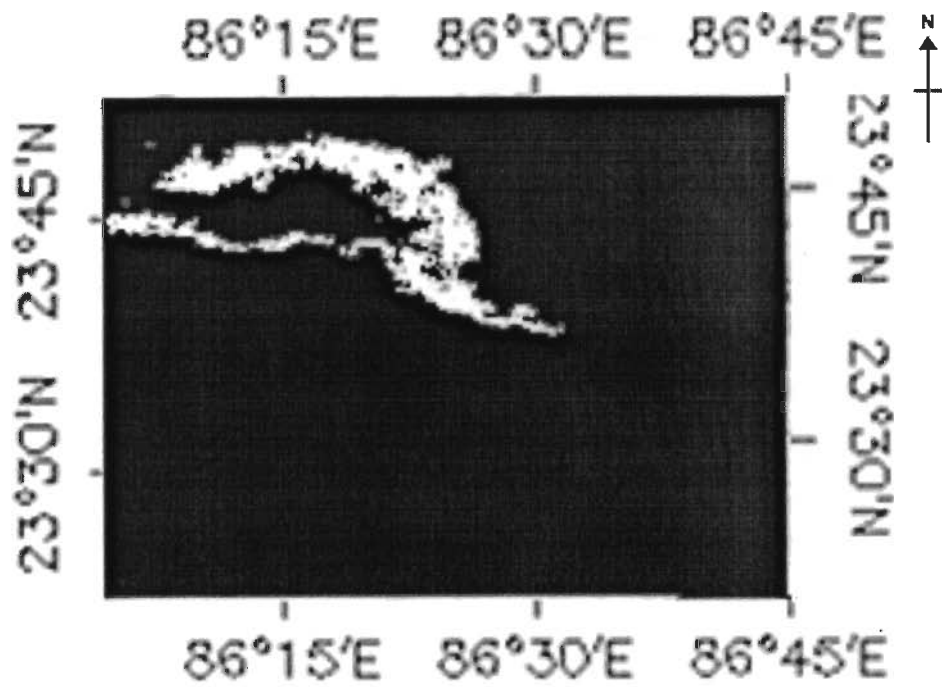


Fig. 5.12. Hotspot and non-hotspot regions classified for the month of February 2004

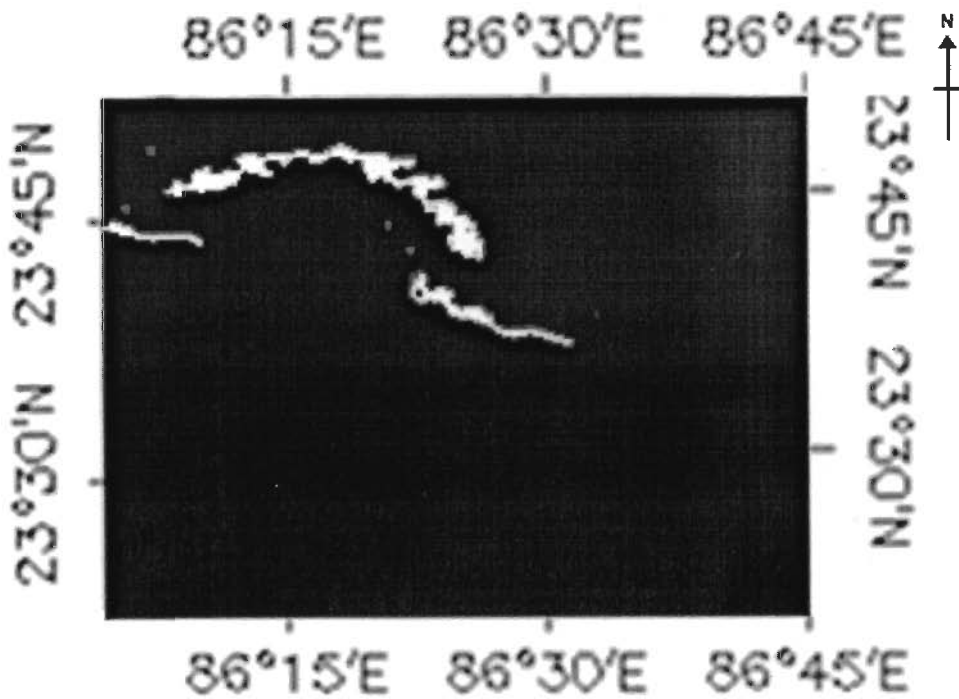


Fig. 5.13. Hotspot and non-hotspot regions classified for the month of November 2004

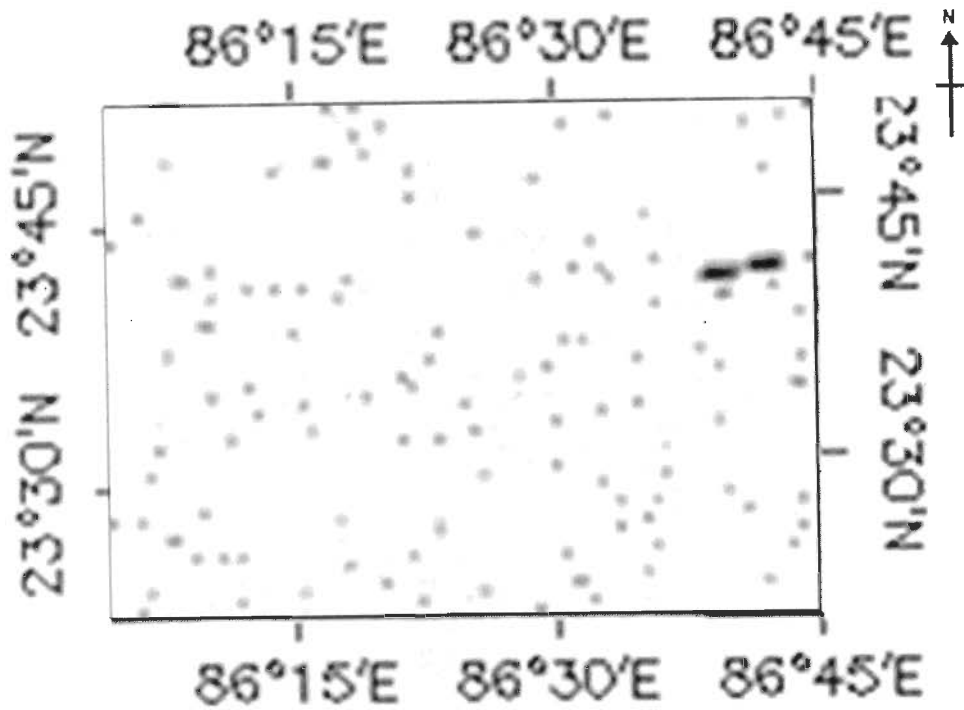


Fig. 5.14a. MODIS Most Confident Fire of February 2004(d3) of MOD14A2

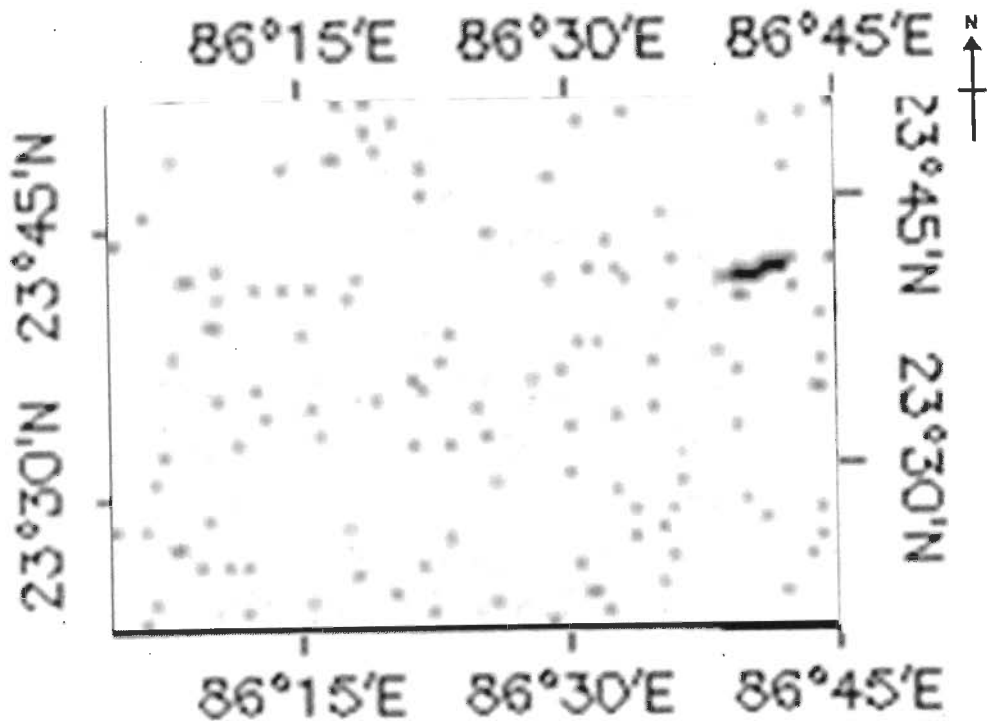


Fig. 5.14b. MODIS Most Confident Fire of November 2004 (d4) of MOD14A2

In due course, the Most Confident Fire product data id d3 and d4 are georeferenced and subset to the Jharia region (fig. 5.14a and fig. 5.14b respectively). HCA is computed and it shows that HCA is zero, as the correctly classified hotspot is zero for both images d3 and d4. It infers that the most confident fire product of MODIS i.e., MOD14A2 is giving false hotspot region whereas fusion of MODIS band with LISS bands are giving quite good accuracy to classify hotspot and non-hotspot regions.

## **5.6. Conclusion**

In this chapter, classification of hotspot and hotspot regions through binary division algorithm for the Jharia coalfield in Jharkhand is presented. The subsurface fire is one of the most important problem of the Jharia region of India, where large amount of coal is burning and giving a lot of problem to environment, economy etc. Therefore, in this chapter, the MODIS band 1 and band2, LISS-III band 2 and band 3 images are considered to dealt with hotspot and non-hotspot regions classification. Although MODIS provides a special product MOD14A2 for fire product classification. But this special product is not only sufficient for hotspot and non-hotspot regions classification. This chapter, thereby provides the necessary technique for classifying hotspot and non-hotspot region with the MODIS images. A quite satisfactory results have been observed which enforce to enhance the applicability of MODIS images.

## Chapter 6

# Multitemporal Harmonic Analysis of MODIS Indexes

---

### 6.1. Introduction

Nowadays mankind is interfering in nature everywhere on Earth. Sometimes even in not easily reachable regions. Some of these manmade changes have enormous effects on nature and whole ecosystems. Recent advances in remote sensing technology and theory have expanded opportunities to characterize the seasonal and interannual dynamics of natural and managed Land use/ land cover communities. Studies have shown that the temporal domain of multispectral image frequently provides more information about land cover and land use than the spatial, spectral, or radiometric domains (Briggs and Nellis 1991, Kremer and Running 1993, Eastman and Fulk 1993, Samson 1993, Reed et al. 1994) and the detailed literature survey is carried out at the section 2.7

The normalized difference vegetation index (NDVI), which is the normalized reflectance difference between the near infrared (NIR) and visible red bands (Rouse et al. 1973, Tucker 1979) is used extensively in ecosystem monitoring. NDVI measures the changes in chlorophyll content (via absorption of visible red radiation) and in spongy mesophyll (via reflected NIR radiation) within the vegetation canopy. As a



result, higher NDVI values usually represent greater vigor and photosynthetic capacity (or greenness) of vegetation canopy (Tucker 1979, Chen and Brutsaert, 1998). A major advantage of the NDVI is that because of its ratioing properties, it is able to naturally cancel out a large proportion of signal variations due to calibration, noise, and changing irradiance conditions caused by varying sun angles, topography, clouds, shadows and atmospheric conditions NDVI's role in ecosystem monitoring and assessment has been described several times during the last decade (Yang et al. 1998).

The normalized difference water index (NDWI) is another satellite-derived index from the NIR and short wave infrared (SWIR) channels that measures the liquid water molecules that interacted with the incoming solar radiation (McFeeters 1996). It is less sensitive to atmospheric scattering effects than NDVI and NDWI is complementary too, but not a substitute for NDVI (Gao, 1996). NDWI calculated from the 500-m SWIR band of MODIS has recently been used to detect and monitor the moisture condition over large areas (Xiao et al. 2002, Jackson et al. 2004, Maki et al. 2004, Chen et al. 2005b, Delbart et al. 2005).

Harmonic analysis is useful in highlighting the seasonal and intra-seasonal cycles and offers great promise for analyzing seasonal and inter-annual variation in land surface condition as recorded by various indexes (i.e., NDVI and NDWI) calculated from time series remotely sensed image such as the MODIS (Wan et al. 2004, Yingxin Gu et al. 2007). The main objective of this chapter is to quantify the changes related to the vegetation and water in the study area using harmonic analysis.

This chapter is structured as follows: data used for the study has been discussed in section 6.2. Section 6.3 briefly reviews the Fourier analysis. Implementation and results of the used approach is given in section 6.4. In the subsequent section, i.e., in section 6.5 analysis of experimental results are carried out and finally this chapter is concluded in the section 6.6.

## **6.2. Data Used/Study Area**

Western Uttar Pradesh and part of Uttarakhand, India is considered as the study area and the detailed clarification about the study area is given in the section 1.3.3.

### 6.2.1. Data used

The MODIS image considered is MODIS/Terra Surface Reflectance 8-Day L3 Global 500m SIN Grid (MOD09A1) and totally 40 images from 2001 to 2008 are considered in this analysis and the image acquired details are tabulated in the table 6.1.

**Table 6.1.** Data sets Details

<b>Data id</b>	<b>Data set</b>	<b>Date of Acquisition</b>
1.1	MOD09A1.A2001057.h24v06.005.2006365121813.hdf	26 <sup>th</sup> February 2001
1.2	MOD09A1.A2001065.h24v06.005.2007002183549.hdf	6 <sup>th</sup> March 2001
1.3	MOD09A1.A2001073.h24v06.005.2007005151635.hdf	14 <sup>th</sup> March 2001
1.4	MOD09A1.A2001081.h24v06.005.2007009180424.hdf	22 <sup>th</sup> March 2001
1.5	MOD09A1.A2001089.h24v06.005.2008277183431.hdf	30 <sup>th</sup> March 2001
2.1	MOD09A1.A2002057.h24v06.005.2008236065943.hdf	26 <sup>th</sup> February 2002
2.2	MOD09A1.A2002065.h24v06.005.2008238031637.hdf	6 <sup>th</sup> March 2002
2.3	MOD09A1.A2002073.h24v06.005.2008239100154.hdf	14 <sup>th</sup> March 2002
2.4	MOD09A1.A2002081.h24v06.005.2007136042309.hdf	22 <sup>th</sup> March 2002
2.5	MOD09A1.A2002089.h24v06.005.2007137102718.hdf	30 <sup>th</sup> March 2002
3.1	MOD09A1.A2003057.h24v06.005.2007286074626.hdf	26 <sup>th</sup> February 2003
3.2	MOD09A1.A2003065.h24v06.005.2008300163445.hdf	6 <sup>th</sup> March 2003
3.3	MOD09A1.A2003073.h24v06.005.2007292074115.hdf	14 <sup>th</sup> March 2003
3.4	MOD09A1.A2003081.h24v06.005.2008307195247.hdf	22 <sup>th</sup> March 2003
3.5	MOD09A1.A2003089.h24v06.005.2007300163248.hdf	30 <sup>th</sup> March 2003
4.1	MOD09A1.A2004057.h24v06.005.2007251185417.hdf	26 <sup>th</sup> February 2004
4.2	MOD09A1.A2004065.h24v06.005.2007255053021.hdf	5 <sup>th</sup> March 2004
4.3	MOD09A1.A2004073.h24v06.005.2007258043831.hdf	13 <sup>th</sup> March 2004
4.4	MOD09A1.A2004081.h24v06.005.2007261150328.hdf	21 <sup>th</sup> March 2004
4.5	MOD09A1.A2004089.h24v06.005.2007264062800.hdf	29 <sup>th</sup> March 2004
5.1	MOD09A1.A2005057.h24v06.005.2008200033550.hdf	26 <sup>th</sup> February 2005
5.2	MOD09A1.A2005065.h24v06.005.2008011023701.hdf	6 <sup>th</sup> March 2005

5.3	MOD09A1.A2005073.h24v06.005.2008011211036.hdf	14 <sup>th</sup> March 2005
5.4	MOD09A1.A2005081.h24v06.005.2008013050946.hdf	22 <sup>th</sup> March 2005
5.5	MOD09A1.A2005089.h24v06.005.2008013131059.hdf	30 <sup>th</sup> March 2005
6.1	MOD09A1.A2006057.h24v06.005.2008085013438.hdf	26 <sup>th</sup> February 2006
6.2	MOD09A1.A2006065.h24v06.005.2008087085529.hdf	6 <sup>th</sup> March 2006
6.3	MOD09A1.A2006073.h24v06.005.2008092222722.hdf	14 <sup>th</sup> March 2006
6.4	MOD09A1.A2006081.h24v06.005.2008095053310.hdf	22 <sup>th</sup> March 2006
6.5	MOD09A1.A2006089.h24v06.005.2008097124026.hdf	30 <sup>th</sup> March 2006
7.1	MOD09A1.A2007057.h24v06.005.2007087150042.hdf	26 <sup>th</sup> February 2007
7.2	MOD09A1.A2007065.h24v06.005.2007088103122.hdf	6 <sup>th</sup> March 2007
7.3	MOD09A1.A2007073.h24v06.005.2007098184729.hdf	14 <sup>th</sup> March 2007
7.4	MOD09A1.A2007081.h24v06.005.2007096012108.hdf	22 <sup>th</sup> March 2007
7.5	MOD09A1.A2007081.h24v06.005.2007096012108.hdf	30 <sup>th</sup> March 2007
8.1	MOD09A1.A2008057.h24v06.005.2008067153432.hdf	26 <sup>th</sup> February 2008
8.2	MOD09A1.A2008065.h24v06.005.2008076025452.hdf	5 <sup>th</sup> March 2008
8.3	MOD09A1.A2008073.h24v06.005.2008082161414.hdf	13 <sup>th</sup> March 2008
8.4	MOD09A1.A2008081.h24v06.005.2008093154953.hdf	21 <sup>th</sup> March 2008
8.5	MOD09A1.A2008089.h24v06.005.2008099223434.hdf	29 <sup>th</sup> March 2008

In this chapter, Band 1, Band 2 and Band 7 of the MOD09A1 are considered. The MOD09A1 generates only 500m resolution for all bands hence band 1, band 2 and band 7 are having resolution of 500m. Band 1 is having spectral resolution of 620–670 nm and 841–876 nm is the spectral resolution of band 2 and 2105–2155 nm is the spectral resolution of the band 7.

### 6.3. Theoretical Basis

**6.3.1. Normalized Difference Vegetation Index (NDVI).** The detailed discussion is carried out in the section 5.3.3 and hence from this section, NDVI values were computed using eq. 5.13, and this equation is repeated here as the eq. 6.1

$$NDVI = \frac{(NIR - R)}{(NIR + R)} = \frac{Band\ 2 - Band\ 1}{Band\ 2 + Band\ 1} \quad (6.1)$$

**6.3.2. Normalized Difference Water Index (NDWI).** The spectral reflectance values in the infrared (NIR) channel (841–876 nm) and the short wave infrared (SWIR) channel (2105-2155 nm) are used for the computation of NDWI values, as per the eq. 6.2 (Yingxin et al. 2007)

$$NDWI = \frac{(NIR - SWIR)}{(NIR + SWIR)} = \frac{Band\ 2 - Band\ 7}{Band\ 2 + Band\ 7} \quad (6.2)$$

NDWI values also ranges between  $-1$  and  $1$ , with values above  $0$  indicating presence of water (Yingxin Gu et al. 2007).

### 6.3.3. Harmonic Analysis

Harmonic analysis also termed spectral analysis or Fourier analysis is performed to quantify some fundamental characteristics related to the phenology of vegetation and water from time series of MODIS image. Harmonic analysis permits a complex curve to be expressed as the sum of a series of cosine waves (terms) and an additive term (Davis 1986, Rayner 1971, Jakubauskas et al. 2001, Jakubauskas et al. 2002). Each wave is defined by a unique amplitude and a phase angle where the amplitude value is half the height of a wave and the phase angle (or simply, phase) defines the offset between the origin and the peak of the wave over the range  $0 - 2\pi$  (fig. 6.1a). Each term designates the number of complete cycles completed by a wave over the defined interval (e.g., the second term completes two cycles, fig. 6.1b). Successive harmonic terms are added to produce a complex curve (fig. 6.1c) and each component curve or term accounts for a percentage of the total variance in the original time-series data set.

Let  $f(x)$  be a continuous function on  $[0, T]$ , the Fourier series representation for  $f(x)$  is defined as eq. 6.3 (Davis 1986, Rayner 1971, Jakubauskas et al. 2001, Jakubauskas et al. 2002).

$$f(x) = \frac{a_0}{2} + \sum_{n=1}^{\infty} \left( a_n \cos \frac{2\pi nx}{T} + b_n \sin \frac{2\pi nx}{T} \right) \quad (6.3)$$

Two waves in eq. 6.3 are combined into a single cosine wave, which has characteristic amplitude (size of the wave) and phase angle (offset of the wave)

(Davis 1986, Rayner 1971, Jakubauskas et al. 2001, Jakubauskas et al. 2002).

$$f(x) = A_0 + \sum_{n=1}^L A_n \cos\left(\frac{2\pi n x}{T} - \theta_n\right) \quad (6.4)$$

$$A_n = \begin{cases} \sqrt{a_n^2 + b_n^2} & (n = 1, 2, \dots) \\ \frac{a_0}{2} & (n = 0) \end{cases} \quad (6.5)$$

$$\theta_n = \begin{cases} \arctan\left(\frac{b_n}{a_n}\right) & (n = 1, 2, \dots) \\ 0 & (n = 0) \end{cases} \quad (6.6)$$

Fourier coefficients  $a_n$  and  $b_n$  are computed for each term and are then used to calculate the value of the additive term ( $A_0$ ) and the amplitudes value ( $A_n$ ) for each of the harmonic components for each pixel in the MODIS NDVI and NDWI data set. For a finite data set  $\{y(j); j = 1, 2, \dots, N\}$ , Fourier coefficient  $a_n$  and  $b_n$  are defined as follows (Davis 1986, Rayner 1971, Jakubauskas et al. 2001, Jakubauskas et al. 2002)

$$a_n = \frac{1}{N-1} \left( y(1) + y(N) + 2 \sum_{j=2}^{N-1} y(j) \cdot \cos \frac{2\pi n(j-1)}{N-1} \right) (n \geq 0) \quad (6.7)$$

$$b_n = \frac{1}{N-1} \left( 2 \sum_{j=2}^{N-1} y(j) \sin \frac{2\pi n(j-1)}{N-1} \right) (n \geq 1) \quad (6.8)$$

In this study,  $N=5$ , as in this chapter, only 5 images is considered for the March month for every years from 2001 to 2008. The value of the additive term,  $A_0$  implies the arithmetic mean of NDVI over the time-series (5 periods) and represents the overall greenness of a land-cover type of particular month March. Similarly for the NDWI, it represents the water land cover type of particular month March of every year. The amplitude term,  $A_1$  of one year period measures the maximum variability of the NDVI and NDWI values from the minimum to the maximum values. In this thesis, March month is considered, therefore  $A_1$  in this thesis measures the maximum variability of the NDVI and NDWI values from the minimum to the maximum values of the month March from year 2001 to 2008.

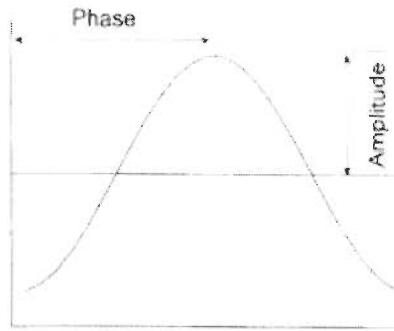


**Fig. 6.1a.** Simple cosine curve representative of the first harmonic (Jakubauskas et al, 2001)

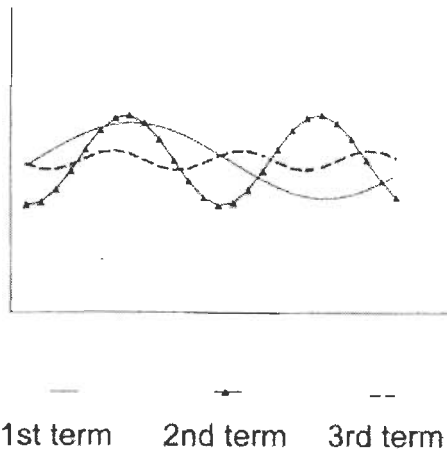


**Fig. 6.1b.** curves for harmonic terms 1, 2, and 3 (Jakubauskas et al, 2001)

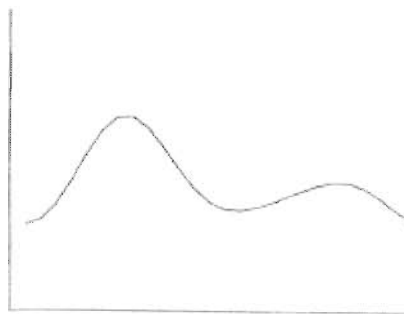


**Fig. 6.1c.** curve produced by addition of curves in (6.1b) (Jakubauskas et al, 2001)

#### 6.4. Implementation of Proposed Approach

Fig. 6.2a and 6.2b shows the methodologies used in this chapter. The downloaded MODIS image is georeferenced then subset to the western Uttar Pradesh and Uttarakhand region. The subsetted MODIS Band 1, Band 2 and Band 7 are considered for the calculation of NDVI and NDWI using eq. 6.1 and 6.2 respectively. From the year 2001 to 2008, totally 40 MODIS images for the month of March is considered (for every year, 5 images are considered, in which one image is of last week of February and the other four image is of the month March and it is assumed that last week February image may be similar to the month March). Eventually the harmonic analysis for every year of month March is carried out and  $A_0$  and  $A_1$  terms are computed using the eq. 6.5 for each year separately. Hence forth, the analysis of agricultural and water changes is carried out for month March.

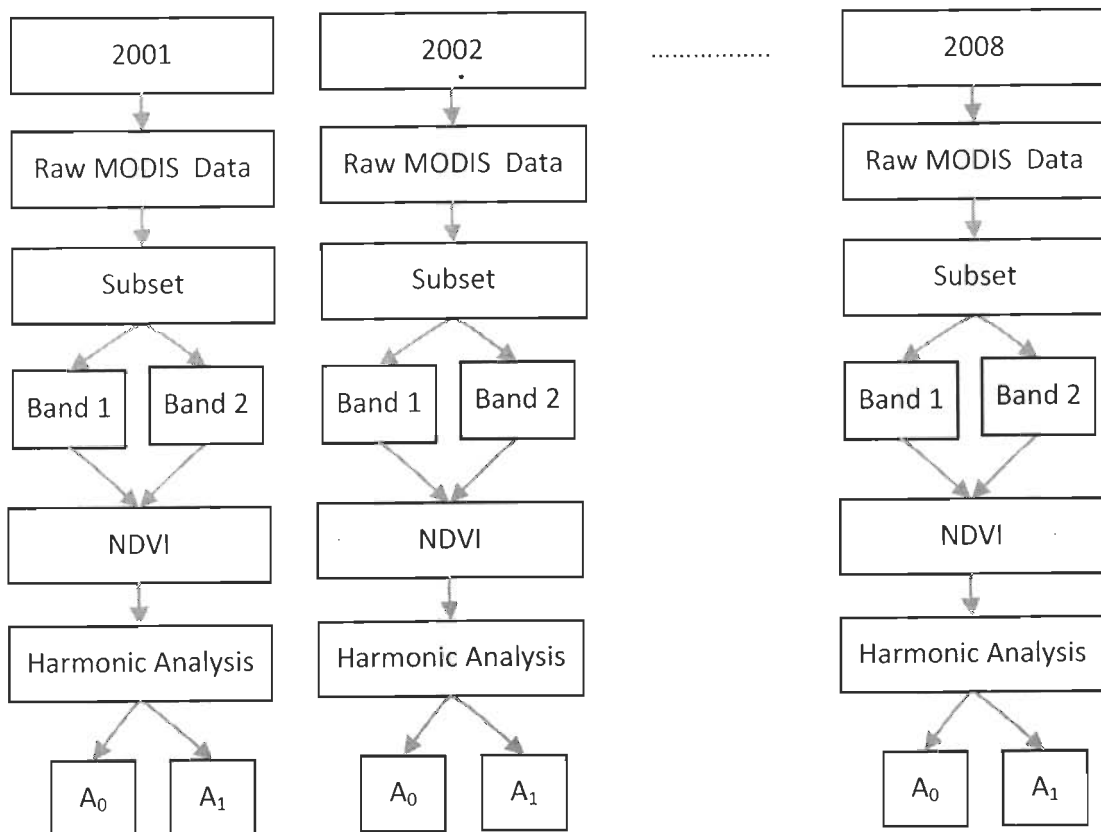


**Fig. 6.2a.** flow graph for NDVI harmonic analysis

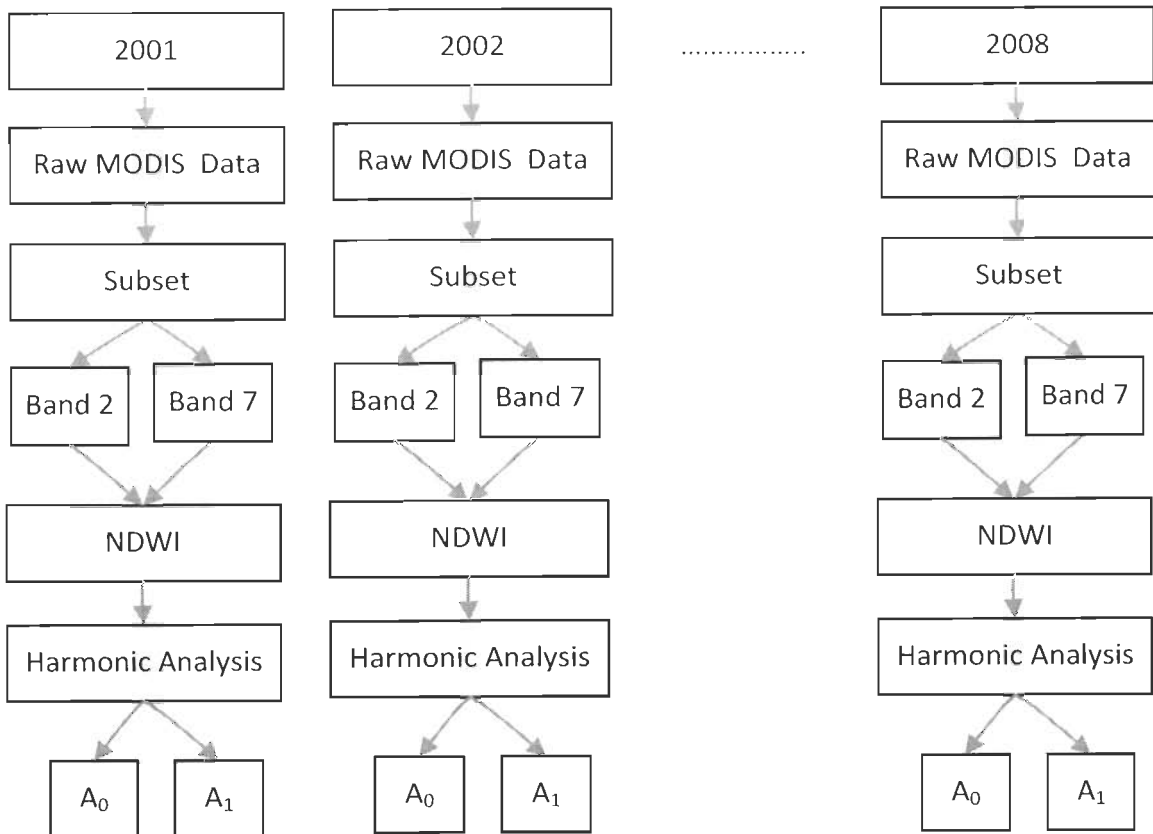


**Fig. 6.2b.** flow graph for NDWI harmonic analysis

## 6.5. Experimental Results

The MODIS Band 1, Band 2 and Band 7 for all the data id as given in table 6.1, are considered. They are georeferenced and consequently subsetted to the study area, as an example the subsetted MODIS Band 1, Band 2 and Band 7 for the data id 1.1 is shown in the fig. 6.3a, 6.3b and 6.3c respectively. The NDVI and NDWI are calculated from equation 6.1 and 6.2 respectively and applied to the data id 1.1 and results are shown in the fig. 6.3d and 6.3e. Fig. 6.3d, the NDVI values range between  $-1$  and  $1$ , where values above  $0$  indicating presence of vegetation (Ma et al. 2007, Stow et al. 2003), and in the fig. 6.3e, the NDWI values also ranges between  $-1$  and  $1$ , where values above  $0$  indicating presence of water (Yingxin Gu et al. 2007). Similarly, for all the data id in the table 6.1, NDVI and NDWI are computed.



For every year 5 data sets (for example for year 2001, the data sets 1.1, 1.2, 1.3, 1.4 and 1.5) have been considered for harmonic analysis using NDVI and NDWI and additive term  $A_0$  and amplitude term  $A_1$  for each year separately are calculated from eq. 6.5. Eventually, the additive term  $A_0$  and amplitude term  $A_1$  for NDVI, and NDWI for every year from 2001 to 2008 are calculated. The Corresponding additive term  $A_0$  and amplitude term  $A_1$  for NDVI is  $NDVI_{A_0}$  and  $NDVI_{A_1}$  respectively. Similarly for NDWI, the additive term  $A_0$  and amplitude term  $A_1$  are  $NDWI_{A_0}$ ,  $NDWI_{A_1}$ . The  $NDVI_{A_0}$ ,  $NDWI_{A_0}$ ,  $NDVI_{A_1}$  and  $NDWI_{A_1}$  for every year from 2001 to 2008 are calculated i.e., we have totally 8 images of  $NDVI_{A_0}$ ,  $NDWI_{A_0}$ ,  $NDVI_{A_1}$  and  $NDWI_{A_1}$ . In this chapter, only for the year 2008, the figures are depicted and the corresponding figures for  $NDVI_{A_0}$ ,  $NDWI_{A_0}$ ,  $NDVI_{A_1}$  and  $NDWI_{A_1}$  are shown in the figs 6.4, 6.5, 6.6 and 6.7 respectively for the year 2008.

For all the year (2001-2008), we have considered the response of greenness and water of the whole area in one hand and in another hand the response of greenness and water of the particular location as considered through the help of Ground Control points (GCPs) thereby we have considered 60 GCPs which represents agriculture and 102 GCPs for water Bodies. These points have been considered on the basis of Ground Survey points and Google earth.

The  $A_0$  and  $A_1$  are computed for these GCPs in one hand and in another hand, the average  $A_0$  and  $A_1$  for whole NDVI and NDWI image is computed. In first case, it represents the effect of  $A_0$  and  $A_1$  on particular GCPs for different year, in second case it tells about the response on the whole region considered.

The average of the  $A_0$  and  $A_1$  of the 60 GCPs (GCP) identified for the agriculture with respect to NDVI are  $NDVI_{R_{A_0}}$  and  $NDVI_{R_{A_1}}$  for the year 2001 to 2008 are computed and are plotted in the figs. 6.8 and 6.10 respectively. Similarly, the average of the  $A_0$  and  $A_1$  of the water GCPs with respect to NDWI are  $NDWI_{R_{A_0}}$  and  $NDWI_{R_{A_1}}$ , are computed for every year from 2001 to 2008 and are plotted in the fig. 6.8 and 6.10 respectively.



**Fig 6.3a.** Subset raw MODIS Band 1 image of  
MOD09A1.A2001057.h24v06.005.2006365121813.hdf



**Fig 6.3b.** Subset raw MODIS Band 2 image of  
MOD09A1.A2001057.h24v06.005.2006365121813.hdf

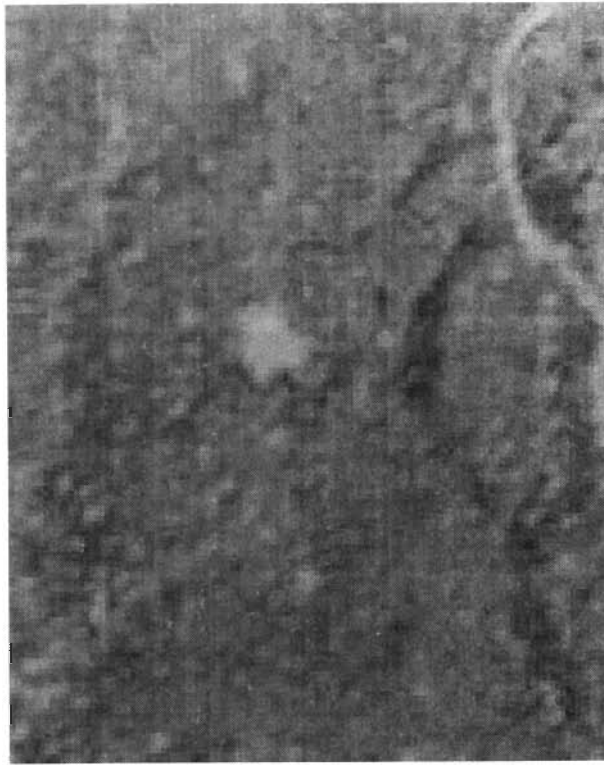


**Fig 6.3c.** Subset raw MODIS Band 7 image of MOD09A1.A2001057.h24v06.005.2006365121813.hdf

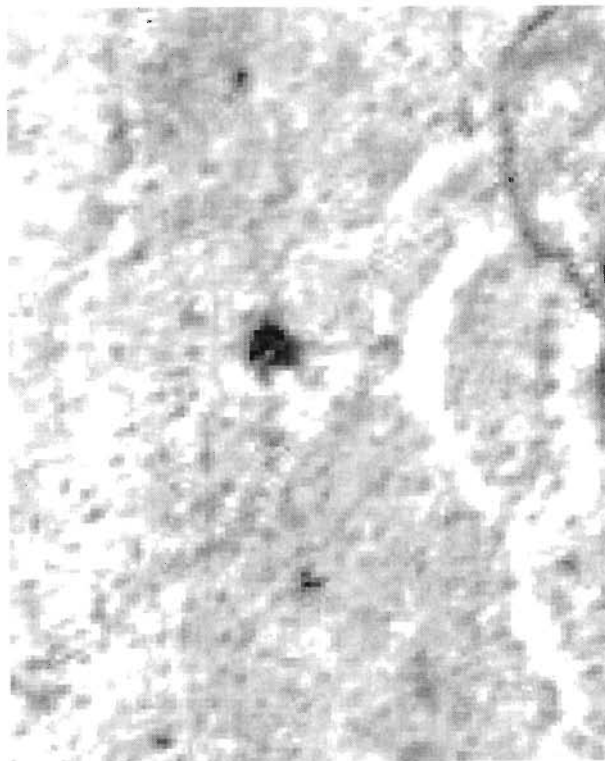


**Fig 6.3d.** NDVI of fig 6.3a and 6.3b

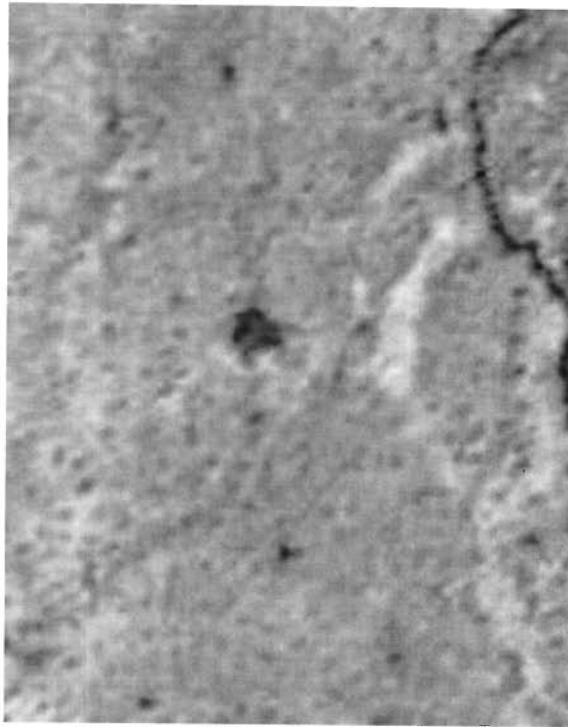


Fig 6.3e. NDWI of fig 6.3b and 6.3c

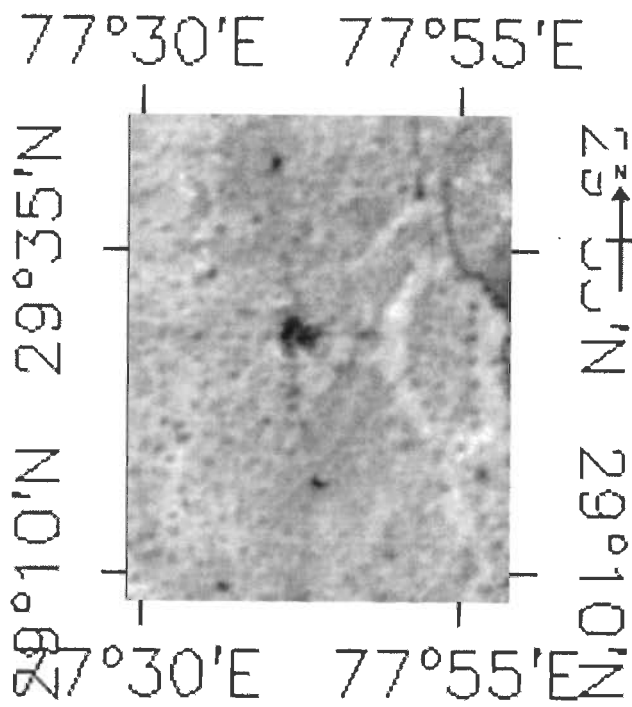


Fig 6.4 NDVI Additive term( $A_0$ ) of the year 2008

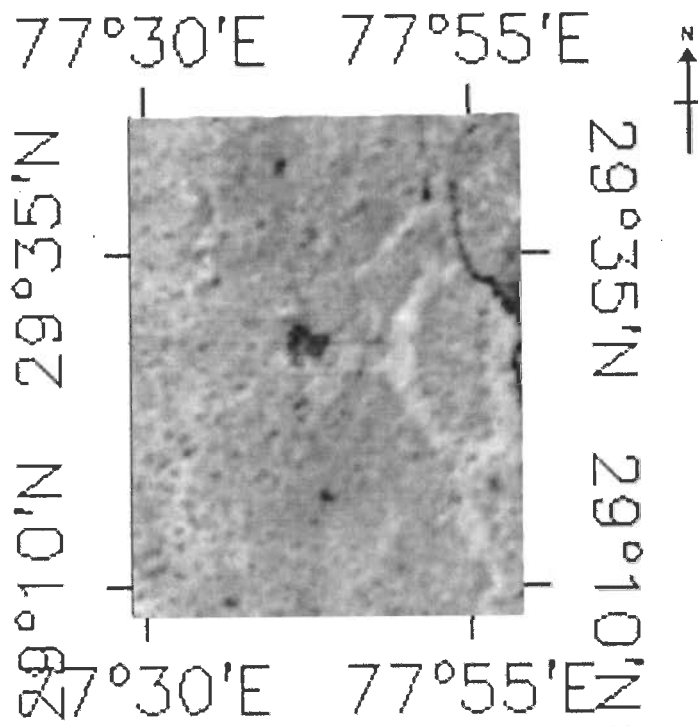


Fig 6.5 NDWI Additive term( $A_0$ ) of the year 2008

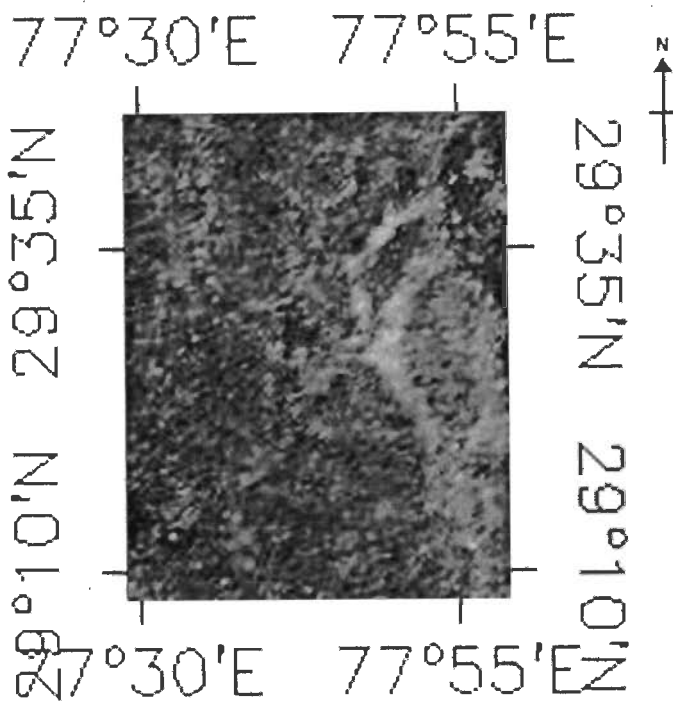


Fig 6.6 NDVI Amplitudes ( $A_1$ ) of the year 2008

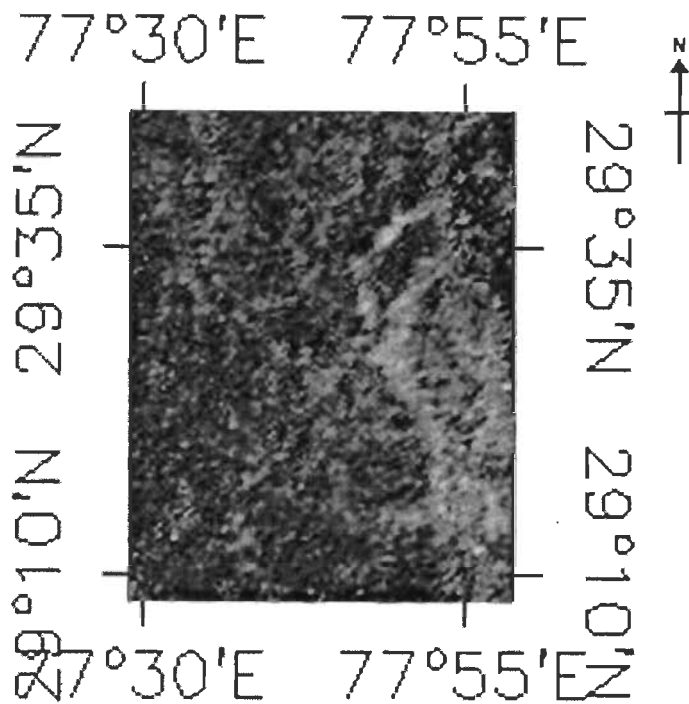


Fig 6.7 NDWI Amplitudes ( $A_1$ ) of the year 2008

The average for the whole image of the NDVI and NDWI Additive term ( $A_0$ ) are  $NDVI_{A\_A_0}$  and  $NDWI_{A\_A_0}$  and are computed for every year from 2001 to 2008 and is plotted in the fig. 6.9. Similarly the average of the NDVI and NDWI Amplitudes term ( $A_1$ ) are  $NDVI_{A\_A_1}$  and  $NDWI_{A\_A_1}$  and are computed for every year from 2001 to 2008 and are plotted in the fig. 6.11.

The overall greenness in response to the agricultural GCPs, in NDVI Additive term ( $A_0$ ) ( $NDVI_{R\_A_0}$ ) was maximum in the year 2005 and was at the minimum in the year 2001 as per the fig. 6.8 and the same pattern followed, i.e., the overall greenness was at the maximum in the year 2005 and minimum in the year 2001, when the whole area is considered, and that is obtained by the average of the NDVI Additive term ( $A_0$ ) ( $NDVI_{A\_A_0}$ ) and is plotted as in the fig. 6.9.

The overall water in response to the water GCPs in NDWI Additive term ( $A_0$ ) ( $NDWI_{R\_A_0}$ ) was maximum in the year 2007 and was at the minimum in the year 2008 as per the fig. 6.8 whereas for the whole considered area the overall water response was maximum in the year 2005 and minimum in the year 2004 that is obtained by the average of the NDWI Additive term( $A_0$ ) ( $NDWI_{A\_A_0}$ ) and is plotted in the fig. 6.9.

High amplitude values for a given term indicate a high level of variation in temporal NDVI and the term in which that variation occurs indicates the periodicity of the event. High first-term amplitude values indicate a unimodal temporal NDVI pattern where a land-use/land-cover has a wide annual range in NDVI values (Jakubauskas et al. 2001). The average of the high NDVI first term amplitude( $A_1$ ) ( $NDVI_{A\_A_1}$ ) values was observed in the year 2004 and low first term amplitude ( $A_1$ ) ( $NDVI_{A\_A_1}$ ) values was observed in the year 2003 as per the plotted fig. 6.11, whereas when the response of the agricultural GCPs are considered a high NDVI first term amplitude ( $A_1$ ) ( $NDVI_{R\_A_1}$ ) values was also observed in the year 2004 whereas the low NDVI first term amplitude ( $A_1$ ) ( $NDVI_{R\_A_1}$ ) values was observed in the year 2001, as shown in the fig. 6.10.

A high NDWI first term amplitude( $A_1$ ) ( $NDWI_{A\_A_1}$ ) values was observed in the year 2004 and low first term amplitude ( $A_1$ ) ( $NDWI_{A\_A_1}$ ) values was observed in the year 2003 as per the plotted in fig. 6.11, whereas when the response of the water GCPs are considered, a high NDWI first term amplitude ( $A_1$ ) ( $NDWI_{R\_A_1}$ ) values was observed in the year 2007, whereas the low NDWI first term amplitude ( $A_1$ ) ( $NDWI_{R\_A_1}$ ) values was observed in the year 2001, as shown in the fig. 6.10.

These results shows that there is some changes occurred during the year 2001 to 2008 and which is quite observable with the harmonic analysis of MODIS image. This chapter has main aim to show the utility of MODIS images with the application of Fourier analysis for observing the land cover changes in which it shows that the applied method on MODIS images may be quite useful in near future for observing the changes over the various land cover. In future, we are trying to get the ground truth information about changes for various classes and will try to check the results.

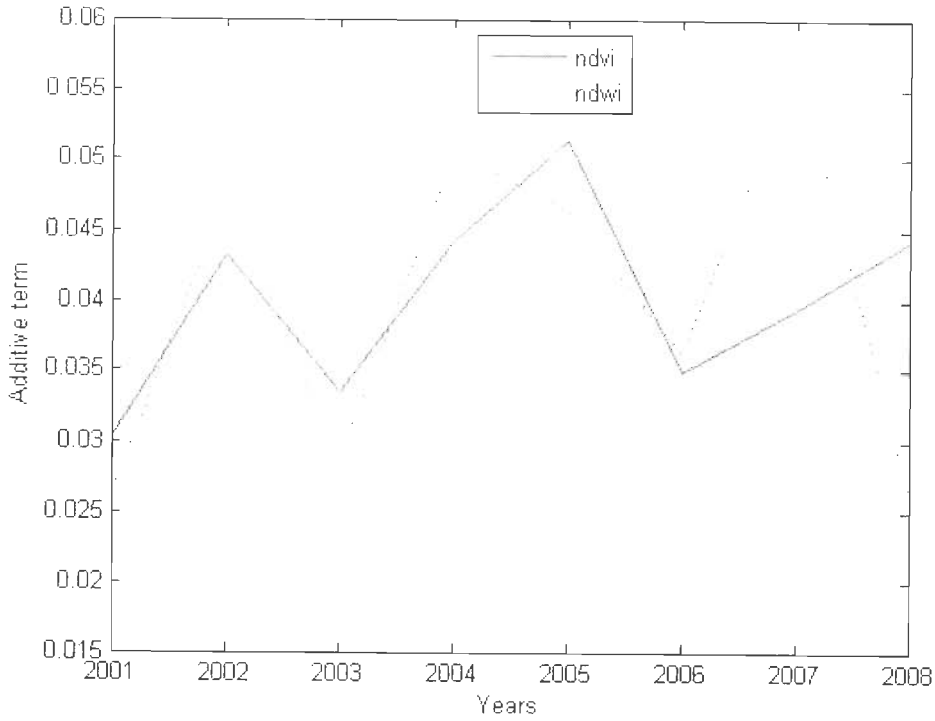


**Fig 6.8.** NDVI and NDWI Additive term( $A_0$ ) with respect to Agricultural ( $NDVI_{R\_A_0}$ ) and Water ( $NDWI_{R\_A_0}$ ) ROIs

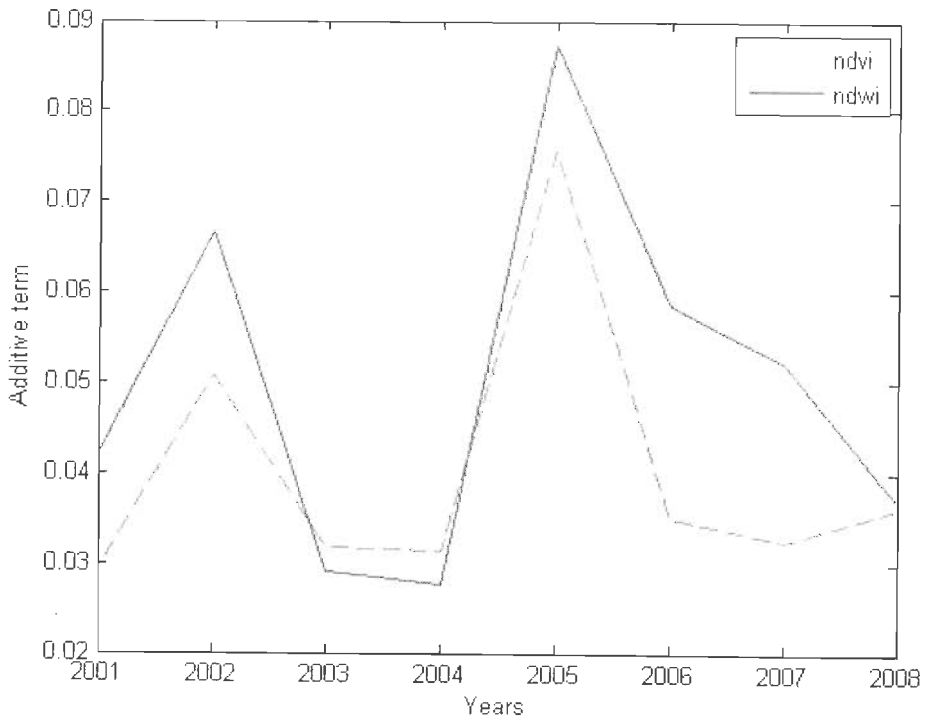


**Fig 6.9.** NDVI ( $NDVI_{A\_A_0}$ ), NDWI ( $NDWI_{A\_A_0}$ ) Additive term( $A_0$ )



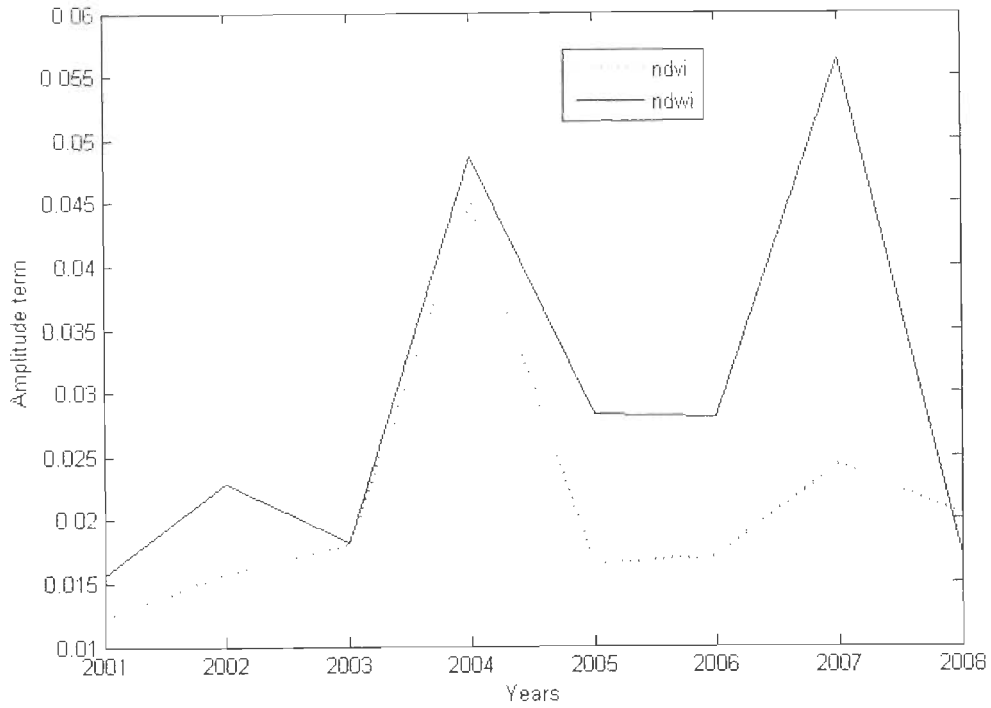


**Fig 6.10.** NDVI and NDWI Amplitudes term( $A_1$ ) with respect to Agricultural ( $NDVI_{R\_A_1}$ ) and Water ( $NDWI_{R\_A_1}$ ) ROIs

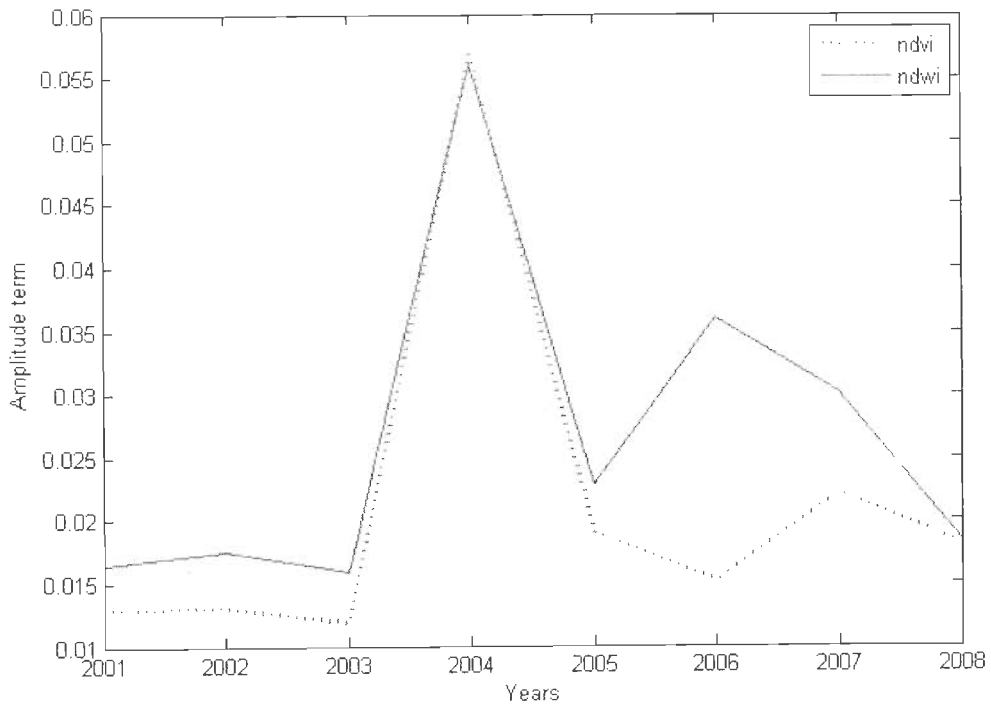


**Fig 6.11.** NDVI ( $NDVI_{A\_A_1}$ ), NDWI ( $NDWI_{A\_A_1}$ ) Amplitudes term( $A_1$ )

## 6.6. Conclusion

A methodology for study of multitemporal changes in the agriculture and water areas is presented in this chapter, through the use of NDVI and NDWI of MODIS images from year 2001 to 2008 by the harmonic analysis. This type of analysis is quite useful for observing the particular changes in the particular month. The considered area of interest for agriculture shows maximum greenness in one hand and in another hand the overall greenness of the whole area was also maximum in the year 2005 where as in the other years changes are observed, but the minimum in the greenness was observed in the year 2001 for the considered area of interest for agriculture and also in the whole area considered. The overall water in response to the water area of interest was maximum in the year 2007 and was at the minimum in the year 2008, whereas the overall water response for the whole considered areas was maximum in the year 2005 and minimum in the year 2004. It shows that particular water areas of interest may be more water in year 2007, whereas overall water in whole considered image is maximum in 2005.

This type of work is giving strength to carry out region specific study for knowing specific changes in particular region.

## Chapter 7

# Conclusions and Future Scope

---

This chapter presents the succinct overview of the layout, results and major inferences of the research work. Scope of the work and possibilities to extend it further constitute the later part of the chapter.

### 7.1. Contributions of the Thesis

The Present work in this thesis started from the observation that a number of satellite images are available for various applications especially land cover application but it is important to select a proper satellite image for the land cover classification. Satellite image properties like resolution and band values are main important parameters for classification. It is also an important challenge to provide this information for various agencies like Govt. planning agency, farmers, Agro-economic developers etc. at minimum cost. Therefore the main aim of this project work is to maximize the use of freely available satellite image especially MODIS. MODIS has 36 bands and each band as designed such as to observe special properties of land, atmosphere, etc. but for land cover classification its resolution is not adequate. Therefore we are not

getting a very good classification accuracy with the MODIS image itself, so it is need of current research to enhance the classification accuracy of MODIS image. Therefore the research work was divided into three main parts for maximizing the use of MODIS image.

1. To enhance the classification accuracy of MODIS image with the fusion of optical as well as radar images.
2. To check the application of MODIS image for particular class enhancement in a single class like hotspot and non-hotspot regions.
3. Application of MODIS images for quantifying the changes in terms of greenness of the particular region as well as amount of water presence in that region.

These three major parts are divided in four chapters in this thesis i.e., chapter 3, chapter 4, chapter 5 and chapter 6. For fulfilling these major task MODIS, ASTER, PALSAR and LISS-III images are used.

- Chapter 3, presents the method of fusion of MODIS and ASTER image for enhancement of classification of the MODIS image as well as the derivation of the fusion coefficient by which fusion complexity may be reduced. The curvelet based and fuzzy based fusion techniques are used for the fusion of high resolution image (i.e., ASTER) with low or moderate resolution image (i.e., MODIS) and the resultant fused image is analyzed in the viewpoint of land cover classification. The fuzzy based fusion technique obtained the higher classification accuracy than the curvelet based fusion. The overall classification accuracy for the fused image is better than the MODIS band 1 and MODIS band 2 for both fusion techniques i.e., curvelet based and fuzzy based fusion. We have also attempted to obtain a fusion coefficient for the particular month (i.e., March) that may be useful for the further years. By this we can avoid to purchase the ASTER image or higher resolution every year. It is found that fusion coefficient may be obtained and that may be quite useful for the fusion of MODIS images of preceding years. The new fusion coefficient is validated with respect to classification accuracy and quality assessment indicators (Correlation Coefficient, Root Mean squared error,

Relative Mean Difference, Relative Variation Difference, Deviation Index, Peak signal-to-noise ratio (PSNR), Universal Image Quality Index). It implies the proposed methodology with fusion coefficient may be used to develop a land cover monitoring system with MODIS image (because it is free and temporal acquisition is high).

- Nowadays synthetic aperture radar (SAR) images are having a lot of attention of various researchers, due to its server advantages over optical images in which SAR with full polarimetric image is providing four band information's like HH, HV, VV and VH, and these hands have spatial characteristic for land cover application therefore chapter 4 is an attempt to fuse to MODIS image with full polarimetric PALSAR images to analyze the fusion effect on classification accuracy. For this purpose, various combination of PALSAR with MODIS images are fused with curvelet based and fuzzy based fusion techniques for assessing the quality of fused images. The fused images are quantitatively analyzed by quality assessment indicators (Correlation Coefficient, Root Mean squared error, Relative Mean Difference, Relative Variation Difference, Deviation Index, Peak signal-to-noise ratio (PSNR), Universal Image Quality Index) in one hand and in another hand land cover classification accuracy is computed. It is observed that both fusion technique i.e., fuzzy and curvelet based are quite enhancing the overall classification accuracy of the fused image in comparison to MODIS band 1 and band 2 images. Curvelet based fusion of MOD12 (Resultant fused image of MODIS band 1 and band 2) with HH PALSAR band which gives the resultant image MO\_PA(HH) are providing the maximum overall classification accuracy. The fused image is also assessed by the various quality assessment indicators which shows that fused image are having quite closer information with MOD12 image, which is the main advantages of these two fusion techniques.
- The Jharia coalfield in Jharkhand is the richest coal bearing area in India which contains a large number of coal mine fires (Hotspot) which have been burning for several decades. This problem paved us, to classify hotspot and non-hotspot regions. Hence in this thesis, chapter 5 is dedicated to this particular problem. The classification of hotspot and non-hotspot regions

through binary division algorithm for the Jharia coalfield in Jharkhand is envisioned. MODIS band 1 and band2, LISS-III band 2 and band 3 images are considered to deal with hotspot and non-hotspot regions classification. Although MODIS provides a special product MOD14A2 for fire classification. But it is observed that this product has limited capability to classify hotspot and non-hotspot regions. Hence, we have developed the methodologies to classify hotspot and non-hotspot regions and thereby maximizing the use of MODIS images and a good classification of hotspot and non-hotspot regions has been obtained.

- The study of multitemporal changes in the agriculture and water areas through the use of NDVI and NDWI of MODIS images from year 2001 to 2008, by the harmonic analysis. For observing the particular changes in the particular month in the agriculture and water areas, this type of analysis is quite useful. Forty MODIS images from year 2001 to 2008 have been used for multitemporal change analysis in this chapter 6. We are interested to highlight the changes in agriculture and water areas of particular month March from year 2001 to 2008. We have taken some specific region of agriculture and water areas and for this we have seen the temporal changes, while we have also computed change in the whole considered image. It is found that the harmonic analysis of MODIS is quite useful for quantitative analyzing the changes in greenness and overall water in the area

## **7.2. Future Scope**

Taking the ground of findings from the implementation of the problems stated in section 1.2, following scope for the research may be outlined:

- The present study is strengthening the concept of enhancement of utilization of MODIS images. It is clearly observed that the classification accuracy of MODIS image will be enhanced by fusing it with high resolution images. Fusion coefficients is one of the better option to the use of number of higher resolution images. But these fusion coefficients will be very much seasonal

and regional specific because satellite images are very much dependant on seasons. So it is important to tune the fusion coefficient. For this purpose more number of higher resolution image may be used to tune the fusion coefficients. This fusion coefficients, may be very helpful for developing a land cover monitoring system.

- It is further required to enhance the use of polarimetric SAR data by developing a method for obtaining fusion coefficients. It may also possible to use radar wave interaction concept with target labeling the various class
- Based on the solutions proposed in the classification of hotspot and non-hotspot in this thesis, a decision support system can be developed which provides automated functionalities for area estimation and monitoring. This system will take input as the satellite image of the affected area and will provide the desired results and information as output.
- A methodology for study of multitemporal changes in the agriculture and water areas was presented in this thesis, only for the month of march only, and in near future it is desired to develop a monitoring system for observing the particular changes in all seasons and in all the month also.

# Bibliography

---

Abdelwahab H. and Nicolas D. G., "A Comparison of mamdani and sugeno fuzzy inference systems for evaluating the quality of experience of haptic-audio-visual applications," IEEE International Workshop on Haptic Audio Visual Environments and their Applications, HAVE 2008, Canada, 2008.

Agarwal R., Singh D., Chauhan D. S. and Singh K. P., "Detection of coal mine fires in the Jharia coal field using NOAA/AVHRR image," Journal of Geophysics and Engineering, vol. 3, pp. 212–218, 2006.

Aguado I., Chuvieco E., Martin P. and Salas J., "Assessment of forest fire danger conditions in southern Spain from NOAA images and meteorological indices," International Journal of Remote Sensing, vol. 24, no. 8, pp. 1653–1668, 2005.

Aiazzi B., Alparone L., Baronti S. and Garzelli A., "Context-driven fusion of high spatial and spectral resolution images based on oversampled multi-resolution analysis," IEEE Transactions on Geoscience and Remote Sensing, vol. 40, no. 10, pp. 2300–2312, 2002.



- Aiazzi B., Alparone L., Baronti S., Garzelli A., Nencini F. and Selva M., "Spectral information extraction by means of ms + pan fusion." Proceedings of ESAEUSC 2004, Spain, ESA SP-553, 2004.
- Akgün A., Eronat A. H. and Türk N., "Comparing different satellite image classification methods: An application in Ayvalik district, western Turkey, " XX<sup>th</sup> International Congress for Photogrammetry and Remote Sensing, Istanbul, Turkey, paper no. 505, 2004
- Alparone L., Aiazzi B., Baronti S., Garzelli A. and Nencini P., "A Global quality measurement of pan-sharpened multispectral imagery," IEEE Geosciences and Remote Sensing Letters, vol. 1, no. 4, pp. 313–317, 2004a.
- Alparone L., Baronti S., Garzelli A. and Nencini F., "Landsat ETM+ and SAR image fusion based on generalized intensity modulation," IEEE Transactions on Geoscience and Remote Sensing, vol. 42, no. 12, 2832–2839, 2004b.
- Alparone L., Wald L., Chanussot L., Thomas C., Gamba P. and Bruce L. M., "Comparison of pansharpening algorithms: Outcome of the 2006 GRS-S data fusion contest," IEEE Transactions on Geosciences and Remote Sensing, vol. 45, pp. 3012–3021, 2007.
- Amarsaikhan D., and Douglas T., "Data fusion and multisource image classification," International Journal of Remote Sensing, vol. 25, no. 17, pp. 3529–3539, 2004.
- Anderson J. R., Hardy E.T., Roach J.T. and Witmer R..E., "A land use and land cover classification system for use with remote sensing data," Professional Paper 964, U.S. Geological Survey, Washington, 1976.
- Anne H. Schistad Solberg, Anil K. Jain and Tofinn Taxt, "Multisource classification of remotely sensed data, fusion of Landsat TM and SAR Images," IEEE Transactions on Geosciences and Remote Sensing, vol. 32, no. 4, pp. 768–778, 1994.
- Antonio Turiel, Jacopo Grazzini and Hussein, Yahia, "multiscale techniques for the detection of precipitation using thermal IR satellite images," IEEE Geosciences and Remote Sensing Letters, vol. 2, no. 4, pp. 447–450, 2005.

- Anyamba A., Tucker C. J. and Mahoney R., "From El Niño to La Niña: vegetation response patterns over east and southern Africa during the 1997–2000 period," *Journal of Climate*, vol. 15, no. 21, pp. 3096–3103, 2002.
- Aplin P., Atkinson P. M. and Curran P. J., "Per-field classification of land use using the forthcoming very fine spatial resolution satellite sensors: problems and potential solutions," In P.M. Atkinson and N.J. Tate (Eds), *Advances in Remote Sensing and GIS Analysis*, pp. 219–239 (New York: John Wiley and Sons), 1999.
- Arino O. and Rosaz J. -M, "1997 and 1998 World ATSR Fire Atlas using ERS-2 ATSR-2 data," *Joint Fire Science Conference*, pp. 177–182, 1999.
- Ball G. H. and Hall D. J., "ISODATA, a novel method of data analysis and classification," *Technical Report*, Stanford University, Stanford, CA, 1965.
- Bannari A., Morin D., Bonn F. and Huete A. R., "A review of vegetation indices," *Remote Sensing Reviews*, vol. 13, pp. 95–120, 1995.
- Barnes W. L., Pagano T. S. and Salomonson V. V. "Prelaunch characteristics of the Moderate Resolution Imaging Spectroradiometer (MODIS) on EOS-AM1," *IEEE Transactions on Geoscience and Remote Sensing*, vol. 36, no. 4, pp. 1088–1100, 1998.
- Barnes W. L., Xiong X. and Salomonson V. V., "Status of Terra MODIS and Aqua MODIS," *Advances in Space Research*, vol. 32, no. 11, pp. 2099–2106, 2003.
- Beaulieu M., Foucher S. and Gagnon L., "Multi-spectral image resolution refinement using stationary wavelet transform," *Proceedings of the IEEE International Geoscience and Remote Sensing Symposium, IGARSS '03*, pp. 4032–4034, 2003.
- Bin L., Weijie L., and Jiaxiong P., "Multispectral image fusion method based on intensity-hue-saturation and nonsubsampling three-channels non-separable wavelets," *Chinese Optics Letters*, vol. 8, pp. 384–387, 2010.
- Bishop C. M., "Neural Networks for Pattern Recognition," Clarendon-Press, Oxford, 1995.

- Bloom A., Fielding E. and Fu X., "A demonstration of stereophotogrammetry with combined SIR-B and Landsat TM images," *International Journal of Remote Sensing*, vol. 9, pp. 1023–1038, 1988.
- Boles S. H. and Verbyla D. L., "Comparison of three AVHRR based fire detection algorithms for interior Alaska," *Remote Sensing Environment*, vol. 72, no. 1, pp. 1–16, 2000.
- Bretschneider T. and Kao, O. D., "Image fusion in remote sensing," *First Online Symposium of Electronics Engineers, OSEE 2000, United States of America, 2000.*
- Briggs J. and Nellis M. D., "Seasonal variation of heterogeneity in the tallgrass prairie: a quantitative measure using remote sensing," *Photogrammetric Engineering and Remote Sensing*, vol. 57, no. 4, pp. 407–411, 1991.
- Brisco B. and Brown R. J., "Multidate SAR/TM synergism for crop classification in western Canada," *Photogrammetric Engineering and Remote Sensing*, vol. 61, no. 8, pp. 1009–1014, 1995.
- Brustet J. M., Vickos J. B., Fontan J., Podaire A. and Lavenu F., "Characterization of active fires in West African savannas by analysis of satellite data: Landsat Thematic Mapper," In *Global Biomass Burning*, J. S. Levine, Ed. Cambridge, MA: MIT Press, pp. 53–60, 1991.
- Butilov V. and Bretschneider T., "Objective content-dependent quality measures for image fusion of optical datam," *International Archives of Photogrammetry and Remote Sensing*, Vol. 33, 2000.
- Bushra N. K., Anwar M. M., Ajmal B. and Haroon I., "Pixel and feature level multiresolution image fusion based on fuzzy logic," Springer, T. Sobh (ed.), *Innovations and Advanced Techniques in Computer and Information Sciences and Engineering*, pp. 129–132, 2007.
- Candès E. J. and Donoho D. L., "Curvelets- A surprisingly effective nonadaptive representation for objects with edges," In *Curve and Surface Fitting*, Nashville, TN: Vanderbilt University Press, 1999.

- Carper W. J., Lillesand T. M. and Kiefer R.W., "The use of Intensity-Hue- Saturation transformations for merging SPOT panchromatic and multispectral Image Data," *Photogrammetric Engineering and Remote Sensing*, vol. 56, no. 4, pp. 459–467, 1990.
- Chatterjee R. S., "Coal fire mapping from satellite thermal IR data – a case example in Jharia coalfield, Jharkhand, India," *ISPRS Journal of Photogrammetry and Remote Sensing*, vol. 60, pp. 113–128, 2006.
- Chatterjee R. S., Wahiduzzaman M., Shah A., Raju E. V. R., Lakhera R. C. and Dadhwal V. K., "Dynamics of coal fire in Jharia coalfield, Jharkhand, India during the 1990s as observed from space," *Current Science*, vol. 92, no. 1, pp. 61–68, 2007.
- Chavez P. S. and Bowell J. A., "Comparison of the spectral information content of Landsat thematic mapper and SPOT for three different sites in the Phoenix, Arizona region," *Photogrammetric Engineering and Remote Sensing*, vol. 54, no. 12, pp. 1699–1708, 1988.
- Chavez P. S. and Kwarteng A. Y., "Extracting spectral contrast in Landsat Thematic Mapper image data using selective principle component analysis," *Photogrammetric Engineering and Remote Sensing*, vol. 55, no. 3, pp. 339–348, 1989.
- Chavez P. S., Slides S. C. and Anderson J. A. "Comparison of three different methods to merge multiresolution and multispectral data: Landsat TM and SPOT panchromatic," *Photogrammetric Engineering and Remote Sensing*, vol. 57, no. 3, pp. 295–303, 1991.
- Chavoshi S. H., Amiri A. and Amini J., "Supervised classification in high resolution images (Quikbird) using Neural network, Fuzzy sets and Minimum distance," *Map Asia 2007 Conference*, Kuala Lumpur, Malaysia, 2007.
- Chen D. and Brutsaert W., "Satellite-sensed distribution and spatial patterns of vegetation parameters over a tallgrass prairie," *Journal of the Atmospheric Sciences*, vol. 55, no. 7, pp. 1225–1238, 1998.

- Chen Y., Fung T., Lin W. and Wang J., "An image fusion method based on object-oriented image classification," *IEEE Transactions on Geoscience and Remote Sensing Symposium IGARSS '05*, vol. 6, pp. 3924–3927, 2005a.
- Chen D., Huang J. and Jackson T. J., "Vegetation water content estimation for corn and soybeans using spectral indices derived from MODIS near- and short-wave infrared bands," *Remote Sensing Environment*, vol. 98, pp. 225–236, 2005b.
- Chibani Y. and Houacine A. "Redundant versus orthogonal wavelet decomposition for multisensor image fusion," *Pattern Recognition*, vol. 36, no. 4, pp. 879–887, 2003.
- Choi M., Kim M. G., Kim T. and Kim R. Y., "Biorthogonal wavelets-based Landsat 7 image fusion," *Proceedings of the 24th Asian Conference on Remote Sensing (ACRS 9' 03) and the International Symposium on Remote Sensing (ISRS)*, Korea, 24, pp. 494–496, 2003.
- Choi M., Kim R. Y. and Kim M. G., "The curvelet transform for image fusion". *International Society for Photogrammetry and Remote Sensing, ISPRS 2004*, vol. 35, no. B8, pp. 59–64, 2004.
- Choi M., Kim R. Y., Nam M. R. and Kim H. O., "Fusion of multispectral and panchromatic satellite images using the curvelet transform," *IEEE Geoscience and Remote Sensing Letters*, vol. 2, no. 2, 136–140, 2005.
- Choi M., "A new intensity–hue–saturation fusion approach to image fusion with a tradeoff parameter," *IEEE Transactions on Geoscience and Remote Sensing*, vol. 44, no. 6, pp. 1672–1682, 2006.
- Chrysoulakis N., Herlin I., Prastacos P., Yahia H., Grazzini J. and Cartalis C., "An improved algorithm for the detection of plumes caused by natural or technological hazards using AVHRR imagery," *Remote Sensing of Environment*, vol. 108, pp. 393–406, 2007.
- Clement V., Giraudon G., Houzelle S. and Sandakly F., "Interpretation of remotely sensed images in a context of multisensor fusion using a multispecialist

- architecture," *IEEE Transactions on Geosciences and Remote Sensing*, vol. 31, no. 4, pp. 779–791, 1993.
- Colditz R. R., Conrad C., Wehrmann T., Schmidt M. and Dech S., "TiSeG – A flexible software tool for time series generation of MODIS data utilizing the quality assessment science data set," *IEEE Transactions on Geoscience and Remote Sensing*, vol. 46, no. 10, 2008.
- Collado A. D., Chuvieco E. and Camarasa A., "Satellite remote sensing analysis to monitor desertification processes in the crop-rangeland boundary of Argentina," *Journal of Arid Environments*, vol. 52, pp. 121–133, 2002.
- Couloigner I., Ranchin T., Valtonen V. P. and Wald L., "Benefit of the future SPOT 5 and of data fusion to urban roads mapping," *International Journal of Remote Sensing*, vol. 19, no. 8, pp. 1519–1532, 1998.
- Craig M. E., "The NASS cropland data layer program," *Third International Conference on Geospatial Information in Agriculture and Forestry*, Denver Colorado, 2001.
- Cuomo V., Lasaponara R. and Tramutoli V., "Evaluation of a new satellite based method for forest fire detection," *International Journal of Remote Sensing*, vol. 22, no. 9, pp. 1799–1826, 2001.
- Danklmayer A., Chandra M. and Lüneburg E., "Principal component analysis in radar polarimetry," *Advances in Radio Science*, vol. 3, pp. 399–400, 2005.
- Davis, J.C., "Statistics and data analysis in geology," Wiley (2nd Ed), New York, 1986.
- De Bethune S., Muller F. and Donnay J. -P., "Fusion of multispectral and panchromatic images by local mean and variance matching filtering techniques," *Proceedings of Fusion of Earth Data*, Sophia Antipolis, Nice, France, IRS–1D Users Handbook (Hyderabad: National Remote Sensing Agency), pp. 31–37, 1998.

- De Beurs K. M. and Henebry G. M., "Land surface phenology, climatic variation, and institutional change: analyzing agricultural land cover change in Kazakhstan," *Remote Sensing of Environment*, vol. 89, no. 4, pp. 423–433, 2004.
- Dean A. M and Smith G. M., "An evaluation of per –parcel land cover mapping using maximum likelihood class probabilities, " *International Journal of Remote Sensing*, vol. 24, no. 14, pp. 2905-2920, 2003.
- Defries R. S. and Townshend J. R. G., "NDVI-derived land cover classifications at a global scale," *International Journal of Remote Sensing*, vol. 15, pp. 3567–3586, 1994.
- Defries R. S., Hansen M. C., Townshend J. R. G. and Sohlberg R. S., "Global land cover classifications at 8 km spatial resolution: The use of training data derived from Landsat imagery in decision tree classifiers," *International Journal of Remote Sensing*, vol. 19, pp. 3141–3168, 1998.
- Dehghani M., "Wavelet based image fusion using a trous algorithm." Poster Session of the Map India Conference, New Delhi, India, 2003.
- Delbart N., Kergoat L., Toan T. L., Lhermitte J. and Picard G., "Determination of phenological dates in boreal regions using normalized difference water index," *Remote Sensing of Environment*, vol. 97, pp. 26–38, 2005.
- Do M. N. and Vetterli M., "The finite ridgelet transform for image representation," *IEEE Transactions on Image Processing*, vol. 12, no. 1, pp. 16–28, 2003.
- Draeger W. C., Holm T. M., Lauer D. T. and Thompson R. J., "The availability of Landsat data: Past, present, and future," *Photogrammetric Engineering and Remote Sensing*, vol. 63, pp. 869–875, 1997.
- Duda R. O., Hart P. E. and Stork D. G., "Pattern Classification," John Wiley 2<sup>nd</sup> Edition, 2001.
- Eastman J. R. and Fulk M., "Long sequence time series evaluation using standardized principal components," *Photogrammetric Engineering and Remote Sensing*, vol. 59, no. 8, pp. 1307–1312, 1993.

- Edwards K. and Davis P. A., "The use of Intensity-Hue-Saturation transformation for producing color shaded-relief images," *Photogrammetric Engineering and Remote Sensing*, vol. 60, no. 11, pp. 1369–1374, 1994.
- Ehlers M., Klonus S., Johan Å. P. and Rosso P., "Multi-sensor image fusion for pansharpening in remote sensing," *International Journal of Image and Data Fusion*, vol. 1, no. 1, pp. 25–45, 2010.
- Eidenshink J. C. and Faundeen J. L., "The 1km AVHRR global land data set: First stages in implementation," *International Journal of Remote Sensing*, vol. 15, no. 17, pp 3443–3462, 1994.
- Erdas, "ERDAS Field Guide™," 5th ed., ERDAS Inc, Georgia, 2002.
- Eva H. and Flasse S., "Contextual and multiple-threshold algorithms for regional active fire detection with AVHRR data," *Remote Sensing of Environment*, vol. 14, pp. 333–351, 1996.
- Eve M. D., Merchant J. W. and Kroll K. C., "A Preliminary Analysis of GAP Land Cover Mapping Procedures," URL: <http://www.gap.uidaho.edu/Bulletins/6/APAGLCMP.htm>(last accessed 05 November 2009), 1997.
- Farina A., Costantini M. and Zirilli F., "Fusion of radar images: techniques and applications," Invited Lecture, Colloquium Entretiens Science et Defense, Topic on Le futur du radar: une synthesis de techniques, pp. 285–296, 1996.
- Fasbender D., Radoux J. and Bogaert P., "Bayesian data fusion for adaptable image pansharpening," *IEEE Transactions on Geosciences and Remote Sensing*, vol. 46, no. 6, pp. 1847–1857, 2008.
- Feitosa R. Q., Meirelles M. S. P. and Blois P. A., "Using linear regression for the automation of supervised classification in multitemporal images," *First International workshop on analysis of multi-temporal remote sensing images – MultiTemp*, 2001.



- Feitosa R. Q., Meirelles M. S. P. and Blois P. A., "Automatic Generation of Training Examples for the Classification of Multitemporal Images." International Workshop on Pattern Recognition for Remote Sensing (PRRS), 2002.
- Filippo Nencini, Andrea Garzelli, Stefano Baronti, Luciano Alparone, "Remote sensing image fusion using the curvelet transform," *Information Fusion*, vol. 8, pp. 143–156, 2007.
- Flannigan M. D. and Vonder Haar T. H., "Forest fire monitoring using NOAA satellite AVHRR," *Canadian Journal of Forest Research*, vol. 16, no. 5, pp. 975–982, 1986.
- Flasse S. P. and Ceccato P., "A contextual algorithm for AVHRR fire detection," *International Journal of Remote Sensing*, vol. 17, no. 2, pp. 419–424, 1996.
- Franklin S. E., Peddle D. R., Dechka J. A. and Stenhouse G. B., "Evidential reasoning with Landsat TM, DEM and GIS data for land cover classification in support of grizzly bear habitat mapping," *International Journal of Remote Sensing*, vol. 23, pp. 4633–4652, 2002.
- Friedl M. A., Mciver D. K., Hodges J. C. F., Zhang X. Y., Muchoney D., Strahler A. H., Woodcock C. E., Gopal S., Schneider A., Cooper A., Baccini A., Gao F. and Gao B., "NDWI—A normalized difference water index for remote sensing of vegetation liquid water from space," *Remote Sensing of Environment*, vol. 58, pp. 257–266, 1996.
- Friedl M. A., McIver D. K., Hodges J. C. F., Zhang X. Y., Muchoney D., Strahler A. H., Woodcock C. E., Gopal S., Schneider A., Cooper A., Baccini A., Gao F. and Schaaf C., "Global land cover mapping from MODIS: algorithms and early results," *Remote Sensing of Environment*, vol. 83, pp. 287–302, 2002.
- Galindo I., Lopez-Perez P. and Evangelista-Salazar M., "Real-time AVHRR forest fire detection in Mexico (1998-2000)," *International Journal of Remote Sensing*, vol. 24, no. 1, pp. 9–22, 2003.
- Gallego F. J., "Remote sensing and land cover area estimation," *International Journal of Remote Sensing*, vol. 25, pp. 3019–3047, 2004.

- Galletti M., Chandra M., Pottier E. and Ghorbani A., "Application of the Cloude-Pottier decomposition to weather radar signatures." *Advances in Radio Science*, vol. 3, pp. 413–420, 2005.
- Galletti M., Chandra M., Borner T. and Bebbington D. H. O., "Degree of polarization for weather radars". *IEEE International Geoscience and Remote Sensing Symposium, IGARSS '07 Proceedings*, pp. 4187-4190, 2007.
- Galletti M., Bebbington D. H. O., Chandra M. and Boerner T., "Measurement and characterization of entropy and degree of polarization of weather radar targets". *IEEE Transactions on Geoscience and Remote Sensing*, Vol. 46, no.10, 2008a.
- Galletti M., Bebbington D., H., O., Chandra M. and Boerner T., "Fully polarimetric analysis of weather radar signatures". *IEEE Radar Conference, RADAR '08*, pp. 1-6, 2008b.
- Gao B. C., "NDWI - A normalized difference water index for remote sensing of vegetation liquid water from space," *Remote Sensing of Environment*, vol. 58, pp. 257–266, 1996.
- Garguet-Duport B., Girel J., Chassery J. M. and Pautou G., "The use of multiresolution analysis and wavelets transform for merging SPOT panchromatic and multispectral image data," *Photogrammetric Engineering and Remote Sensing*, vol. 62, no. 9, pp. 1057–1066, 1996.
- Gautam R. S., Singh D. and Mittal A., "Application of principal component analysis and information fusion technique to detect hotspots in NOAA/AVHRR images of Jharia coalfield," *SPIE Journal of Applied Remote Sensing (JARS)*, vol. 1, 013523, 2007a.
- Gautam R. S., Singh D. and Mittal A., "A fuzzy logic approach to detect hotspots with NOAA/AVHRR image using multi-channel information fusion technique," *Signal, Image and Video Processing*, vol. 1, pp. 347–357, 2007b.
- Gautam R. S., Singh D. and Mittal A., "Detection of hotspots in NOAA/AVHRR images using principal component analysis and information fusion technique,"

- International Archives of Photogrammetry, Remote Sensing and Spatial Information Sciences, vol. 36, no. 4, pp. 951–956, 2007c.
- Gautam R. S., Singh D. and Mittal A., "An efficient contextual algorithm to detect hotspots with NOAA/AVHRR data." IEEE Transactions on Geosciences and Remote Sensing, vol. 46, no. 7, pp. 2005–2015, 2008a.
- Gautam R. S., Singh D., Mittal A. and Sajin P., "Application of SVM on satellite images to detect hotspots in Jharia coal field region of India," Advances in Space Research, vol. 41, pp. 1784–1792, 2008b.
- Giglio L., Kendall J. D. and Justice C. O., "Evaluation of global fire detection algorithms using simulated AVHRR infrared data," International Journal of Remote Sensing, vol. 20, no. 10, pp. 1947–1985, 1999.
- Giglio L., Loboda T., Roy D. P., Quayle B. and Justice C. O., "An active-fire based burned area mapping algorithm for the MODIS sensor," Remote Sensing of Environment, vol. 113, no. 408–420, 2009.
- Gillespie A. R., Kahle A. B. and Walker R. E., "Color enhancement of highly correlated images—II. Channel ratio and 'chromaticity' transformation techniques," Remote Sensing of Environment, vol. 22, pp. 343–365, 1987.
- Gohil B. S., Mathur A. K. and Pandey P. C., "An algorithm for sea surface temperature estimation from ERS-1 ATSR using moisture dependent coefficients: a simulation study," International Journal of Remote Sensing, vol. 15, no.5, pp. 1161–1167, 1994.
- Goldewijk K. K. and Ramankutty N., "Land cover change over the last three centuries due to human activities: the availability of new global data sets," GeoJournal, 61, pp. 335–344, 2004.
- Gonzalez-Audicana M., Saleta J. L. and Catalan R. G., "Fusion of multispectral and panchromatic images using improved IHS and PCA mergers based on wavelet decomposition," IEEE Transactions on Geoscience and Remote Sensing, vol. 42, no. 6, pp. 1204–1211, 2004.

- Gonzalo P. and Jesus M. C., "A wavelet-based image fusion tutorial," *Pattern Recognition*, vol. 37, pp. 1855 – 1872, 2004.
- Goshtasby A. A. and Nikolov S., "Image fusion: advances in the state of the art," *Information Fusion*, vol. 8, no. 2, pp. 114–118, 2007.
- Goward S.N., Turner S., Dye D.G. and Liang S., "The University of Maryland improved global vegetation index product," *International Journal of Remote Sensing*, vol. 15, no. 17, pp. 3365–3395, 1994.
- Grasso D.N. "Applications of the IHS color transformation for 1:24,000-scale geologic mapping: A low cost SPOT alternative," *Photogrammetric Engineering and Remote Sensing*, vol. 59, no. 1, pp. 73–80, 1993.
- Grazzini J., Turiel A. and Yahia H., "Entropy estimation and multiscale processing in meteorological satellite images," *International Conference on Pattern Recognition ICPR'02*, vol. 3, pp. 764 - 767, 2002.
- Grazzini J., Turiel A., Yahia H. and Isabelle H., "Analysis and comparison of functional dependencies of multiscale textural features on monospectral infrared images," *Geosciences and Remote Sensing Symposium, IGARSS 03*, vol. 3, pp. 2045–2047, 2003.
- Gu J., Yang J., Zhang H., Peng Y. and Wang C., "Speckle filtering in polarimetric SAR data based on the subspace decomposition," *IEEE Transactions on Geoscience and Remote Sensing*, vol. 42, no. 8, pp. 1635–1641, 2004.
- Gungor O. and Shan J., "Evaluation of satellite image fusion using wavelet transform." *Proceedings of the ISPRS, Commission VII, WG III/6, Istanbul*, paper no. 236, 2004.
- Gupta R. P. and Prakash A., "Reflectance aureoles associated with thermal anomalies due to subsurface mine fires in the Jharia coalfield, India," *International Journal of Remote Sensing*, vol. 19, no. 14, pp. 2619–2622, 1998.

- Gyanesh Chander, Michael J. Coan and Pasquale L. Scaramuzza, "Evaluation and Comparison of the IRS-P6 and the Landsat Sensors," *IEEE Transactions on Geoscience and Remote Sensing*, vol. 46, no. 1, pp. 209–221, 2008.
- Haack B. and Bechdol M., "Integrating multisensor data and RADAR texture measures for land cover mapping," *Computers & Geosciences*, vol. 26, no. 4, pp. 411–421, 2000.
- Haci Mustafa Palancioglu, "Extracting movement patterns using fuzzy and neuro-fuzzy approaches". PhD Thesis, Spatial Information Science and Engineering, The University of Maine, May, 2003.
- Hall D. L. and Llinas J., "An introduction to multisensor data fusion," *Proc. IEEE*, vol. 85, no. 1, pp. 6–23, 1997.
- Hanaizumi H. and Chino S., "Binary division algorithm using a linear discriminant function for the cluster analysis of remotely sensed multispectral images," *SPIE Proceedings-- Volume 2579, Image and Signal Processing for Remote Sensing II*, pp. 182–187, 1995.
- Hanaizumi H., Chino S. and Fujimura S., "A Binary Division Algorithm for Clustering Remotely Sensed Multispectral Images," *IEEE Transactions on Instrumentation and Measurement*, vol. 44, no 3, pp.759–763, 1995.
- Hansen M. C., Defries R. S., Townshend J. R. G. and Sohlberg R., "Global land cover classification at 1 km spatial resolution using a classification tree approach," *International Journal of Remote Sensing*, vol. 21, no. 6–7, pp. 1331–1364, 2000.
- Hansen M. C., Defries R. S., Townshend J. R. G., Sohlberg R., Dimiceli C. and Carroll M., "Towards an operational MODIS continuous field of percent tree cover algorithm: Examples using AVHRR and MODIS data," *Remote Sensing of Environment*, vol. 83, pp. 303–319, 2002.
- Hansen M. and DeFries R. S., "Detecting long-term global forest change using continuous fields of tree-cover maps from 8km Advanced Very High Resolution Radiometer (AVHRR) data for the years 1982-99," *Ecosystems*, vol. 7, pp. 695–716, 2004.

- Harish K. G. R. and Singh D., "Quality assessment of fused image of MODIS and PALSAR," *Progress In Electromagnetics Research B*, vol. 24, pp. 191–221, 2010.
- Harris J. R., Murray R. and Hirose T., "IHS transform for the integration of radar imagery and other remotely sensed data," *Photogrammetric Engineering and Remote Sensing*, vol. 56, no. 12, pp. 1631–1641, 1990.
- Hegarar-Masclé S., Quesney A., Vidal-Madjar D., Taconet O., Normand M. and Loumagne C., "Land cover discrimination from multitemporal ERS images and multispectral Landsat images: a study case in an agricultural area in France," *International Journal of Remote Sensing*, vol. 21, pp. 435–456, 2000.
- Holben B. N., "Characterization of maximum value composites from temporal AVHRR data," *International Journal of Remote Sensing*, vol. 7, no. 11, pp. 1417–1434, 1986.
- Homer C., Huang C., Yang L., Wylie B. and Coan M., "Development of a 2001 national land-cover database for the United States," *Photogrammetric Engineering and Remote Sensing*, vol. 70, no. 7, pp. 829–840, 2004.
- Hong G. and Zhang Y., "High resolution image fusion based on Wavelet and IHS transformations," *Proceedings of the IEEE/ISPRS Joint Workshop on 'Remote Sensing and Data Fusion over Urban Areas, 2003, Berlin*, pp. 99–104, 2003.
- Hong G. and Zhang Y., "The effects of different types of wavelets on image fusion." *Proceedings of the ISPRS, Commission IV, Istanbul*, paper no. 474, 2004.
- Huang S., "The potential of multi-sensor satellite data for applications in environmental monitoring with special emphasis on land cover mapping, desertification monitoring and fire detection Dissertation," *LMU München: Fakultät für Biologie*, 2005.
- Humayun I., Muhammad K., Abdul B. S. and Ayyaz H., "Image fusion using computational intelligence: A Survey," *International Conference on Environmental and Computer Science*, pp. 128-132, 2009.

- Irina P. and Martina D., "Image fusion on the basis of fuzzy transforms," Research report No. 122, University of Ostrava, 2008.
- Jackson J. T., Chen D., Cosh M., Li F., Anderson M., Walthall C., Doriaswamy P. and Hunt E. R., "Vegetation water content mapping using Landsat data derived normalized difference water index for corn and soybeans," *Remote Sensing of Environment*, vol. 92, pp. 475–482, 2004.
- Jacopo G., Antonio T., Hussein Y. and Isabelle H., "A multifractal approach for extracting relevant textural areas in satellite meteorological images," *Environmental Modelling and Software*, vol. 22, pp. 323–334, 2007.
- Jain A. K., Murty M. N. and Flynn P.J., "Data clustering: a review," *ACM Computing Surveys*, vol. 31, no. 3, pp. 264–323, 1999.
- Jain A. K., Duin R. P. W. and Mao J., "Statistical pattern recognition: A review," *IEEE Transactions on Pattern Analysis and Machine Intelligence*, vol. 22, no. 1, pp. 4–37, 2000.
- Jakubauskas M. E., Legates D. R. and Kastens J., "Harmonic analysis of time-series AVHRR NDVI data," *Photogrammetric Engineering and Remote Sensing*, vol. 67, no. 4, pp. 461–470, 2001.
- Jakubauskas M. E., Legates D. R. and Kastens J. H., "Crop identification using harmonic analysis of time-series AVHRR NDVI data," *Computers and Electronics in Agriculture*, vol. 37, pp. 127–139, 2002.
- James M. E. and Kalluri S. N. V., "The pathfinder AVHRR land data set: an improved coarse resolution data set for terrestrial monitoring," *International Journal of Remote Sensing*, vol. 15, no. 17, pp. 3347–3363, 1994.
- Jang J. S. R. and Sun C. T., "Neuro-Fuzzy modeling and control," *Proceedings of the IEEE*, vol. 83, pp. 378–406, 1995.
- Ji L. and Gallo K., "An agreement coefficient for image comparison," *Photogrammetric Engineering and Remote Sensing Journal*, vol. 72, no. 7, pp. 823–833, 2006.

- Jia Y. and Xiao M., "Fusion of pan and multispectral images based on contourlet transform," In: Wagner W., Székely, B. (eds.): ISPRS TC VII Symposium, IAPRS, Vol. XXXVIII, Part 7, 2010
- John A. R. and Xiuping J., "Remote sensing digital image analysis," Springer Verlag, 4th Edition, 2005.
- Jonathan M., Meirelles M. S. P., Berroir J. P. and Herlin I., "Regional scale land use/land cover classification using temporal series of MODIS data," ISPRS Mid-Term Symposium, Remote Sensing: from Pixel to Process, 2006.
- Jönsson P. and Eklundh L., "Seasonality extraction by function fitting to time-series of satellite sensor data". IEEE Transactions on Geosciences and Remote Sensing, vol. 40, pp. 1824–1832, 2002.
- Judge J., Galantowicz J. F., England A.W., and Dahl P., "Freeze/thaw classification for prairie soils using SSM/I radiobrightnesses, " Geosciences and Remote Sensing Symposium, IGARSS 1996, pp. 827–832, 1996.
- Judge J., Galantowicz J. F., England A. W. and Dahl P., "Freeze/thaw classification for prairie soils using SSM/I radiobrightnesses," IEEE Transactions on Geosciences and Remote Sensing, vol. 35, pp. 827–832, 1997a.
- Judge J., Metcalfe J., McNichol D., Liou Y. A. and England A. W., "Validation of a summertime LSP/Radiobrightness model for bare soils in northern prairie," Geosciences and Remote Sensing Symposium, IGARSS 1997, pp. 211 - 214, 1997b.
- Judge J., England A. W., Crosson W. L., Laymon C. A., Hornbuckle B. K., Boprie D. L., Kim E. J. and Yuei-An Liou, "A growing season land surface process/radiobrightness model for wheat-stubble in the Southern Great Plains," IEEE Transactions on Geosciences and Remote Sensing, vol. 37, pp. 2152-2158, 1999.
- Judge J., Galantowicz J. F. and England A. W., "Comparison of ground-based and satellite-borne microwave radiometric observations in the Great Plains". IEEE Transactions on Geosciences and Remote Sensing, vol. 39, pp. 1686–1696, 2001.



- Justice C. O., Malingreau J. -P. and Setzer A. W., "Satellite remote sensing of fires: potential and limitations," *Fire in the Environment*, pp. 77–88, 1993.
- Justice C. O., Kendall J. D., Dowty P. R. and Scholes R. J., "Satellite remote sensing of fires during the SAFARI campaign using NOAA-AVHRR data," *Journal of Geophysical Research*, vol. 101, pp. 23851–23863, 1996.
- Justice C. O., Vermote E. Townshend J. G. R., et al, "The moderate resolution imaging spectroradiometer (MODIS): land remote sensing for global change research," *IEEE Transactions on Geoscience and Remote Sensing*, vol. 36, pp. 1228–1249, 1998.
- Justice C. O. and Townshend J. R. G., "Special issue on the moderate resolution imaging spectroradiometer (MODIS): A new generation of land surface monitoring," *Remote Sensing of Environment*, vol. 83, pp. 1–2, 2002.
- Justice C. O., Townshend J. R. G., Vermote E. F., Masuoka E., Wolfe R. E., El Saleous N. Z., Roy D. P. and Morisette J. T., "An overview of MODIS Land data processing and product status," *Remote Sensing of Environment*, vol. 83, no. 1–2, pp. 3–15, 2002.
- Kalluri S., Gilruth P. and Bergman R., "The potential of remote sensing data for decision makers at the state, local and tribal level: experiences from NASA's Synergy program," *Environmental Science & Policy*, vol. 6, pp. 487–500, 2003.
- Kamran U. K. and Yang J., "Polarimetric synthetic aperture radar image classification by a hybrid method," *Tsinghua Science and Technology*, vol. 12, no. 1, pp. 97–104, 2007.
- Karathanassi V., Kolokousis P. and Ioannidou S., "A comparison study on fusion methods using evaluation indicators," *International Journal of Remote Sensing*, vol. 28, no. 10, 2309–2341, 2007.
- Kaufman Y. J., Herring D. D., Ranson K. J. and Collatz G. J., "Earth observing system AM1 mission to Earth," *IEEE Transactions on Geoscience and Remote Sensing*, vol. 36, pp. 1045–1055, 1998.

- Kennedy P. J., Belward A. S. and Gregoire J. -M., "An improved approach to fire monitoring in West Africa using AVHRR data, " *Int. J. Remote Sens.*, vol. 15, no. 11, pp. 2235–2255, Jul. 1994.
- King R. L. and Wang J. W., "A wavelet based algorithm for pan sharpening Landsat 7 imagery," *Geosciences and Remote Sensing Symposium, IGARSS 2001*, pp. 849 - 851, 2001.
- King M. D., Closs J., Wharton S., Myers M. and Parkinson C. L., "EOS data products handbook – Volume 1,," NASA Goddard Space Flight Center, Greenbelt, MA, 2004.
- Klir G. J. and Folger T. A., "Fuzzy sets, uncertainty, and information," Prentice Hall, Englewood Cliffs, NJ, 1988.
- Kremer R. G. and Running S. W., "Community type differentiation using NOAA/AVHRR data within a sagebrush-steppe ecosystem," *Remote Sensing of Environment*, vol. 46, pp. 311–318, 1993.
- Kucera J., Yasuoka Y., and Dye D. G., "Creating a forest fire database for the Far East of Asia using NOAA/AVHRR observation," *International Journal of Remote Sensing*, vol. 26, no. 11, pp. 2423–2439, 2005.
- Kuenzer C., Hecker C., Zhang J., Wessling S. and Wagner W., "The potential of multidiurnal MODIS thermal band data for coal fire detection," *International Journal of Remote Sensing*, vol. 29, no. 3, pp. 923–944, 2008.
- Kumar R., Sarkar A. and Pandey P. C., "Estimation of ocean depths off Goa coast using ERS-1 synthetic aperture radar," *Continental Shelf Research*, vol. 19, no. 2, pp. 171–181, 1999.
- Labib A., Harpreet S. and Sushil P., "A neuro fuzzy logic approach to material processing," *IEEE Transactions on Systems, Man, and Cybernetics, Part C: Applications and Reviews*, vol. 29, no. 3, pp. 362 -370, 1999.
- Lambin E. F., Turner B.,L., Geist H.,J., Agbola S. B., Angelsen A., Bruce J. W., Coomes O. T., Dirzo R., Fischer G., Folke C., George P. S., Homewood K.,

- Imbernon J., Leemans R., Li X., Moran E. F., Mortimore M., Ramakrishnan P. S., Richards J. F., Skanes H., Steffen W., Stone G. D., Svedin U., Veldkamp T. A., Vogel C. and Xu J., "The causes of land use and land cover change: Moving beyond the myths". *Global Environment Change*, vol. 11, pp. 261–269, 2001.
- Leckie D., "Synergism of SAR and visible/infrared data for forest type discrimination," *Photogrammetric Engineering and Remote Sensing*, vol. 56, pp. 1237–1246, 1990.
- Lee T. M. and Tag P. M., "Improved detection of hotspots using the AVHRR 3.7 um channel," *Bull. Amer. Meteor. Soc.*, vol. 71, pp. 1722–1730, 1990.
- Li J., "Spatial quality evaluation of fusion of different resolution images". *International Archives of Photogrammetry and Remote Sensing*, vol. 33, 2000.
- Li Z., Nadon S. and Cihlar J., "Satellite-based detection of Canadian boreal forest fire: development and application of the algorithm," *International Journal of Remote Sensing*, vol. 21, no. 16, pp. 3057–3069, 2000.
- Li Z., Kaufman Y. J., Ichoku C., Fraser R., Trishchenko A., Giglio L., Jin J. and Yu X., "A Review of AVHRR-based active fire detection algorithms: Principles, Limitations, and Recommendations," In: *Global and Regional Vegetation Fire Monitoring from Space: Planning a Coordinated International Effort*, The Hague, The Netherlands: SPB Academic Publishing, pp. 199–225, 2001.
- Li S., Kwok J. T. and Wang Y., "Using the discrete wavelet frame transform to merge Landsat TM and SPOT panchromatic images," *Information Fusion*, vol. 3, pp. 17–23, 2002.
- Li Q. and Hu Q., "3D wavelet compression to multiple band remote sensing images based on edge reservation," *Proceedings of the ISPRS, Commission VII, Istanbul*, paper no. 11, 2004.
- Li R. -R., Kaufman Y. J., Hao W. M., Salmon J. M. and Gao B. -C., "A technique for detecting burn scars using MODIS data," *IEEE Transactions on Geoscience and Remote Sensing*, vol. 42, pp. 1300–1308, 2004.

- Liu J. G., "Smoothing filter-based intensity modulation: A spectral preserve image fusion technique for improving spatial details," *International Journal of Remote Sensing*, vol. 21, no. 18, pp. 3461–3472, 2000.
- Liu X. H., Skidmore A. K. and Oosten V. H., "Integration of classification methods for improvement of land-cover map accuracy," *ISPRS Journal of Photogrammetry and Remote Sensing*, vol. 56, pp 257-268, 2002.
- Lohani B., Mason D. C. and Bist H. S., " semi-automatic multi-level approach for extraction of tidal channels from aerial photographs and hyperspectral data," *Proceedings of Map India 2004*, pp. 28-30, 2004.
- Lohani B. and Mason D. C., "A case study on error identification and minimization in Airborne Altimetric LiDAR data," *International Journal of Geoinformatics*, vol. 1, no. 3, pp. 53–61, 2005.
- Long Z., Baochang X., Weilong T. and Zhe C., "A pixel-level multisensor image fusion algorithm based on fuzzy logic," Springer-Verlag Berlin Heidelberg, FSKD, LNAI 3613, pp. 717–720, 2005.
- Loveland T. R., Merchant J. W., Ohlen D. O. and Brown J. F., "Development of a land cover characteristics database for the conterminous U.S," *Photogrammetric Engineering and Remote Sensing*, vol. 57, no. 11, pp. 1453–1463, 1991.
- Loveland T. R., and Belward A. S., "The IGBP–DIS global 1 km land cover data set, DISCover: First results," *International Journal of Remote Sensing*, vol. 18, no.15, pp. 3289–3295, 1997.
- Loveland T. R., Reed B. C., Brown J. F., Ohlen D. O., Zhu Z., Yang L., et al., "Development of a global land cover characteristics database and IGBP DISCover from 1 km AVHRR data," *International Journal of Remote Sensing*, vol. 21, no. 6–7, pp. 1303–1330, 2000.
- Lu H., Raupach M. R., Mcvicar T. R. and Barrett D. J., "Decomposition of vegetation cover into woody and herbaceous components using AVHRR NDVI time series," *Remote Sensing of Environment*, vol. 86, no. 1, pp. 1–18, 2003.

- Lucas N. S., Sanjeevi S. and Barnsley M., "Sub-pixel habitat mapping of a coastal dune ecosystem." *Applied Geography*, vol. 22, pp. 253–270, 2002.
- Luis A. J. and Pandey P. C., "Characteristics of atmospheric divergence and convergence in the Indian Ocean inferred from scatterometer winds," *Remote Sensing of Environment*, vol. 97, no.2, pp. 231–237, 2005.
- Ma M., Wang X., Frank V. and Dong L., "Change in area of the Ebinur Lake during the 1998–2005 period," *International journal of remote sensing*, vol. 28, pp. 5523–5533, 2007.
- Madhavan B. B., Venkataraman G., Shah S. D. and Mohan B. K., "Revealing the geology of the great nicobar island, Indian ocean, by the interpretation of airborne synthetic aperture radar images," *International Journal of Remote Sensing*, vol. 18, no. 13, pp. 2723–2742, 1997.
- Madhavan B. B., Venkataraman G., Mohan B. K. and Shah S. D., "Airborne SAR and IRS-1A LISS II data interpretation of coastal geomorphology in godavari delta, India," *Geocarto International*, vol. 14, no. 2, pp. 52–61, 1999.
- Maiden M. E. and Greco S., "NASA's pathfinder data set programme: land surface parameters," *International Journal of Remote Sensing*, vol. 15, no.17, pp. 3333–3345, 1994.
- Maki M., Ishiara M. and Tamura M., "Estimation of leaf water status to monitor the risk of forest fires by using remotely sensed data," *Remote Sensing Environment*, vol. 90, pp. 441–450, 2004.
- Mallat S., "A theory for multiresolution signal decomposition: the wavelet representation," *IEEE Transactions on Pattern Analysis and Machine Intelligence*, vol. 11, no. 7, pp. 674–693, Jul. 1989.
- Mamdani E. H., "Applications of fuzzy algorithms for simple dynamic plant," *Proceedings of IEEE*, vol. 121, no. 12, pp. 1585–1588, 1974.

- Mamdani E. H. and Assilian S., "An experiment in linguistic synthesis with a fuzzy logic controller," *International Journal of Man-Machine Studies*, vol. 7, no. 1, pp. 1–13, 1975.
- Maragos P., Schafer R. W. and Butt M. A., "Mathematical Morphology and its Applications to Image and Signal Processing," Kluwer Academic Publishers, Boston, 1996
- Margarita H., Javier L., Alicia P., Fernando M., Ana S. and Paula E., "Assessment of forest fire seasonality using MODIS fire potential: A time series approach," *Agricultural and Forest Meteorology*, vol 149, no. 11, pp. 1946–1955, 2009.
- Martha T. R., Bhattacharyak A. and Kumar K. V., "Coal-fire detection and monitoring in Raniganj coalfield, India – a remote sensing approach, " *Current Science*, vol. 88, no. 1, pp. 21–24, 2005.
- Masce S. H., Bloch I. and Vidal-Madjar D., "Introduction of neighborhood information in evidence theory and application to data fusion of radar and optical images with partial cloud cover," *Pattern Recognition*, vol. 34, pp. 1811–1823, 1998.
- Masuoka E., Fleig A., Wolfe R. W. and Patt F., "Key characteristics of the MODIS data products," *IEEE Transactions on Geoscience and Remote Sensing*, vol. 36, pp. 1313–1323, 1998.
- Mathworks, "Fuzzy Logic Toolbox™ 2 - User's Guide," 2006.
- Mc feeters S. K., "The use of the Normalized Difference Water Index (NDWI) in the delineation of open water features, " *International Journal of Remote Sensing*, vol. 17, pp. 1425–1432, 1996.
- McNeill D. and Freiburger P., "Fuzzy Logic: The Discovery of a Revolutionary Computer Technology-and How it is Changing Our World," Simon and Schuster, New York, 1993.

- Meitzler T., Arafeh L., Singh H. and Gerhart G., "Fuzzy logic approach for computing the probability of target detection in cluttered environments," *Optical Engineering*, vol. 35, pp. 3623–3636, 1996.
- Mendel J. M. and Mouzouris G. C., "Designing fuzzy logic systems," *IEEE Transaction Circuit and Systems-II: Analog and Digital Signal Processing*, vol. 44, pp. 885–895, 1997.
- Metwalli M. R., Nasr A. H., Farag A. O. S., El-Rabaie S. and Abd E. Fathi. E., "Satellite image fusion based on principal component analysis and high-pass filtering," *Journal of the Optical Society of America A*, vol. 27, no. 6, pp. 1385–1394, 2010.
- Mitianoudis N. and Stathaki T., "Pixel-based and region-based image fusion schemes using ICA bases," *Information Fusion*, vol. 8, no. 2, pp. 131–142, 2007.
- Mota G., Pakzad K., Muller S., Meirelles M. S. P., Feitosa R., coutinho H. and Luis C., "A Framework for Automatic Low-Resolution Satellite Image Interpretation Based on Spectral, Contextual and Multitemporal Knowledge," *International Society Phtogrammetry and Remote Sensing XXth Congress*, 2004.
- Mota G., Feitosa R., Coutinho H., Luis C., Liedtke C. E., Muller S., Pakzad K. and Meirelles M. S. P., "Multitemporal Fuzzy Classification Model Based on Class Transition Possibilities," *ISPRS Journal of Photogrammetry and Remote Sensing*, vol. 62, pp. 182–200, 2007.
- Muhammad M. K., Jocelyn C., Laurent C. and Annick M., "Indusion: Fusion of Multispectral and Panchromatic Images Using the Induction Scaling Technique," *IEEE geoscience and remote sensing letters*, vol. 5, no. 1, pp. 98–102, 2008.
- Murtagh F. and Starck J. L., "Image processing through multiscale analysis and measurement noise modeling," *Statistics and computing*, vol. 10, no. 2, pp. 95–103, 2000.
- Murthy C. A., Chatterjee N., Shankar B. U. and Majumder D. D., "IRS image segmentation: Minimum distance classifier approach," *11<sup>th</sup> International Conference on Pattern Recognition, ICPR 92*, pp. 781–784, 1992.

- Nagarajan R. and Venkataraman G., "Reflectance characteristics of rocks in geological remote sensing," *Journal of the Indian Society of Remote Sensing*, vol. 16, no.1, pp. 11–14, 1988.
- Nakayama M., Maki M., Elvidge C. D. and Liew S. C., "Contextual algorithm adapted for NOAA–AVHRR fire detection in Indonesia," *International Journal of Remote Sensing*, vol. 20, no. 17, pp. 3415–3421, 1999.
- Nezry E. and Yakam-Simen F., "On the preservation of polarimetric signatures and polarimetric texture signatures by fully polarimetric MAP filters," *Geosciences and Remote Sensing Symposium, IGARSS 99*, vol. 3, pp. 1555–1557, 1999.
- Nuñez J., Otazu X., Fors O., Prades A., Palà V. and Arbiol R., "Multiresolution-based image fusion with additive wavelet decomposition," *IEEE Transactions on Geosciences and Remote Sensing*, vol. 37, no. 3, pp. 1204–1211, 1999.
- Ostermeier R., Rogge H. I. and Auernhammer H., "Multisensor data fusion implementation for a sensor based fertilizer application system," *Agricultural Engineering International: the CIGR E-journal* , IX, 2007.
- Ozesmi S. L. and Bauer M., "Satellite Remote Sensing of Wetlands," *Wetlands Ecology and Management*, vol. 10, pp. 381-402, 2002.
- Pal S. K., Majumdar T. J. and Bhattacharya A. K., "ERS-2 SAR and IRS-1C LISS III data fusion: A PCA approach to improve remote sensing based geological interpretation," *ISPRS Journal of Photogrammetry and Remote Sensing*, vol. 61, pp. 281–297, 2007.
- Pandey P. C. and Kakar R., "An empirical microwave emissivity model for a foam-covered sea," *IEEE Journal of Oceanic Engineering*, vol. 7, no.3, pp. 135–140, 1982.
- Pandey P. C. and Hariharan T. A., "Advances in microwave remote sensing of the ocean and atmosphere," *Journal of Earth System Science*, vol. 93, no.3, pp. 257–282, 1984.



- Pandey P. C., Gairola R. M. and Gohil B. S., "Wind-wave relationship from SEASAT radar altimeter data," *Boundary-Layer Meteorology*, vol. 37, no. 3, pp. 263–269, 1986.
- Parkinson C. L., "Aqua: an earth-observing satellite mission to examine water and other climate variables," *IEEE Transactions on Geoscience and Remote Sensing*, vol. 41, no. 2, pp. 173–183, 2003.
- Parrt W., Sier A. R., Battarbee R. W., Mackay A. and Burgess J., "Detecting environmental change: science and society perspectives on long-term research and monitoring in the 21st century," *The Science of the Total Environment*, pp. 1-8, 2003.
- Piella G., "A general framework for multiresolution image fusion: from pixels to regions," *Information Fusion*, vol. 4, no. 4, pp. 259–280, 2003.
- Piella G. and Heijmans H., "A new quality metric for image fusion," *Proceedings of IEEE International Conference on Image Processing*, vol. 3, pp.173–176, 2003.
- Pohl C. and Van Genderen J. L., "Multisensor image fusion in remote sensing: concepts, methods and applications," *International Journal of Remote Sensing*, vol. 19, no. 5, pp. 823–854, 1998.
- Pozo D., Olmo F. J. and Alados-Arboledas L., "Fire detection and growth monitoring using a multitemporal technique on AVHRR mid-infrared and thermal channels," *Remote Sensing of Environment*, vol. 60, pp. 111–120, 1997.
- Prakash A., "Remote sensing-GIS based geo-environmental studies in Jharia Coalfield, India, with special reference of coalmine fires," Ph.D. Thesis, Department of Earth Sciences, UOR, Roorkee, India, 194 p, 1996.
- Prakash A., Gupta R. P. and Saraf A. K., "A Landsat TM based comparative study of surface and subsurface fires in the Jharia coalfield, India," *International Journal of Remote Sensing*, vol. 18, no. 11, pp. 2463–2469, Jul. 1997.

- Prakash A. and Gupta R. P., "Land-use mapping and change detection in a coal mining area – a case study in the Jharia coalfield, India," *International Journal of Remote Sensing*, vol. 19, no. 3, pp. 391–410, 1998.
- Prakash A. and Gupta R. P., "Surface fires in Jharia coalfield, India – their distribution and estimation of area and temperature from TM data," *International Journal of Remote Sensing*, vol. 20, no. 10, pp. 1935–1946, 1999.
- Prakash A., Gens R. and Vekerdy Z., "Monitoring coal fires using multi-temporal night-time thermal images in a coalfield in north-west China," *International Journal of Remote Sensing*, vol. 20, no. 14, pp. 2883–2888, 1999.
- Prins E. M. and Menzel W. P., "Trends in south American biomass burning detected with the GOES VISSR radiometer atmospheric sounder from 1983 to 1991," *Journal of Geophysical Research* 99, pp. 16719–16773, 1994.
- Pu R., Gong P., Li Z. and Scarborough J., "A dynamic algorithm for wildfire mapping with NOAA/AVHRR data," *International Journal of Wildland Fire*, vol. 13, pp. 275–285, 2004.
- Raghavawamy V., Gautam N. C., Padmavathi M. and Badarinath K. V. S., "Studies on microwave remote sensing data in conjunction with optical data for land use/land cover mapping and assessment," *Geocarto International* vol. 11, no. 4, pp. 25–31, 1996.
- Ranchin T. and Wald L., "Fusion of high spatial and spectral resolution images: The ARSIS concept and its implementation," *Photogrammetric Engineering and Remote Sensing*, vol. 66, no. 1, pp. 49–61, 2000.
- Ranchin T., Aiazzi B., Alparone L., Baronti S., and Wald L., "Image fusion—The ARSIS concept and some successful implementation schemes," *ISPRS Journal Photogrammetric Engineering and Remote Sens.*, vol. 58, pp. 4–18, 2003.
- Rauste Y., Herland E., Frelander H., Soini K., Kuoremaki T. and Ruokari A., "Satellite-based forest fire detection for fire control in boreal forests," *International Journal of Remote Sensing*, vol. 18, no. 12, pp. 2641–2656, 1997.

- Rayner, J. N., "An Introduction to Spectral Analysis," Pion Ltd, London, pp. 174, 1971.
- Reed B., Brown J., Vanderzee D., Loveland T., Merchant J. and Ohlen D. O., "Measuring phenological variability from satellite imagery," *Journal of Vegetation Science*, vol. 5, pp. 703–714, 1994.
- Ressl R., Lopez G., Cruz I., Colditz R. R., Schmidt M., Ressler S. and Jiménez R., "Operational active fire mapping and burnt area identification applicable to Mexican Nature Protection Areas using MODIS and NOAA-AVHRR direct readout data," *Remote Sensing of Environment*, vol. 113, pp. 1113–1126, 2009.
- Richards J. A. and Jia X., "Remote sensing digital image analysis," 4th ed. Berlin, Heidelberg: Springer-Verlag, 2006.
- Richards J. A., "Analysis of remotely sensed data: The formative decades and the future," *IEEE Transactions on Geoscience and Remote Sensing*, vol. 43, no. 3, pp. 422–432, 2005.
- Rouse J. W., JR., Haas H. R., Deering D. W., Schell J. A. and Harlan J. C., "Monitoring the vernal advancement and retrogradation (green wave effect) of natural vegetation," *Goddard Space Flight Center GSFC Type II Final Report*, Greenbelt, Maryland, pp. 87, 1973.
- Rosenqvist, A., Shimada, M., Ito, N. and Watanabe, M., "ALOS PALSAR: a pathfinder mission for global-scale monitoring of the environment," *IEEE Transactions on Geoscience and Remote Sensing*, vol. 45, pp. 3307–3316, 2007.
- Roy D. P., Borak J. S., Devadiga S., Wolfe R. E., Zheng M. and Desloires J., "The MODIS Land product quality assessment approach," *Remote Sensing of Environment*, vol. 83, no.1-2, pp. 62–76, 2002.
- Samson S. A., "Two indices to characterize temporal patterns in the spectral response of vegetation," *Photogrammetric Engineering and Remote Sensing*, vol. 59, no. 4, pp. 511–517, 1993.

- Sanjeevi S., "Morphology of dunes of the Coromandel coast of Tamil Nadu. A satellite data based approach for coastal landuse planning," *Landscape and Urban Planning*, vol. 34, pp. 189–195, 1996.
- Sanjeev B., Amritphale S. S. and Chandra N., "Utilisation of toxic solid waste generated in a nonferrous metal industry for making frit/glazing material and its application for glazing of ceramics," In: P.R. Rao, R. Kumar, S. Srikanth and N.G. Goswami, Editors, *Proc. Nonferrous Extractive Metallurgy in the New Millenium*, NML, Jam shedpur, India, pp. 375–384, 1999.
- Sanjeevi S., Vani K. and Lakshmi K., "Comparison of conventional and wavelet transform techniques for fusion of IRS-1C LISS-III and Pan images". *Proceedings of the 22nd Asian Conference on Remote Sensing, ACRS'01*, pp. 140–145, 2001.
- Saraf A. K., Prakash A., Sengupta S. and Gupta R. P., "Landsat-TM data for estimating ground temperature and depth of coal fire in the Jharia coalfield, India, " *Internatinal Journal of Remote Sensing*, vol. 16, no. 12, pp. 2111–2124, 1995.
- Saraf A. K., "IRS-1C-LISS-III and PAN data fusion: an approach to improve remote sensing based mapping techniques, " *International Journal of Remote Sensing*, vol. 20, no. 10, pp. 1929–1934, 1999.
- Schetselaar E. M., "Fusion by the IHS transform: Should we use cylindrical or spherical coordinates?, " *Internatinal Journal of Remote Sensing*, vol. 19, no. 4, pp. 759–765, 1998.
- Schetselaar E. M., "On preserving spectral balance in image fusion and its advantages for geological image interpretation," *Photogrammetric Engineering and Remote Sensing*, vol. 67, no. 8, pp. 925–934, 2001.
- Schistad-Solberg A., Jain A. and Taxt T., "Multisource classification of remotely sensed data: fusion of Landsat TM and SAR images," *IEEE Transactions on Geoscience and Remote Sensing*, vol. 32, pp. 768–778, 1994.
- Schmullius C., "Monitoring Siberian Forests and Agriculture with the ERS-1 Windscatterometer," *IEEE Transactions on Geoscience and Remote Sensing*, vol. 35, no. 5, pp. 1363–1366, 1997.

- Sellers P. J., "Vegetation-canopy spectral reflectance and biophysical processes," In G. Asrar, *Theory and applications of optical remote sensing*, New York: Wiley, pp. 297–335, 1989.
- Shamshad A., Wan H. W.M.A. and MOHD S. S.A., "Comparison of different data fusion approaches for surface features extraction using Quickbird images," Japan–Vietnam Geoinformatics Consortium, *Geoinformatics for Spatial-Infrastructure Development in Earth and Allied Sciences (GIS-IDEAS)*, Hanoi, Vietnam, 2004.
- Shen S. S., "Summary of types of data fusion methods utilized in workshop papers. Multisource Data Integration in Remote Sensing," *Proceedings of Workshop, Maryland, U.S.A., 14 - 15 June, NASA Conference Publication 3099 (Greenbelt, MD: NASA)*, pp. 145–149, 1990.
- Shensa M. J., "The discrete wavelet transform: Wedding the à Trous and Mallat algorithms," *IEEE Transactions on Geoscience and Remote Sensing*, vol. 40, no. 10, pp. 2464–2482, 1992.
- Shi W. Z., Zhu C. Q., Zhu C.Y. and Yang X. M., "Multi-bandwavelet for fusing SPOT panchromatic and multi-spectral images," *Photogrammetric Engineering Remote Sensing*, vol. 69, no. 5, pp. 513–520, 2003.
- Simone G., Farina A., Morabito F. C., Serpico S. B. and Bruzzone L., "Image fusion techniques for remote sensing applications," *Information Fusion*, vol. 3, pp. 3–15, 2002.
- Singh H., Raj J. and Kaur. G., "Image Fusion Using Fuzzy Logic and Application," *Proceedings of IEEE International Conference on Fuzzy Systems*, vol. 1, pp. 337–340, 2004.
- Singh R. P., Cervone G., Kafatos M., Prasad A. K., Sahoo A. K., Sun D., et al., "Multi-sensor studies of the Sumatra earthquake and tsunami of 26 December 2004," *International Journal of Remote Sensing*, vol. 28, no. 13–14, pp. 2885–2896, 2007.
- Starck J. L., Candès E. J. and Donoho D. L., "The curvelet transform for image denosing," *IEEE Transactions Image Processing*, vol. 11, pp. 670–684, 2002.

- Starck J. L., Candès E. J. and Donoho D. L., "gray and color image contrast enhancement by the curvelet transform," *IEEE Transactions Image Processing*, vol. 12, no. 6, pp. 706–717, 2003.
- Stow D., Daeschner S., Hope A., Douglas D., Petersen A., Myneni R., Zhou L. and Oechel W., "Variability of seasonally integrated normalized difference vegetation index across the North Slope of Alaska in the 1990s," *International Journal of Remote Sensing*, vol. 24, pp. 1111–1117, 2003.
- Strobl D., Ragga J. and Buchroithner M., "Terrain correction geocoding of a multi-sensor image data set," *Proceedings of the 10th Earsel Symposium, Toulouse, France*, pp. 98–107, 1990.
- Stuckens J., Coppin P. R. and Bauer M. E., "Integrating contextual information with per-pixel classification for improved land cover classification," *Remote Sensing of Environment*, vol. 71, pp. 282–296, 2000.
- Sugeno M., "Industrial applications of fuzzy control," Elsevier Science Pub. Co., 1985.
- Teggi S., Cecchi R. and Serafini F., "TM and IRS-1C-PAN data fusion using multiresolution decomposition methods based on the 'atrous' algorithm," *International Journal of Remote Sensing*, vol. 24, pp. 1287–1301, 2003.
- Temimi M., Leconte R., Brssette F. and Chaouch N., "Flood monitoring over the Mackenzie River Basin using passive microwave data," *Remote Sensing of Environment*, vol. 98, no. 2–3, pp. 344–355, 2005.
- Thomas M. L., Claudia G. and Klaus S., "Survey: interpolation methods in medical image processing," *IEEE Transactions on medical imaging*, vol. 18, no. 11, pp. 1049–1075, 1999.
- Thomas C., Ranchin T., Wald L. and Chanussot J., "Synthesis of multispectral images to high spatial resolution: A critical review of fusion methods based on remote sensing physics," *IEEE Transactions on Geosciences and Remote Sensing*, vol. 46, pp. 1301–1312, 2008.

- Tizhoosh H. R. and Haußecker H., "Fuzzy Image Processing: An Overview," In: Jähne B., Haußecker H. (Eds.), *computer vision and applications: A guide for students and practitioners*, Academic Press, Boston, ISBN 0-12-379777-2, pp. 541–576, 2000.
- Tong S. and Yrjö N., "Detail-preserving median based filters in image processing," *Pattern Recognition Letters*, vol. 15, no. 4, pp. 341–347, 1994.
- Townshend J. R. G., "Global data sets for land applications from the advanced very high resolution radiometer: an introduction," *International Journal of Remote Sensing*, vol. 15, no. 17, pp. 3319–3332, 1994.
- Townshend J. R. G. and Justice C.O., "Towards operational monitoring of terrestrial systems by moderate-resolution remote sensing," *Remote Sensing of Environment*, vol. 83, no. 1–2, pp. 351–359, 2002.
- Toyra J., Pietroniro A., Martz L. W. and Prowse T. D., "A multi-sensor approach to wetland flood monitoring," *Hydrological Processes*, vol. 16, pp. 1569–1581, 2002.
- Tu T. M., Su S. C., Shyu H. C. and Huang P. S., "A new look at IHS-like image fusion methods," *Information Fusion*, vol. 2, no. 3, pp. 177–186, 2001.
- Tucker C. J., "Red and photographic infrared linear combinations for monitoring vegetation," *Remote Sensing of Environment*, vol. 8, pp. 127–150, 1979.
- Tucker C. J., Dregne H. W. and Newcomb W. W., "AVHRR datasets for determination of desert spatial extent," *International Journal of Remote Sensing*, vol. 15, pp. 3547–565, 1994.
- Vani K., Sanjeevi S. and Marruthachalam M., "Fusion of IRS -LISS III and PAN images using different resolution ratios," *Proceedings of the 22nd Asian Conference on Remote Sensing, ACRS'01*, pp. 140–145, 2001.
- Varma A. K., Pokhrel S., Gairola R. M. and Agarwal V. K., "An empirical algorithm for cloud liquid water from MSMR and its utilization in rain identification," *IEEE Transactions on Geoscience and Remote Sensing*, vol. 41, no.8, pp. 1853–1858, 2003.

- Varma A. K. and Liu G., "A near-global survey of the horizontal variability of rainfall," *Monthly Weather Review*, 2004.
- Varma A. K. and Liu G., "Small-scale horizontal rain-rate variability observed by satellite," *Monthly Weather Review*, vol. 134, no.10, pp. 2722–2733, 2006.
- Varma A. K., Pokhrel S., Gairola R. M. and Agarwal V. K., "Study of geophysical parameters associated with the Orissa super cyclone using active and passive microwave remote sensing measurements," *International Journal of Remote Sensing*, vol. 27, no.18, pp. 3753–3765, 2006.
- Varshney P. K., "Multisensor data fusion," *Electronics & Communication Engineering Journal*, pp. 245–263, 1997.
- Venkataraman G., Madhavan B. B., Ratha D. S., Antony J. P., Goyal R. S., Banglani S. and Roy S. S., "Spatial modeling for base-metal mineral exploration through integration of geological data sets," *Natural Resources Research*, vol. 9, no.1, pp. 27–42, 2000.
- Venkataraman G., Mahato B. C., Ravi S., Rao Y. S., Mathur P., Snehmani, " Fusion of optical and microwave remote sensing data for snow cover mapping, " *Geosciences and Remote Sensing Symposium, IGARSS 2004*, vol.4, pp. 2554 - 2557, 2004.
- Verbyla D., "Satellite remote sensing of natural resources," Boca Raton: Lewis Publishers, 1995.
- Vijayaraj V., Younan N. H. and O'Hara C. G., "Quality Metrics for Multispectral Image Processing," *Proceedings of the Annual ASPRS Conference*, 2004.
- Voegtle T. and Steinle E., "Fusion of 3D building models derived from first and last pulse laser scanning data," *Information Fusion*, vol. 6, no. 4, pp. 275–281, 2005.
- Vogelmann J. E., Howard S. M., Yang L., Larson C. R., Wylie B. K. and Van Driel J. N., "Completion of the 1990's National Land Cover data set for the conterminous United States," *Photogrammetric Engineering and Remote Sensing*, vol. 67, pp. 650–662, 2001.



- Vrabel J., "Multispectral imagery advanced band sharpening study," *Photogrammetric Engineering and Remote Sensing*, vol. 66, no. 1, pp. 73–79, 2000.
- Vrcelj B. and Vaidyanathan P. P., "Efficient implementation of all-digital interpolation," *IEEE Transactions on Image Processing*, vol. 10, pp. 1639-1646, 2001.
- Wald L., "An overview of concepts in fusion of Earth data," *Future Trends in Remote Sensing*, Denmark, pp. 385–390, 1997.
- Wald L., Ranchin T., and Mangolini M., "Fusion of satellite images of different spatial resolutions: Assessing the quality of resulting images," *Photogrammetric Engineering and Remote Sensing*, vol. 63, no. 6, pp. 691–699, 1997.
- Wald L., "Some terms of reference in data fusion," *IEEE Transactions on Geosciences and Remote Sensing*, vol. 37, no. 3, pp. 1190–1193, 1999.
- Wald L. and Ranchin T., "Comment: Liu smoothing filter-based intensity modulation: a spectral preserve image fusion technique for improving spatial details," *International Journal of Remote Sensing*, vol. 23, no. 3, pp. 593–597, 2002.
- Wan Z., Wang P. and Li X., "Using MODIS land surface temperature and normalized difference vegetation index for monitoring drought in the southern Great Plains, USA," *International Journal of Remote Sensing*, vol. 25, pp. 61–72, 2004.
- Wang L. X., "Adaptive fuzzy systems and control," Prentice-Hall, Englewood-Cliffs, New Jersey Wang, 1994.
- Wang Z. and Bovik A. C., "A Universal Image Quality Index," *IEEE Signal Processing Letters*, vol. 9, no.3, pp.81–84, 2002.
- Wang Z., Bovik A. C., Sheik H. and Simoncelli E., "Image quality assessment: From error visibility to structural similarity," *IEEE Transactions on Image Processing*, vol. 13, no. 4, pp. 600–612, 2004.
- Wang Z., Ziou D., Armenakis C., Li D. and Li Q., "A Comparative Analysis of Image Fusion Methods," *IEEE Transactions on Geosciences and Remote Sensing*, vol. 43, no. 6, pp.1391–1402, 2005.

- Welch R. and Ehlers M., "Cartographic feature extraction with integrated SIR-B and Landsat TM images," *International Journal of Remote Sensing*, vol. 9, no. 5, pp. 873–889, 1988.
- Wessels K. J., Defries R. S., Dempewolf J., Anderson L. O., Hansen A. J., Powell S. L. and Moran E. F., "Mapping regional land cover with MODIS data for biological conservation: Examples from the Great Yellowstone Ecosystem, USA and Para State," *Brazil, Remote Sensing of Environment*, vol. 92, pp. 67–83, 2004.
- Westra T. and De W. R. R., "Monitoring Sahelian floodplains using Fourier analysis of MODIS time-series data and artificial neural networks," *International Journal of Remote Sensing*, vol. 8, no. 7, pp. 1595–1610, 2007.
- Williams M. L., Wilson R. C. and Hancock E. R., "Deterministic search for relational graph matching," *Pattern Recognition*, vol. 32, no. 7, pp. 1255–1516, 1999.
- Willmott C. and Matsuura K., "Advantages of the mean absolute error (MAE) over the root mean square error (RMSE) in assessing the average model performance," *Climate Research*, vol. 30, pp. 79–82, 2005.
- www1, "[https://lpdaac.usgs.gov/lpdaac/products/modis\\_products\\_table/surface\\_reflectance/8\\_day\\_13\\_global\\_250m/v5/terra](https://lpdaac.usgs.gov/lpdaac/products/modis_products_table/surface_reflectance/8_day_13_global_250m/v5/terra)," last accessed on November 2008.
- www2, "[http://www.ccrs.nrcan.gc.ca/resource/tutor/fundam/chapter3/08\\_e.php](http://www.ccrs.nrcan.gc.ca/resource/tutor/fundam/chapter3/08_e.php)," last accessed on June 2009.
- Xiao X., Boles S., Liu J., Zhuang D. and Liu M., "Characterization of forest types in northeastern China, using multi-temporal SPOT-4 VEGETATION sensor data," *Remote Sensing of Environment*, vol. 82, pp. 335–348, 2002.
- Xiong X. and Barnes W. L., "An overview of MODIS radiometric calibration and characterization," *Advances in Atmospheric Sciences*, vol. 23, no. 1, pp. 69–79, 2006.
- Yahia H. A., Turiel N., Chrysoulakis J., Grazzini P., Prastacos and Herlin I., "Multifractal pre-processing of AVHRR images to improve the determination of

- smoke plumes from large fires," *Geosciences and Remote Sensing Symposium, IGARSS 2007*, pp. 5335 - 5338, 2007.
- Yamaguchi Y., Kahle A., Tsu H., Kawakami T. and Pniel M., "Overview of Advanced Spaceborne Thermal Emission and Reflection Radiometer (ASTER)," *IEEE Transactions on Geosciences and Remote Sensing*, vol. 36, no. 4, pp. 1062–1071, 1999.
- Yang L., Wylie B. K., Tieszen L. L. and Reed B. C., "An analysis of relationships among climate forcing and time-integrated NDVI of grasslands over the U. S. northern and central Great Plains," *Remote Sensing of Environment*, 65, pp. 25–37, 1998.
- Yang J., Xiong T. and Peng Y., N., "Polarimetric SAR image classification by using generalized optimization of polarimetric contrast enhancement," *International Journal of Remote Sensing*, vol. 27, no. 16, pp. 3413–3424, 2006.
- Yang J., She X. and Xiong T., "Iteration based polarimetric SAR image classification," *PIER online*, vol. 3, no. 5, pp. 625–628, 2007.
- Yifang B., Hongtao H. and Rangel I. M., "Fusion of Quickbird MS and RADARSAT SAR data for urban land-cover mapping: object-based and knowledge-based approach," *International Journal of Remote Sensing*, vol 31, no. 6, pp. 1391–1410, 2010.
- Yingxin G., Brown J. F., Verdin J. P. and Wardlow B., "A five-year analysis of MODIS NDVI and NDWI for grassland drought assessment over the central Great Plains of the United States," *Geophysical Research Letters*, vol. 34, 106407, 2007.
- Yocky D. A., "Image merging and data fusion using the discrete two dimensional wavelet transform," *Journal of the Optical Society of America A*, vol. 12, no. 9, pp. 1834–1841, 1995.
- Yocky D. A., "Multiresolution wavelet decomposition image merger of Landsat Thematic Mapper and SPOT panchromatic Data," *Photogrammetric Engineering and Remote sensing*, vol. 62, no. 3, pp. 295–303, 1996.

- Zadeh L. A., "Fuzzy Sets," *Information and control*, vol. 8, no. 3, pp. 338–353, 1965.
- Zadeh L. A., "Outline of a new approach to the analysis of complex systems and decision processes," *IEEE Transactions on Systems, Man, and Cybernetics*, vol. 3, no. 1, pp. 28–44, 1973.
- Zhan X., Sohlberg R. A., Townshend J. R. G., Dimiceli C., Carroll M. L., Eastman J. C., Hansen M. C. and Defries R. S., "Detection of land cover changes using MODIS 250 m data," *Remote Sensing of Environment*, vol. 83, pp. 336–350, 2002.
- Zhang J., Wagner W., Prakash A., Mehl H. and Voigt S., "Detecting coal fires using remote sensing techniques," *International Journal of Remote Sensing*, vol. 25, no. 16, pp. 3193–3220, 2004.
- Zhang Q., Wang C., Shinohara F. and Yamaoka T., "Automatic extraction of water body based on EOS/MODIS remotely sensed imagery," *Proceedings of the SPIE*, Volume 6786, pp. 678642, 2007.
- Zhang X. M., "Coal Fires in Northwest China – detection, monitoring and prediction using remote sensing data," PhD thesis, University of Delft, ITC Publication, no. 58, 1998.
- Zhang X. M., Cassells C. J. S. and van Genderen J. L., "Multi-sensor data fusion for the detection of underground coal fires" *Geologie en Mijnbouw*, vol. 77, pp. 117–127, 1999.
- Zhao L., Xu B., Tang W. and Chen Z., "A Pixel-Level Multisensor Image Fusion Algorithm Based on Fuzzy Logic," Springer-Verlag Berlin Heidelberg, FSKD, LNAI 3613, pp. 717–720, 2005.
- Zheru C., Hong Y. and Tuan P., "Fuzzy Algorithms: With applications to image processing and pattern recognition," World Scientific Publication, 1996.
- Zhou J., Civco D. L. and Silander J. A., "A wavelet transform method to merge Landsat TM and SPOT panchromatic data," *International Journal of Remote Sensing*, vol. 19, no. 4, pp. 743–757, 1998.

Zhu Z. Y., "A novel image fusion approach based on rough set and wavelet analysis,"  
Key Engineering Materials, vol 439–440, pp. 1069–1074, 2010

Zimmermann H. J., "Fuzzy sets theory and its applications," Kluwer Academic  
Publishers, Boston, 1991.

# Author's Publications

## **International Journals**

1. Harish K. G. R. and Singh D., "Quality assessment of fused image of MODIS and PALSAR," Progress In Electromagnetics Research B, vol. 24, pp. 191–221, 2010.

## **International Journals (communicated)**

1. Harish K. G. R. and Singh D., "Curvelet Based Fusion of MODIS and ASTER data," communicated to International Journal of Advances in Space Research, Elsevier publications (under review).
2. Harish K. G. R. and Singh D., "Multitemporal Harmonic Analysis of MODIS indexes images from the year 2001 to 2008," communicated to Geomatics, Natural Hazards and Risk, Taylor & Francis (under review).

## **International Conferences**

1. Harish K. G. R. and Singh D., "Application of Binary Division Algorithm for Image Analysis and Change Detection to identify the hotspots in MODIS

Images," International Archives of Photogrammetry, Remote Sensing and Spatial Information Sciences, vol. 36, no. 4, pp. 140–145, 2006.

2. Harish K. G. R., Singh D. and Ankush M., "Fusion of MODIS, AVHRR and ASTER data using curvelet transform for land cover classification," Geosciences and Remote Sensing Symposium, IGARSS 2007, IEEE International, pp. 3082–3085, 2007.
3. Harish K. G. R. and Singh D., "A Pixel Purity Index and Curvelet based approach for the Fusion of ASTER and MODIS data for land cover classification, " 37th COSPAR scientific Assembly Montreal, Canada, 13th July-20th July, 2008.
4. Harish K. G. R. and Singh D., "Fusion of MODIS and PALSAR principal component images through curvelet transform for land cover classification," communicated to COSPAR Scientific Assembly 2010 (Accepted).
5. Harish K. G. R. and Singh D., "Fusion of ASTER and MODIS Principal Component images through Curvelet transform for land cover classification," communicated to Geoscience and Remote Sensing Symposium, IGARSS 2010 (Accepted).

#### **National Seminar/ Conferences**

1. Harish K. G. R. and Singh D., "Fusion of MODIS and ASTER data using fuzzy logic," National Seminar on Radar Remote Sensing and Its Applications, IIT Roorkee, 25-26 September, pp. 25, 2009.
2. Harish K. G. R. and Singh D., " Fusion of MODIS and PALSAR Data using ATrous Transform for land cover enhancement," Ucost, 6-7 February 2010.